Advanced Radiance Transformation System (ARTS) For Space-borne Microwave Instruments

Hu(Tiger) Yang[1], Fuzhong Weng[2], Ninghai Sun[2]
Wanchun Chen[2], Lin Lin[2] , Miao Tian[1]

1. Earth Science System Interdisciplinary Center, University of Maryland
2. NOAA Center for Satellite Applications and Research, USA

huyang@umd.edu

May 12, 2014

Introduction

NOAA request a full radiance based calibration algorithm for consistent calibration for historical, present and future microwave sounding instruments

- Weather forecast application require continuous improving for satellite instrument calibration accuracy
- Satellite climate study need to develop and implement a robust, sustainable and scientifically defensible calibration system to producing and preserving climate records from satellite data

Present microwave calibration system is derived in temperature space, which is not consistent with historical full radiance calibration system developed in NOAA

- R-J approximation corrected calibration algorithm will cause scene dependent calibration error
- New sciences established from solid study of SNPP ATMS are need to be included to improve the calibration accuracy

An Advanced Radiance Transformation System (ARTS) is developed for microwave sounding instruments in JPSS era

- Full radiance calibration system applicable to different sensors
- New science for improving the calibration accuracy

ARTS System and Software Engineering

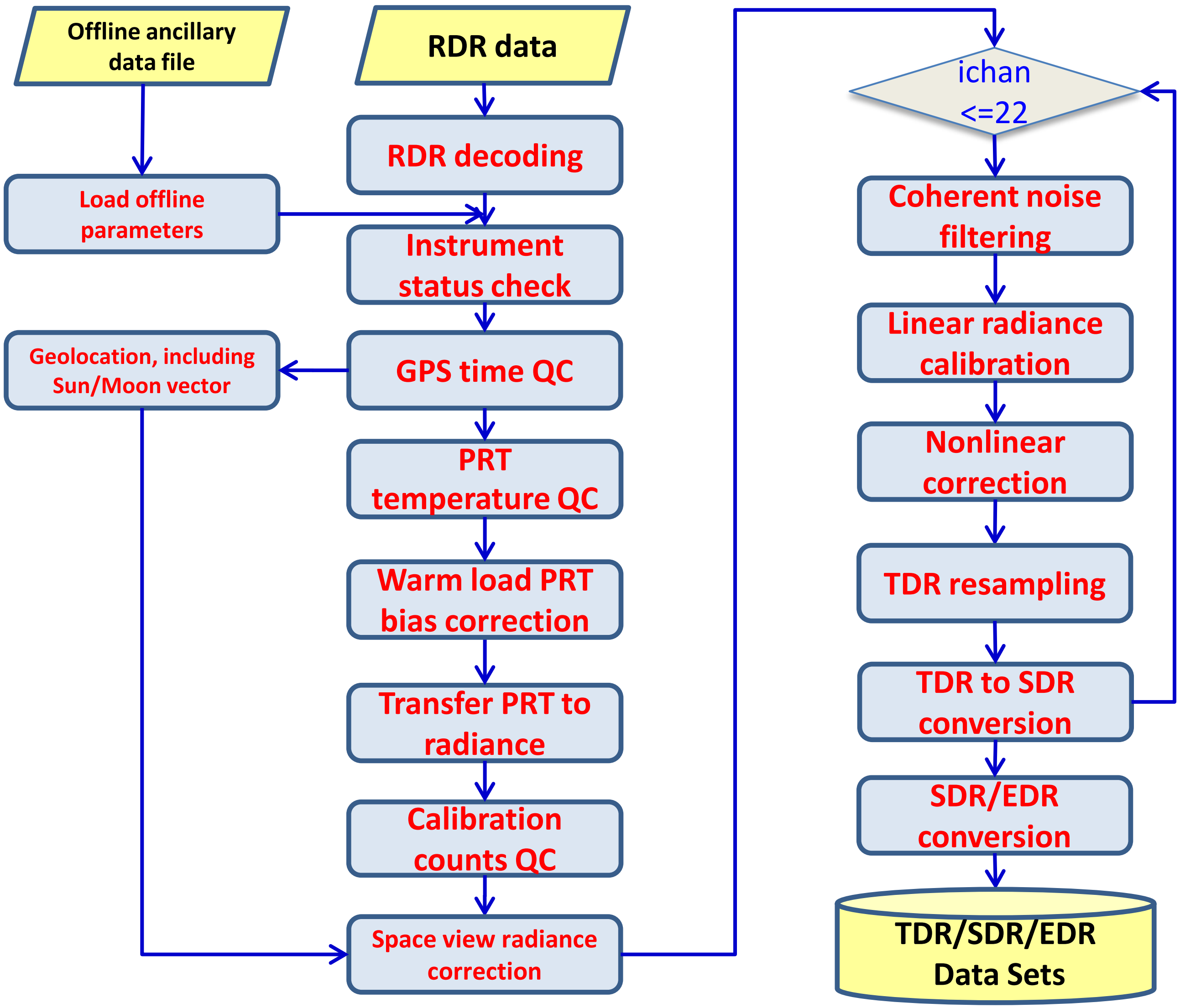

- Consistent calibration algorithm for different sensors
- Full radiance calibration system with improved two-point calibration algorithm
- Data resampling ability to generate TDR with different spatial resolutions

Quality Control in ARTS

Different level of Quality control with PCT as inputs makes system being sustainable

Granule Level

Quadratic Correction(i.e., Nonlinearity)

Scan Level

Instrument mode
Health and status
PRT conversion
PRT temperature limit
PRT temperature consistency
Scan time/Data gap check

Channel Level

Lunar contamination
Gain error
Insufficient warm target observations
Insufficient cold space observations
Calibration counts out of range
Warm target view inconsistency check

Supported Platforms

- Supports both big and little endian platforms
- Comparable processing efficiency with IDPS

OS	C compiler	C++ compiler	Fortran 90 compiler
AIX 5.3.0.0 or later	IBM XL C/C++ Enterprise Edition for AIX, V10.1	IBM XL C/C++ Enterprise Edition for AIX, V10.1	IBM XL Fortran Enterprise Edition for AIX, V12.1
LINUX (Red Hat Enterprise 5)	GCC 4.3.2	GCC 4.3.2	Intel Fortran version 11 or later
Windows XP/Vista running Cygwin	GCC 4.3.2	GCC 4.3.2	gfortran

Main ARTS Modules

- Satellite geolocation
- Full radiance calibration
- B-G resampling
- Coherent noise filtering
- Lunar contamination correction

Geolocation

- Geolocation module includes GPS based and TLE based algorithms
- Primary algorithm uses GPS measurements of satellite position/velocity
- TLE is used as backup when no GPS data or large data gap exists in raw data
- ATMS geolocation error relative to VIIRS is about 3-4km

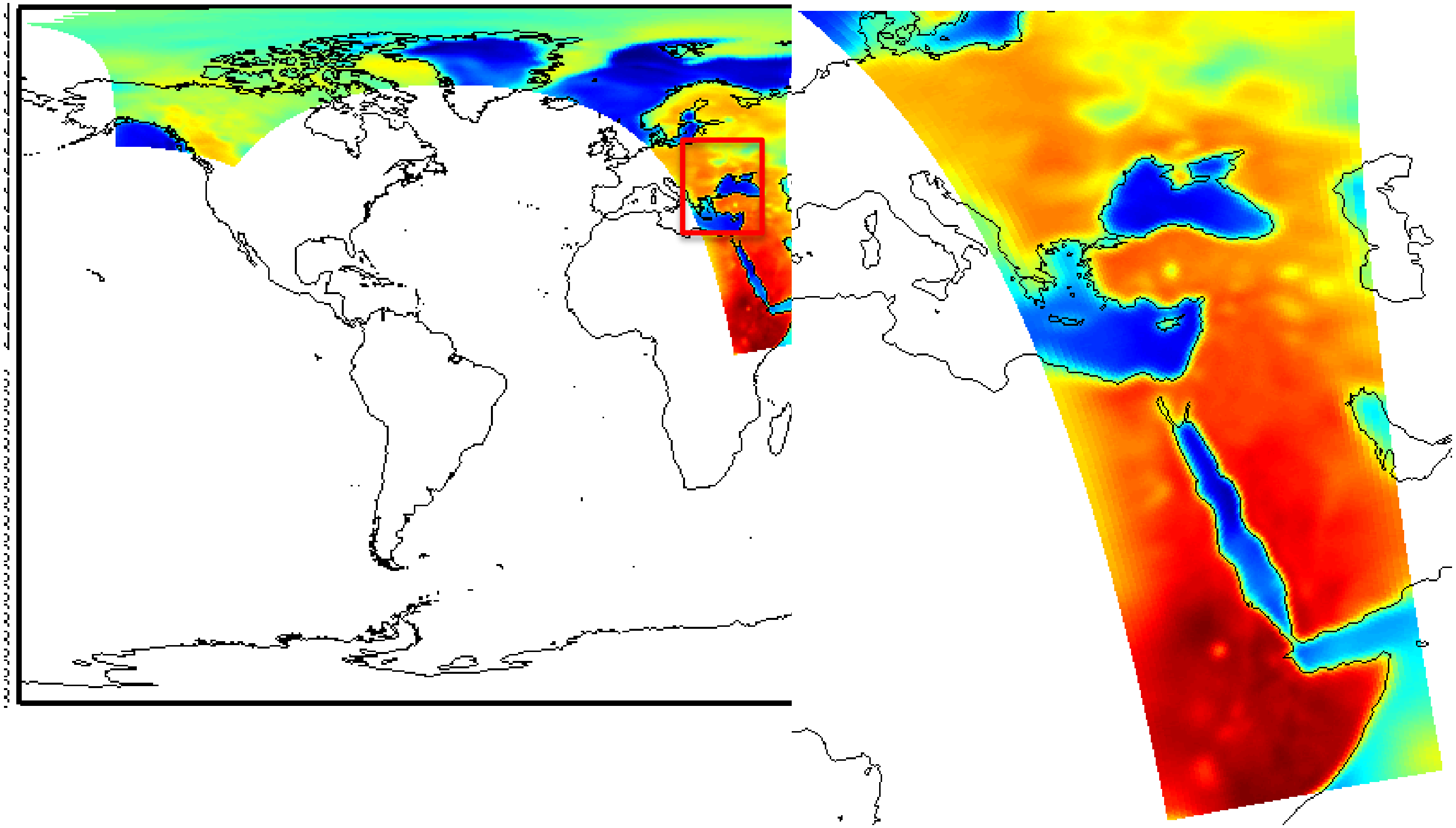

Full Radiance Calibration

- Calibrated space view scene brightness temperatures from IDPS are not equal to the cosmic background temperature 2.73K
- Abnormal scan angle dependent feature existed in calibrated TDR products

ATMS TDR at Ch18 on February 20, 2012

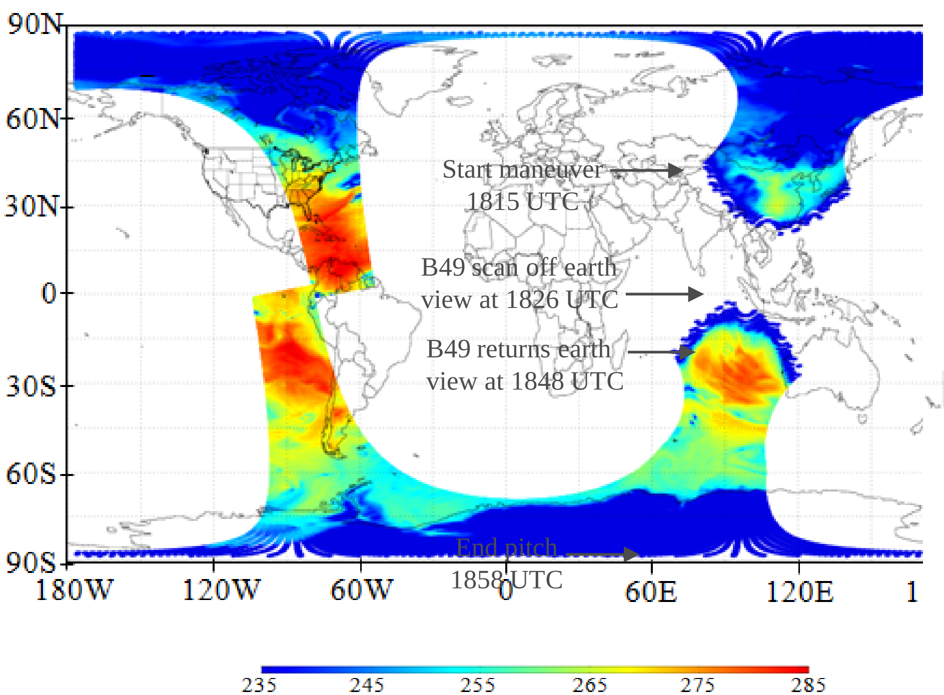

Channel 1

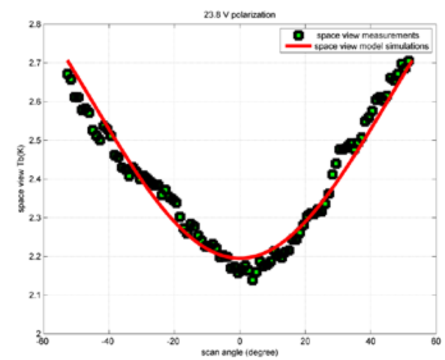

Channel 2

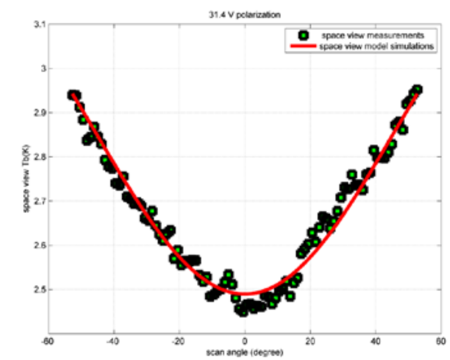

Channel 3

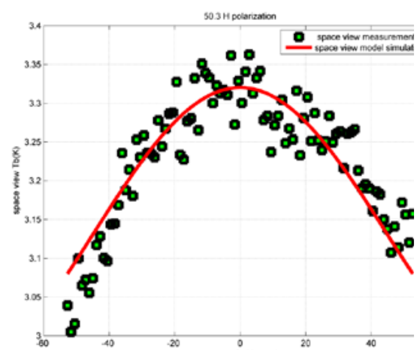

Channel 4

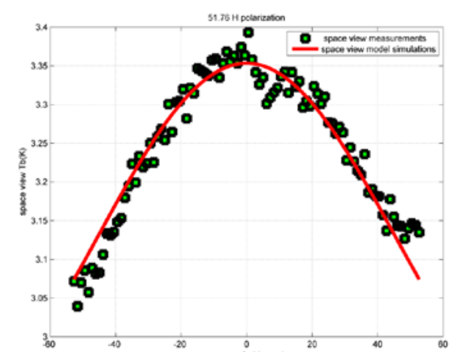

Calibration Error in IDPS

- Normally, a scene temperature dependent term and a constant bias term are used in R-J calibration equation
- However, after applying correction by them it will still have residual errors that are dependent to temperature and frequency in the corrected calibrated temperature
- Especially, when the scene temperature is close to cosmic background temperature, large bias will present when applying the R-J calibration equation with Tc correction.

$$T_s = \delta(T_h - T_c) + T_c + (\Delta T_c - \Delta T_s)$$

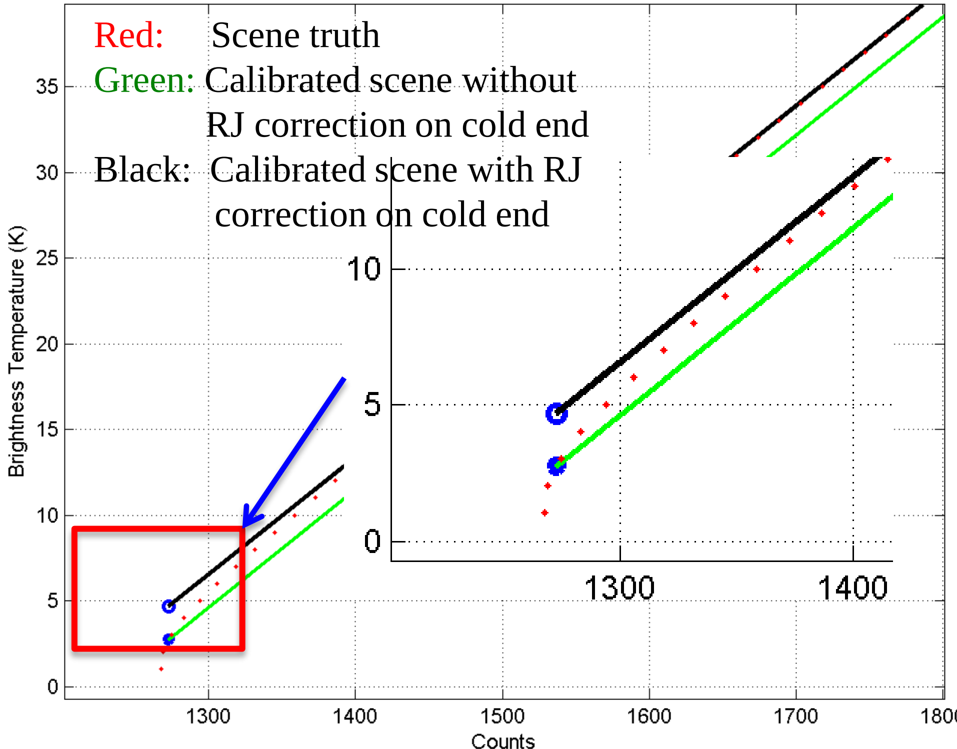

New Two-Point Calibration Model in ARTS

Antenna emission including near-field radiation effect is modeled as function of scan angle and included in the calibration. Cold space observations from pitch maneuver operation are clean and used to derive model parameters for different channels. Such new algorithm can only be delivered in full radiance calibration system.

Corrected Two Point Calibration Equation in ARTS

For Vertical Polarization Channels:

$$\boxed{R_s = \delta[(R_h - R_c) + \beta_1(sin^2\theta_h - sin^2\theta_c)] + R_c + \beta_1(sin^2\theta_s - sin^2\theta_c)}$$

For Horizontal Polarization Channels:

$$\boxed{R_s = \delta[(R_h - R_c) + \beta_1(cos^2\theta_h - cos^2\theta_c)] + R_c + \beta_1(cos^2\theta_s - cos^2\theta_c)}$$

Rs: Calibrated antenna radiance

Rh: Warm load radiance

Rc: Cold space radiance (equal to 2.73K)

θ_{h}: Scan angles of warm load measurements

θ_{c}: Scan angles of space view

θ_{s}: Scan angles of Earth view (i.e., each FOV)

δ: Defined as (Cs - Cc) /(Ch - Cc), where Ch/Cc/Cs are receiver output counts of warm load, cold space and earth view, respectively

Space View BT Calibrated by ARTS

Channel -1

ARTS IDPS

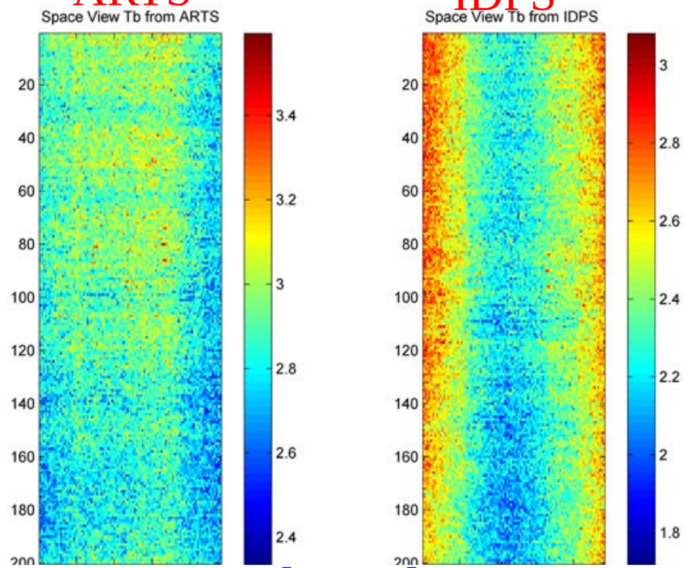

Channel -2

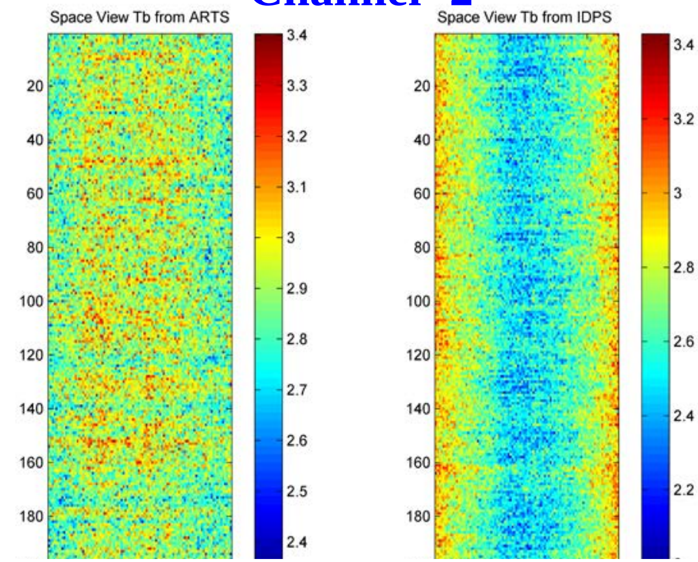

Channel -14

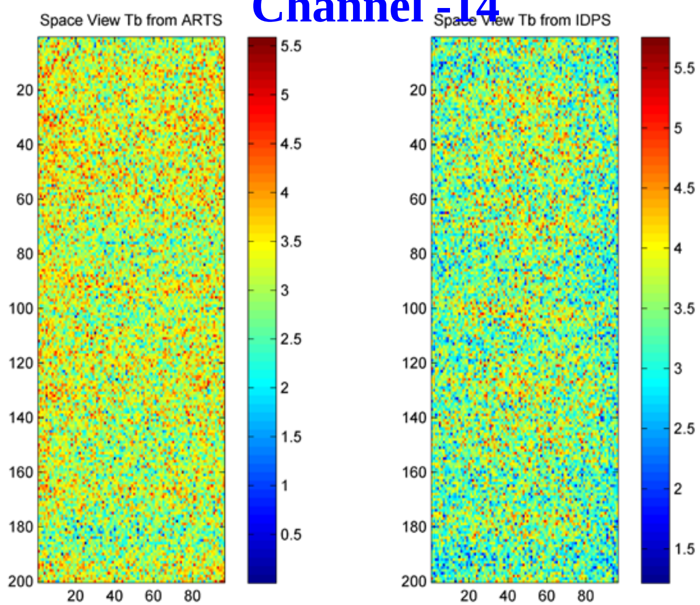

Channel -18

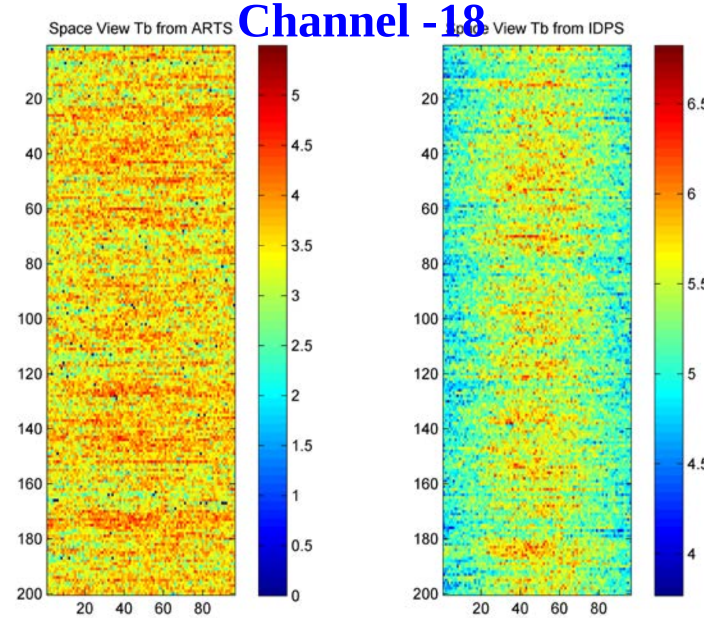

Scan Angle Dependent in TDR from ARTS

For space view BT corrected by ARTS: No scan angle dependent feature, and close to cosmic background 2.73K

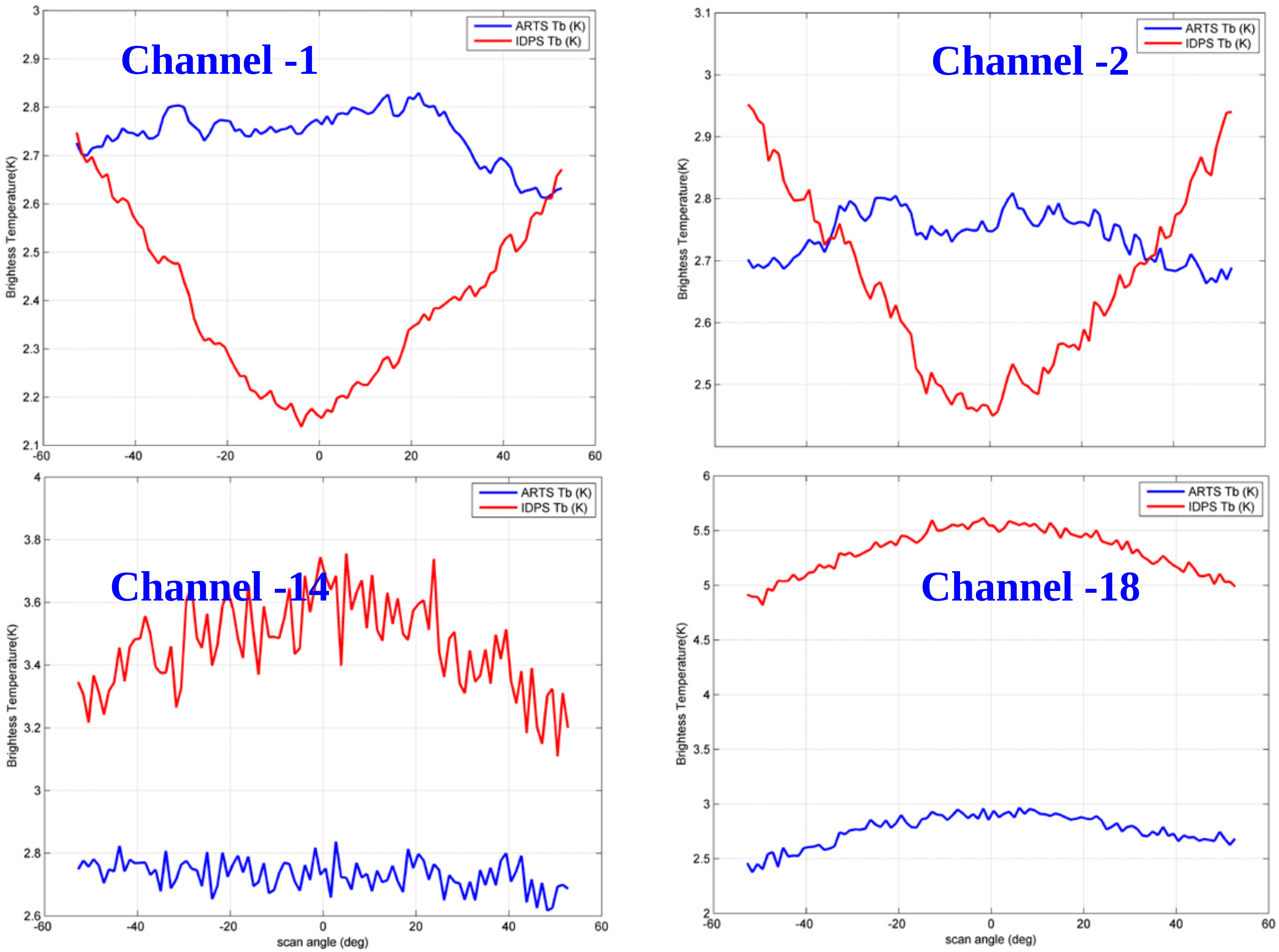

Resampling TDR

Resolution Reduction

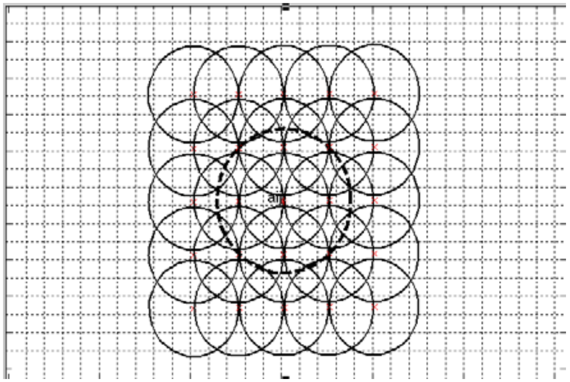

Resolution Enhancement

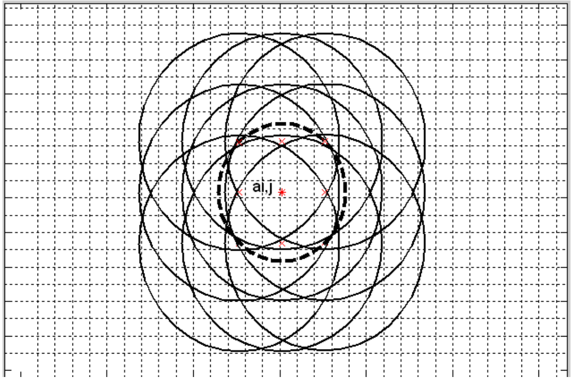

FOV 2.2°

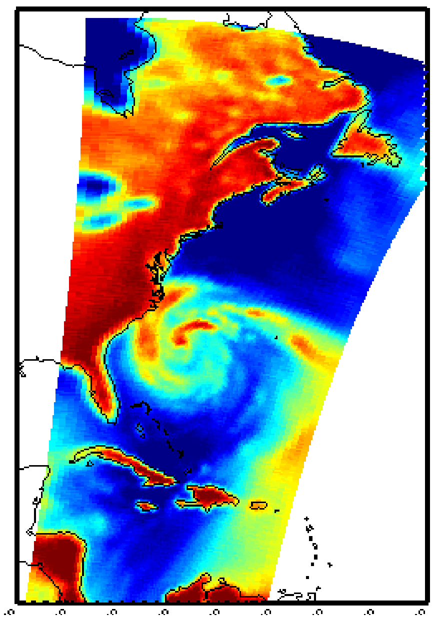

FOV 3.3

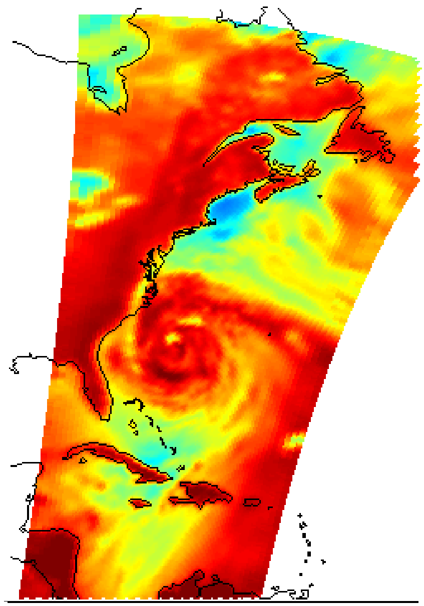

- Explore the potential of the oversampling characteristic of ATMS observations and generate observations at different frequencies with consistent FOV size

- Backus-Gilbert observation reconstruction algorithm is used for remapping TDR to expected spatial resolution

- Remapping coefficients are tuned to ensure the remapped TDR products are in best balance between noise and spatial resolution

Coherent Noise Filtering

Based on frequency spectrum analysis of the receiver output calibration counts, a low-pass filter with sinc window function is developed to effectively remove the high-frequency components (rapid fluctuations) while keep the low-frequency components (gain variations) unchanged.

Sinc Window Function

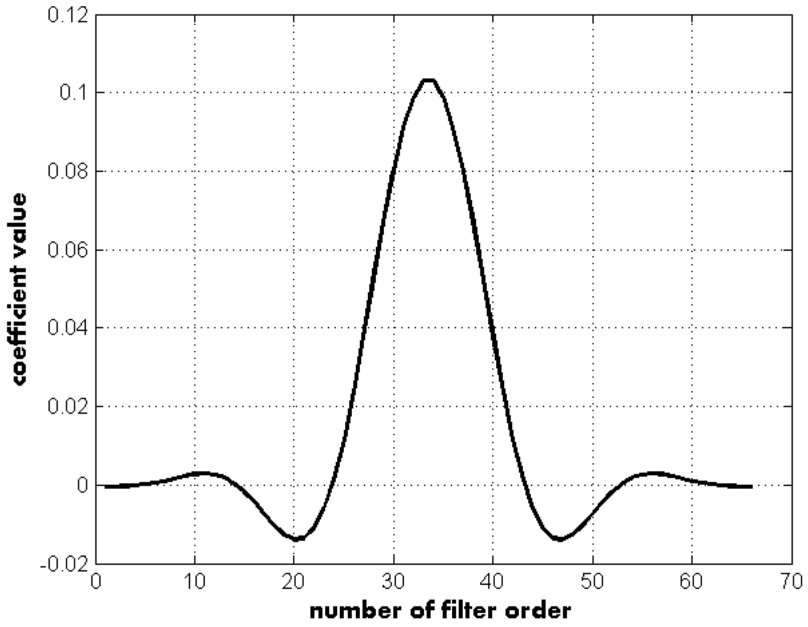

Calibrated Tb with and without calibration counts noise filtering

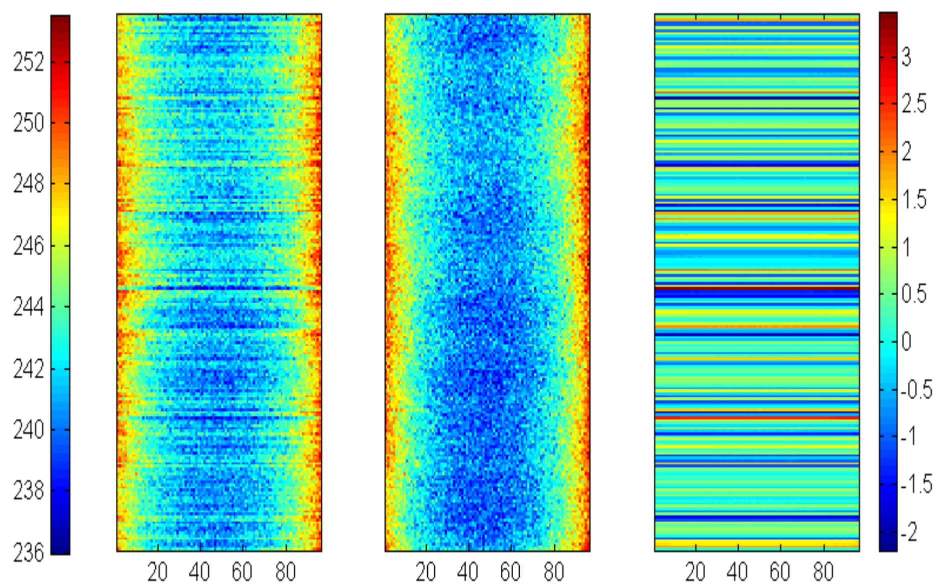

Lunar Contamination Correction

Brightness temperature increment arising from lunar contamination is modeled as function of lunar solid angle, antenna response and radiation from the Moon

$$\Delta T_{moon} = G * \Omega * T_{moon}$$

G: Antenna response function

Ω_{moon} Weights of the Moon in Isaac Moradi <imoradi@umd.edu> **antenna pattern:**

T_{moon}: Brightness temperature of the Moon

- LI happens when $\beta' = \beta - \alpha_l \leq 1.25 \cdot \theta_{3dB}$
- Lunar contamination impacts to the four space view counts are different.
- The increased brightness temperature due to the lunar contamination can be accurately identified and quantified from the model.

Sketch plot of lunar contamination in space view

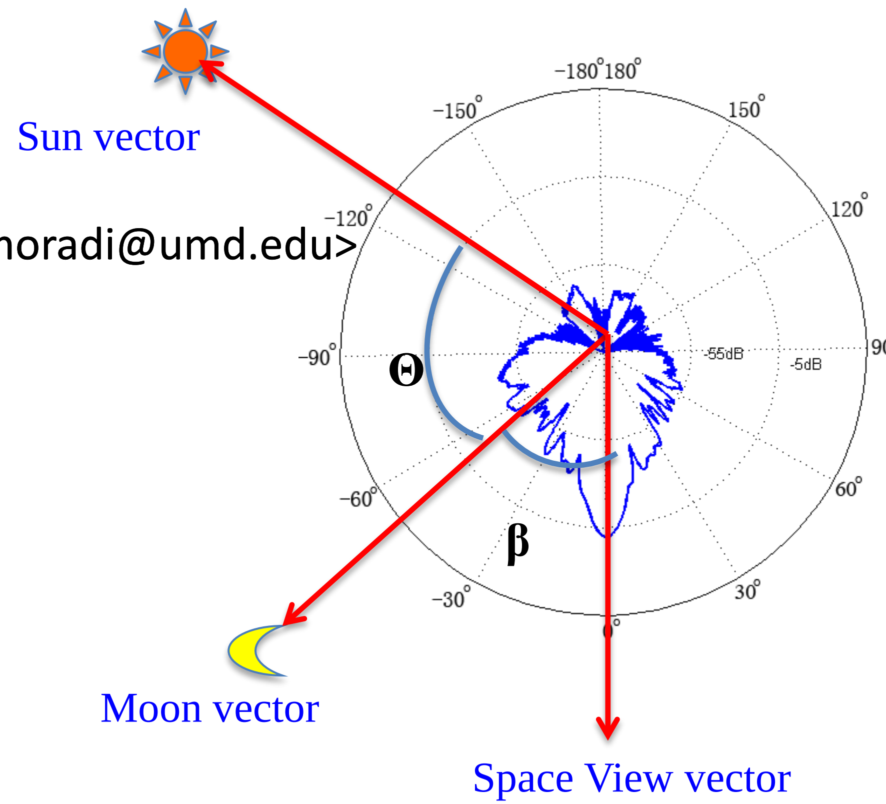

ATMS SDR Lunar Intrusion Identification and Correction Activities and Results

ICVS Monitoring Results of Lunar Intrusion

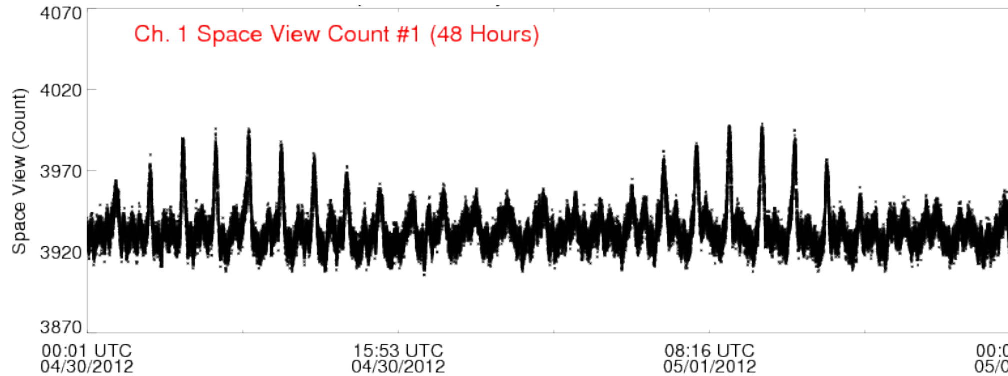

Operational SDR without LI correction

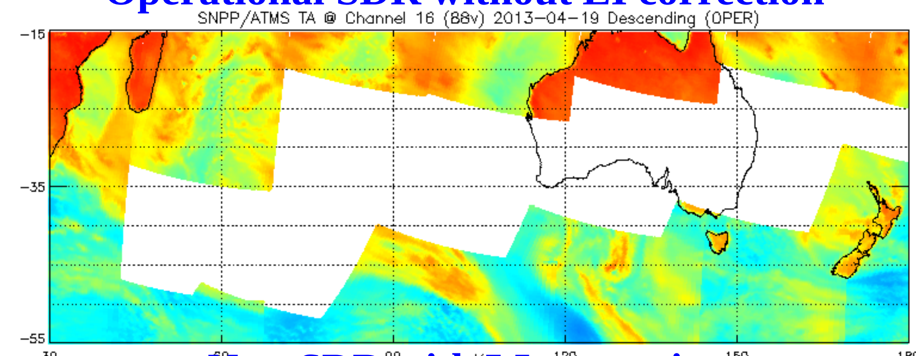

New SDR with LI correction

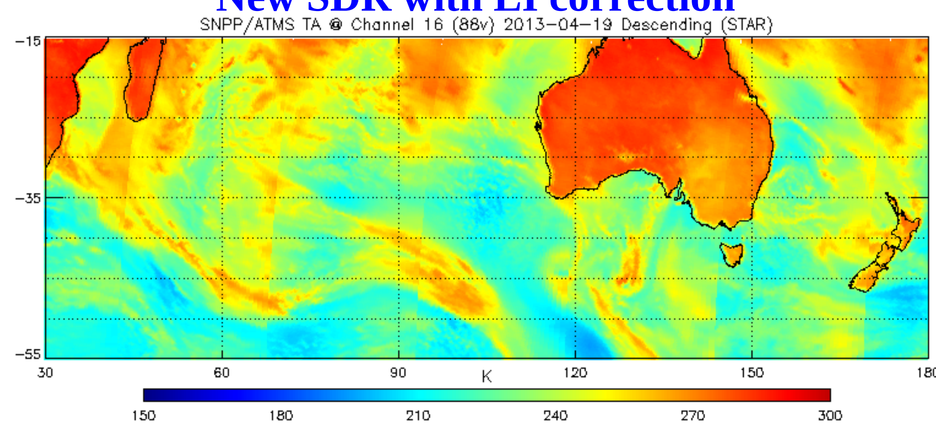

Activities

- ATMS RDR dataset was re-processed using the latest ATMS SDR algorithm code and PCT to evaluate lunar intrusion (LI) detection and correction performance
- The potential impact of current TDR with LI on NWP model was evaluated in GSI
- New metrics and physical model was developed for LI identification and correction
- Different approaches for LI correction was compared and tested in ARTS, optimal algorithm was selected and implemented in current operational calibration system

Results

- Lunar intrusion was accurately identified and correctly flagged in SDR datasets
- Data gap was removed after LI correction, residual correction error is below the instrument noise
- New scheme for LI detection and correction was developed for future improvement of current IDPS

TDR Products from ARTS

- TDR products are generated on the daily basis
- TB difference ARTS and IDPS is scene and frequency dependent.

TDR from ARTS   ATMS Channel-01   TDR from IDPS

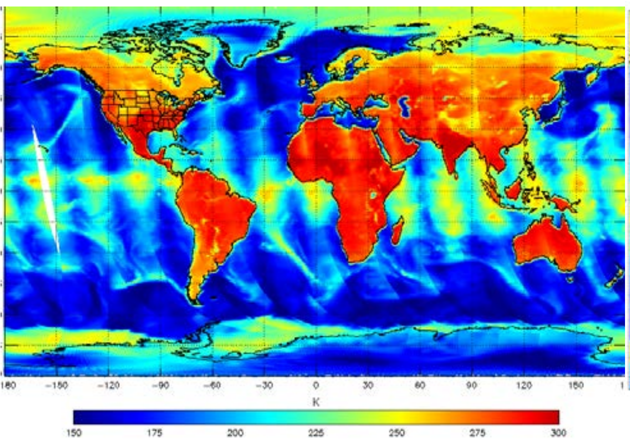

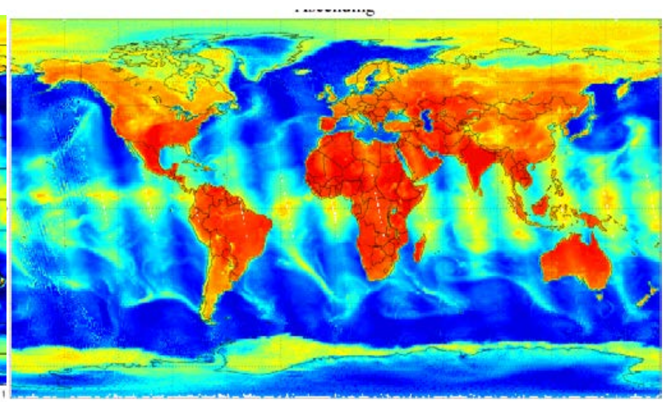

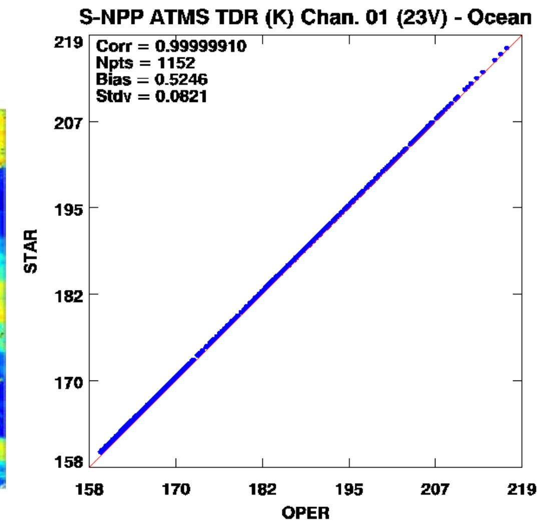

ATMS Channel-17

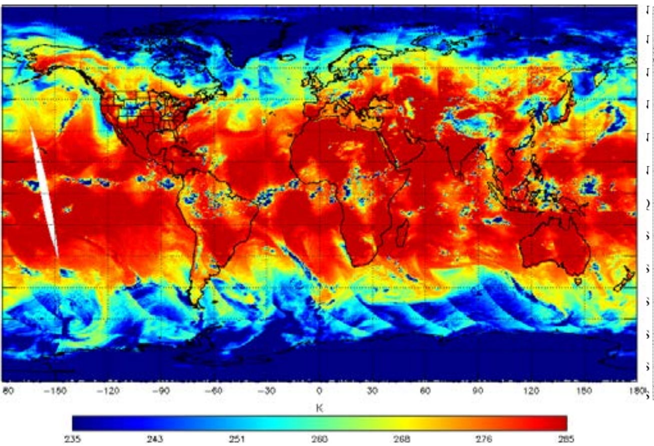

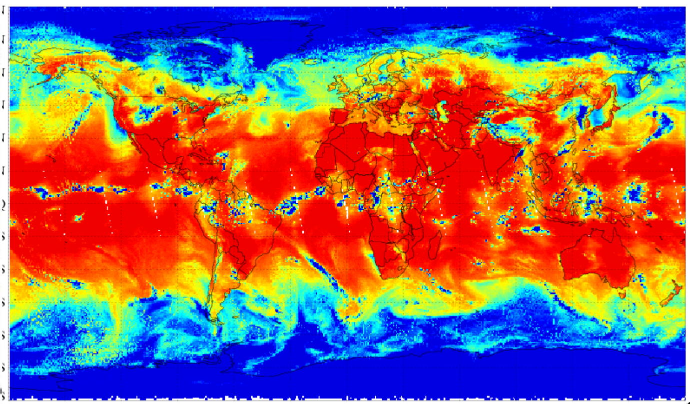

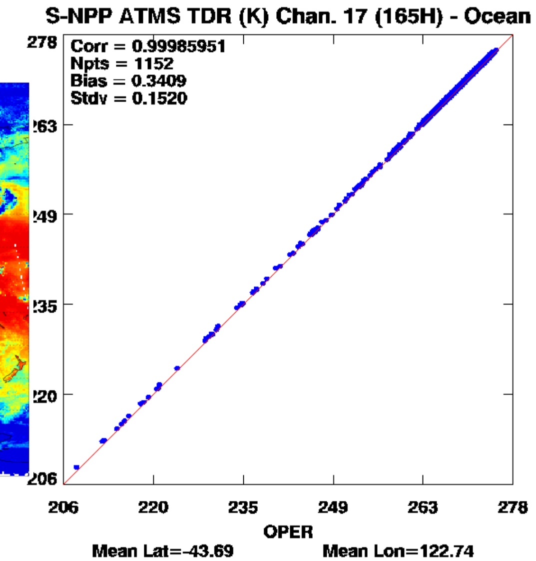

Conclusions and Future Works

- ARTS is a full radiance calibration system designed for microwave sounding instruments. With new sciences developed from solid study of SNPP ATMS, the calibration accuracy of TDR products from future JPSS satellite will be improved

- ARTS is designed as a robust, sustainable and scientifically defensible operational calibration system for future JPSS satellite, and also can be used as test bed for developing new algorithm.

- Future work will focus on reprocessing SNPP ATMS data using ARTS, generating 2.2^{o} resolution TDR products for use in weather and climate study

Pertinent Publications

- Fuzhong Weng, Hu Yang, Xiaolei Zou, 2012, “On Convertibility From Antenna to Sensor Brightness Temperature for ATMS”, IEEE Geoscience and Remote sensing Letters, Vol.99, pp 1-5
- Fuzhong Weng, Xiaolei Zou, Ninghai Sun, Hu Yang, Xiang Wang, Lin Lin, Miao Tian, and Kent Anderson, 2013, “Calibration of Suomi National Polar-Orbiting Partnership (NPP) Advanced Technology Microwave Sounder (ATMS) ”, Journal of Geophysical Research, Vol.118, No.19, PP. 11,187~11,200
- Fuzhong Weng, Xiaolei Zou, 2013, “Errors from Rayleigh-Jeans approximation in satellite microwave radiometer calibration systems”, 52 (3) PP. 505-508
- Hu Yang and Xiaolei Zou, 2014, “OPTIMAL ATMS REMAPPING ALGORITHM FOR CLIMATE RESEARCH”, IEEE Transaction on Geoscience and Remote sensing, in print
- Xiaolei Zou, Fuzhong Weng, and Hu Yang, 2014, “Connection the Time Series of Microwave Sounding Observations from AMSU to ATMS for Long-Term Monitoring of Climate Change”, Journal of Climate, accepted for publication
- Hu Yang and Fuzhong Weng, 2014, “On-Orbit ATMS Lunar Contamination Corrections”, Submitted to IEEE Transaction on Geoscience and Remote Sensing

ATMS Optimal Striping Filters

X. Zou[1], Y. Ma[1] and F. Weng[2]

[1]Department of EOAS, Florida State University

[2]Center for Satellite Applications and Research, NOAA

May 13, 2014

Outline

- ATMS TDR/SDR Striping Issues
- User Complains
- Requirements for Characterization and Correction
- AMSU-A/MHS/AMSU-B
- ATMS Striping (TVAC, Pitchover Data, Earth Scene ...)
- De-striping Methodology
- Optimal Striping Filters for Radiances
- Optimal Striping Filters for Calibration Counts

Qin, Z., X. Zou and F. Weng, 2013: Analysis of ATMS and AMSU striping noise from their earth scene observations. *J. Geophy. Res.*, **118**, 13,214-13,229.

PCA Decomposition for ATMS Channel 10

The ATMS data can then be expressed as in PCA:

$$\mathbf{A} = \sum_{j=1}^{96} \vec{e}_j \vec{u}_j$$

PC mode PC coefficient

$$\mathbf{A} = \begin{pmatrix} TB_{1,1} & TB_{1,2} & \cdots & TB_{1,j} & \cdots & TB_{1,K} \\ TB_{2,1} & TB_{2,2} & \cdots & TB_{2,j} & \cdots & TB_{2,K} \\ \vdots & & \ddots & & & \\ TB_{k,1} & & & TB_{k,j} & & TB_{k,K} \\ \vdots & & & & \ddots & \\ TB_{96,1} & & & & & TB_{96,K} \end{pmatrix}$$

K -total number of scanlines

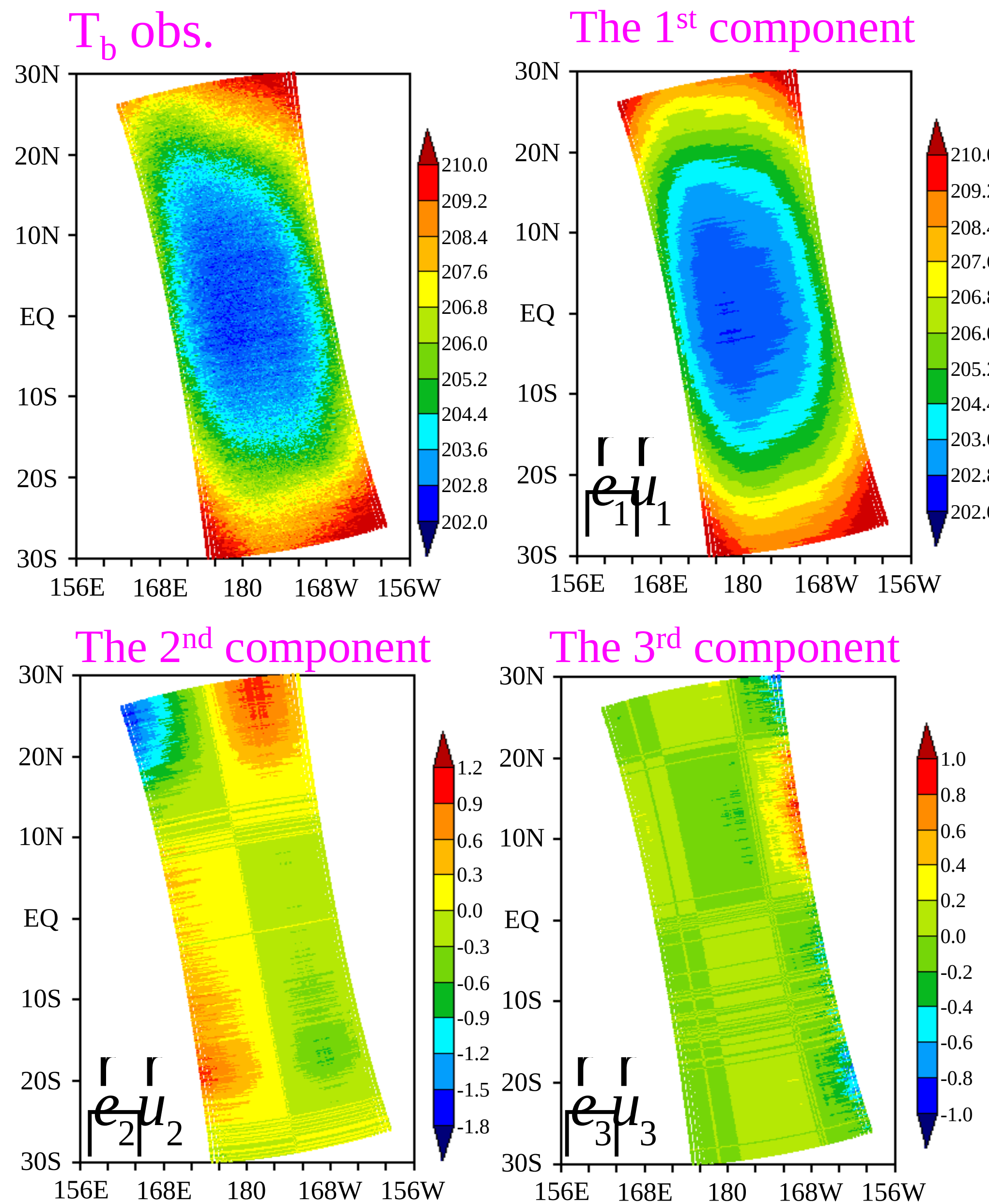

The First Three IMFs of ATMS Ch10 Obs.

The 1st PC Component at Nadir

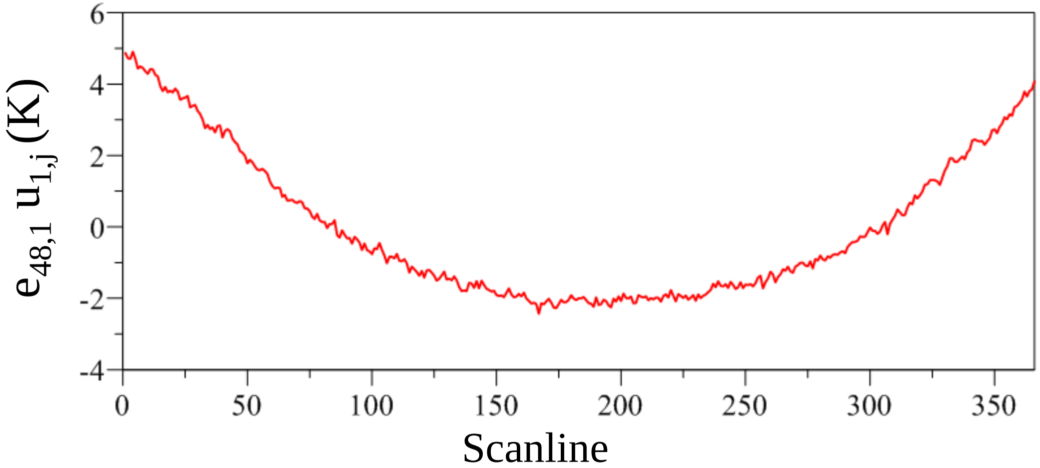

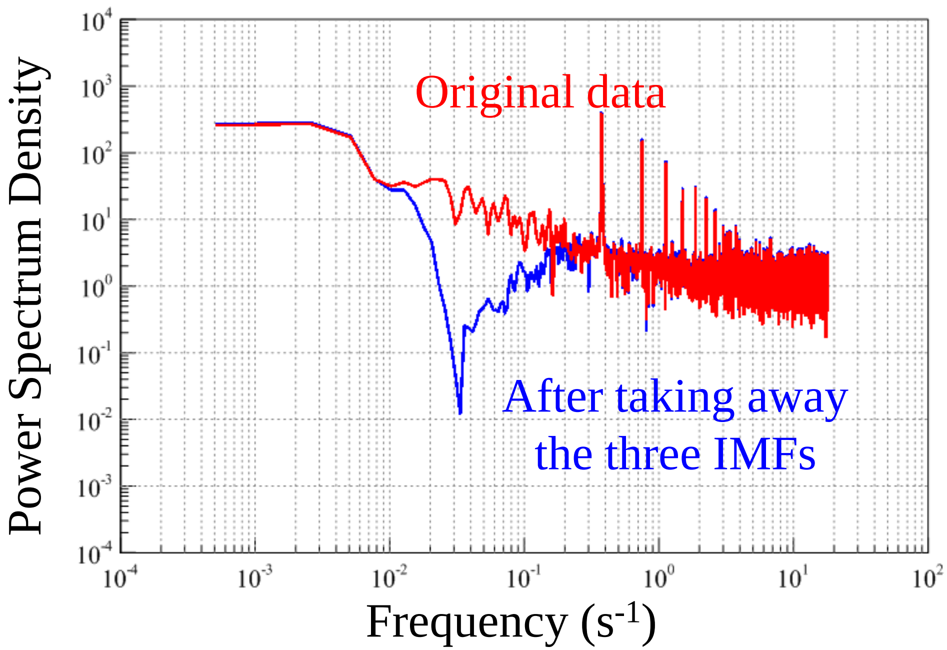

The 1st IMF

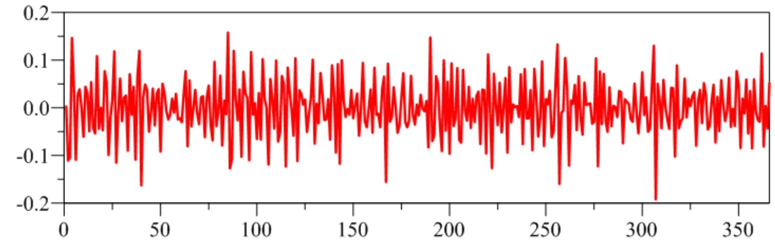

The 2nd IMF

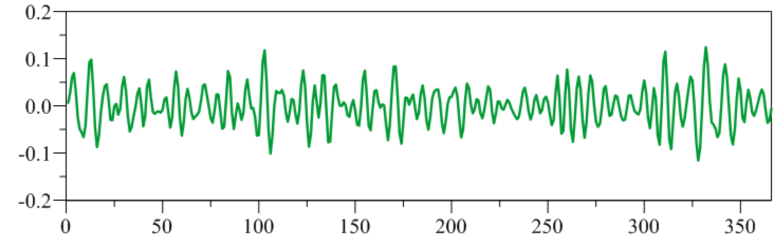

The 3rd IMF

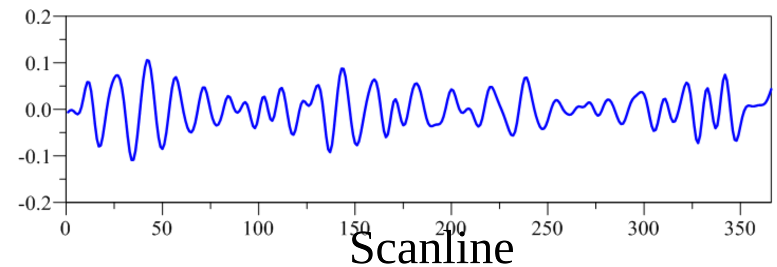

The Optimal Striping Filters: Mathematical Formula

The first PC coefficient

$$\{u_{1,k}\}\ (k = 1, 2, \ldots, K)$$

$$\begin{cases} \min_{\alpha_n} J = \min \sum_{k=1}^{K} \left(\sum_{n=-N}^{N} \alpha_n u_{1,k+n} - \bar{u}_{1,k}^{eemd} \right)^2 \\ \sum_{n=-N}^{N} \alpha_n = 1, \quad \alpha_n = \alpha_{-n} \end{cases}$$

where $\bar{u}_{k,1}^{eemd} = u_{k,1} - \sum_{m=1}^{L} IMF_m(k)$

The filtered first PC coefficient

$$\bar{u}_{1,k} = \sum_{n=-N}^{N} \alpha_n u_{1,k+n}, \quad \alpha_n = \alpha_{-n}$$

$$u_{1,k} = \sum_{m=0}^{K-1} C_m e^{-i\frac{2\pi mk}{K}} \qquad \bar{u}_{1,k} = \sum_{m=0}^{K-1} \bar{C}_m e^{-i\frac{2\pi mk}{K}}$$

$$r_m = \sum_{n=0}^{N} \alpha_n \cos(2\pi f \Delta t)$$

$$\bar{C}_m = r_m C_m, \; f = \frac{m}{K\Delta t}, \Delta t = \frac{8}{3} s$$

$$T_{b,k,i}^{destriping} = e_{1,i} \sum_{n=-N}^{N} \alpha_n u_{1,k+n} + \sum_{j=2}^{96} e_{j,i} u_{j,k}$$

$i = 1, 2, \ldots, 96$ represents scan position

$k = 1, 2, \ldots, K$ represents scan line

Power Spectrum Density of the First Seven IMFs and Residuals of ATMS Brightness Temperatures

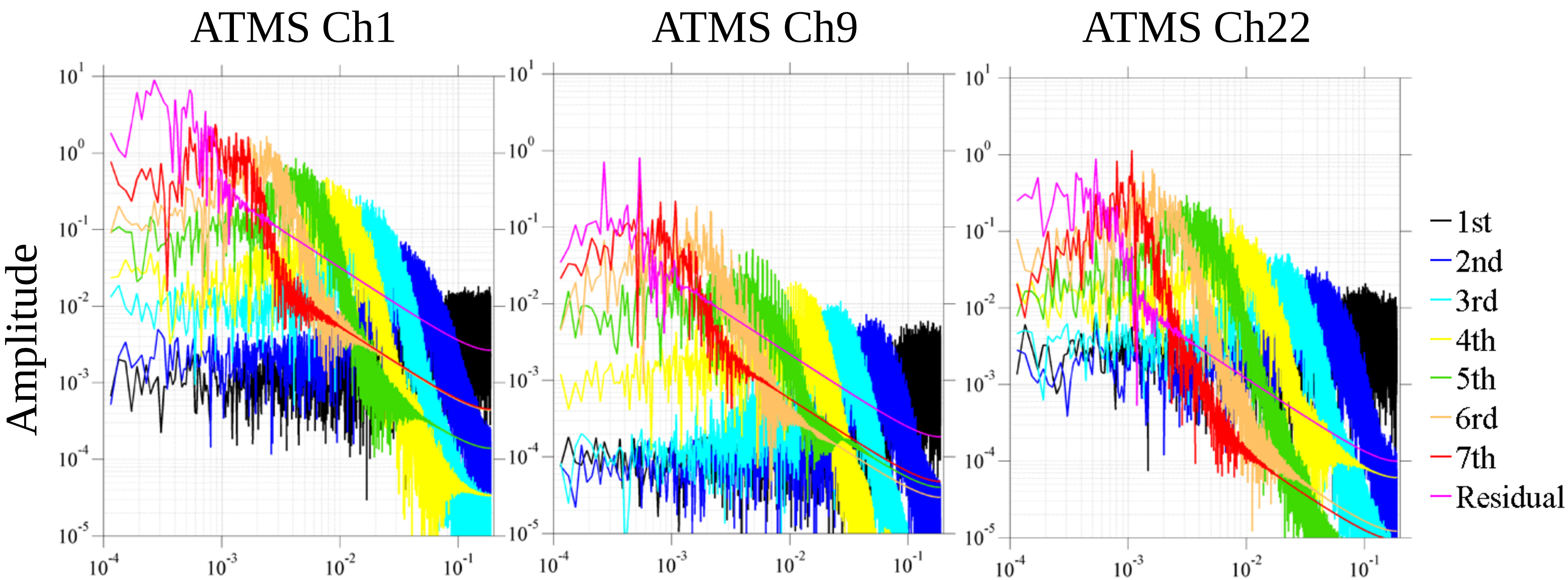

Decision:

The total number of IMFs removed are two for channels 1-2 and three for channels 3-22.

The Optimal Striping Filters: Numerical Results

$$J = \sum_{k=1}^{K}\left(\sum_{n=-N}^{N} \alpha_n u_{1,k+n} - \bar{u}_{1,k}^{eemd}\right)^2$$

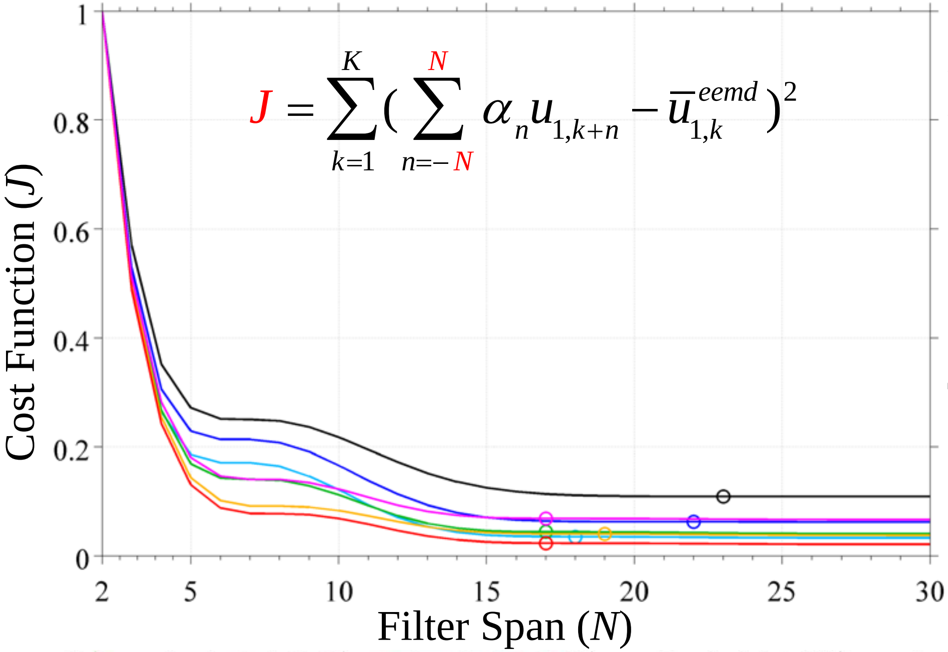

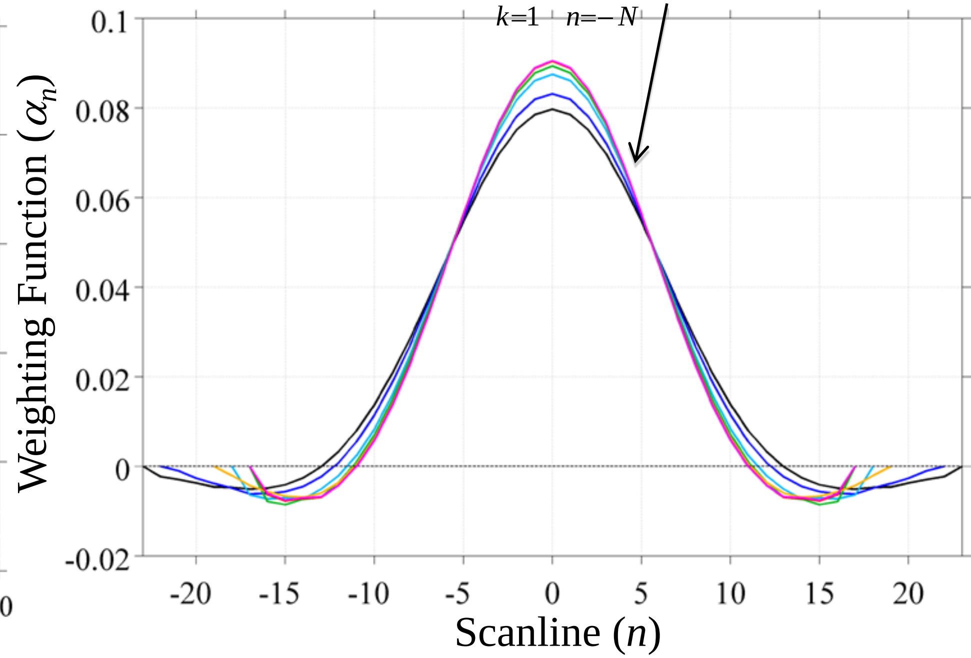

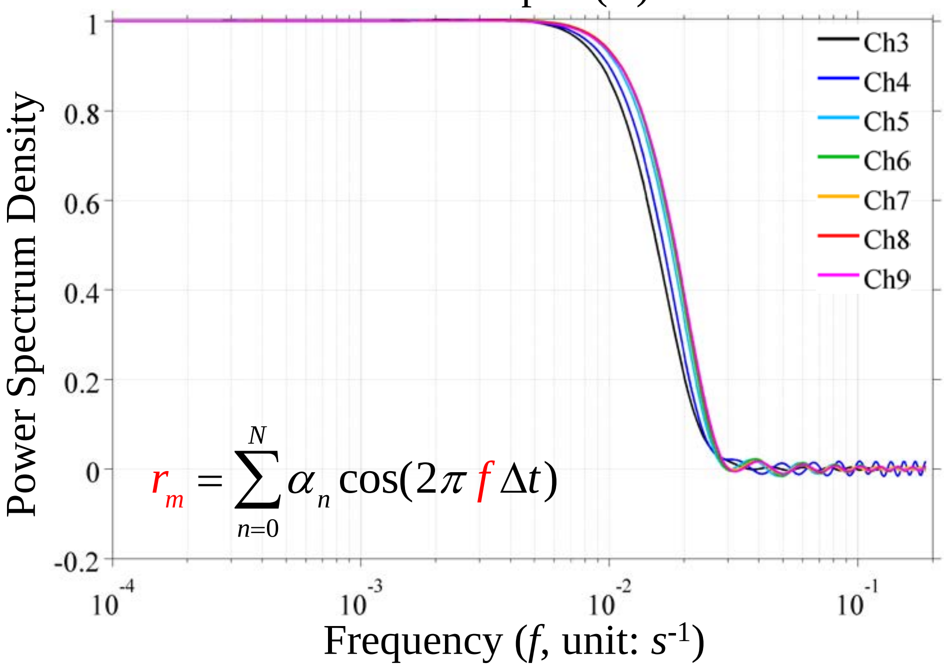

This is a set of optimal filters for ATMS radiances designed to smooth out the striping noise but not to alter lower frequency weather signals.

Variation of Cost Function *J* with Filter Span

$$J = \sum_{k=1}^{K} \left(\sum_{n=-N}^{N} \alpha_n u_{1,k+n} - \bar{u}_{1,k}^{eemd} \right)^2$$

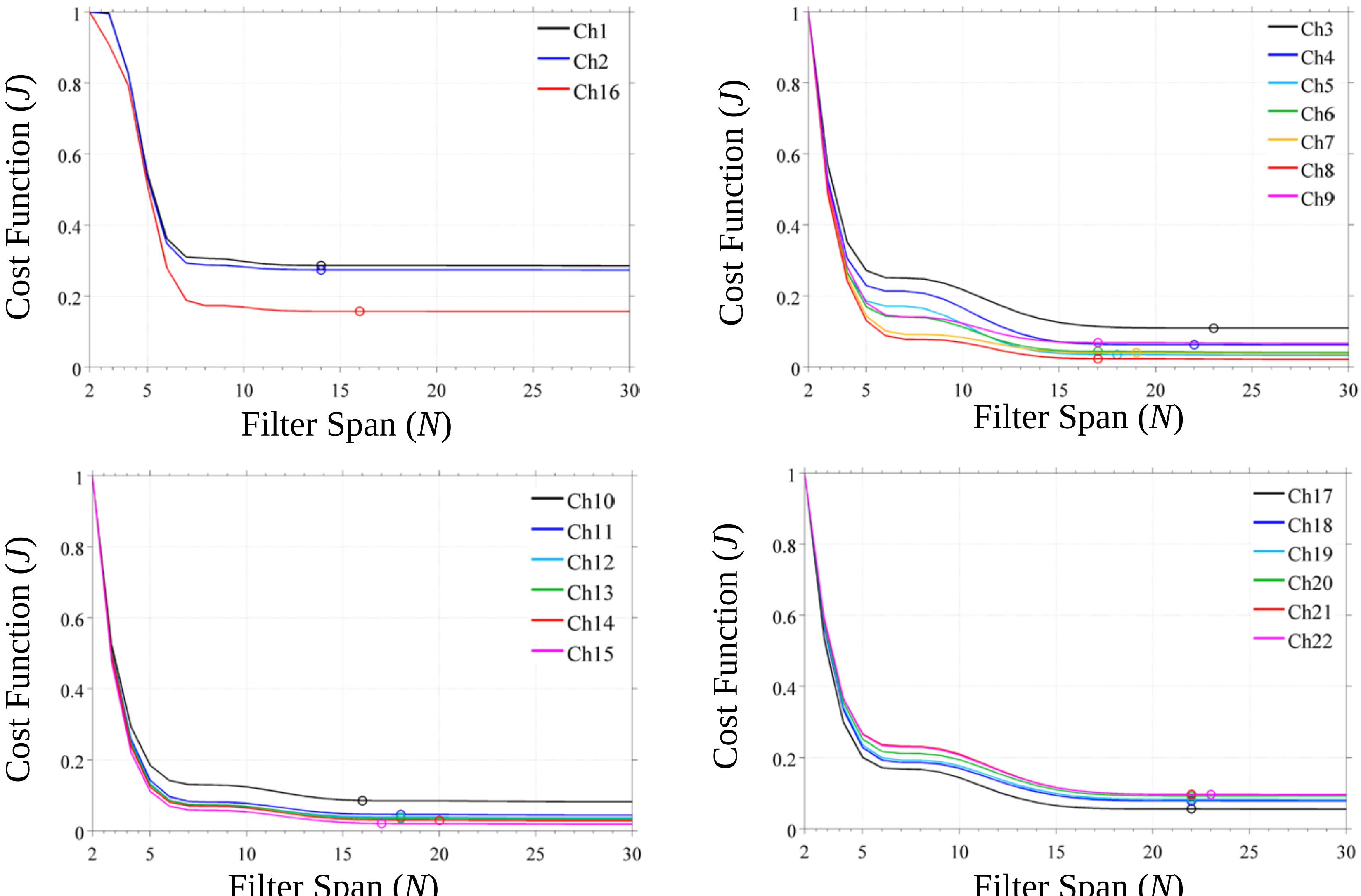

Optimal Weighting Coefficients

$$J = \sum_{k=1}^{K} \left(\sum_{n=-N}^{N} \alpha_n u_{1,k+n} - \bar{u}_{1,k}^{eemd} \right)^2$$

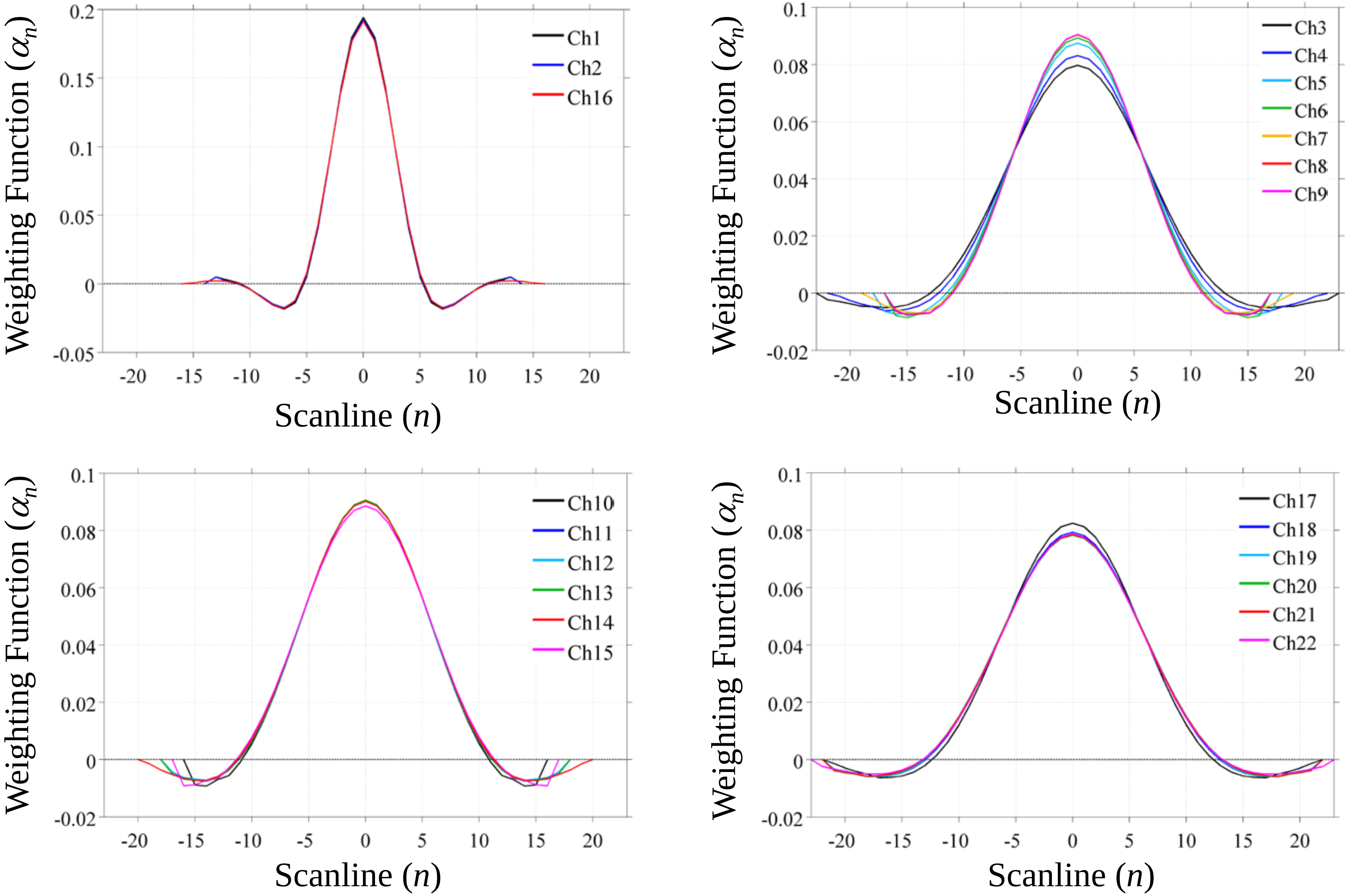

Response Functions of the Optimal Striping Filters

$$r_m = \sum_{n=0}^{N} \alpha_n \cos(2\pi f \Delta t)$$

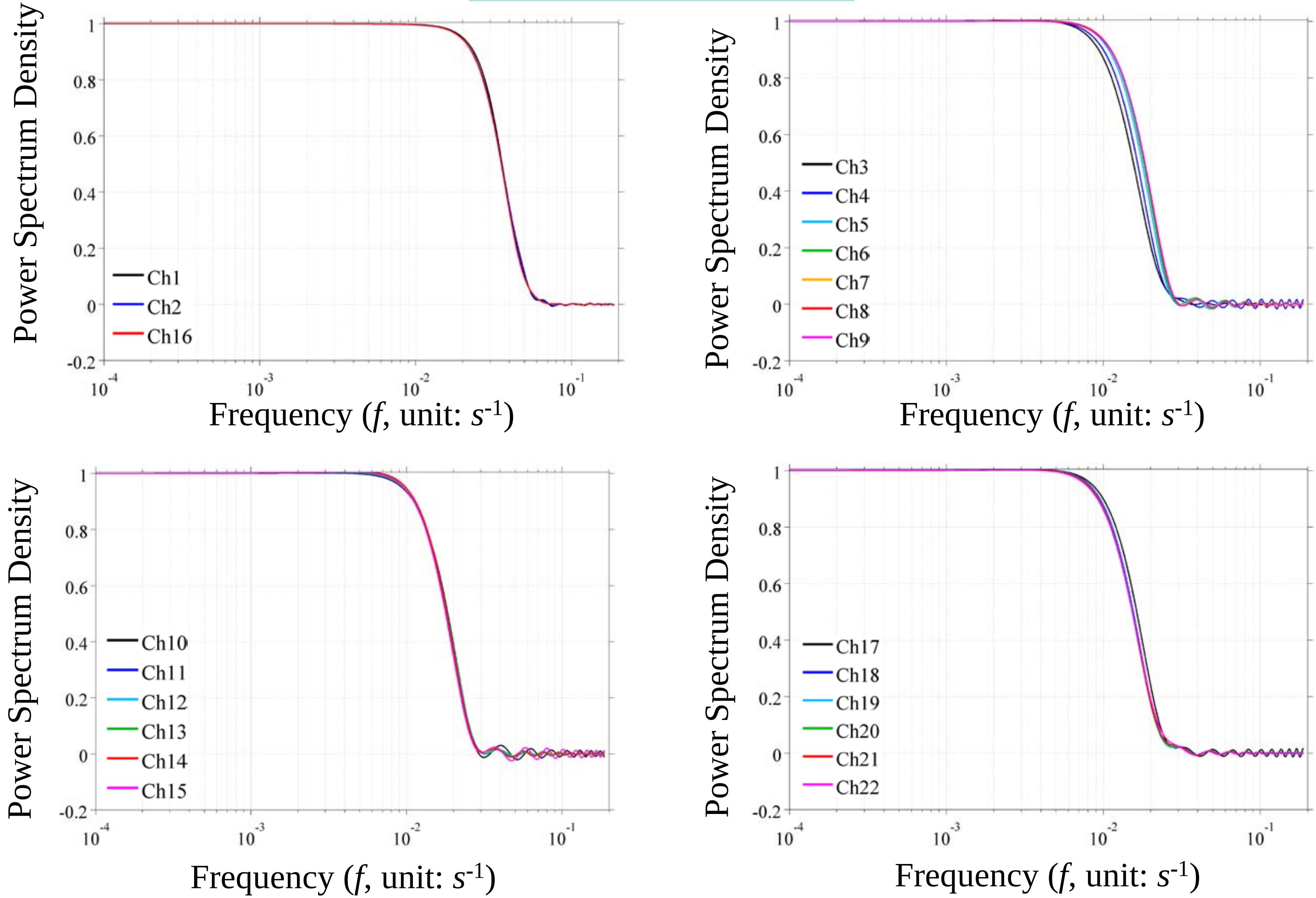

Striping noise Spectrum removed by the optimal striping filters

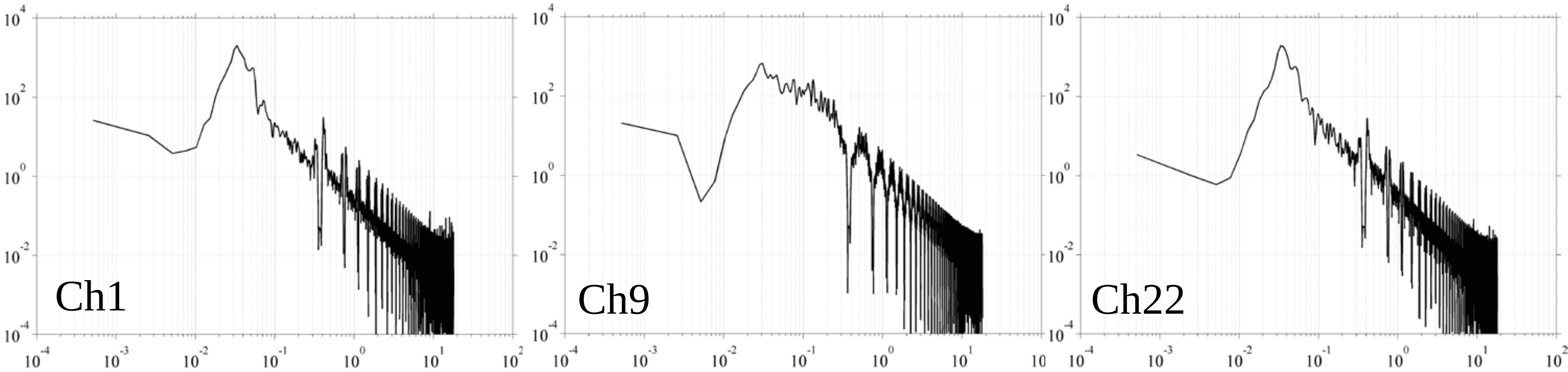

Global O-B Spectrum with and without Applying the Optimal Striping Filter

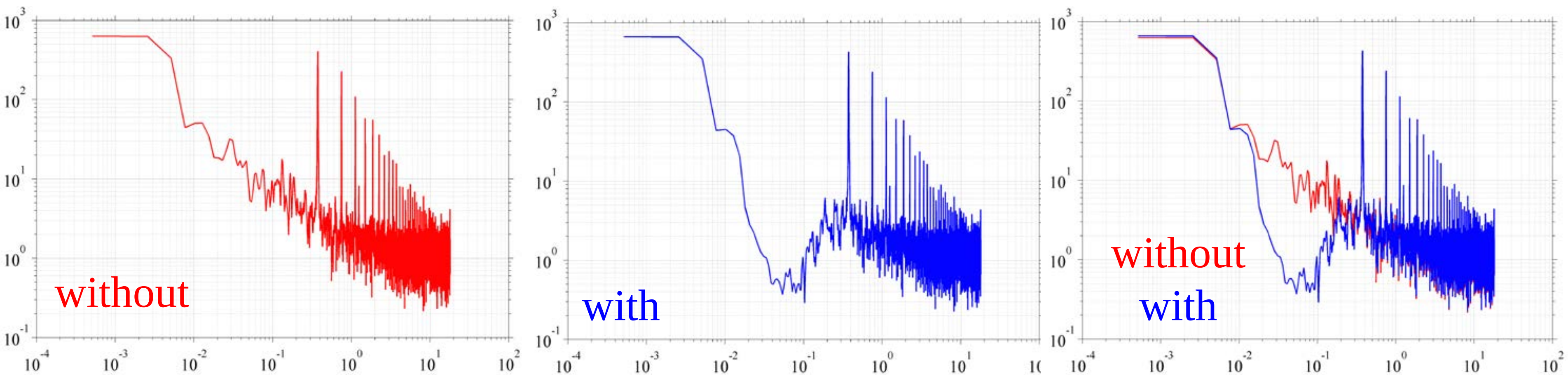

Global O-B Distributions of ATMS Channel 8

Before

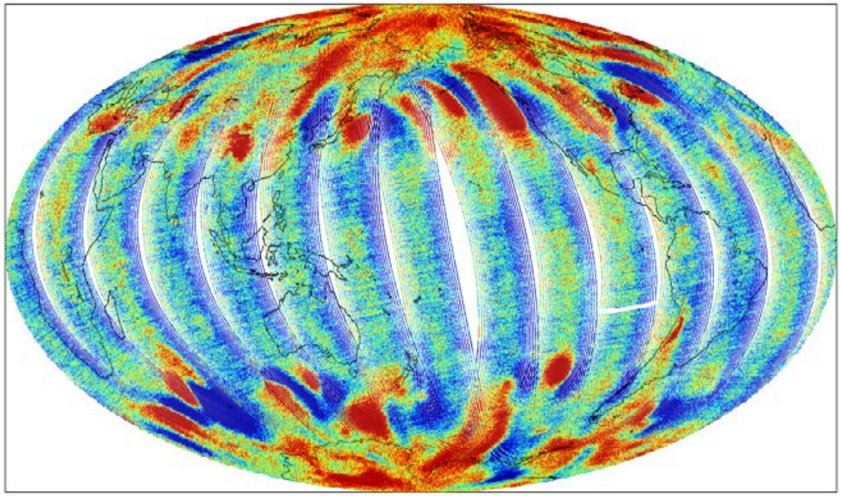

After

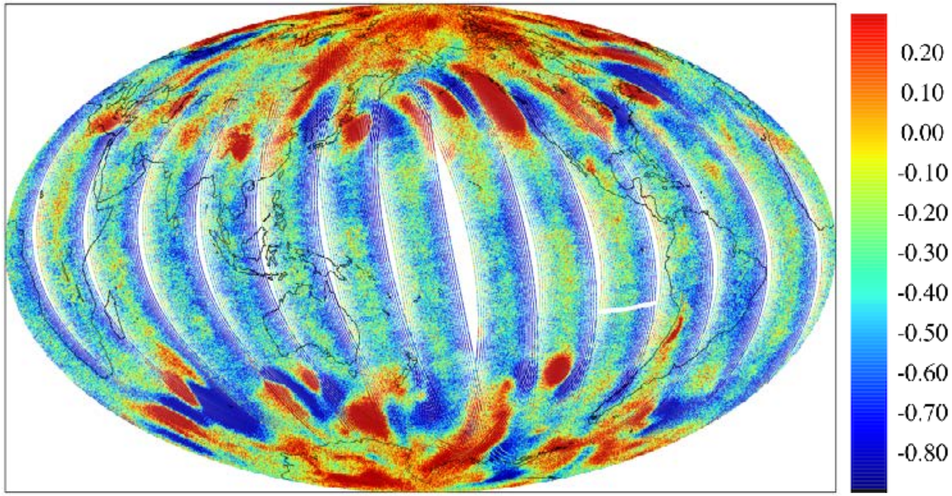

Before minus After

Striping noise

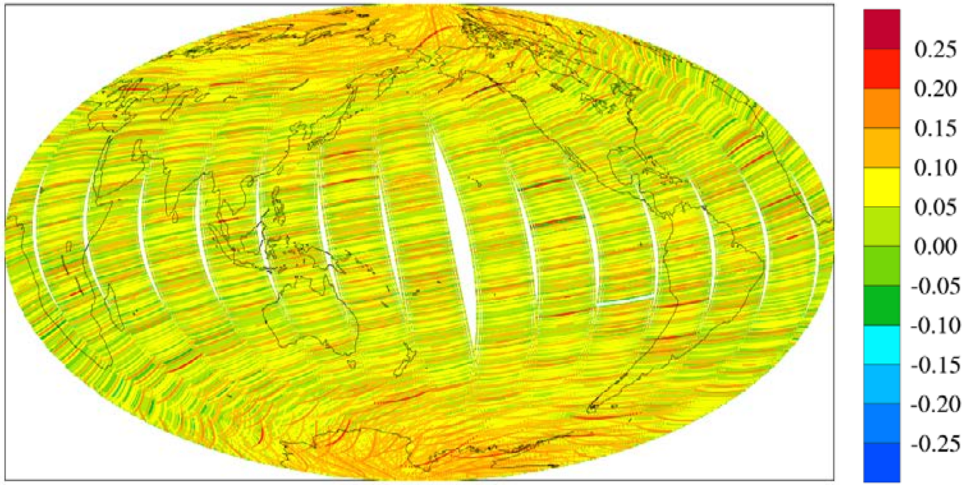

Pitch-Over Maneuver Data with and without Optimal Filtering

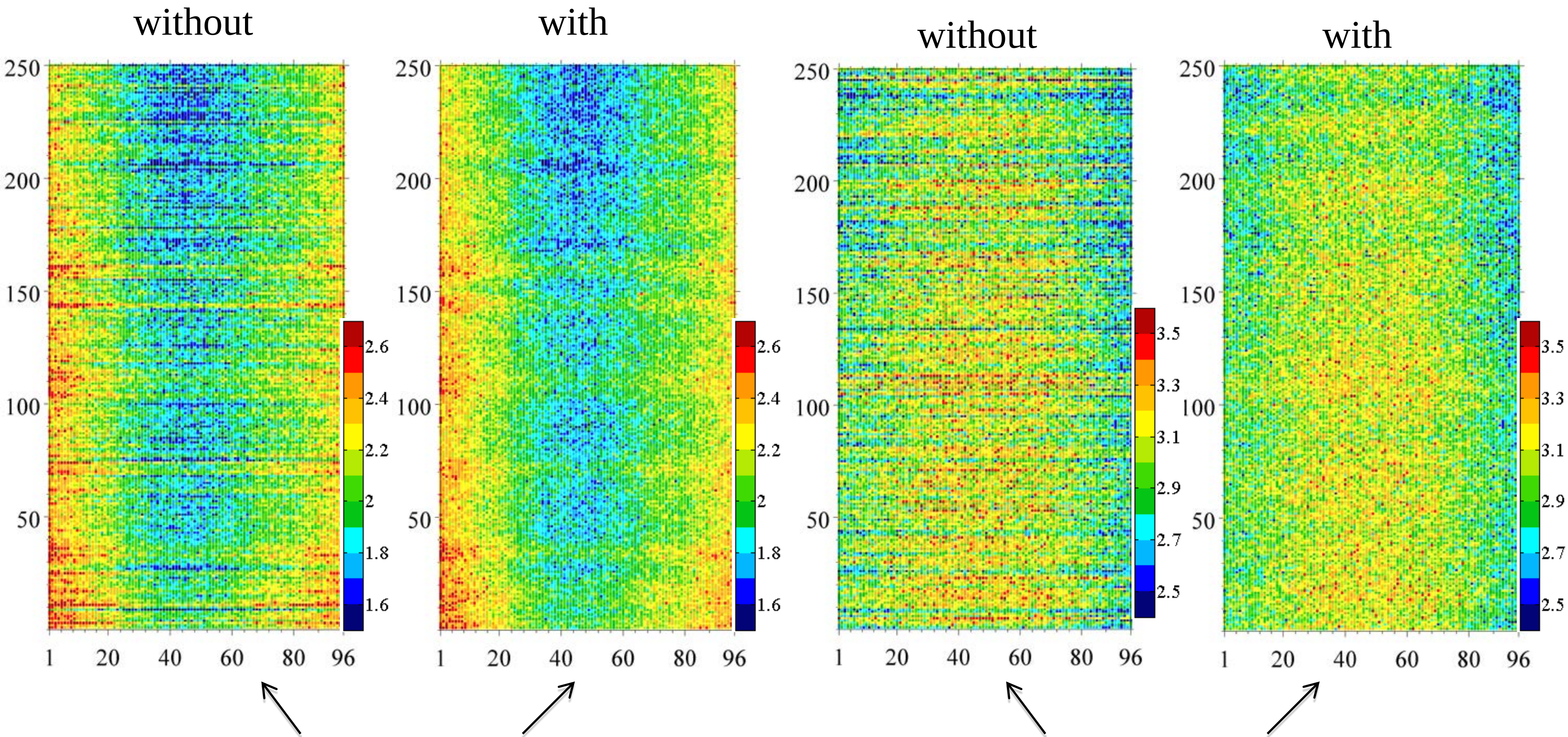

ATMS Channel 1

ATMS Channel 9

Striping Index (SI)

$$SI = \frac{V_{along}}{V_{cross}}$$

Along-track variance

$$V_{along} = \frac{1}{N}\sum_{j=1}^{N}\left(\frac{1}{M}\sum_{k=1}^{M}\left(T_b(k,j) - \frac{1}{M}\sum_{k=1}^{M}T_b(k,j)\right)^2\right)$$

Cross-track variance

$$V_{cross} = \frac{1}{M}\sum_{k=1}^{M}\left(\frac{1}{N}\sum_{j=1}^{N}\left(T_b(k,j) - \frac{1}{N}\sum_{j=1}^{N}T_b(k,j)\right)^2\right)$$

Striping Index (SI) of Pitch-Over Maneuver Data

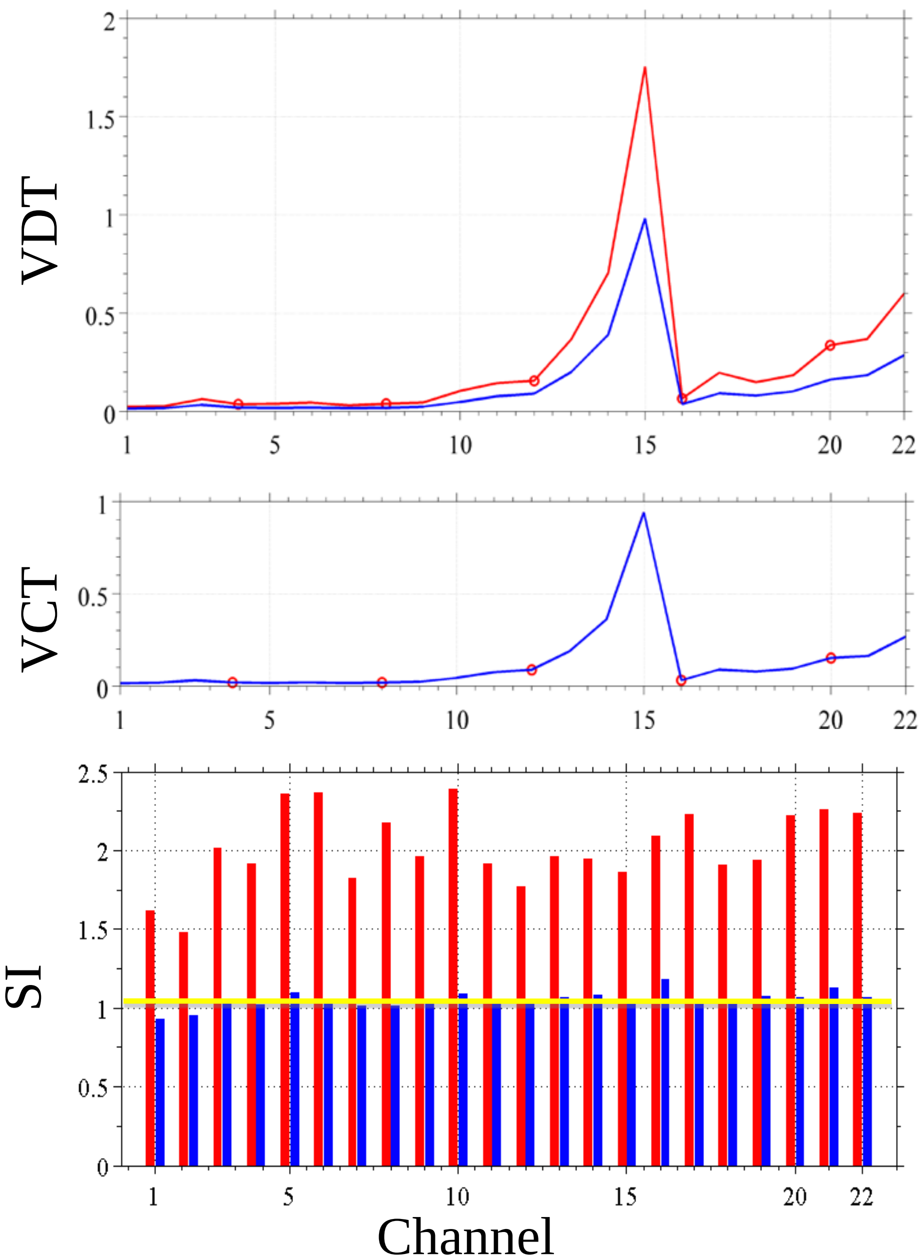

Variance of down-track (VDT), variance of cross-track (VCT), and striping index (SI) before (red) and after (blue) applying the optimal striping filter.

SI is significantly reduced to one for ATMS all channels.

Summary

- Twenty two optimal striping filters are developed for 22 ATMS channels

- Two months of de-striping ATMS data are being produced for NWP impact test

Future Plan

Similar optimal striping filters will be developed for calibration counts, and impact of striping noise on NEDT will be quantified.

Towards Establishing A Benchmark Instrument for Microwave Sounders

Lin Lin[1, 2], Fuzhong Weng[3] and Xiaolei Zou[4]

[1] Joint Center for Satellite Data Assimilation, College Park, Maryland, USA
[2] I. M. Systems Group, Inc., Rockville, Maryland, USA
[3] National Environmental Satellite, Data, & Information Service, National Oceanic and Atmospheric Administration, Washington, D. C., USA
[4] Department of Earth, Ocean and Atmospheric Sciences, Florida State University, USA

Outline

1. Introduction
2. A Brief Description of GPS RO Data
3. GPS RO Derived Scan Bias and Bias Correction
4. MonoRTM Simulations Using Measured and Boxcar SRF
5. Long Term Monitoring of ATMS Bias Characterization Using Collocated COSMIC RO Data
6. Summary

Introduction

- For both NWP and climate applications, it is important to know the satellite instrument's on-orbit accuracy. However, lack of on-orbit truth measurement makes it challenging.
- The Global Positioning System (GPS) Radio Occultation (RO) data have high accuracy and precision on atmospheric temperature, and also have high vertical resolution under all weather conditions.
- Current radiative transfer (RT) models are accurate for ATMS temperature sounding channels since the O_2 absorption coefficient for frequency between 50-70 GHz is accurately derived in lab.
- This research presents a method of using the GPS RO data and atmospheric RT models, such as the U.S. Joint Center of Satellite Data Assimilation (JCSDA) Community Radiative Transfer Model (CRTM) and the line-by-line RT model, to assess ATMS on-orbit accuracy.

A Brief Description of GPS RO

1. High vertical resolution
2. No contamination from clouds
3. No system calibration required
4. High accuracy and precision:
    a. The global mean differences between COSMIC and high-quality reanalyses is ~0.65K between 8 and 30km (Kishore et al. 2008)
    b. The precision of COSMIC GPS RO soundings is ~0.05K in the upper troposphere and lower stratosphere (Anthes et al. 2008)

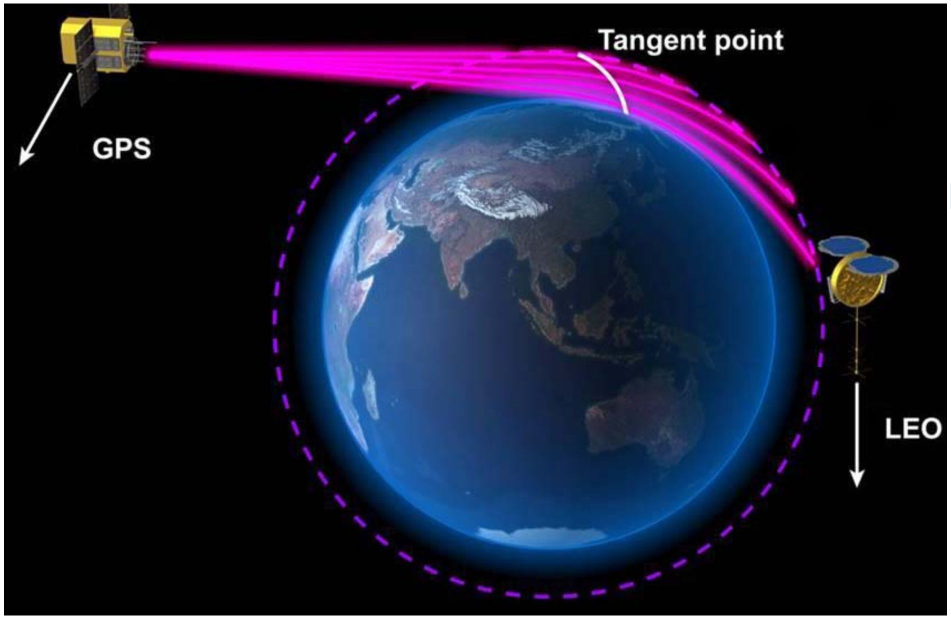

Collocation of GPS and ATMS

Temporal difference ≤ ±3 hrs

Spatial distance ≤ 50 km

Use COSMIC geolocation at the altitude of maximum WF for spatial collocation

Channel- and FOV- Dependent

ATMS Weighting Function (U.S. Standard Atmosphere)

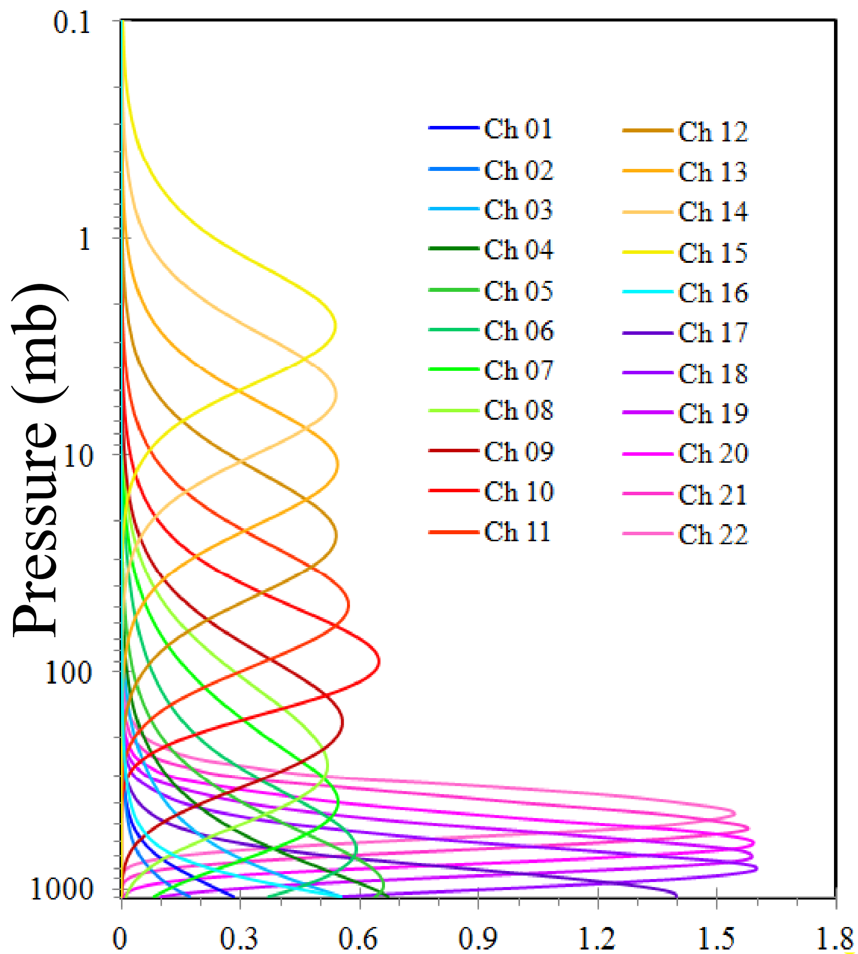

ATMS Weighting Function (U.S. Standard Atmosphere)

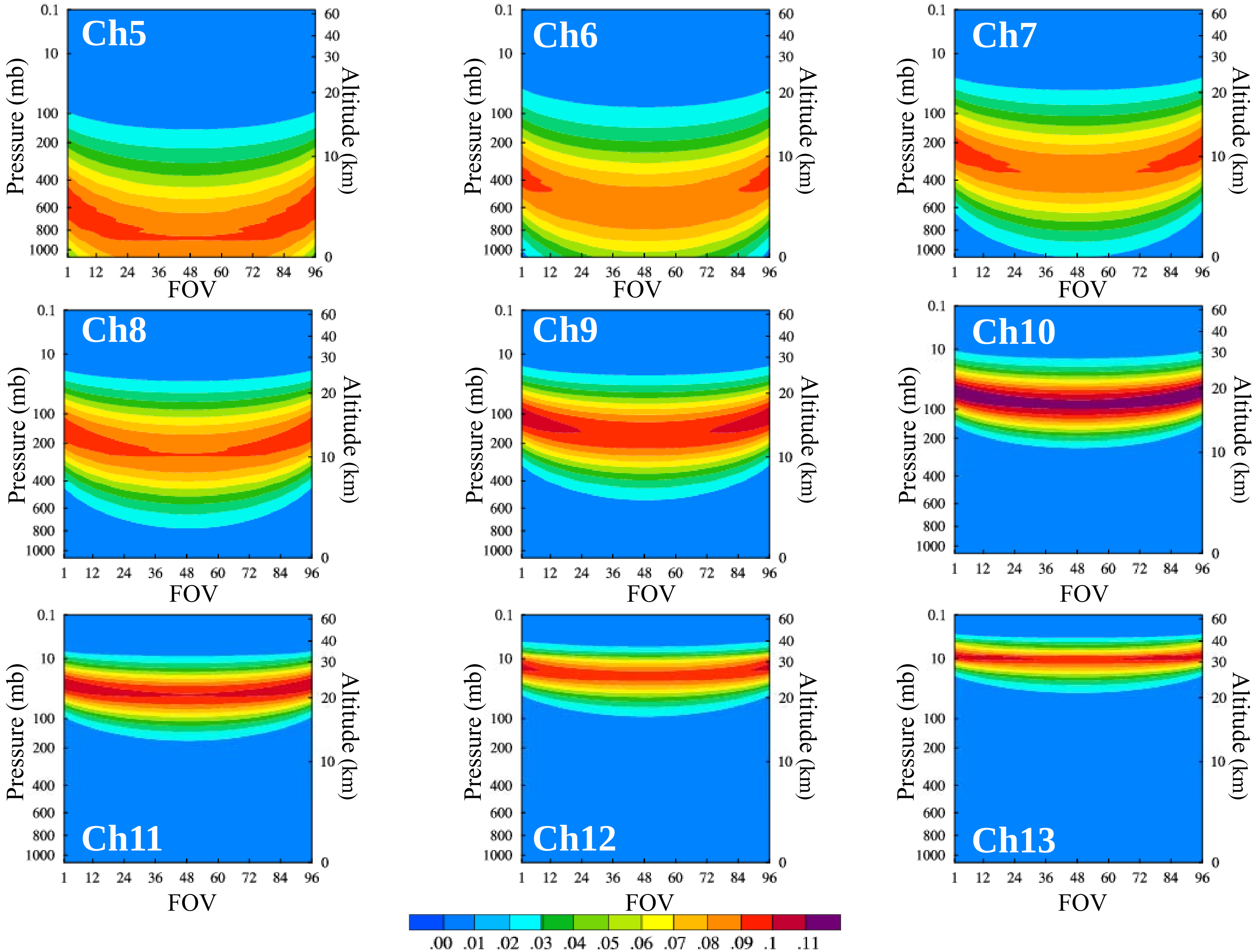

Distribution of Matchups

Clear-sky, over ocean, 60°S ~ 60°N, Dec. 10, 2011 ~ Jun. 30, 2012

Channel 6:
16,701 in total

Similar patterns for other channels 5, 7-13.

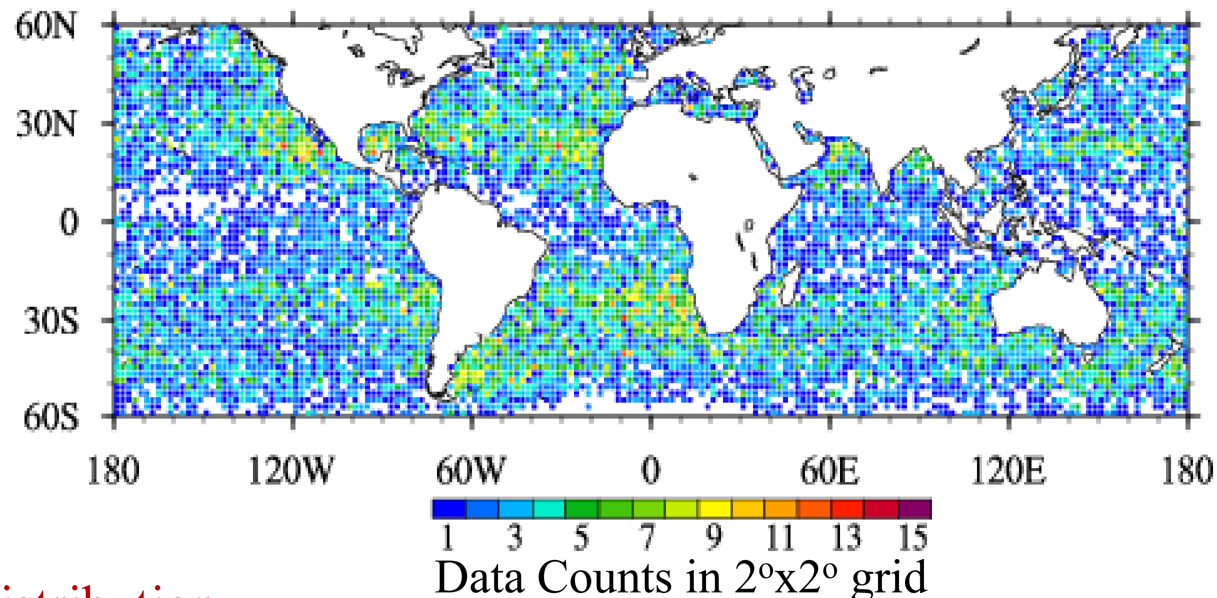

Latitudinal Distribution

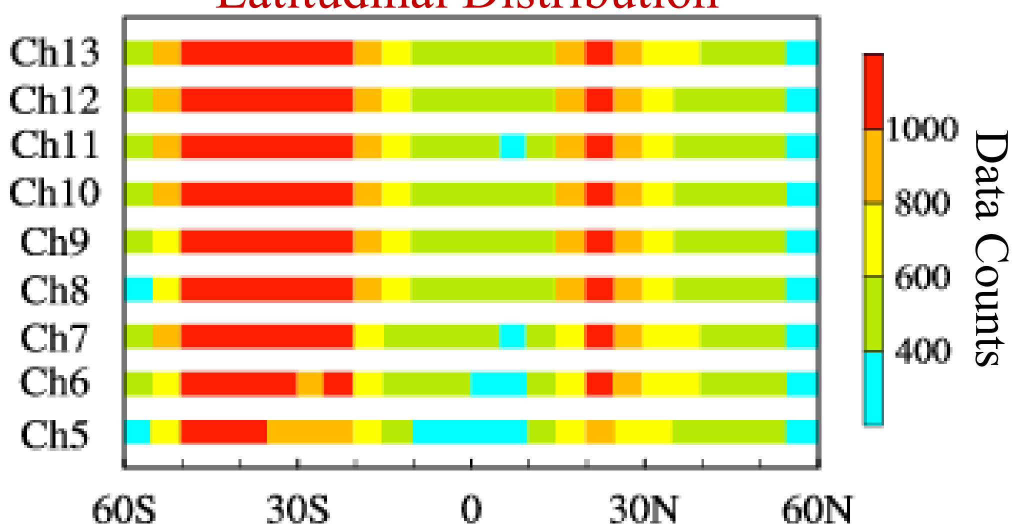

Most collocated data are located in subtropical in Northern Hemisphere and middle latitudes in Southern Hemisphere.

ATMS Observation and GPS Simulation

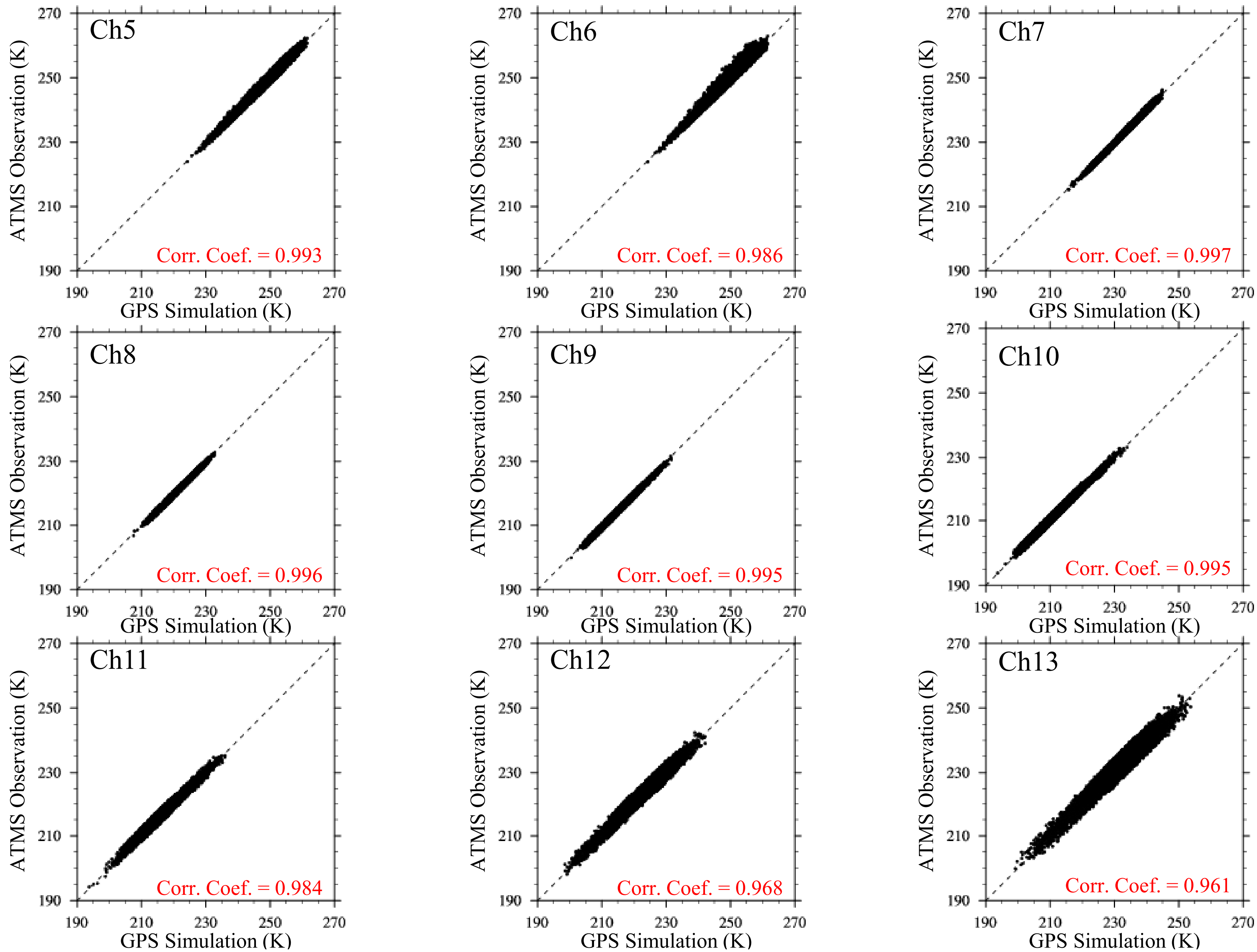

GPS RO Derived Scan Bias

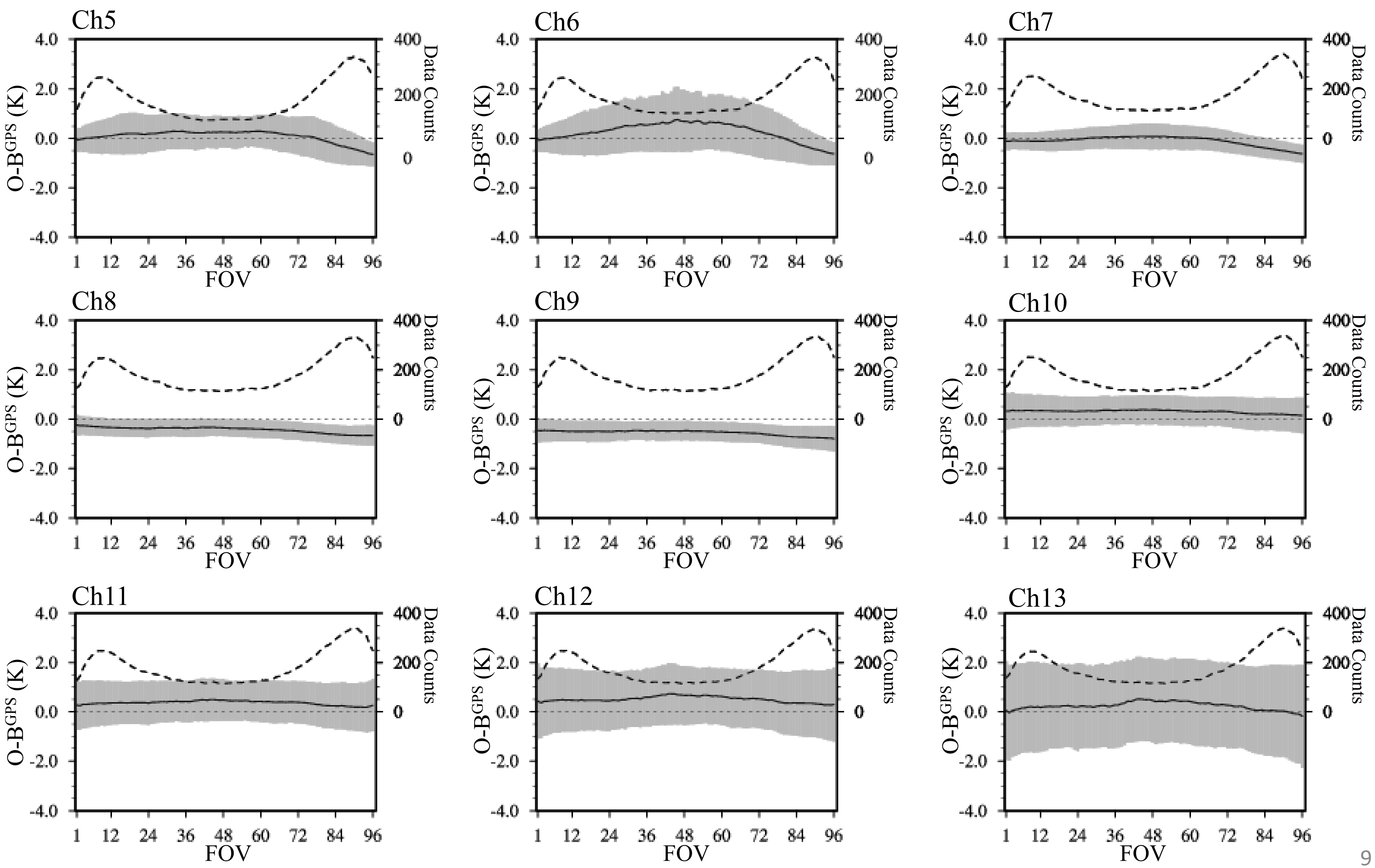

Bias Before/After Scan Bias Correction

Before:

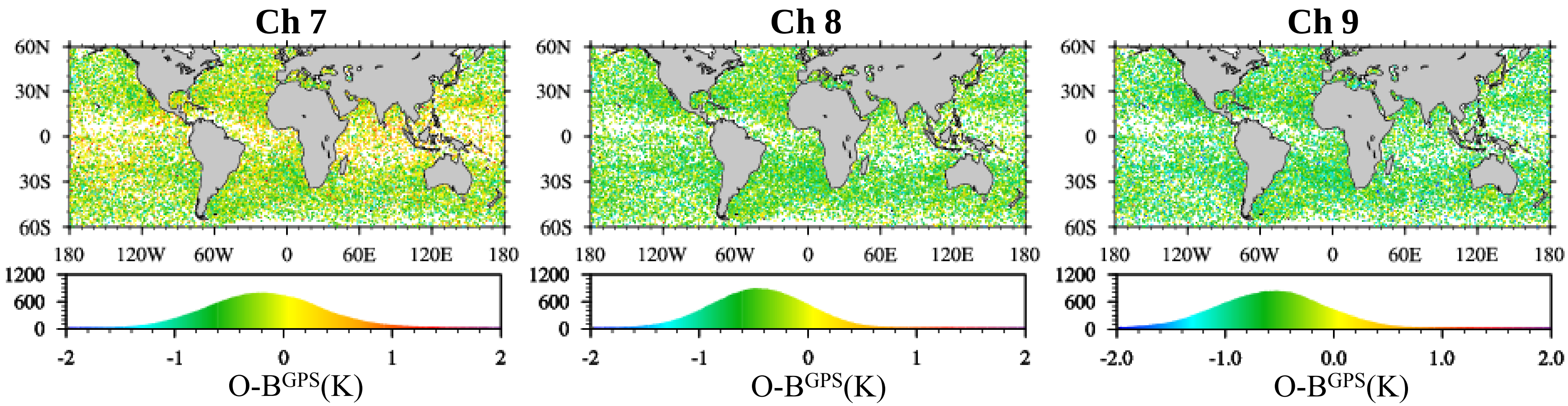

After:

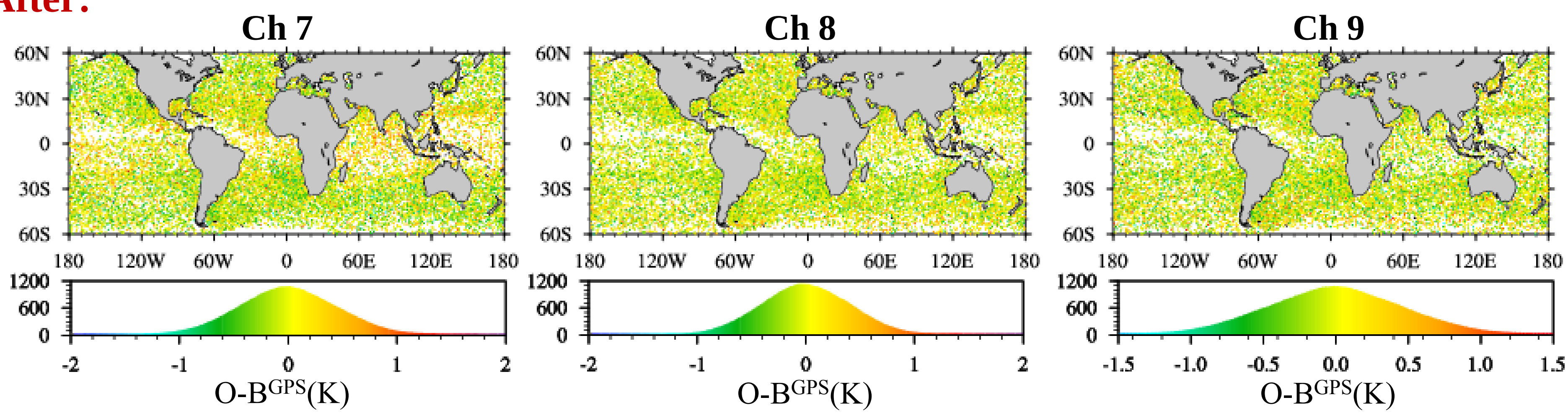

Bias Before/After Scan Bias Correction (Cntd')

Before:

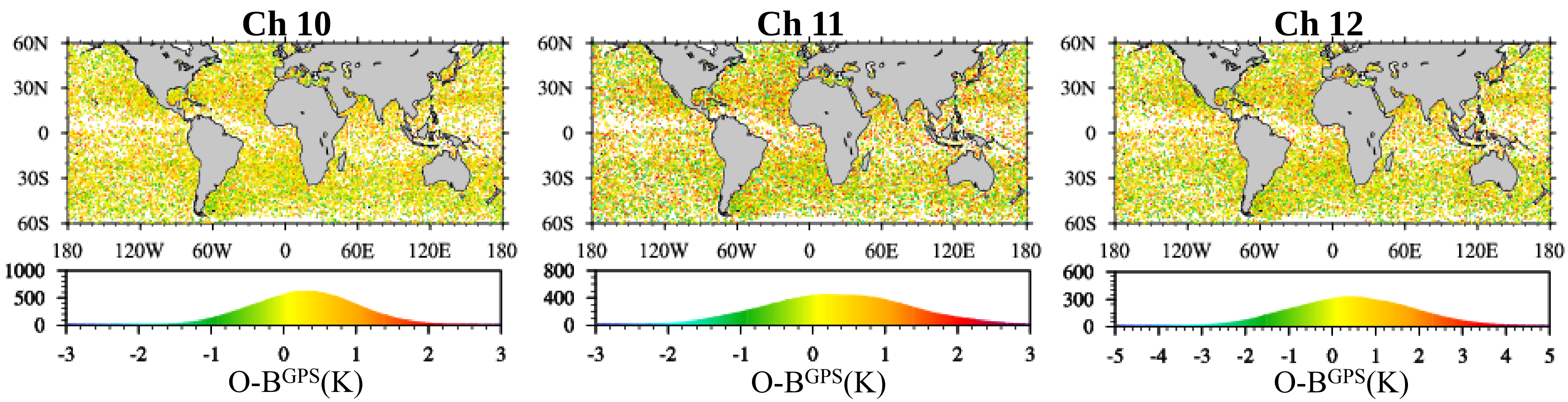

After:

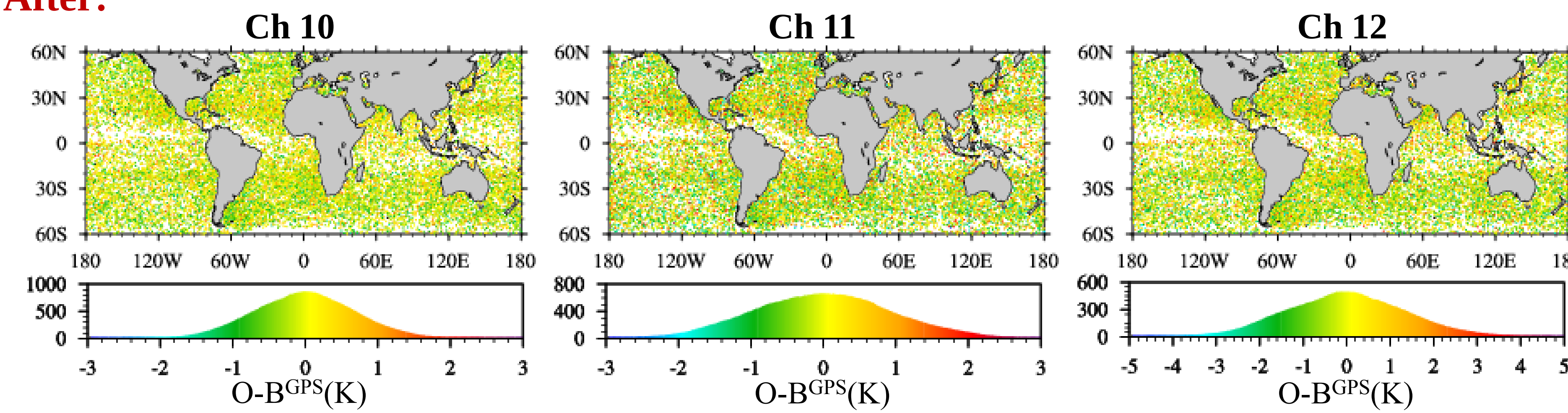

PDF of Bias Before/After Scan Bias Correction

Before:

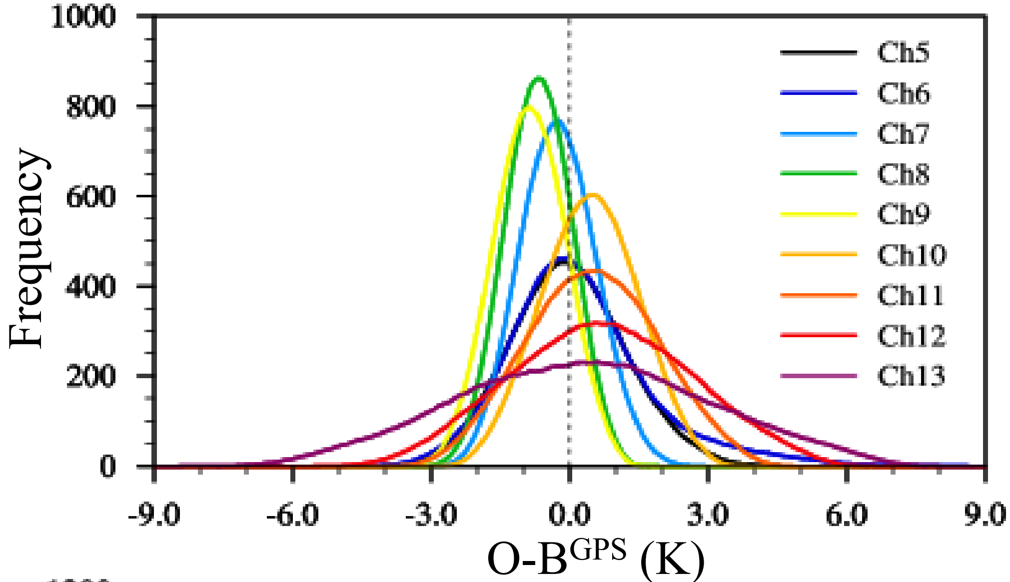

Different channels have different biases (i.e., in PDF).

After:

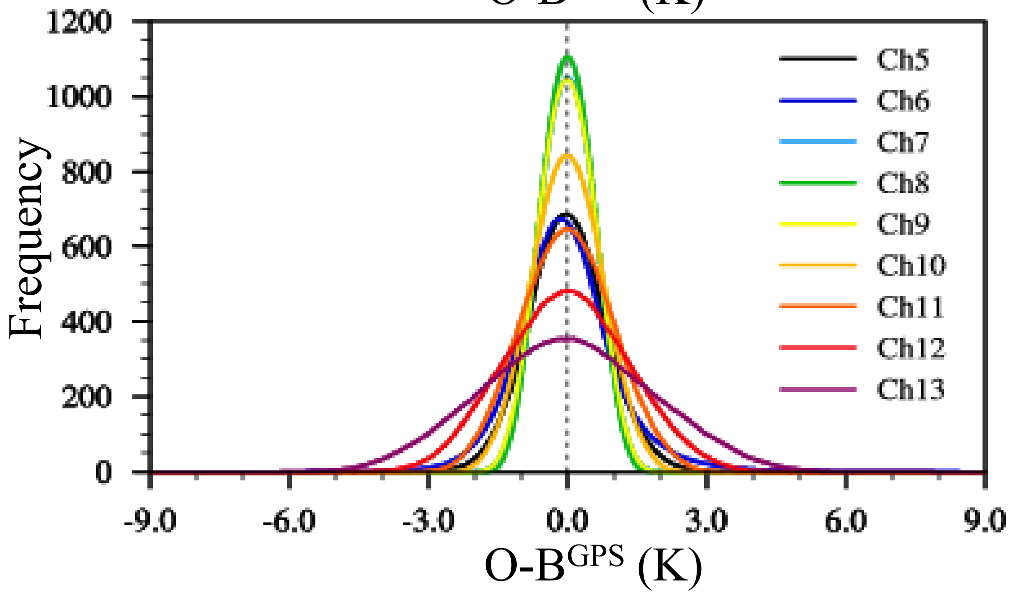

After calibrated using GPS RO data, biases of all channels are very close to normal distribution.

More, magnitudes of these calibrated biases are about an order smaller than the original TDR data.

MonoRTM

- A line-by-line (LBL) radiative transfer calculation
- Accurate atmospheric spectroscopy data base
- Only gaseous absorption
- Vertical stratification

For microwave sounding channels at 50-60 GHz, the O_2 absorption band can be best simulated under a cloud-free atmosphere using the LBL calculation.

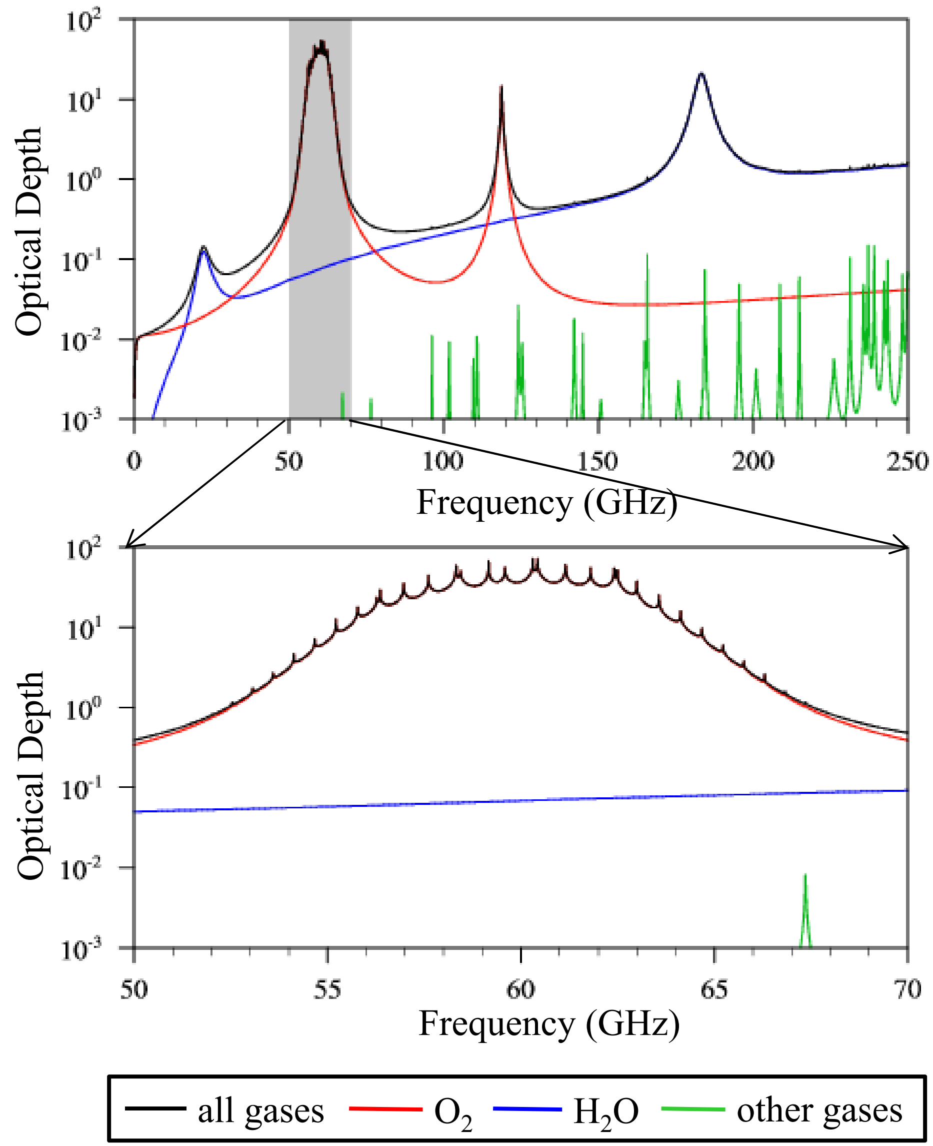

Total Number of Absorption Lines Used in ATMS SRFs Before/After -20dB Truncation

ATMS Channel Number	Number of Line		Frequency Resolution (mHz)
	Original	**-20dB**	
5	1001	664	0.600
6	2002	1188	0.300
7	1001	708	0.600
8	1001	705	0.600
9	1001	690	0.500
10	2002	1788	0.185
11	2002	1422	0.125
12	2002	982	0.165
13	2002	1004	0.075

- To save computational time, the SRF is truncated at -20dB to keep the 99% of the maximum SRF for each band of each channel.
- Compared to 256 lines for Boxcar SRF, the number of lines for truncated measured SRF is at least tripled for each channel.

SRFs after the -20dB Truncation for CP at 20^{o}C

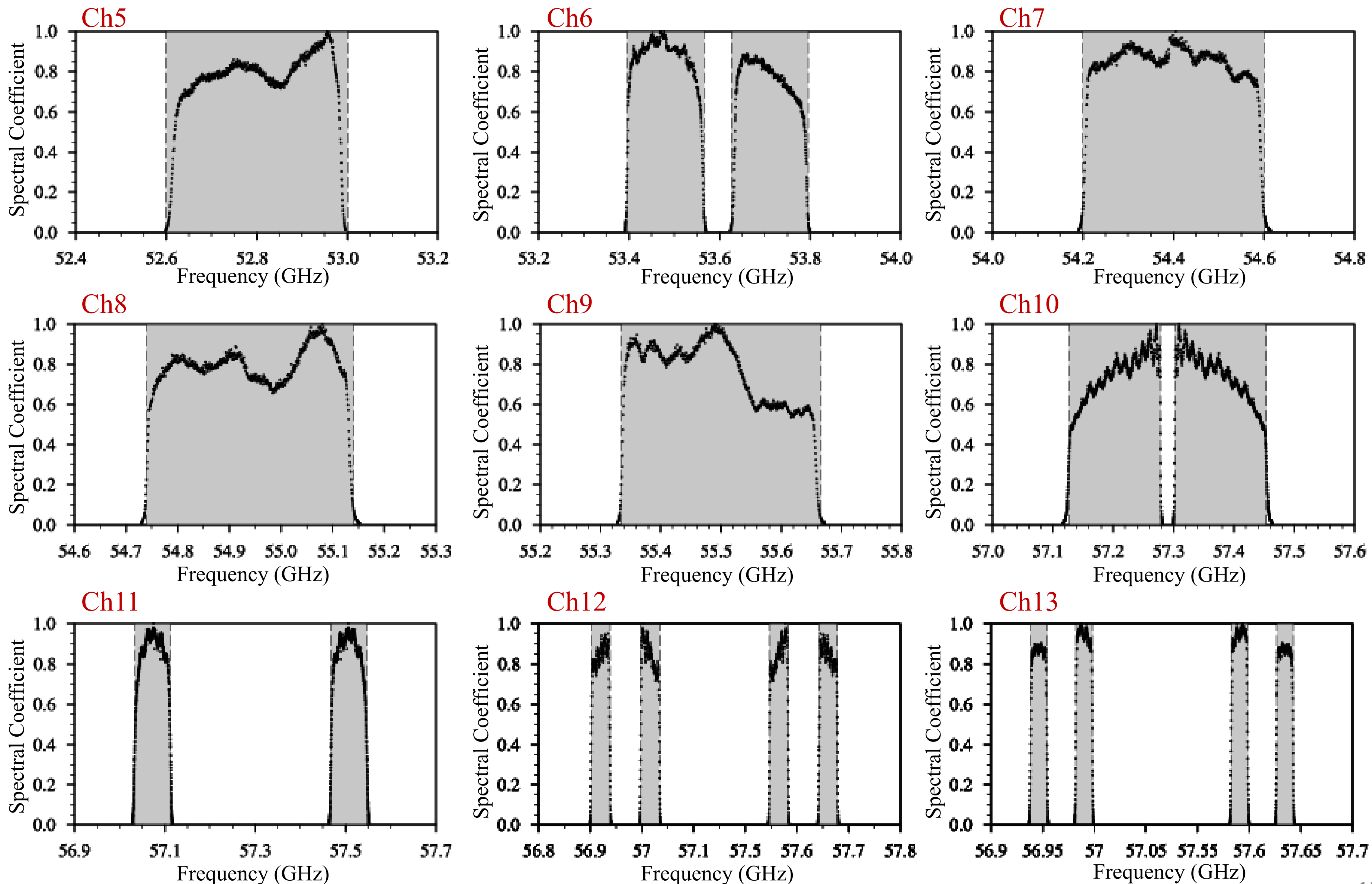

MonoRTM Simulation (M^{SRF}-M^{BoxCar})

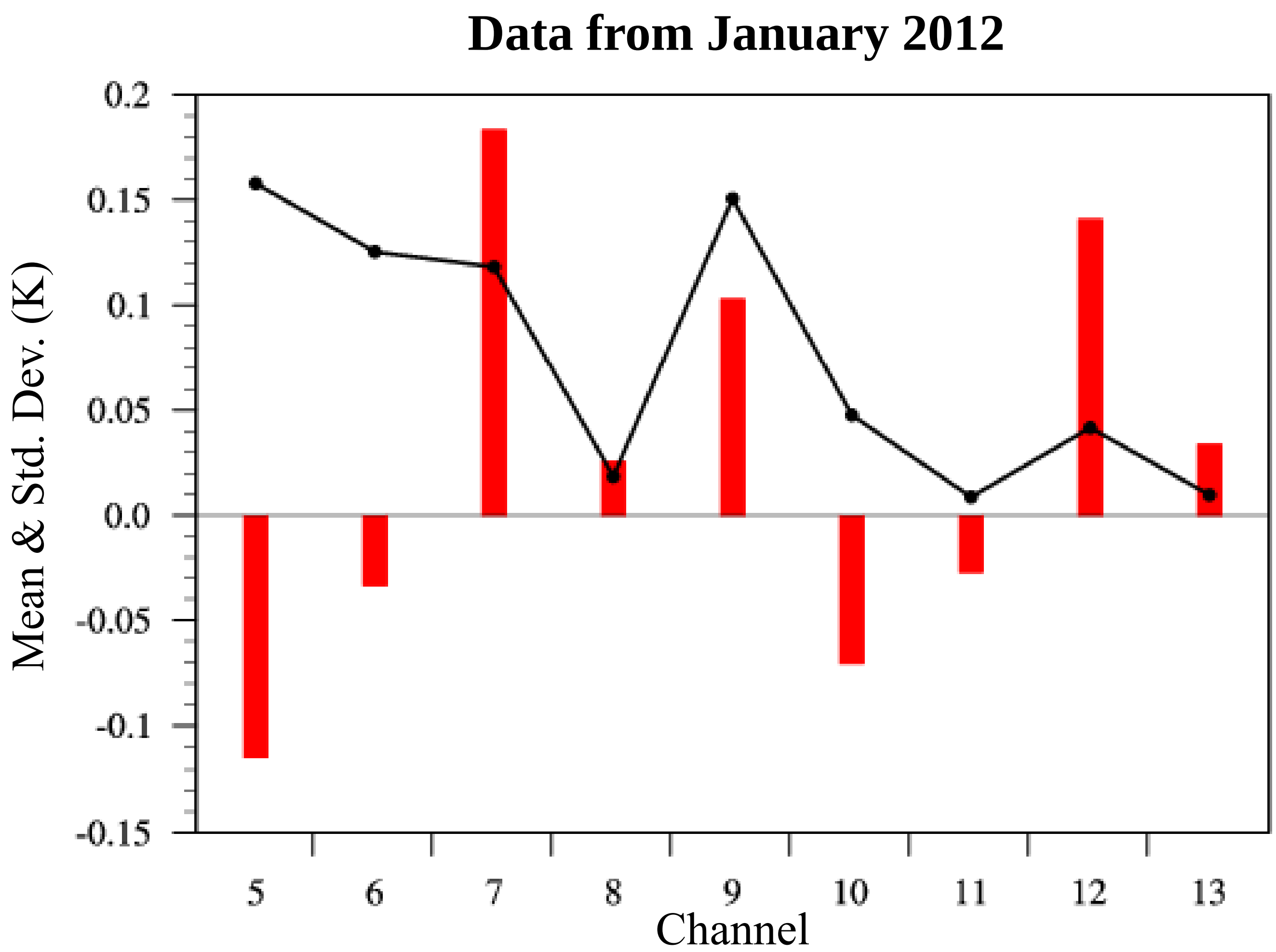

The mean difference is within ± 0.2K.

The Std. Dev. is within 0.2K.

Long Term Monitoring of ATMS Bias Characterization Using Collocated COSMIC RO Data

Clear-sky, over ocean, 60°S ~ 60°N, Dec. 10, 2011 ~ Dec. 31, 2013

Ch 6

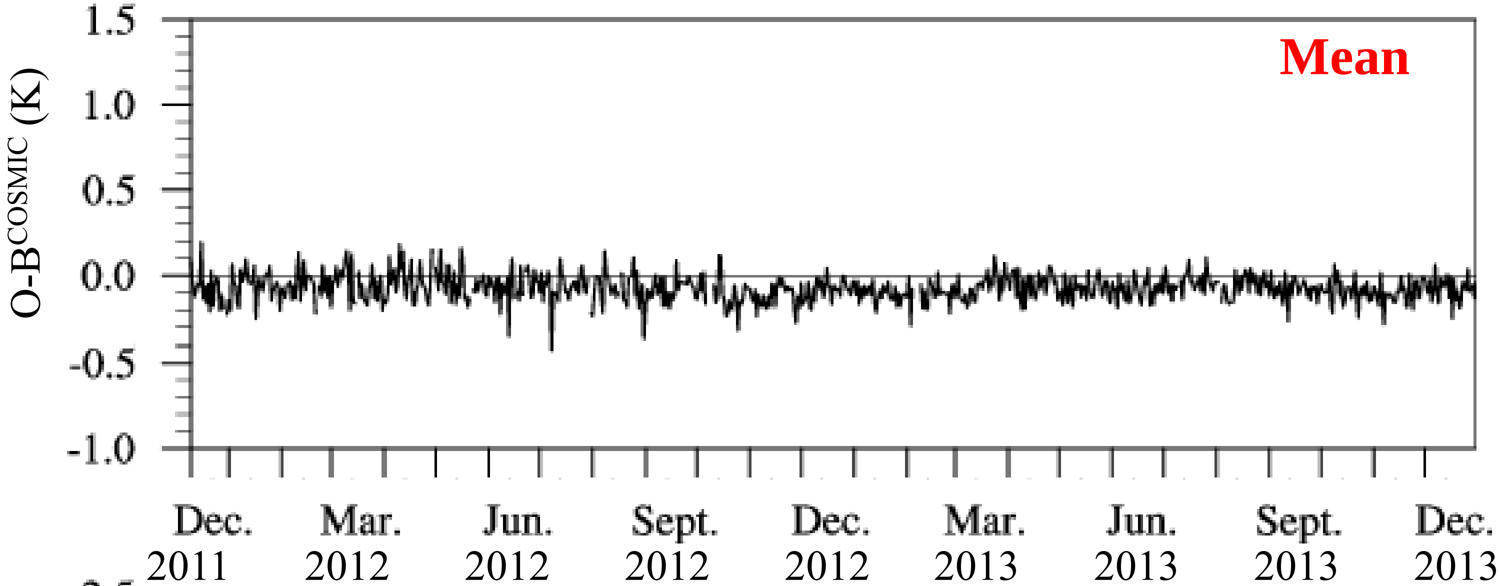

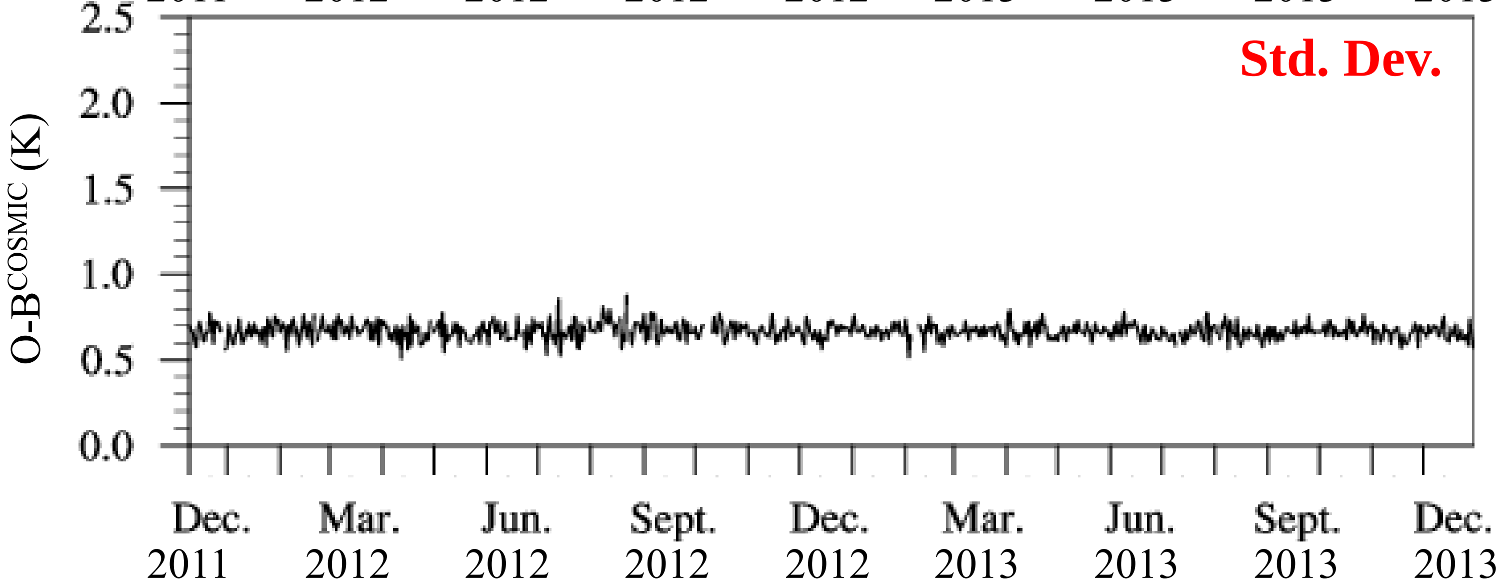

Daily Mean and Std. Dev. of O-B^{COSMIC}

Clear-sky, over ocean, 60°S ~ 60°N, Dec. 10, 2011 ~ Dec. 31, 2013

Ch 7

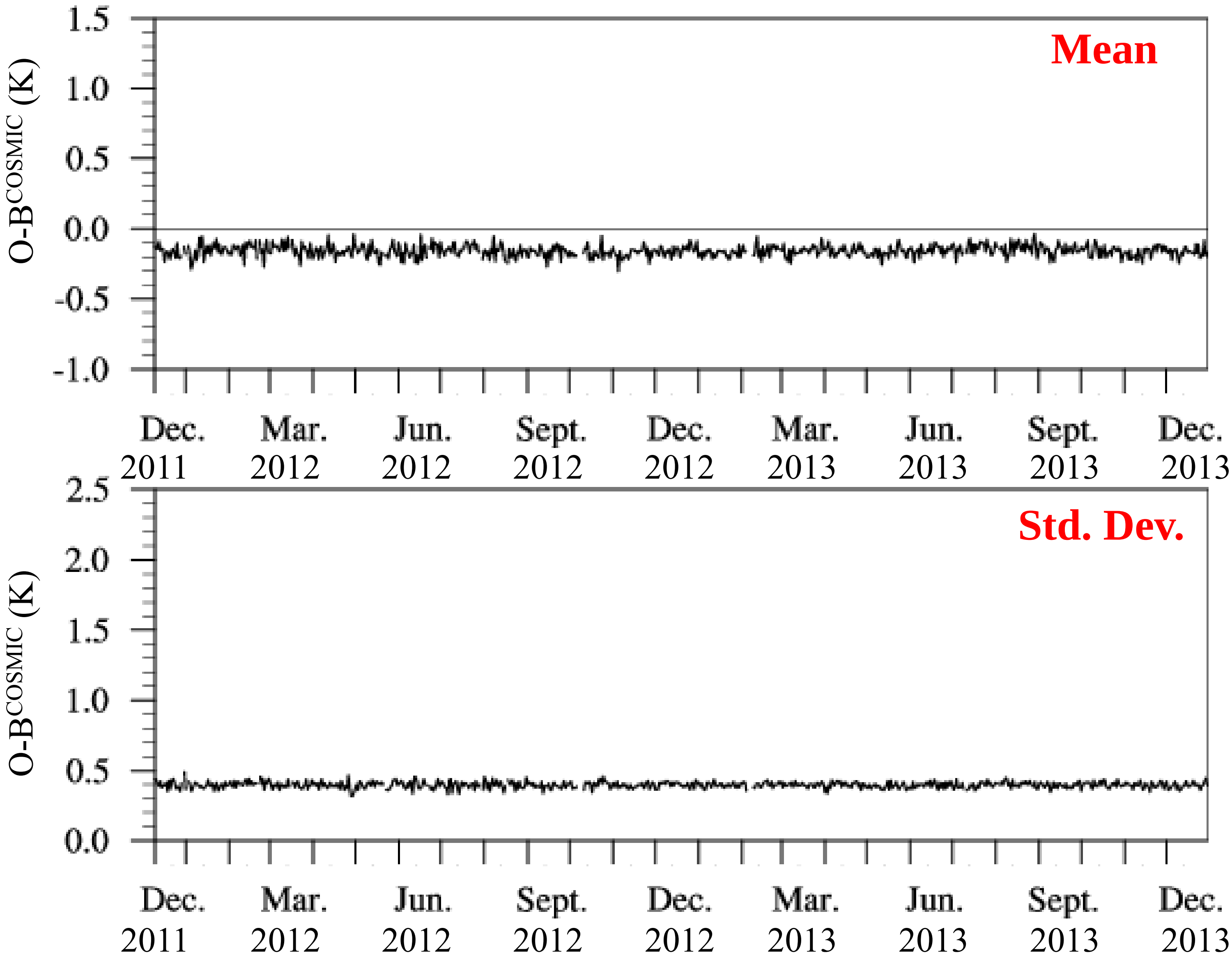

Daily Mean and Std. Dev. of O-B^{COSMIC}

Clear-sky, over ocean, 60°S ~ 60°N, Dec. 10, 2011 ~ Dec. 31, 2013

Ch 8

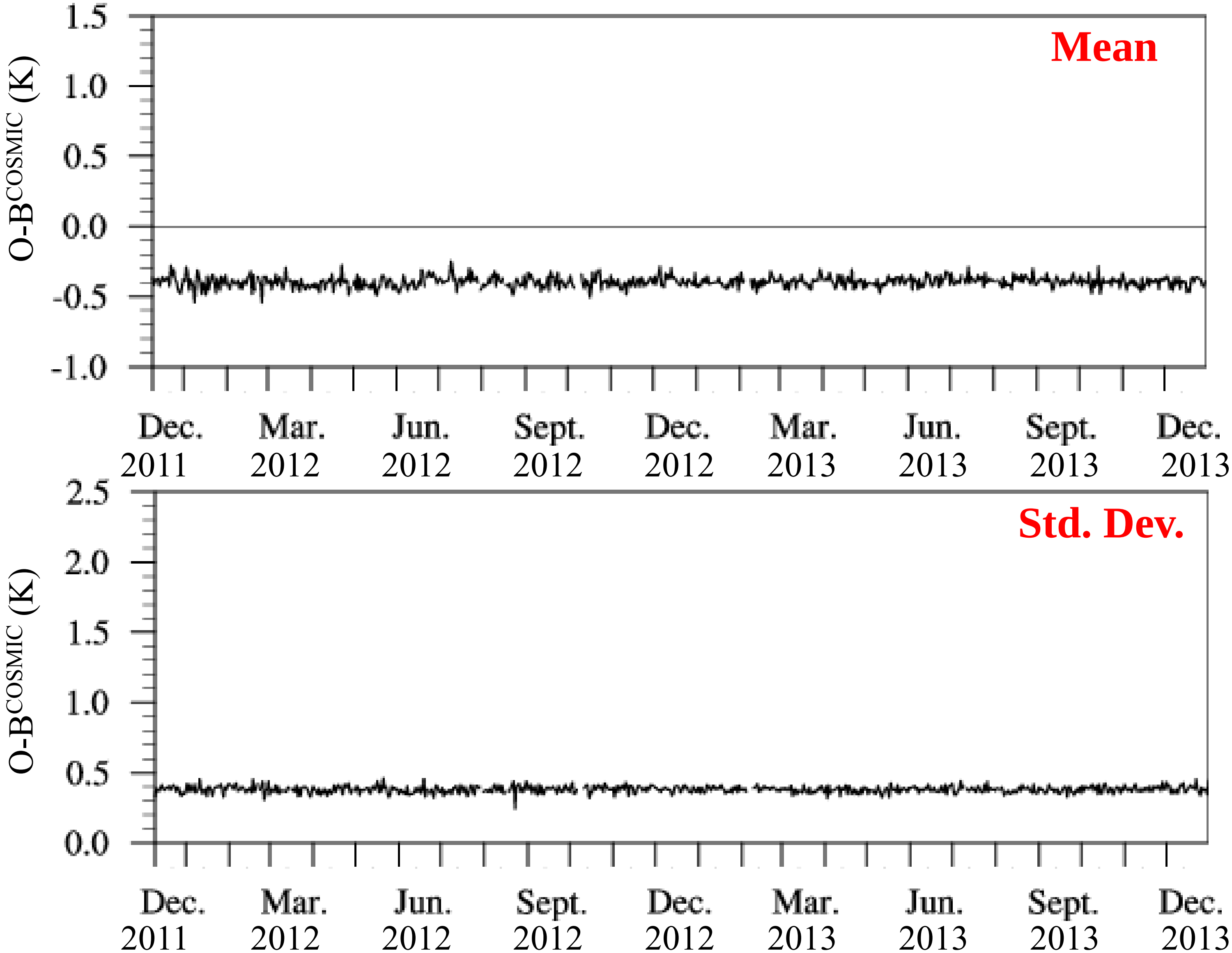

Daily Mean and Std. Dev. of O-B^{COSMIC}

Clear-sky, over ocean, 60°S ~ 60°N, Dec. 10, 2011 ~ Dec. 31, 2013

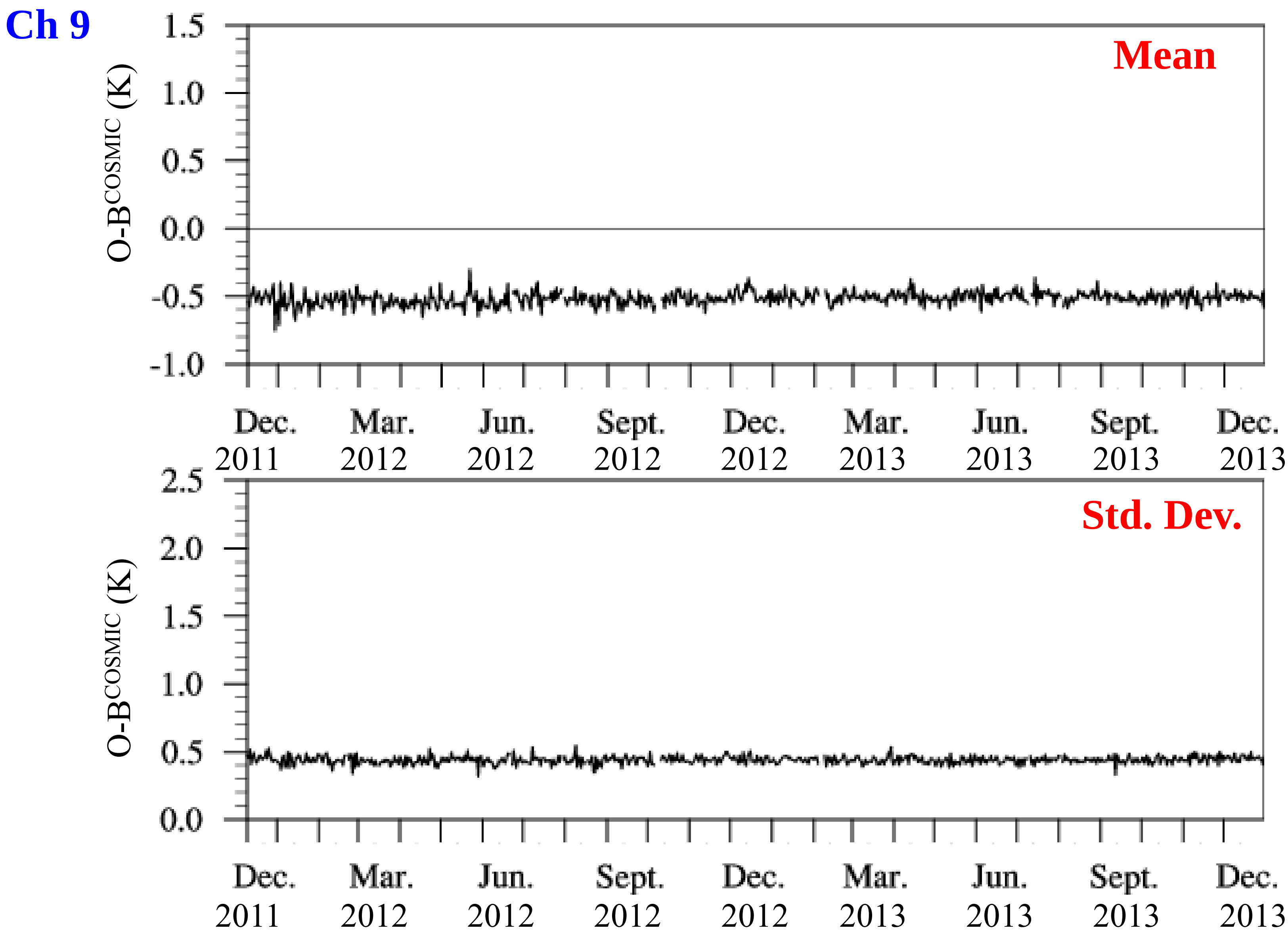

Daily Mean and Std. Dev. of O-B^{COSMIC}

Clear-sky, over ocean, 60°S ~ 60°N, Dec. 10, 2011 ~ Dec. 31, 2013

Ch 10

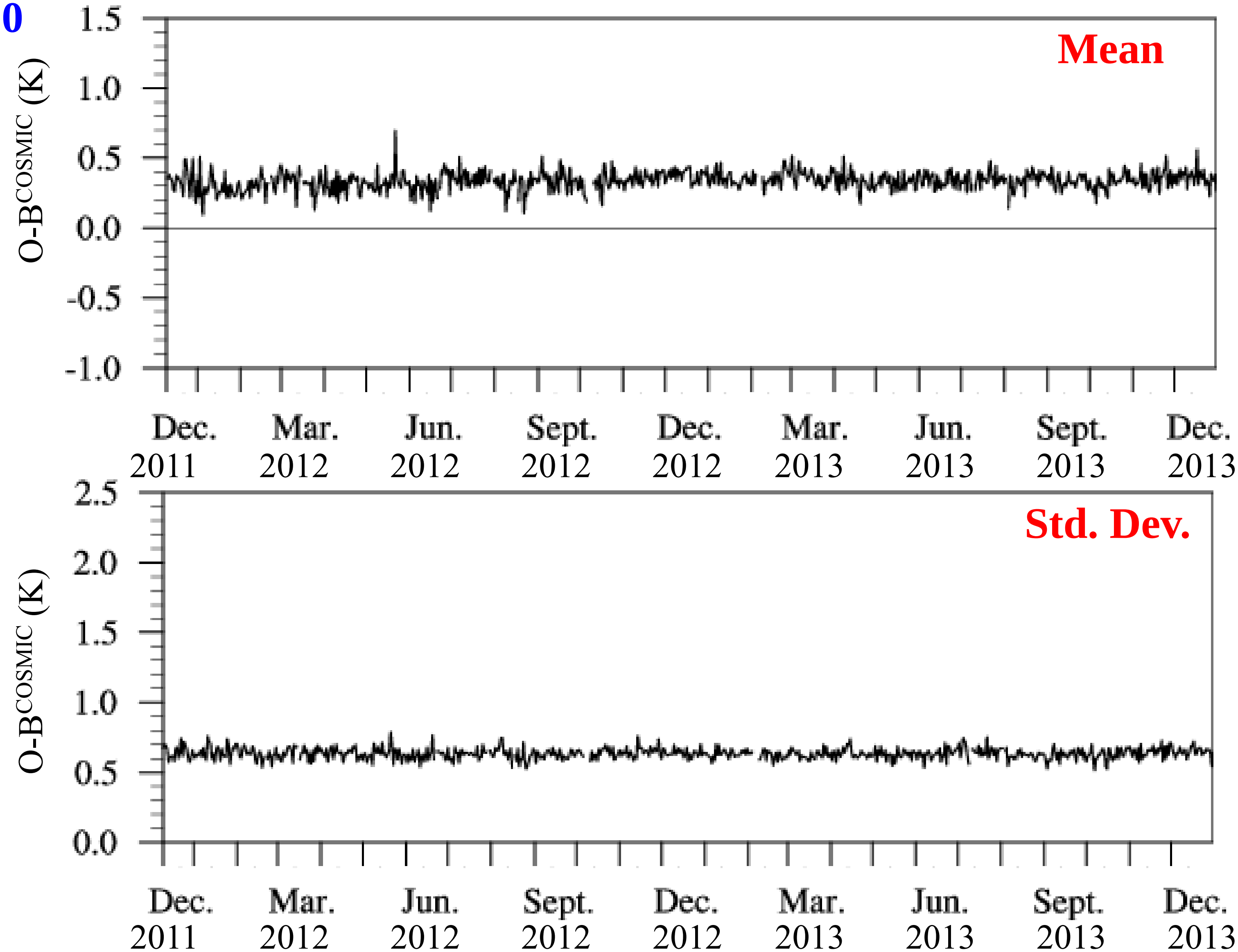

Daily Mean and Std. Dev. of O-B^{COSMIC}

Clear-sky, over ocean, 60°S ~ 60°N, Dec. 10, 2011 ~ Dec. 31, 2013

Ch 11

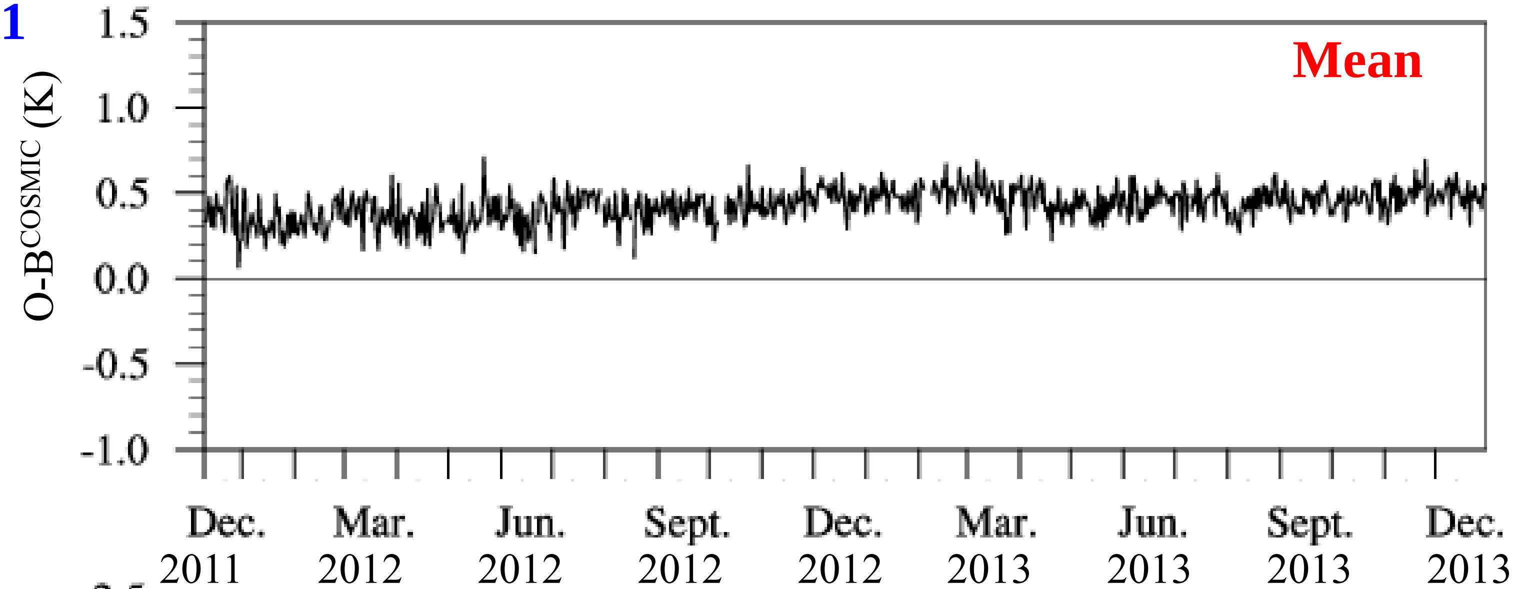

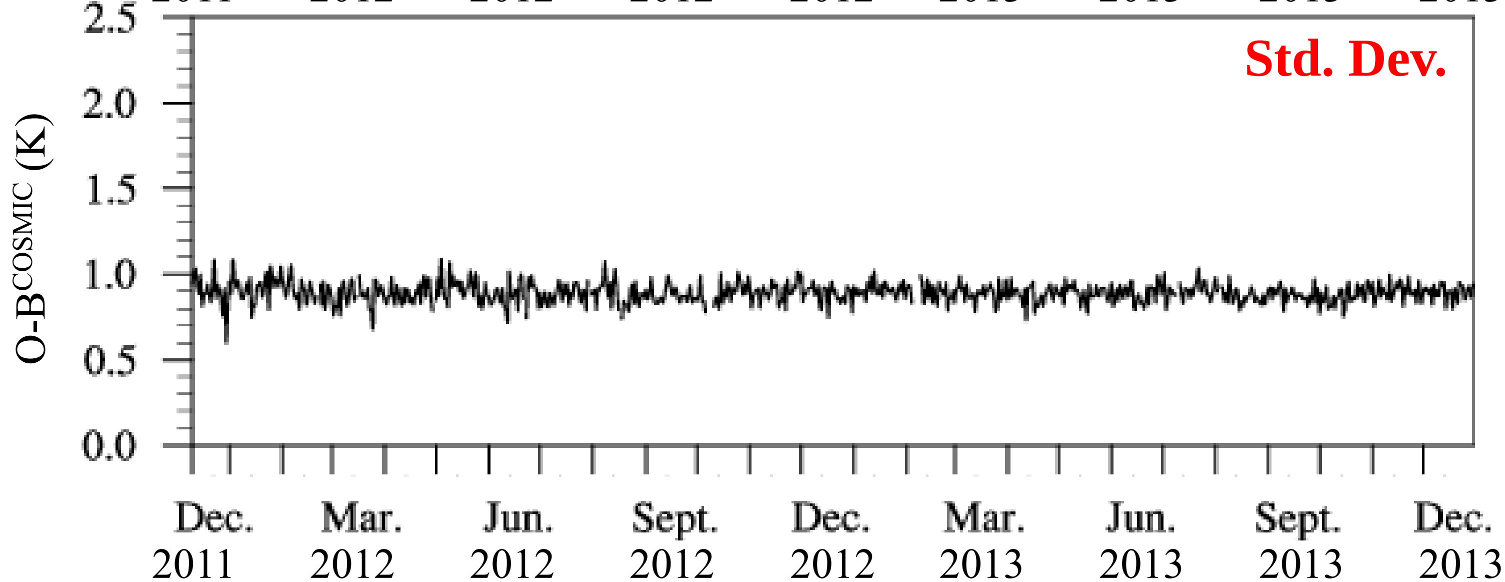

Daily Mean and Std. Dev. of O-B^{COSMIC}

Clear-sky, over ocean, 60^{o}S ~ 60^{o}N, Dec. 10, 2011 ~ Dec. 31, 2013

Ch 12

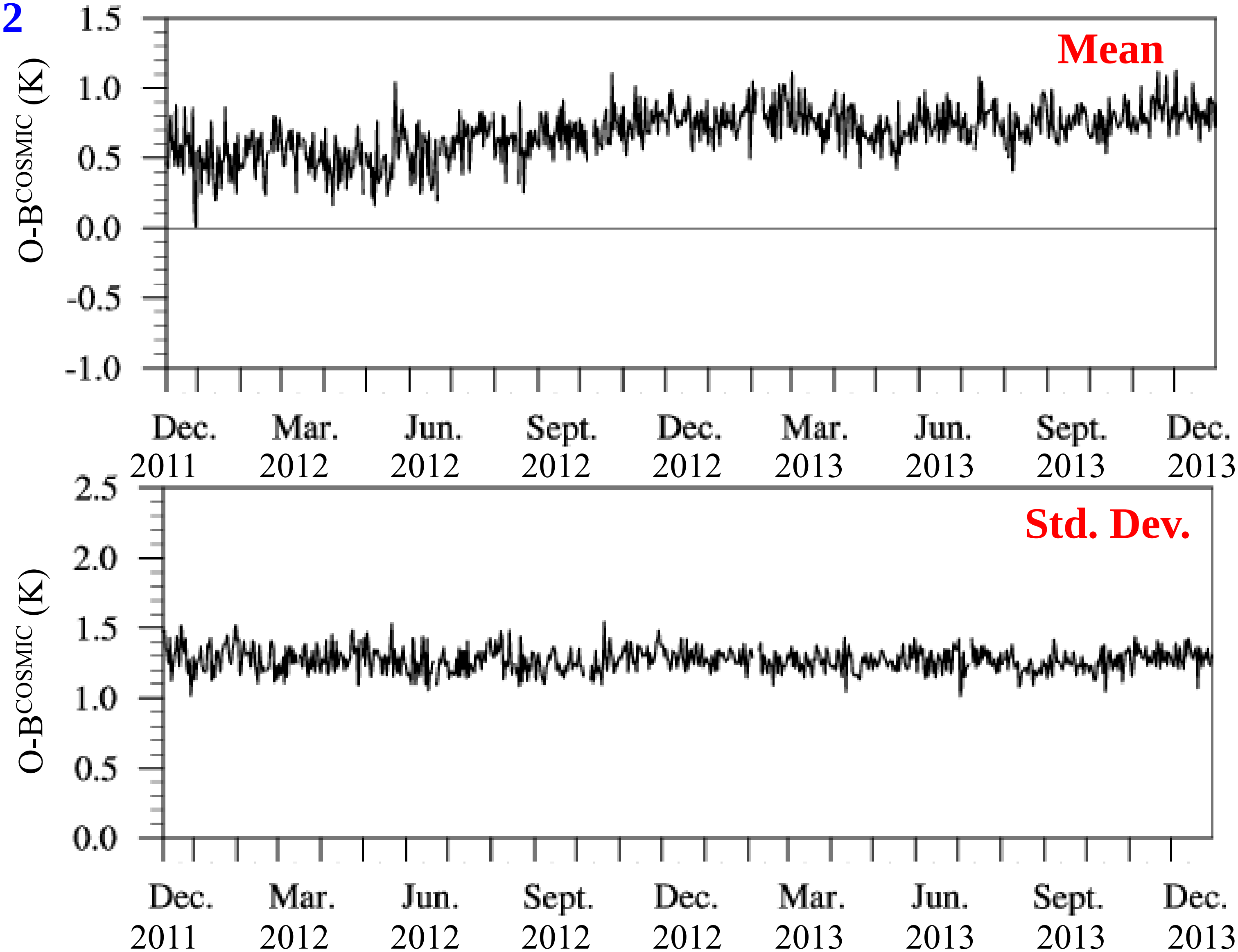

Daily Mean and Std. Dev. of O-B^{COSMIC}

Clear-sky, over ocean, 60°S ~ 60°N, Dec. 10, 2011 ~ Dec. 31, 2013

Ch 13

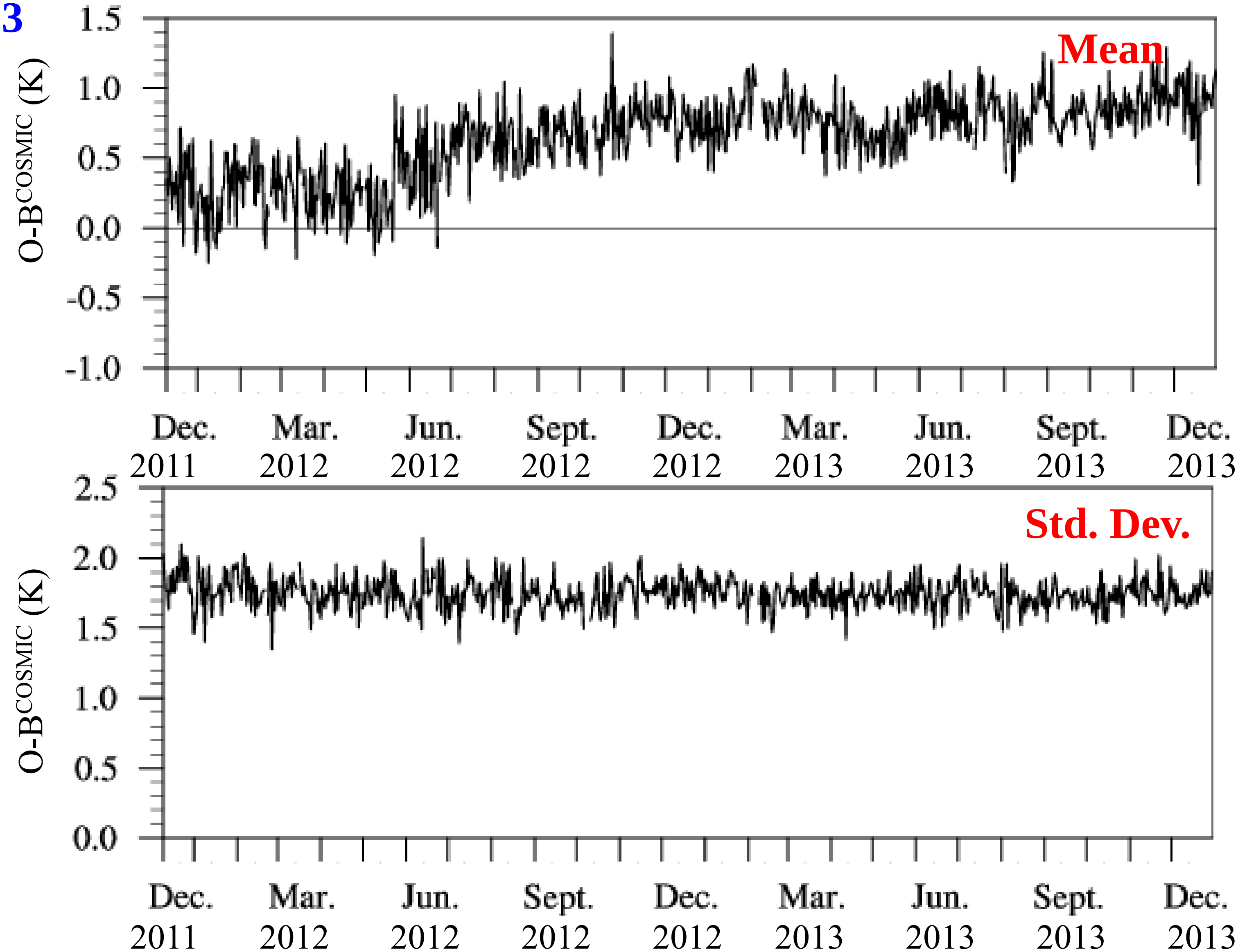

Monthly Mean of O-B^{COSMIC}

Clear-sky, over ocean, 60°S ~ 60°N, Dec. 10, 2011 ~ Dec. 31, 2013

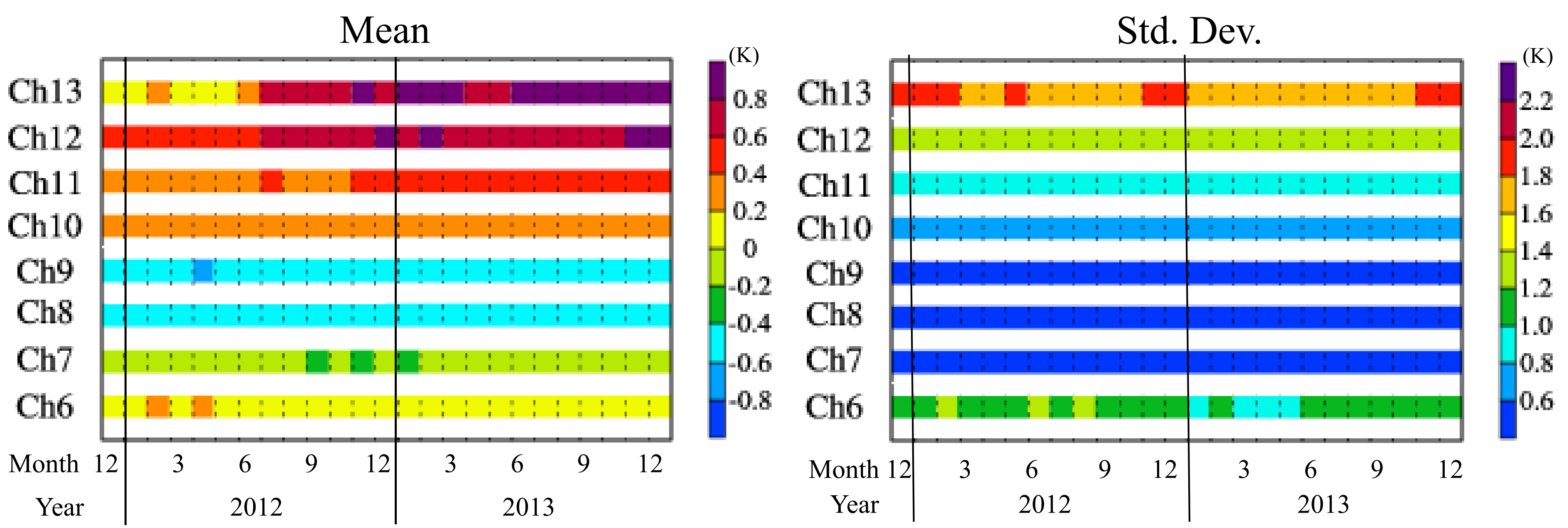

Channels 6 to 11 show consistently stable mean O-B and standard deviation.

Monitoring of ATMS Bias Characterization

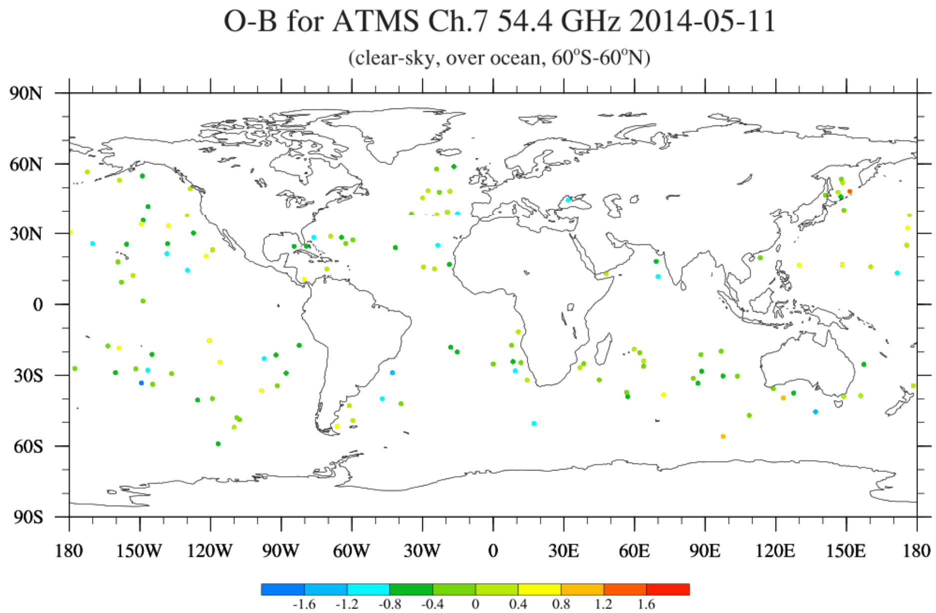

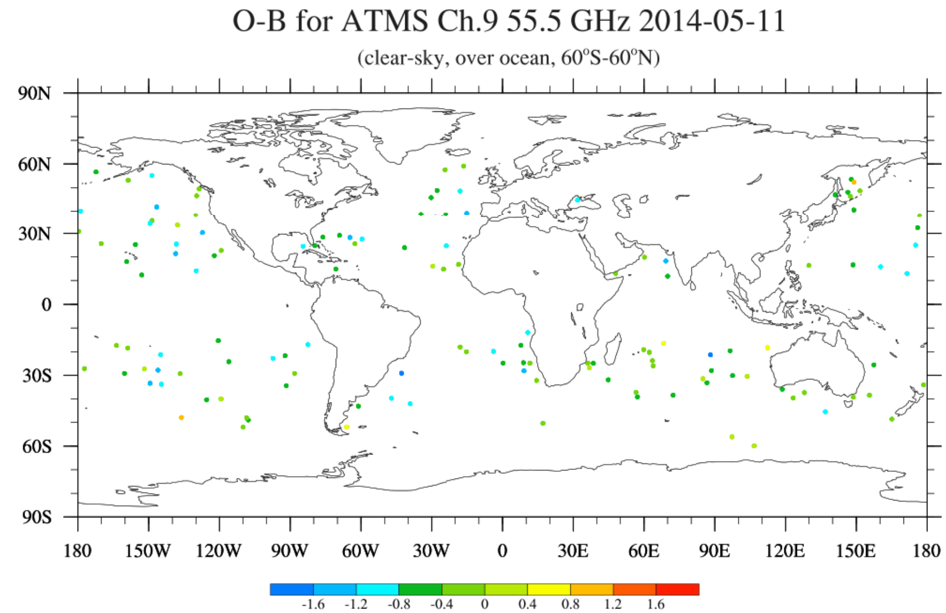

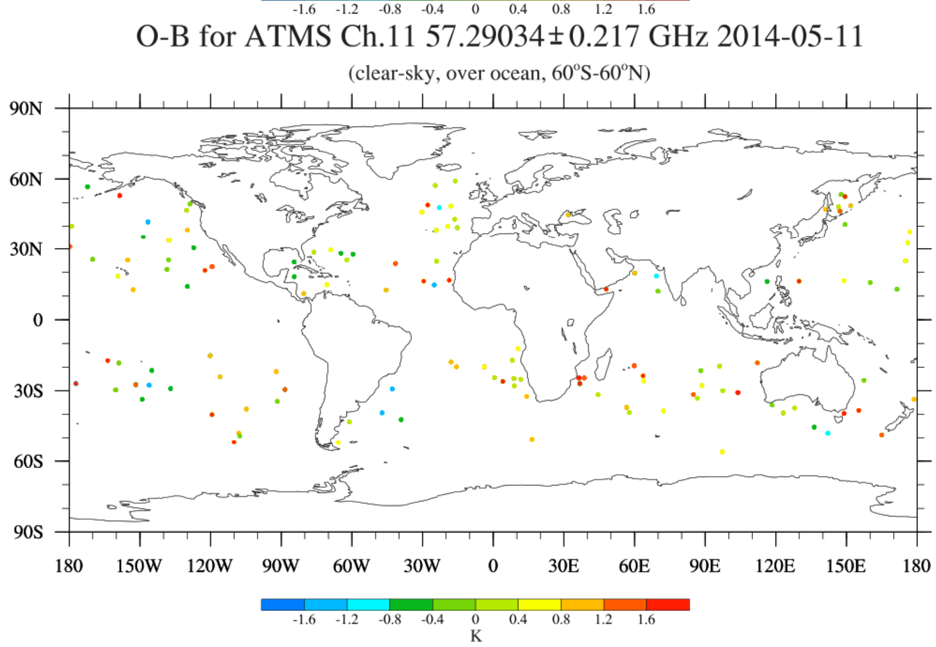

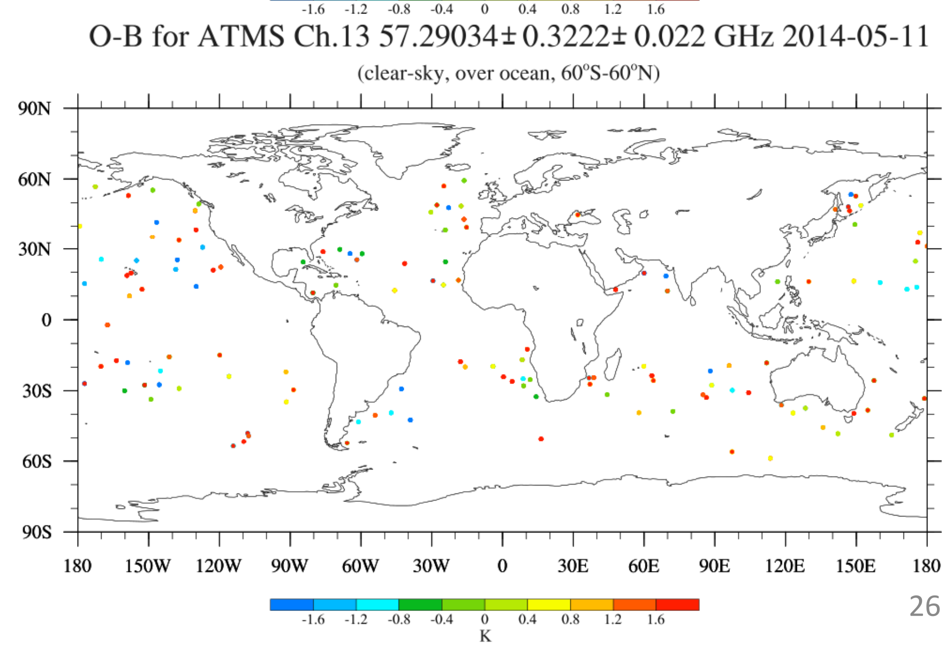

Summary

- Since Dec. 2012, COSMIC RO data are collocated with ATMS observations for channels 5-13. Clear-sky conditions over ocean within 60^{o}S~60^{o}N are examined.
- ATMS global BT biases for channels 5-13 derived from GPS RO are asymmetric to scan angle and within ±0.7K. After scan bias correction, the biases become Gaussian, and the magnitudes are one order smaller.
- The SRF comparison presents biases less than ±0.2K. It suggests that forward RTM should either use the measured SRFs or remove the model biases introduced by the Boxcar SRFs that currently used in CRTM.
- Moreover, the biases and standard deviations of channels 6-11 are stable and consistent with each other; but for channels 12 and 13 their biases increase since July 2012.
- To deduce a long-term climate trend with high accuracy, precision, stability, and consistency, this study can significantly contribute to a better refined post-launch calibration of ATMS, and future integration of ATMS data into long-term satellite climate data records (CDRs).

ATMS Airborne SDR Validation, Spectral Analysis, & Correlation Analysis

Vince Leslie, Bill Blackwell, Mike DiLiberto, Idahosa Osaretin, Erik Thompson, and Mark Tolman

STAR JPSS Annual Meeting

13 May 2014

LINCOLN LABORATORY
MASSACHUSETTS INSTITUTE OF TECHNOLOGY

Outline

- **NAST-M cross-validation from S-NPP Field Campaign**
- **S-NPP and J1 ATMS Spectral Analysis**
- **S-NPP and J1 ATMS Correlation Coefficients Analysis**

Radiance Versus Modeling Verification

Radiance to Radiance Comparisons

- Separate sensors measuring nearly the same point at the same time
- Examples include Simultaneous Nadir Observations (SNO) or aircraft underflights
- Pros: same atmosphere and surface conditions with similar instrumentation
- Cons: Different spectral or spatial characteristics and small data sets

Radiance to Model Comparisons

- Model the sensor and the atmosphere
- Examples include using state-of-the-art NWP, radiative transfer, and surface models
- Pros: large amounts of data
- Cons: Idealized or measured spectral or spatial characteristics and modeling errors

Airborne Validation Status

- **Calibrated NAST-M (V-band & upper G-band) in altitude chamber using precision microwave calibration target from 100-325 K at the instrument's high-altitude operating temperature**

- **NAST-M calibrated to these residual errors:**
  - **V-band: <0.25 K from 200-325 K**
  - **G-band: <0.30 K from 200-325 K**

- **Compared S-NPP ATMS measurements against NAST-M for the 10May2013 sortie**

S-NPP Mission Cal/Val Campaign

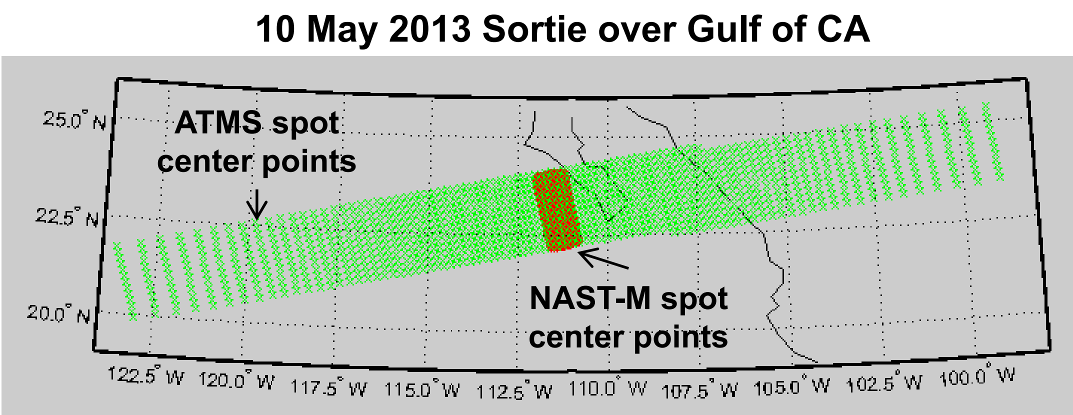

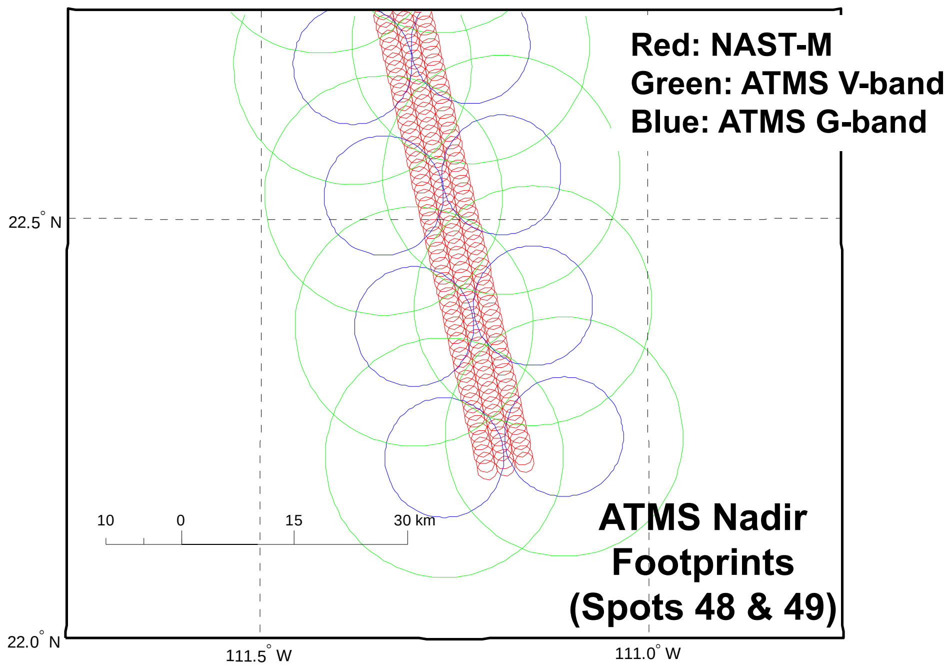

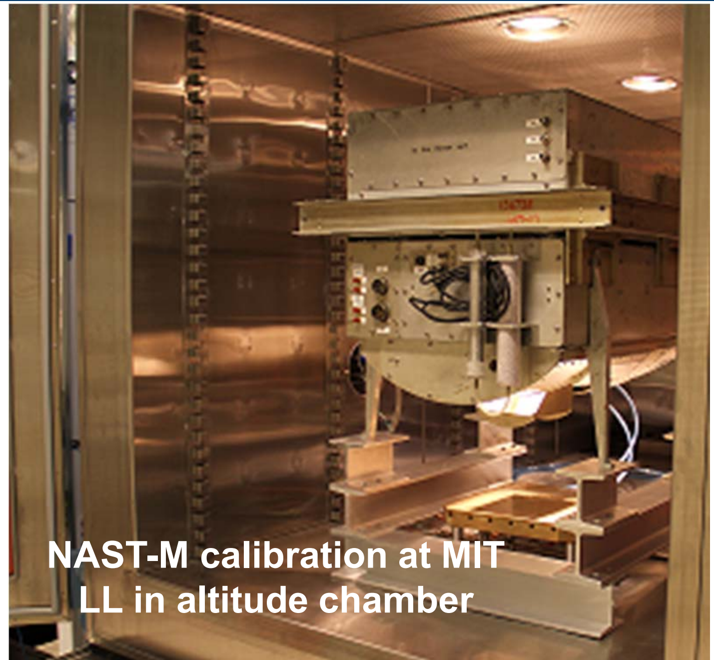

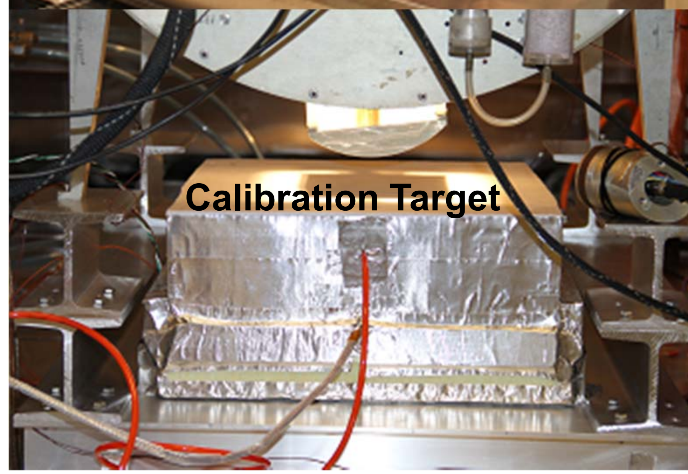

Science Sorties During S-NPP Mission

NAST-M has data from 12 flights ~81 hours

Data Collected
No Data Collected

Data Source	May 7th	May 10th	May 15th	May 16th	May 18th	May 20th	May 22nd	May 23rd	May 24th	May 30th	May 31th	June 1st
NAST-M												
GPS												
Video												
ER-2 NAV												
Drop Sonde												
Radioondes												
Salton Sea												
NAM												
ECMWF												
Overpass												
NPP												
Aqua												
Metop-A												
Metop-B												
Conditions												
Time Of Day	Day	Day	Day	Day	Day	Day	Day	Day	Day	Night	Night	
Surface type	Ocean	Mixed	Mixed	Mixed	Land	Land	Land	Ocean	Land	Ocean	Mixed	
Weather	Cloudy	Clear	Clear	Scattered	Thin Cirrus	Scattered	Clear	Cloudy	Scattered	Scattered	Clear	
Flight Time (H)	6.35	5.98	7.63	8.13	6.25	8.47	9.2	6.58	8.03	6.22	8.18	0

Collected data from 9 S-NPP overflights

LINCOLN LABORATORY
MASSACHUSETTS INSTITUTE OF TECHNOLOGY

NAST-M Calibration Accuracy: 54 GHz Band

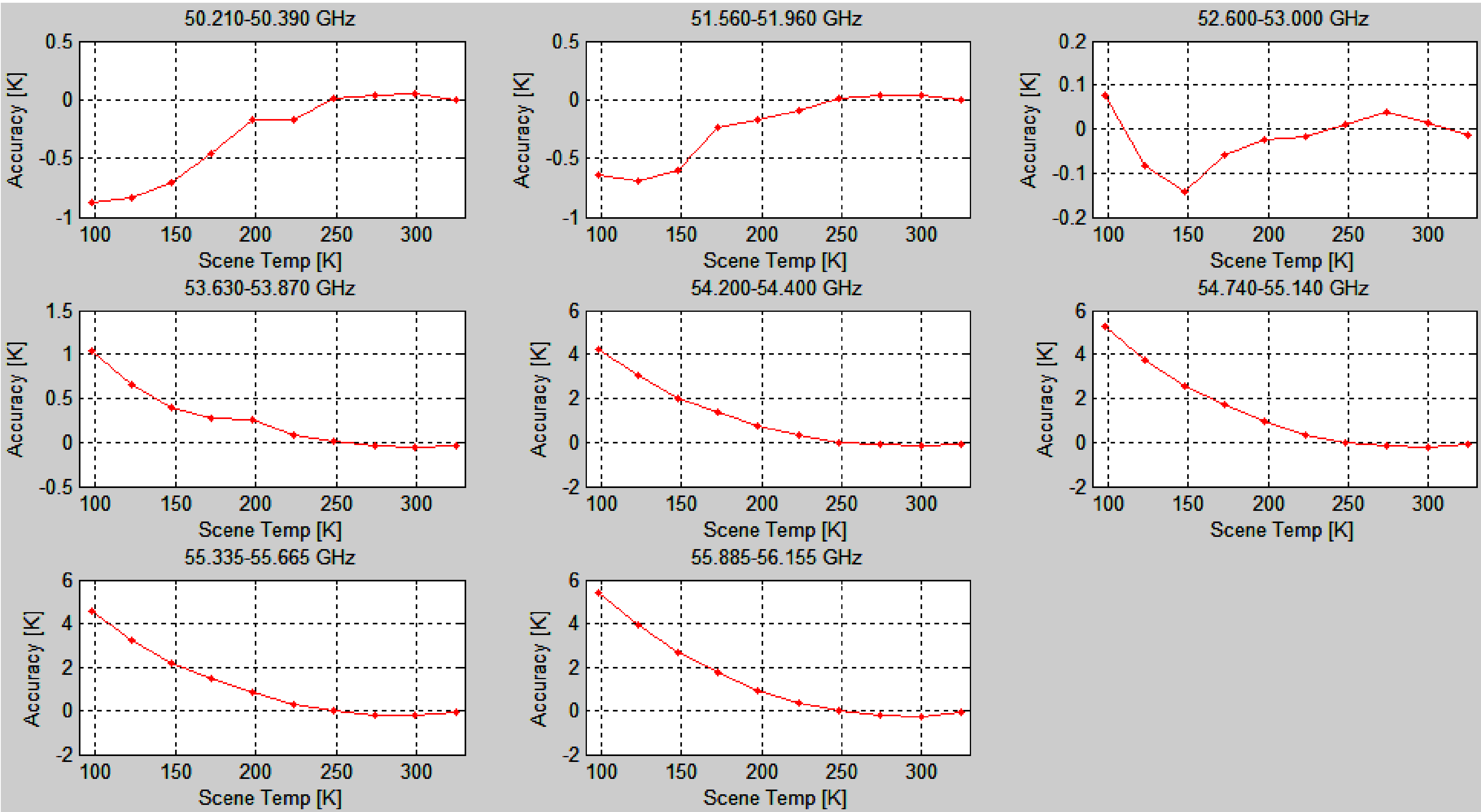

NAST-M Calibration Accuracy: 183 GHz Band

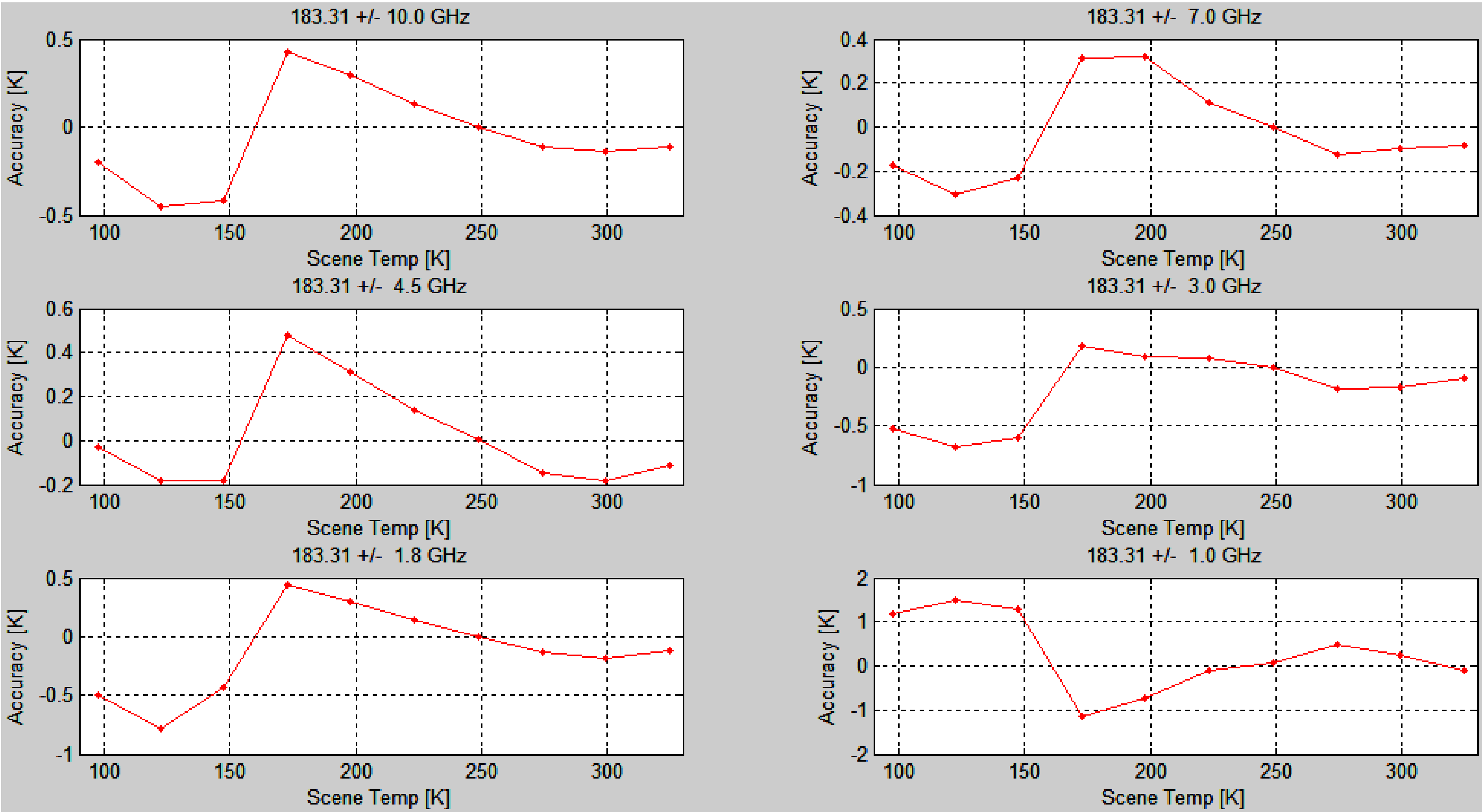

Matchup Flowchart

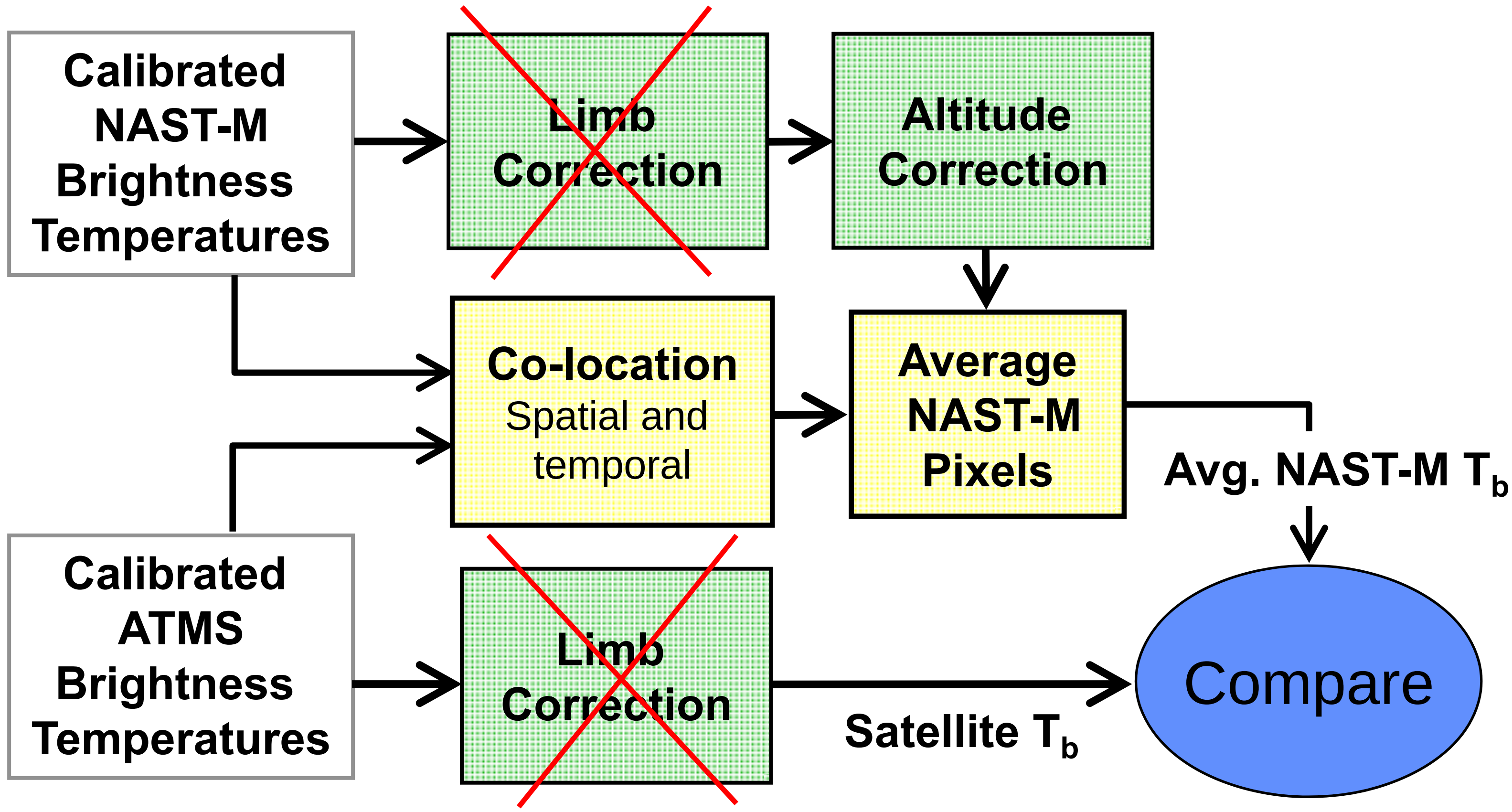

Green boxes need one of these:

1) **Radiosonde or dropsonde** **(Most desirable)**
2) **Simulated model output (e.g., ECMWF)**
3) **Retrieved profile from a different instrument**

Altitude-Corrected Aircraft Brightness Temperature (T_b)

AC– Aircraft
NWP– Numerical Weather Prediction
SAT– Satellite
TOA– Top of Atmosphere

NWP

Temperature
Pressure
H_2O
O_3

Radiative Transfer Model

$T_b^{NWP}\left(\text{sim} \updownarrow^{x}_{\text{Surface}}\right)$

T_b^{SAT}

$$T_b^{\Delta} = T_b^{SAT} - T_b^{AC}$$
$$\approx 0.1 \leftrightarrow 1\,\text{K}\,(54\,\text{GHz})$$
$$\approx 0.01 \leftrightarrow 0.1\,\text{K}\,(183\,\text{GHz})$$

T_b^{AC}

<u>Use Simulated Brightness Temperatures</u>

$$T_b^{SAT} \approx T_b^{NWP}\left(\text{sim} \updownarrow^{\text{TOA}}_{\text{Surface}}\right)$$
$$T_b^{AC} = T_b^{NWP}\left(\text{sim} \updownarrow^{\text{AC}}_{\text{Surface}}\right)$$

Surface

$$T_b^{\text{Alt-Corrected}} = T_b^{AC}\left(\text{meas} \updownarrow^{\text{AC}}_{\text{Surface}}\right) + T_b^{\Delta}$$

S-NPP 10 May 2013 Matchup

Residual Error between ATMS measurements and NAST-M (ATMS – NAST-M) at nadir

Lower V-Band ATMS Channels

ATMS	Ch. 3	Ch. 4	Ch. 5	Ch. 6	Ch. 7	Ch. 8	Ch. 9
TDR	0.95	-0.22	-1.6	0.59	-0.07	0.00	-0.36
SDR	1.38	0.34	-0.89	1.04	0.41	0.35	-0.19

Upper G-Band ATMS Channels

ATMS	Ch. 18	Ch. 19	Ch. 20	Ch. 21	Ch. 22
TDR	-2.52	-2.11	-2.23	-1.24	1.58
SDR	-3.38	-2.93	-3.08	-2.11	0.62

TDR = Temperature Data Record or antenna temperature
SDR = Sensor Data Record or brightness temperature (scan bias corrected)

TDR-to-SDR Results: K and Lower V Band

ATMS Residuals of SDR and TDR against ECMWF/CRTM for May 24, 2013 over ocean and under clear skies from STAR

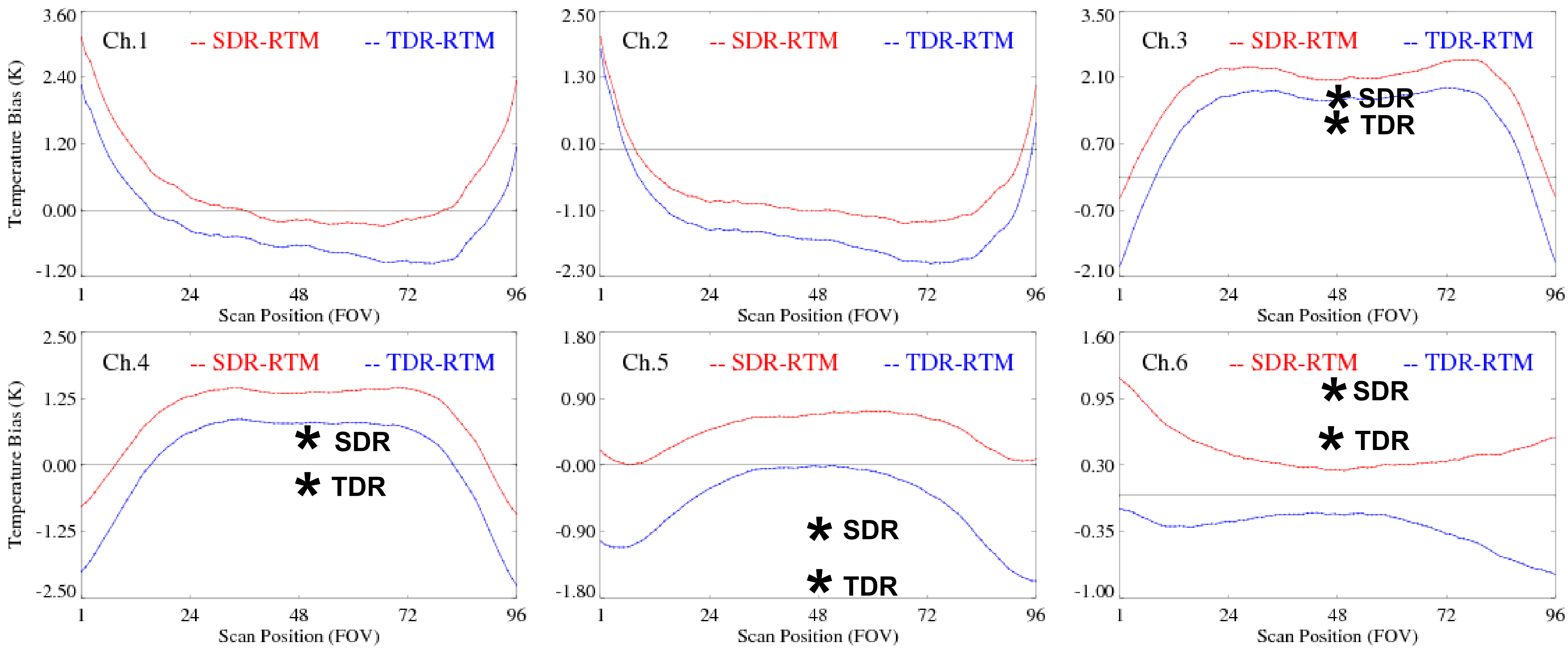

*** NAST-M Result from 10 May 2013; clear skies over ocean with limited # of high quality matchups**

TDR-to-SDR Results: Upper Air Sounding

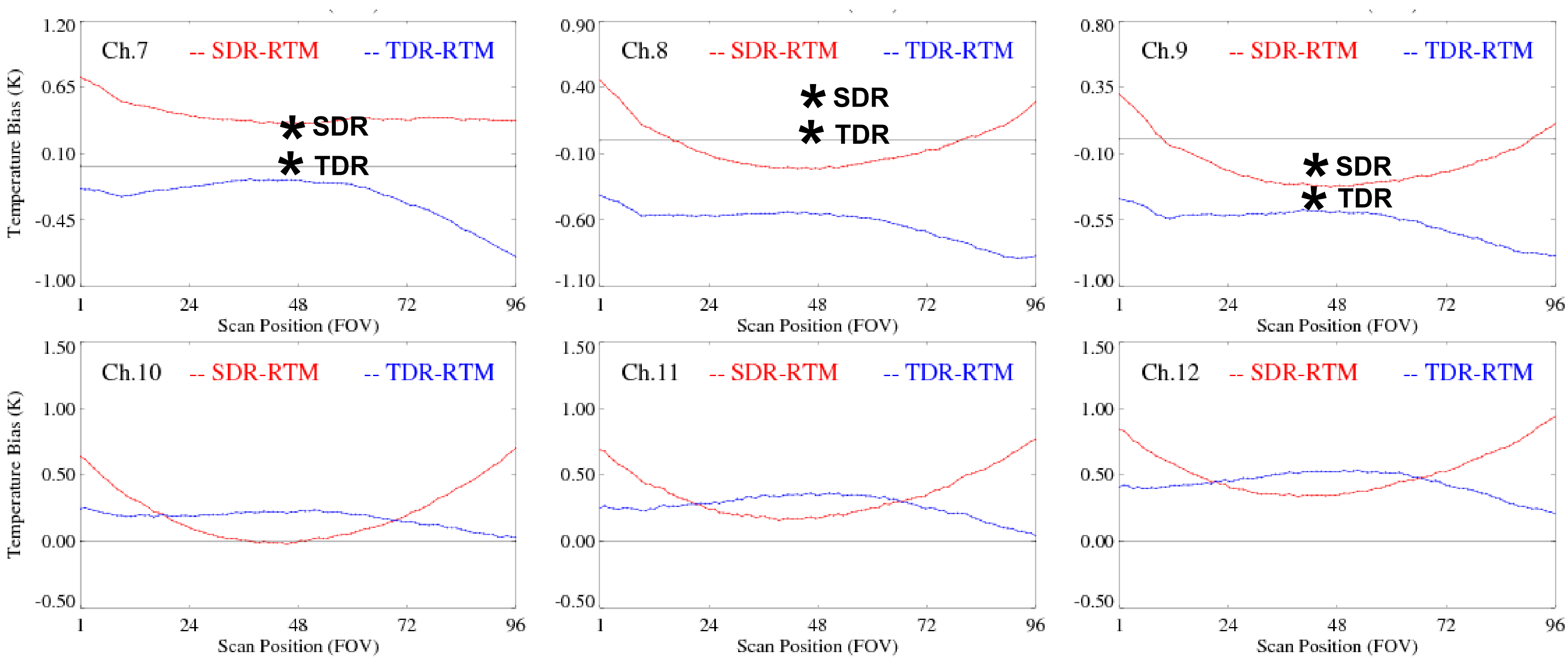

* NAST-M Result from 10 May 2013; clear skies over ocean

TDR-to-SDR Results for W/G Band

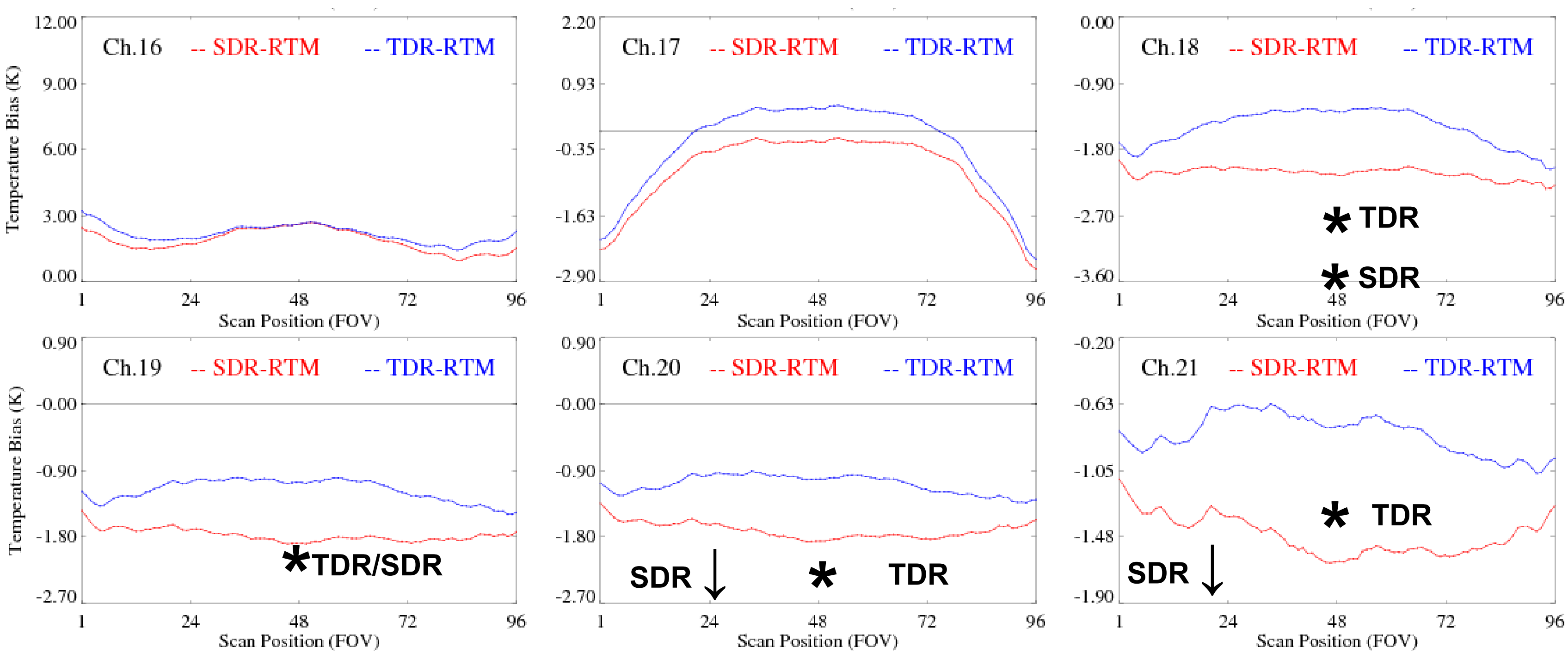

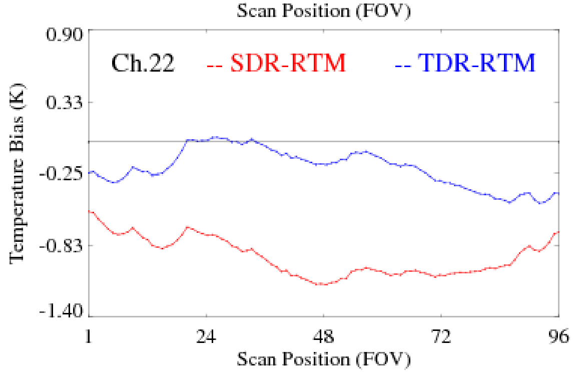

TDR/SDR ↑

*** NAST-M Result from 10 May 2013; clear skies over ocean with limited # of high quality matchups**

Example Power Spectral Densities

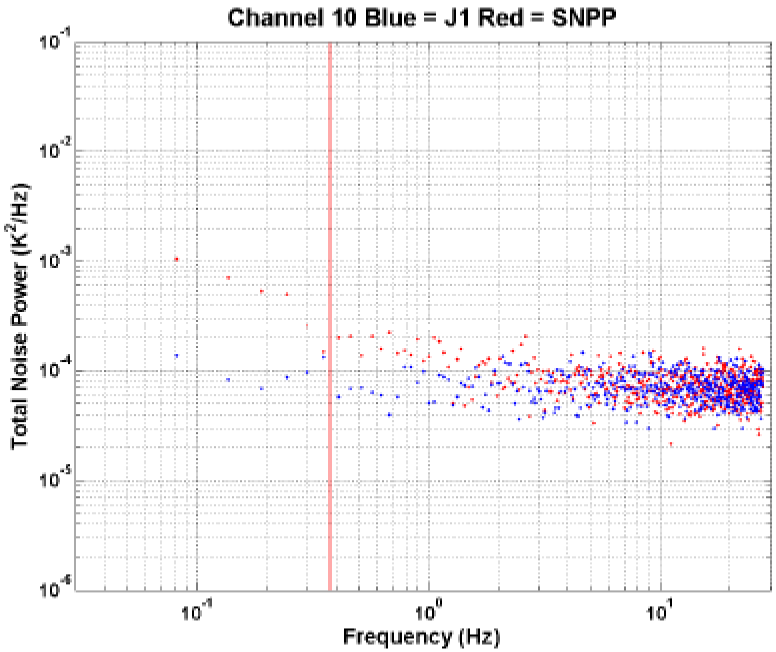

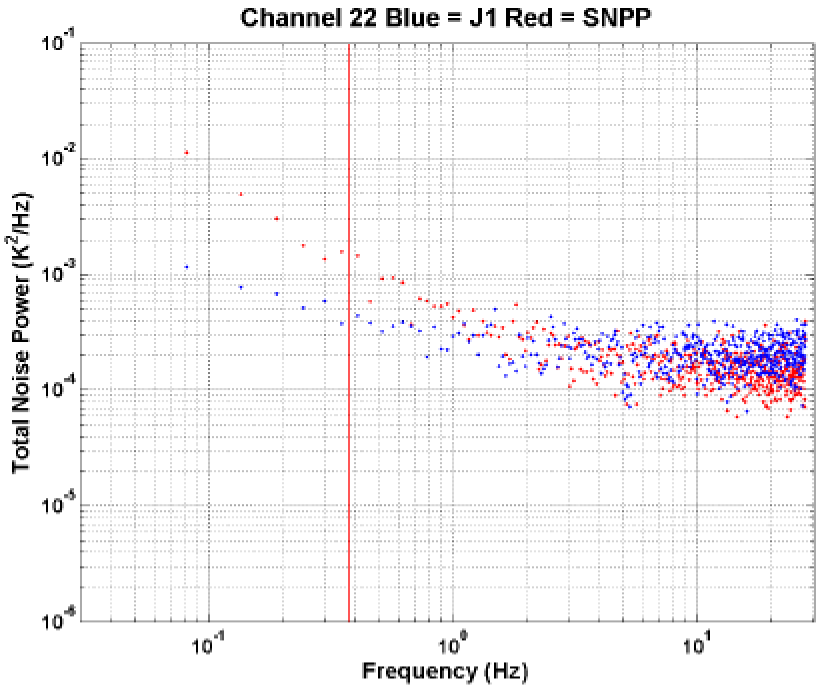

- **PSD show the 1/f noise on the left and the thermal noise to the right**
- **The red vertical line is the calibration frequency (scan period) and the calibration algorithm effectively applies a highpass filter to the spectrum**

Brightness Temperature Correlation

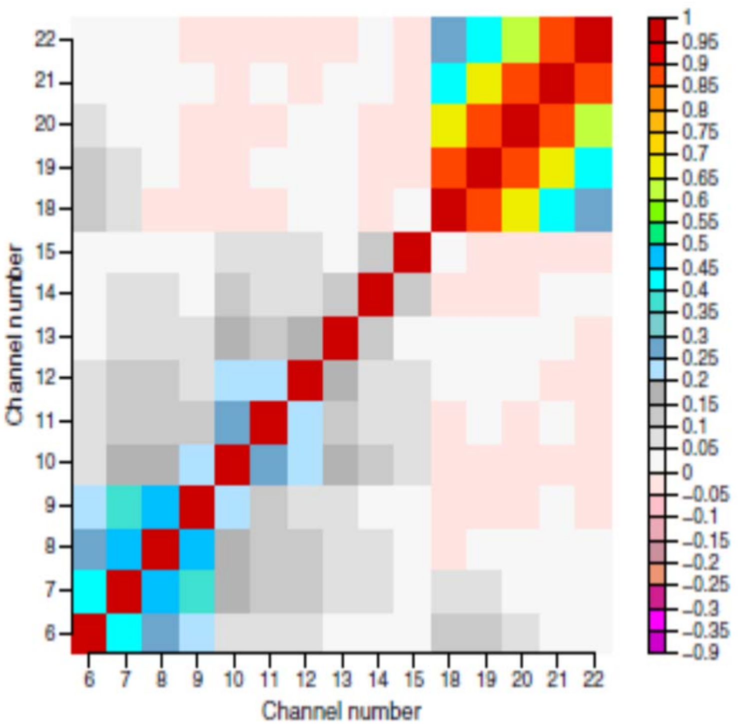

Figure 6. Estimates of interchannel error correlations based on the Desroziers diagnostics for ATMS. Statistics are based on used data over sea for 1–31 July 2012 (only scenes for which all considered channels are assimilated).

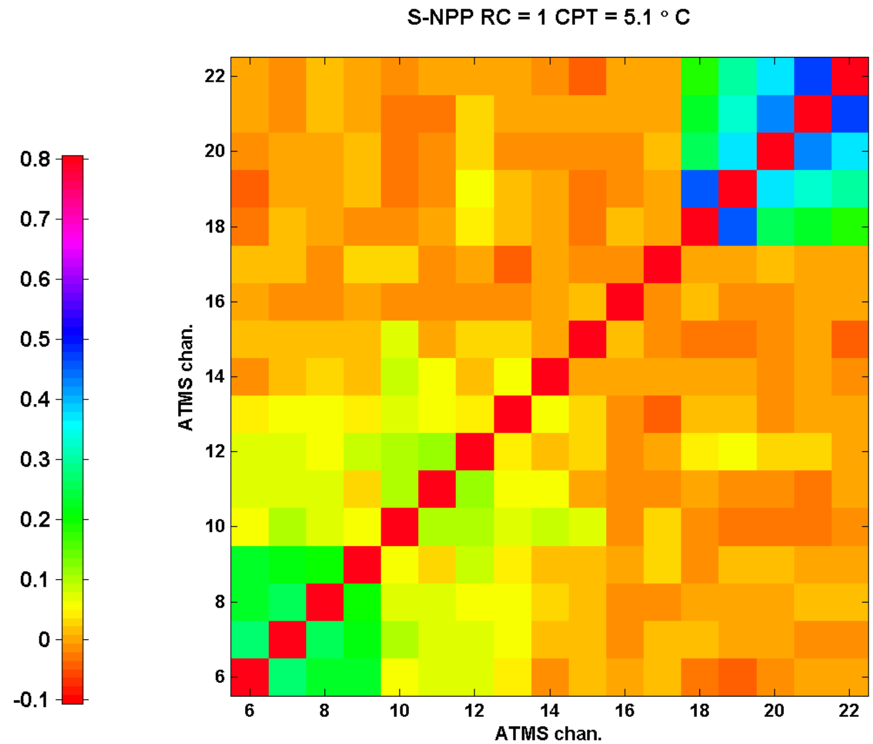

S-NPP Brightness temperature correlation coefficient matrix from pre-launch TVAC calibration

Bormann et al., "Evaluation and assimilation of ATMS data in ECMWF" JGR-A Vol. 118 12,970-12,980

Correlation and the Calibration Algorithm

- **Pre-launch TVAC**
- **Two external targets and internal target**
- **Correlation matrix calculated for eleven scene temperatures**
- **Correlation matrices averaged after Fisher transform**
- **DN cold is the averaged four Space View measurements**
- **Gain uses eight scans in calculation**

$$T_b = gain \times (DN_{scene} - DN_{cold\ target}) + T_{cold\ target}$$

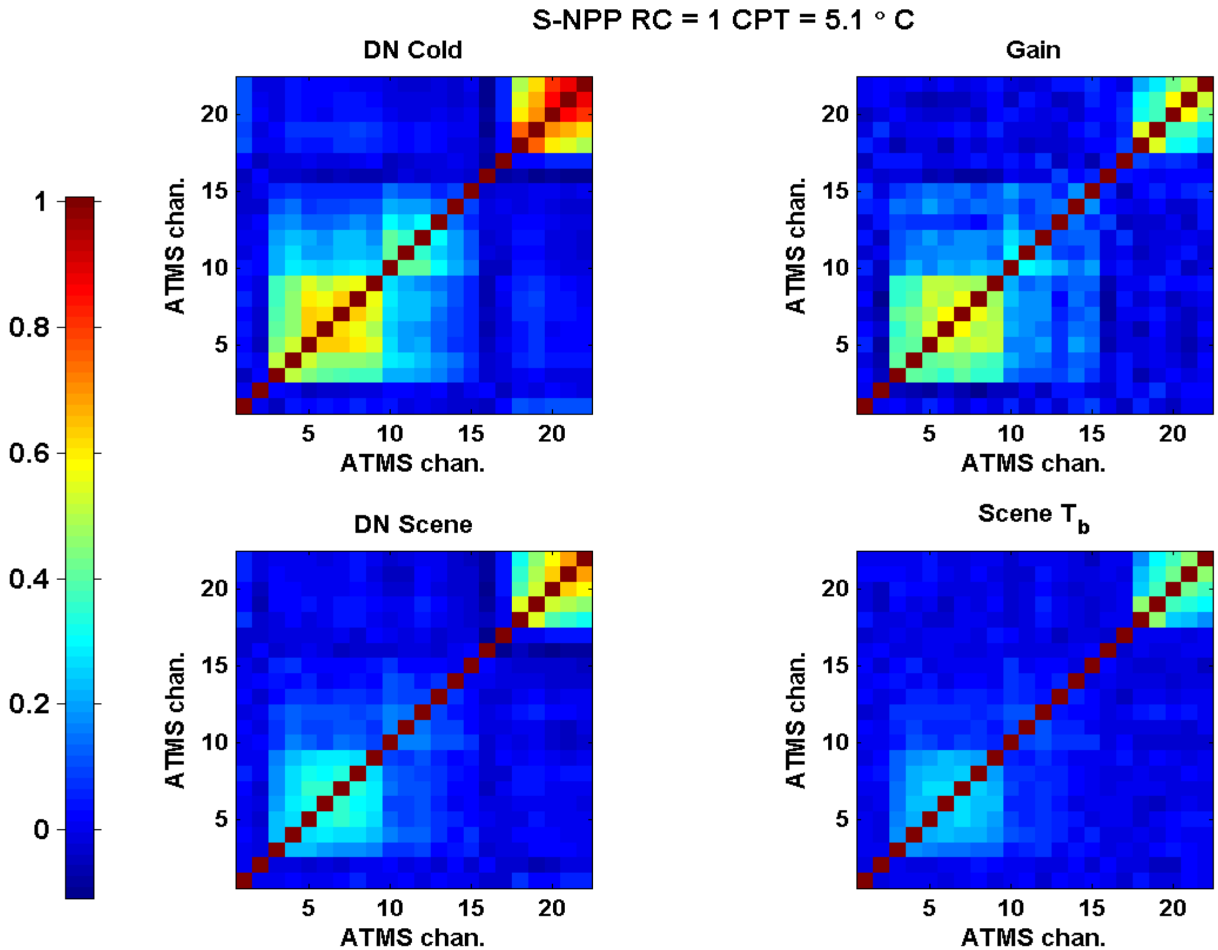

J1 ATMS Results

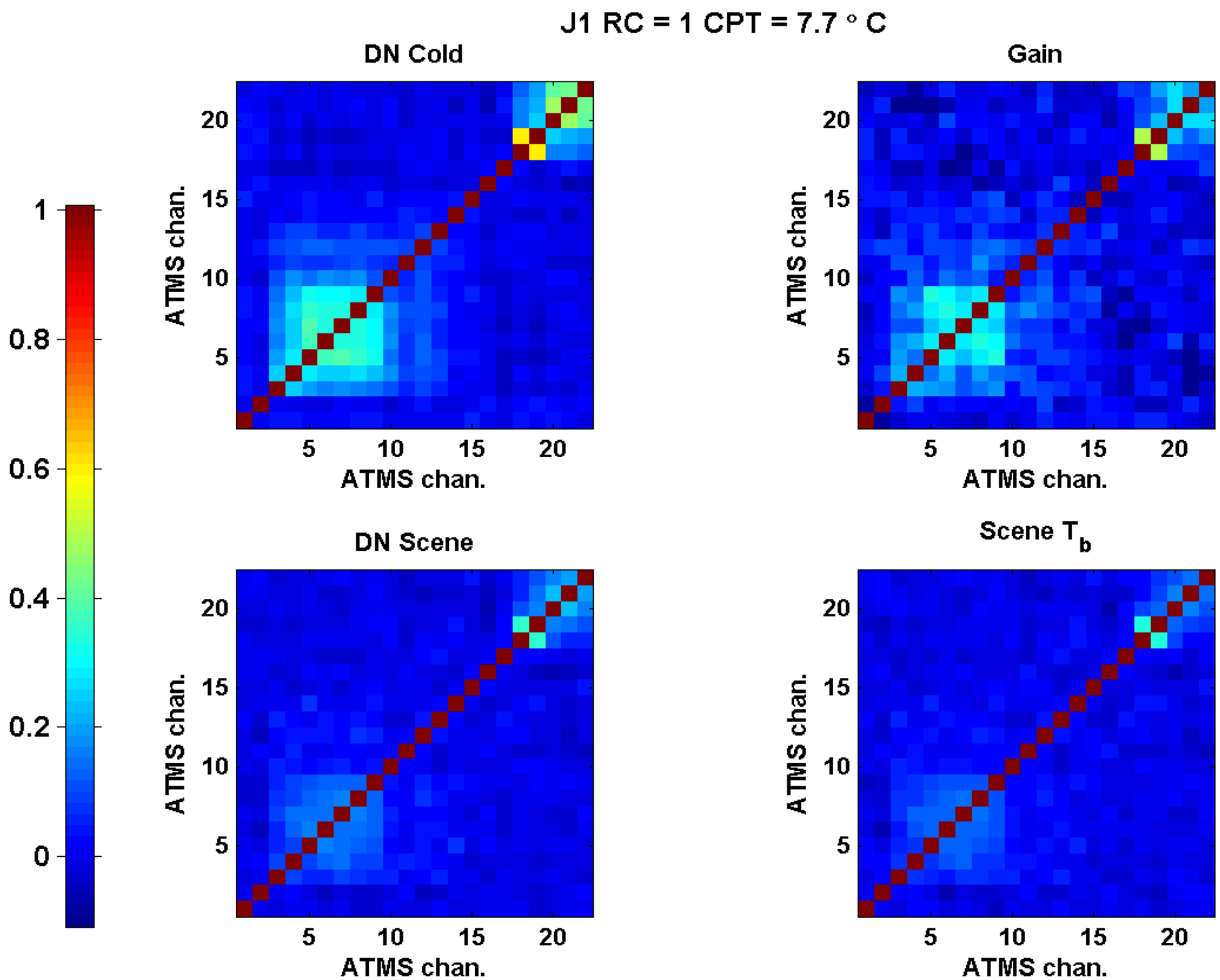

Summary

- **Successful airborne campaign, but need to finish processing all sorties and investigate ATMS bias**
- **J1 ATMS 1/f noise and correlation is lower than S-NPP ATMS**
- **Need to analyze how the J1 & S-NPP spectra and correlation matrices impact data products and instrumentation**

JPSS1 ATMS Thermal Vacuum Calibration Early Results

2014 STAR JPSS Science Team Meeting

Kent Anderson, Edward Kim, and Otto Bruegman

with contributions from Joseph Lyu, Vince Leslie, and Hemanshu Patel

13 May, 2014

NORTHROP GRUMMAN

JPSS1 ATMS Instrument Calibration Test Profiles

- **Testing performed for 4 redundancy configurations at each calibration step**
- **For each calibration step, 278 scans of data processed to yield 271 scans of derived accuracy data**

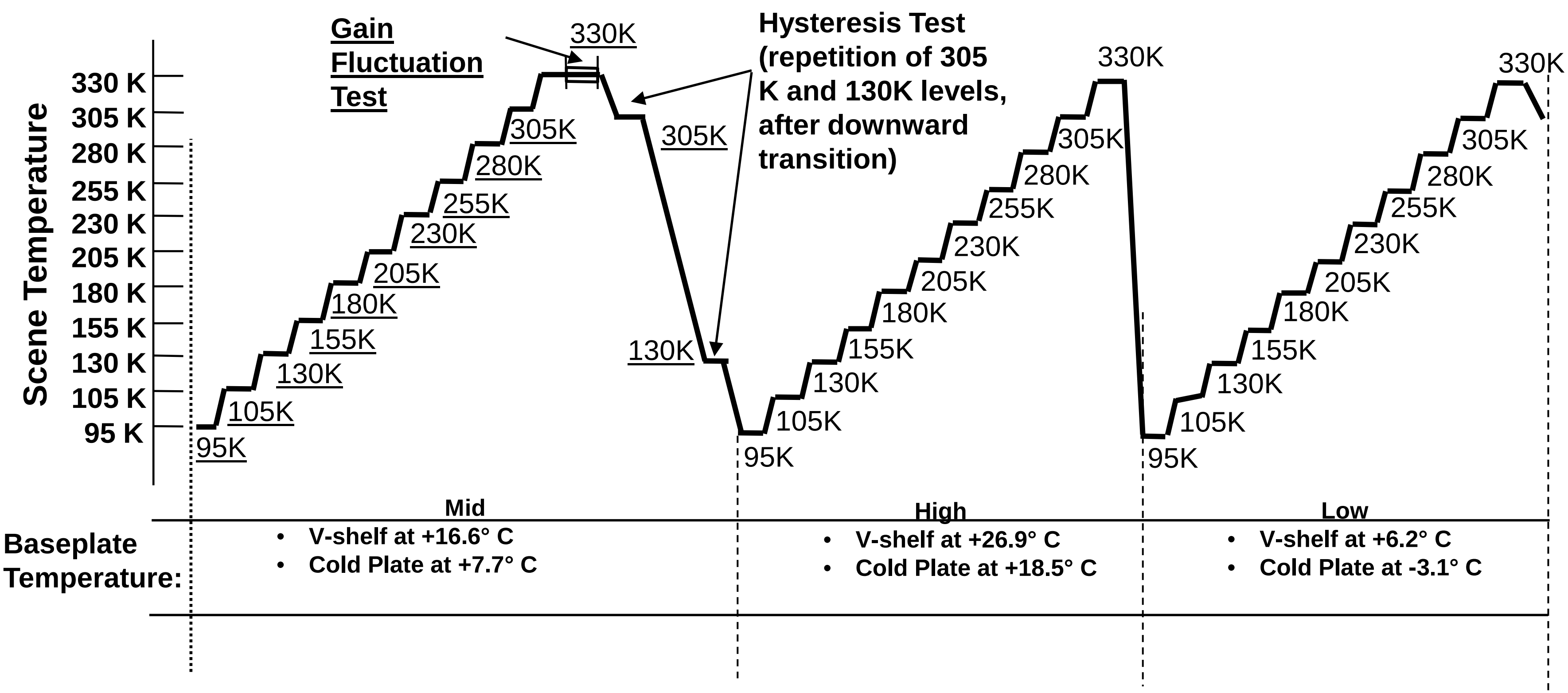

NORTHROP GRUMMAN

JPSS1 ATMS NEDT Performance

- Worst Case of 4 Redundancy Configurations
- Scene temperature at 300 K

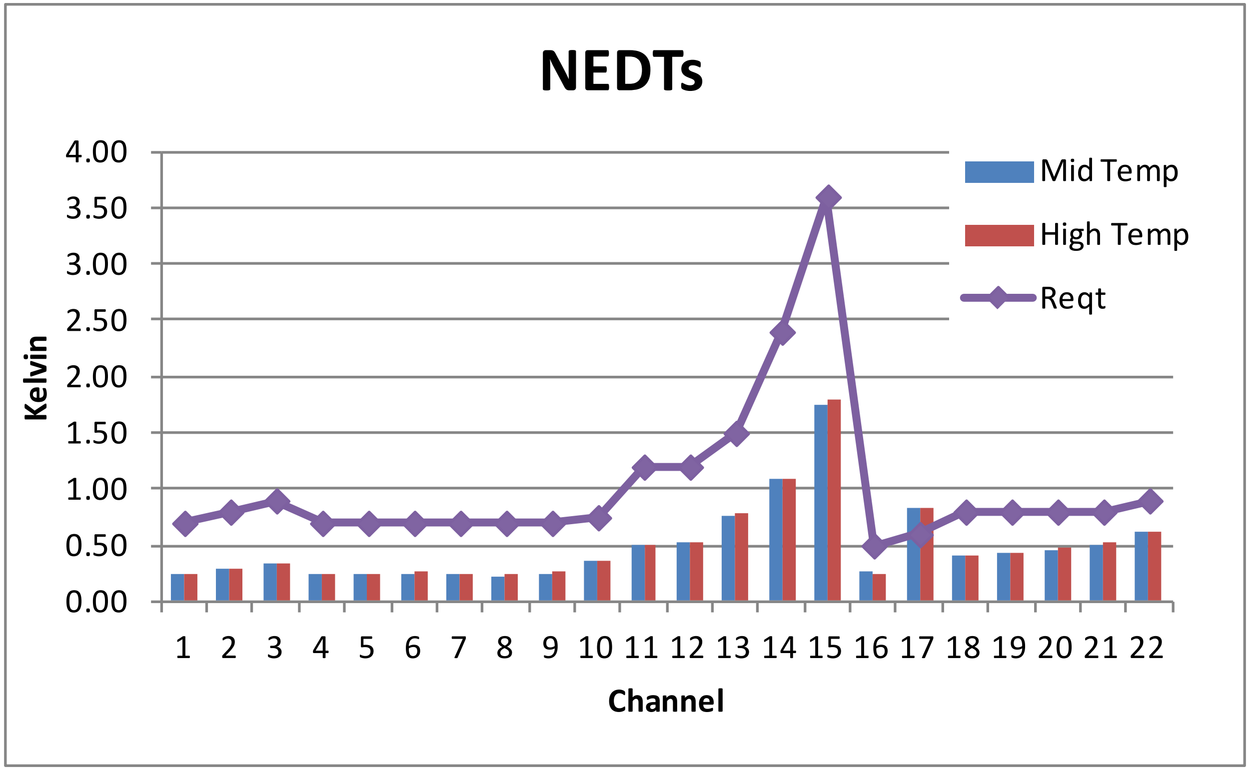

- Waiver request will be submitted for Channel 17 NEDT
- All other channels compliant

JPSS1 ATMS NEDT Performance

- Worst Case of 4 Redundancy Configurations
- Scene temperature interpolated to 300 K

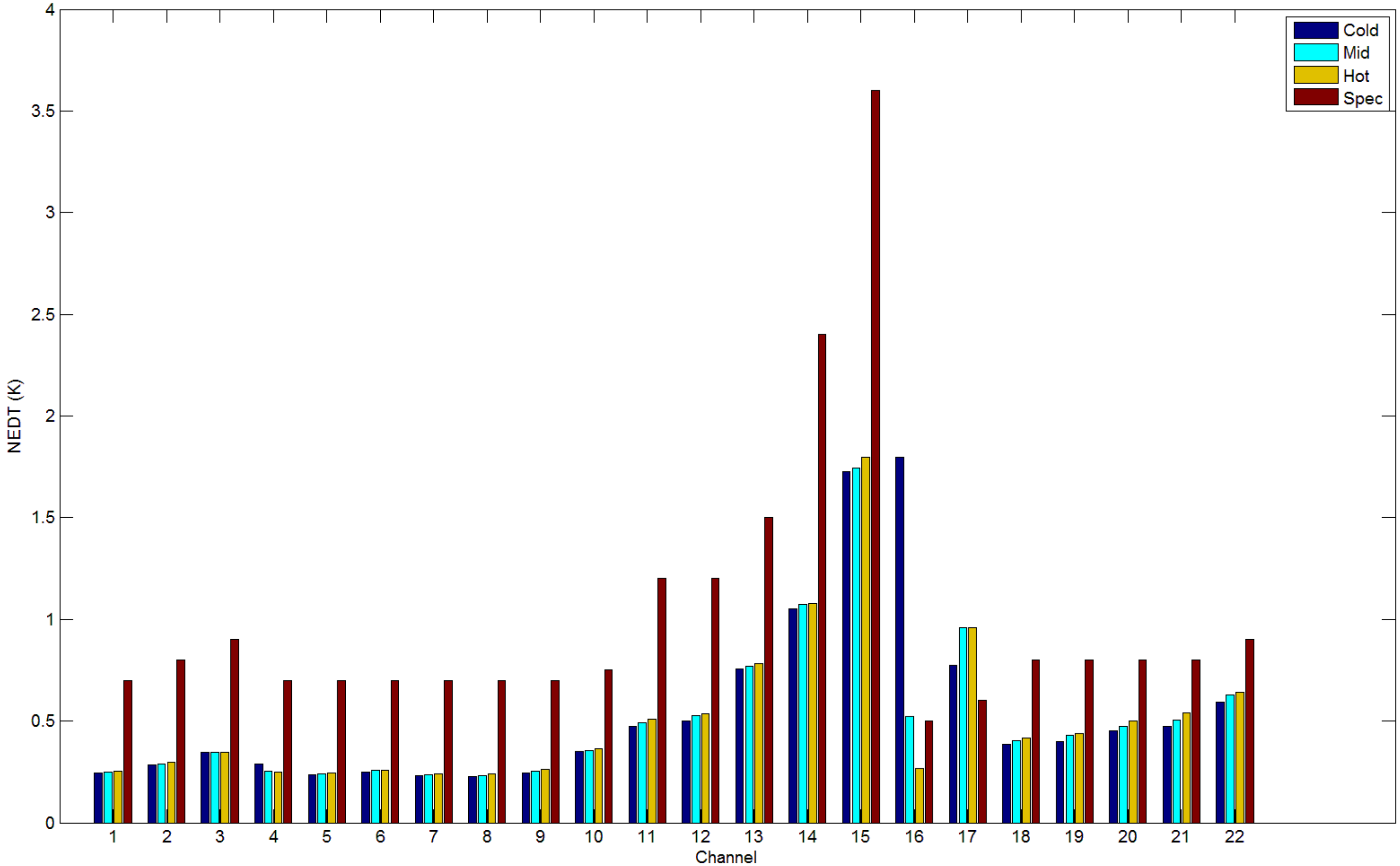

JPSS1 ATMS On-Orbit Accuracy

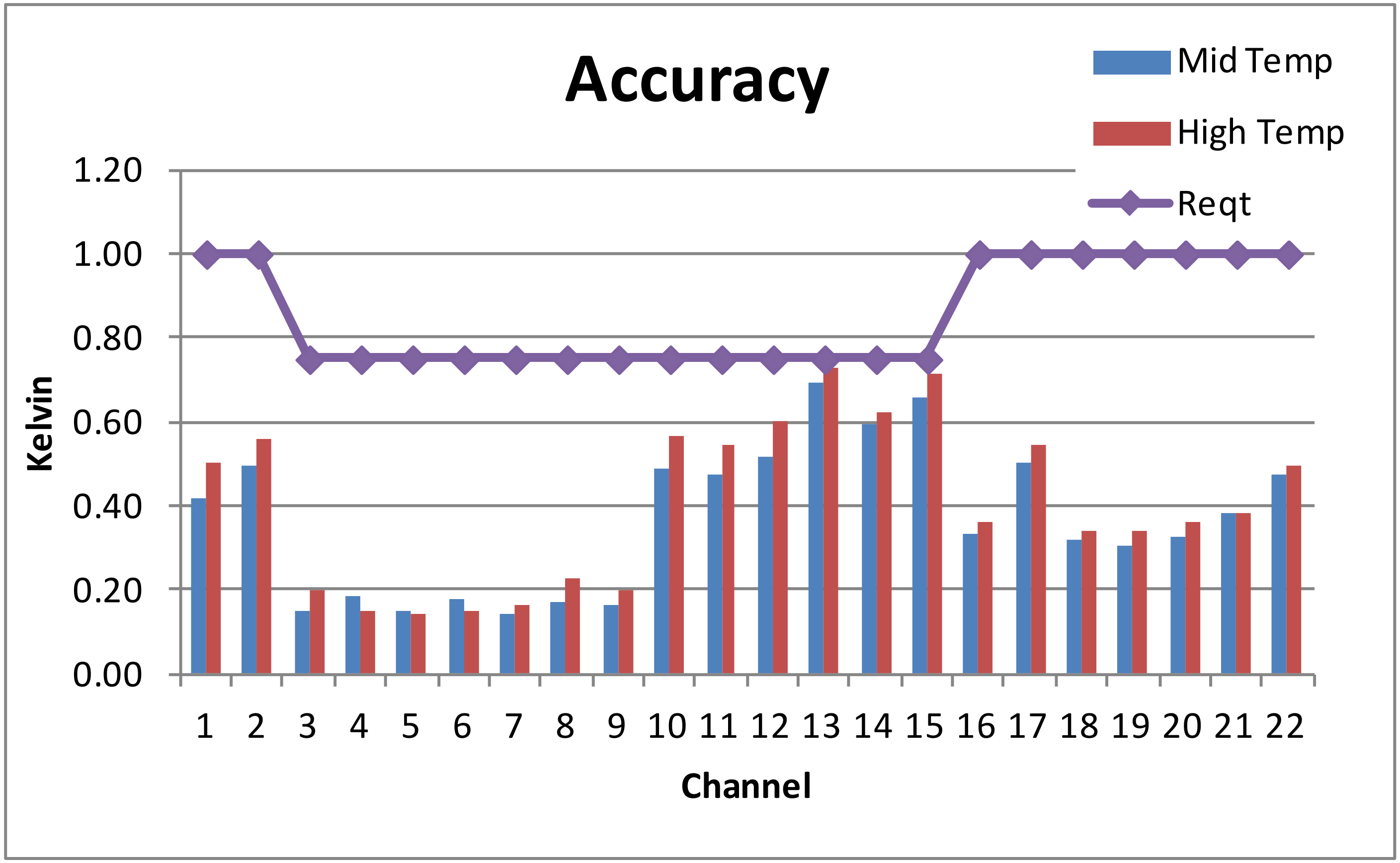

- Worst Case of 4 Redundancy Configurations
- All channels compliant

NORTHROP GRUMMAN

Radiometric Transfer Functions

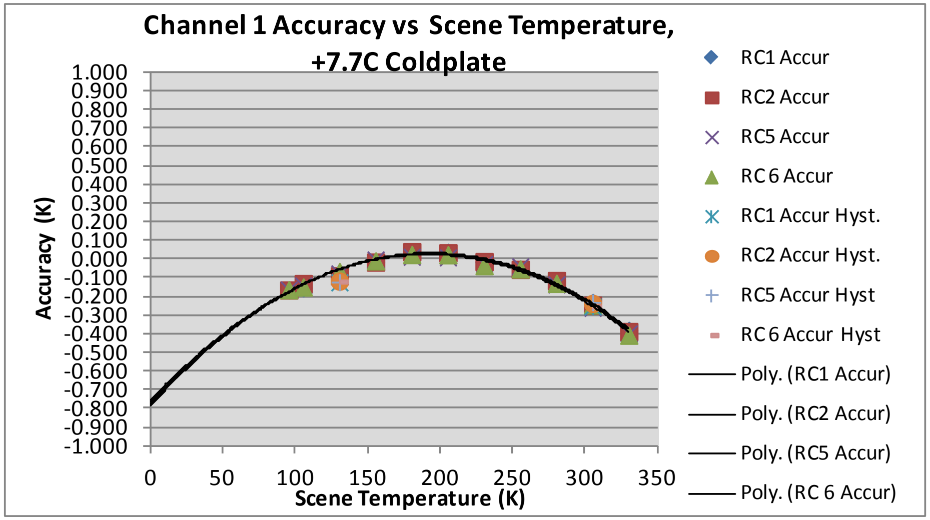

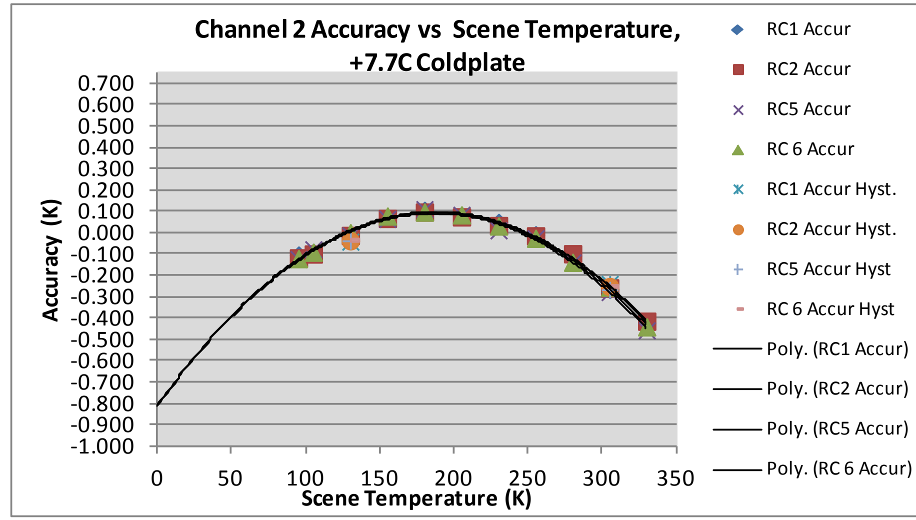

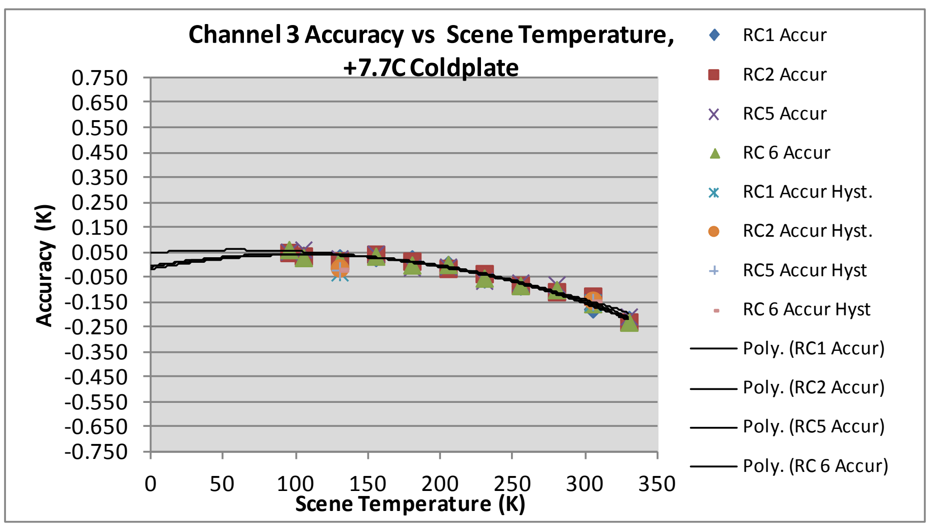

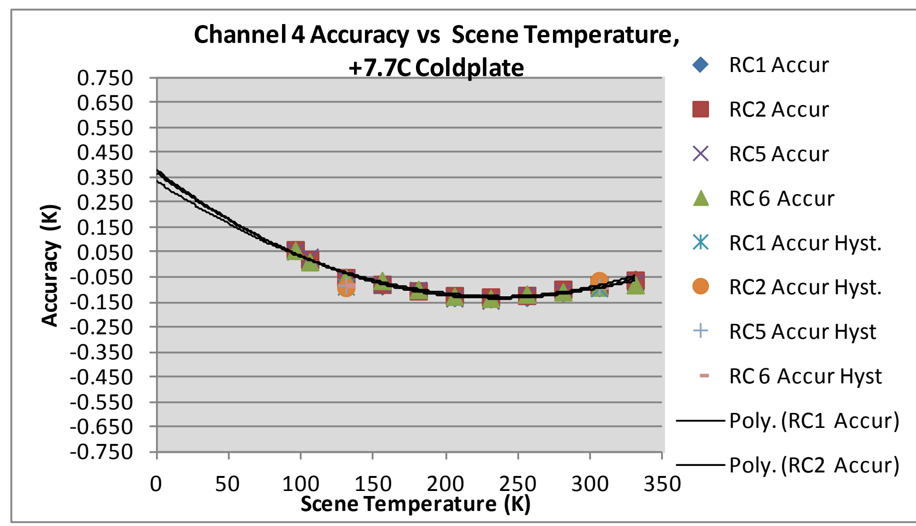

Radiometric Transfer Functions(cont.)

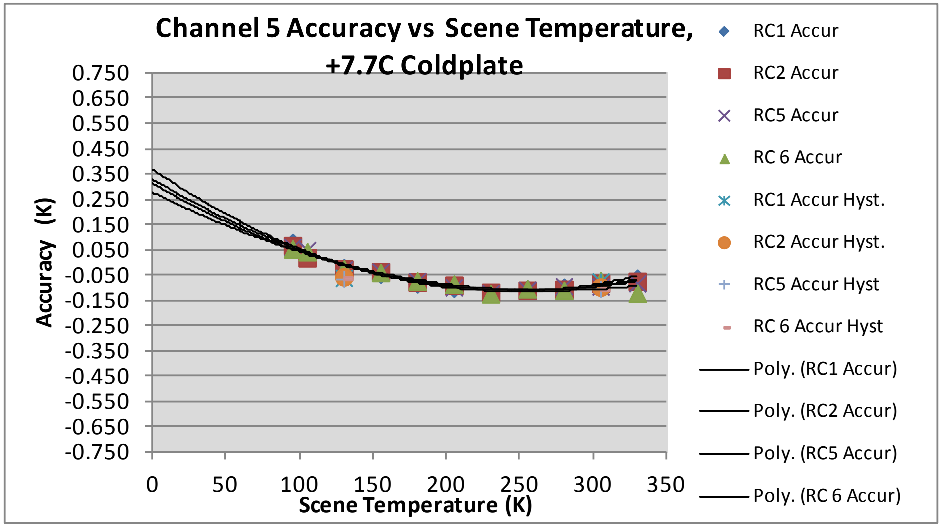

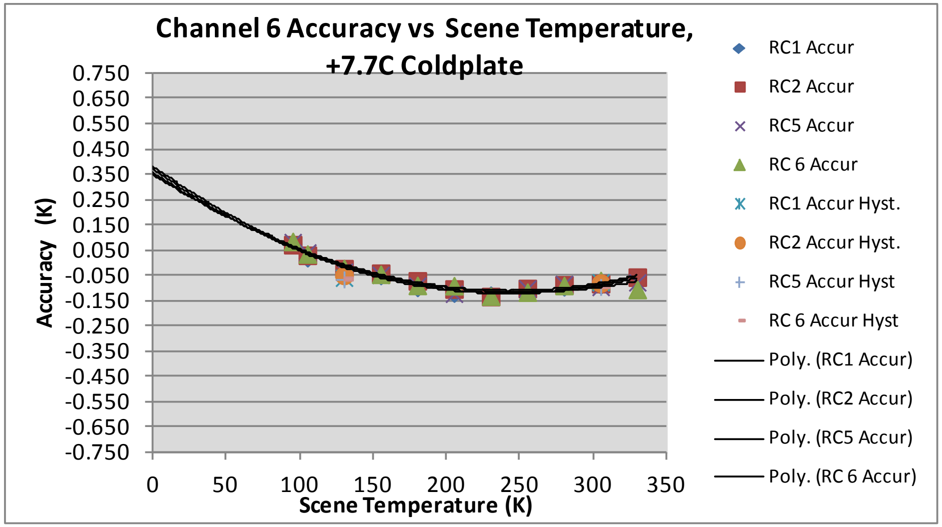

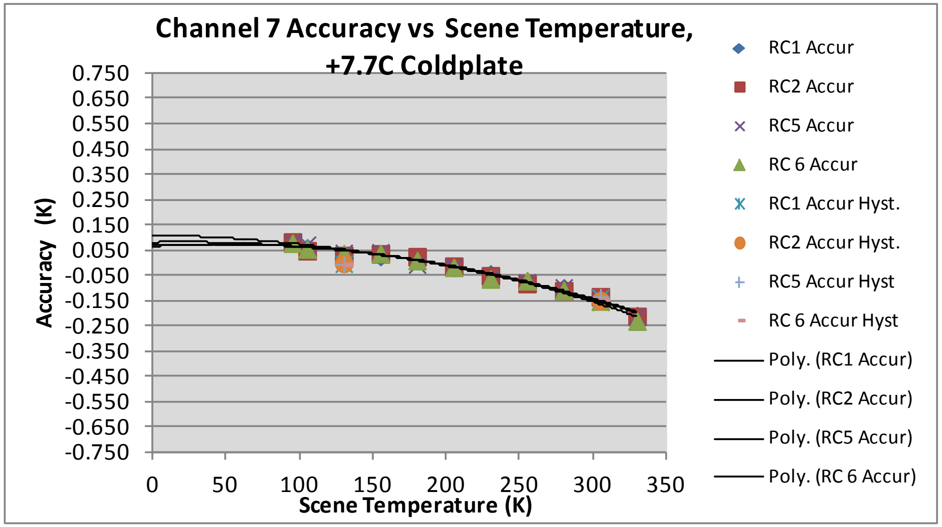

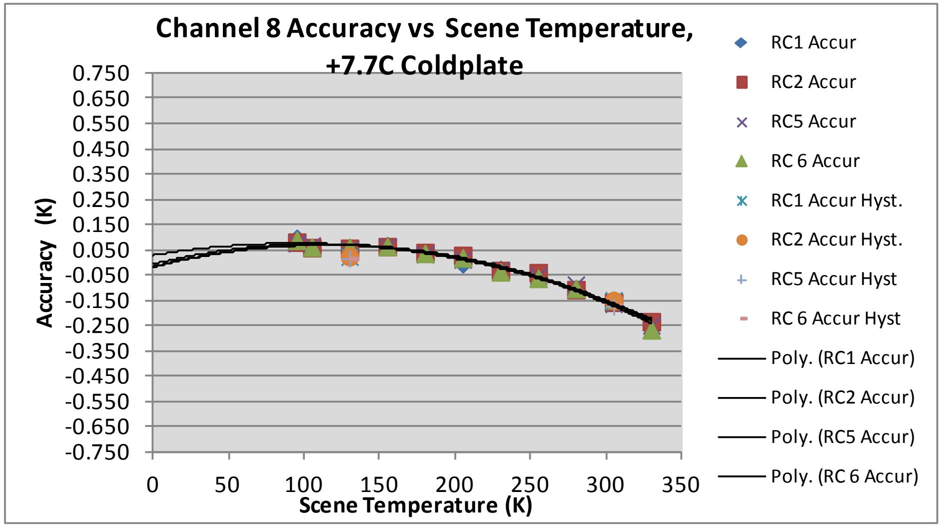

Radiometric Transfer Functions(cont.)

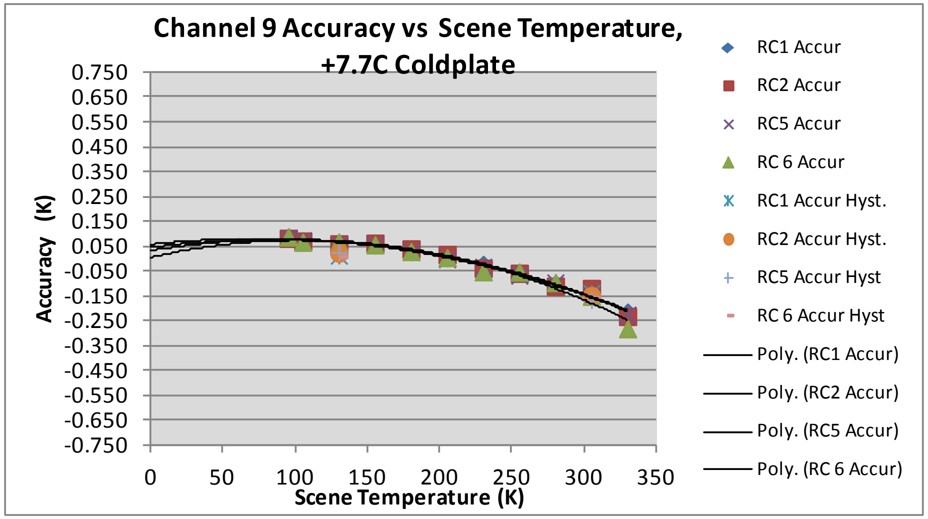

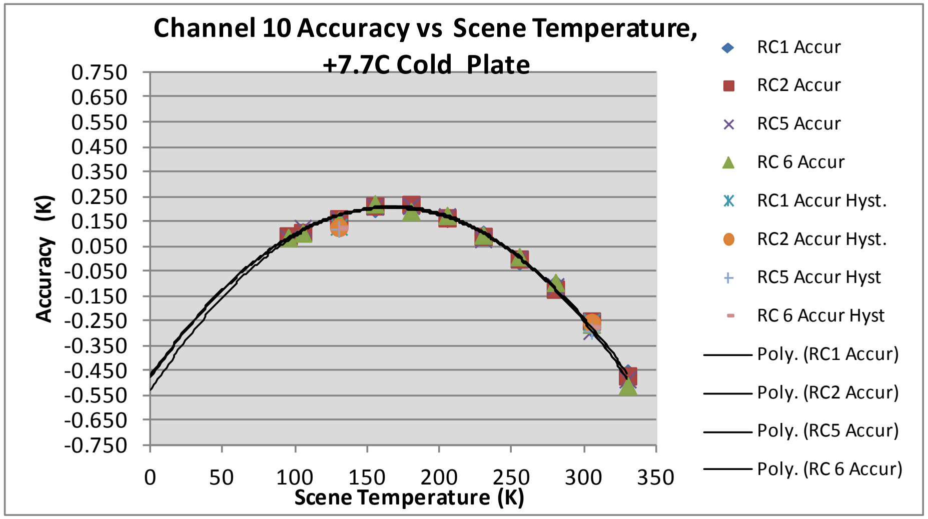

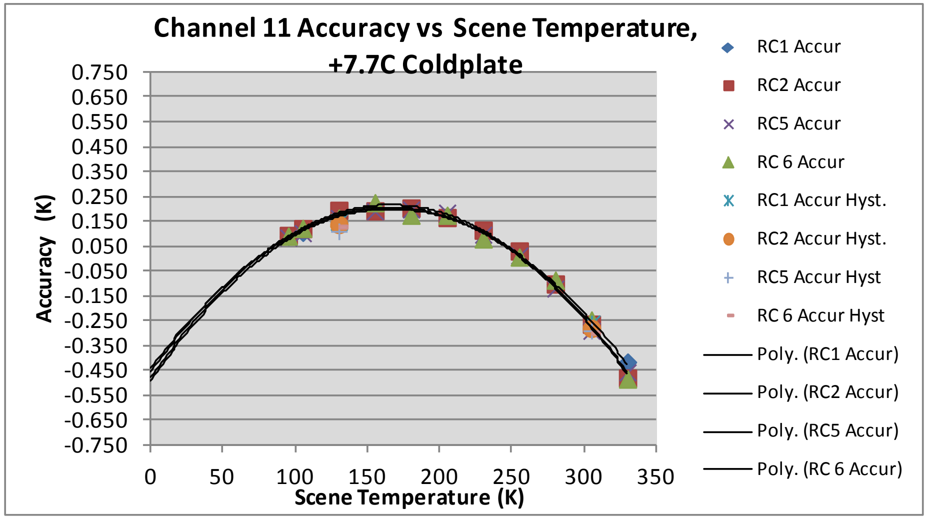

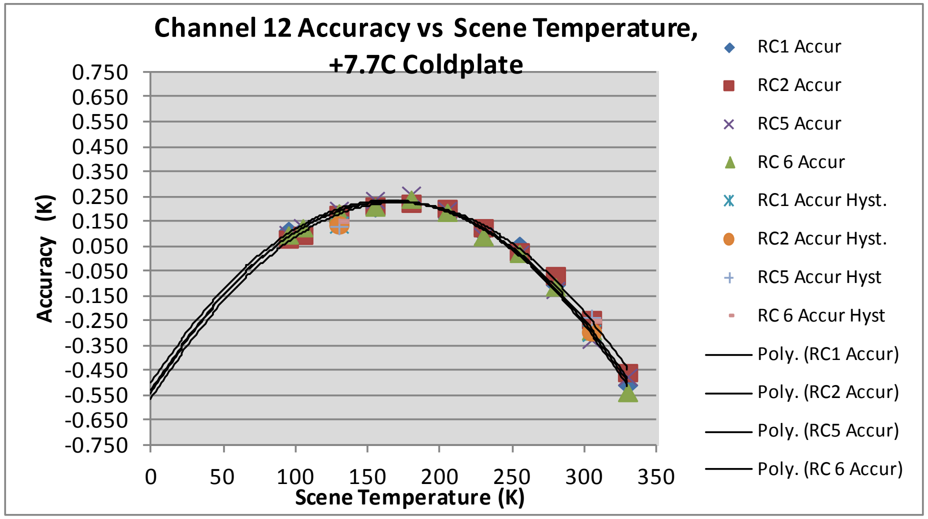

Radiometric Transfer Functions (cont.)

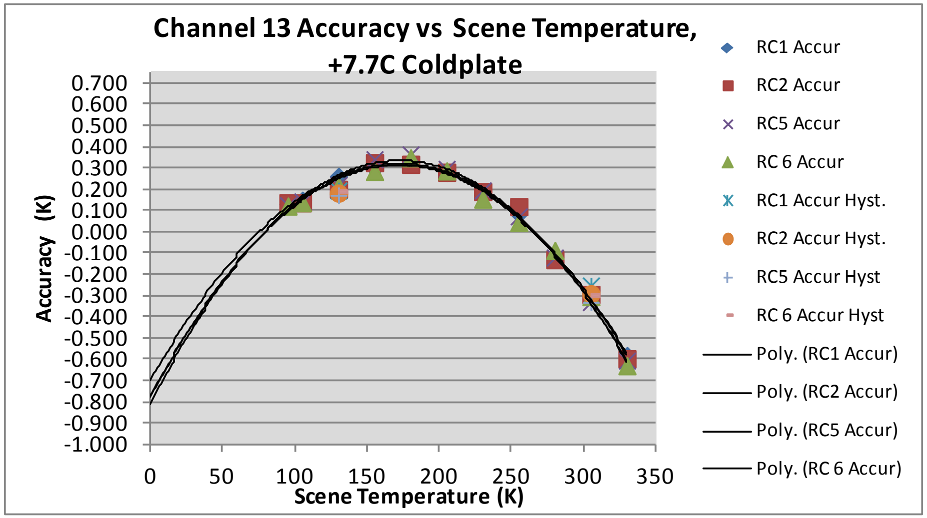

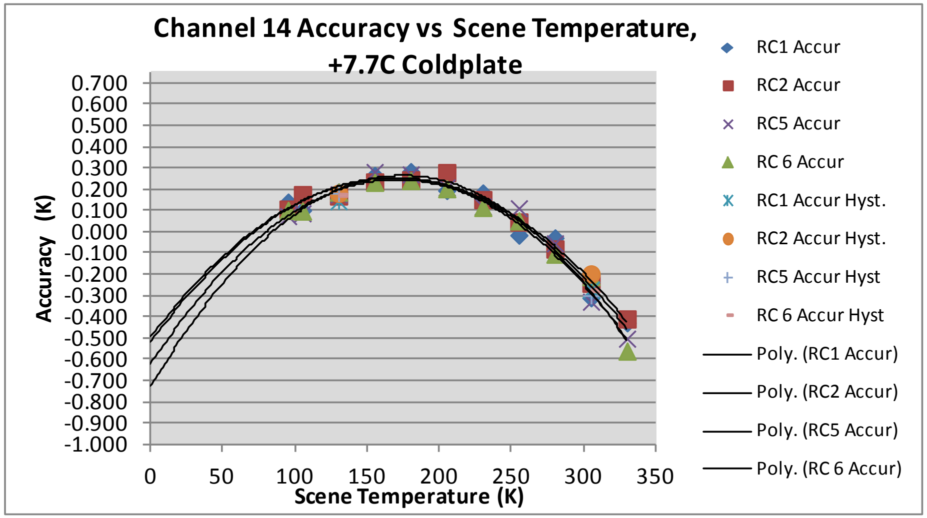

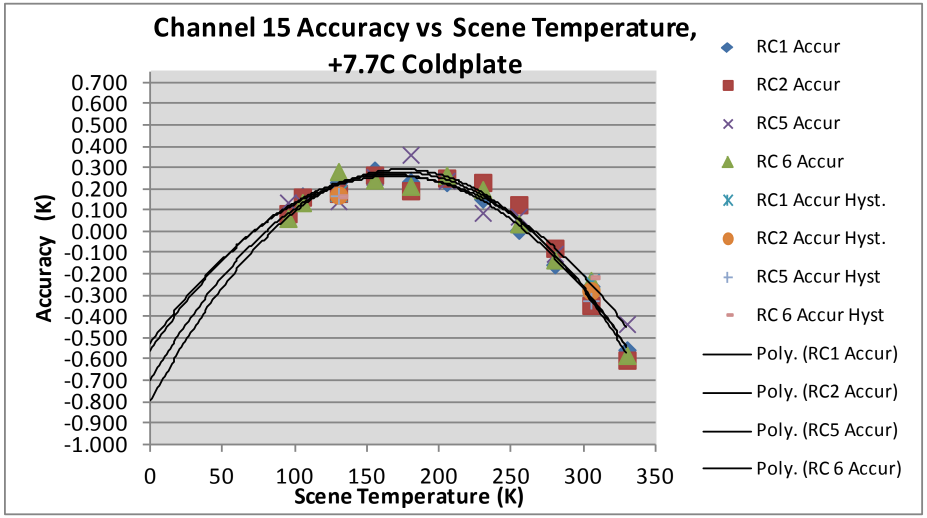

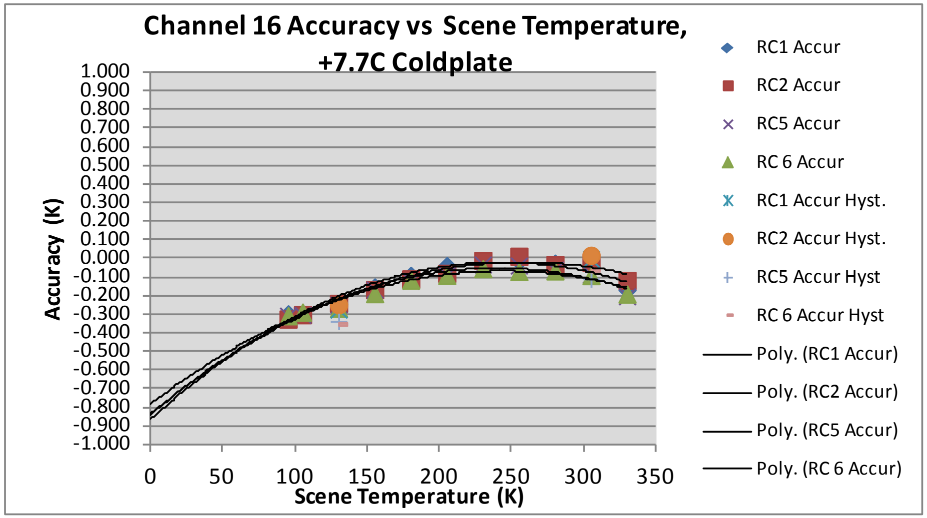

Radiometric Transfer Functions (cont.)

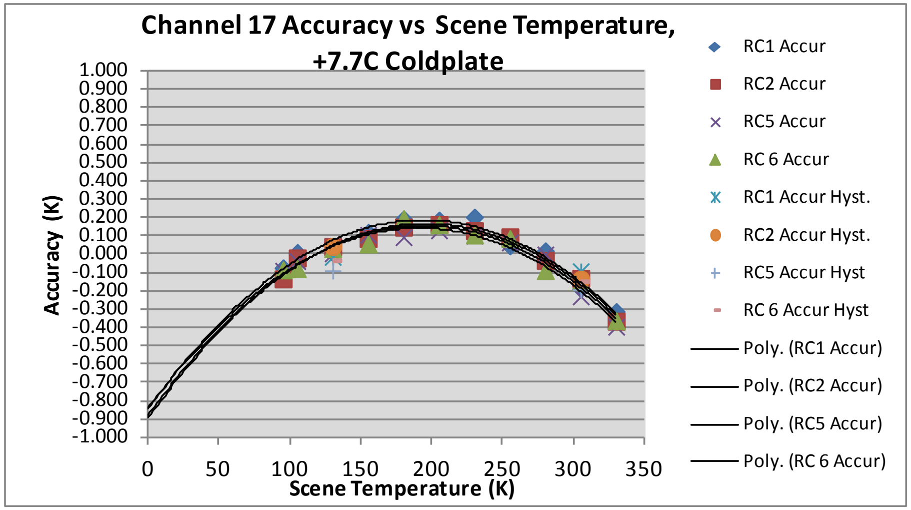

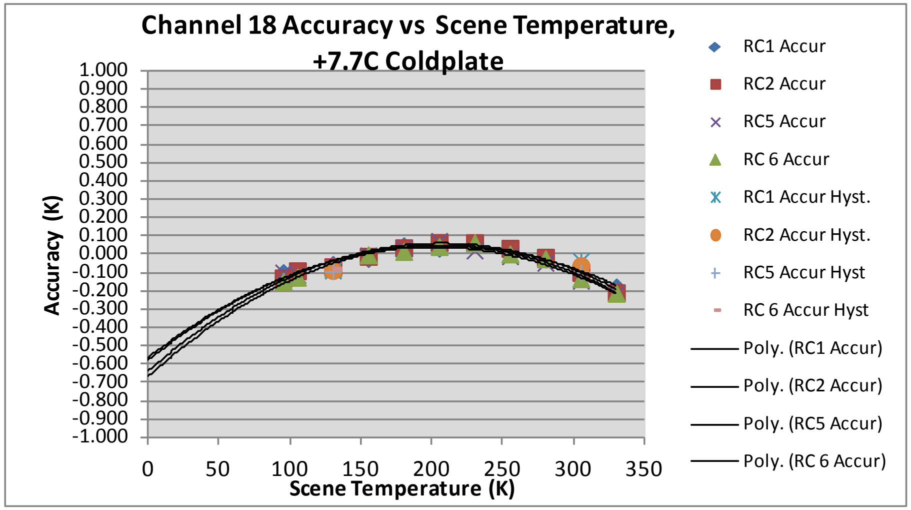

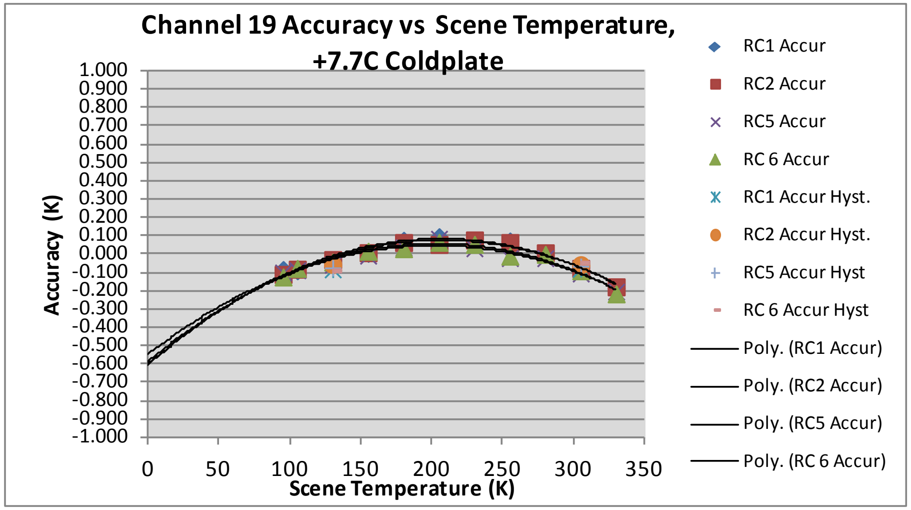

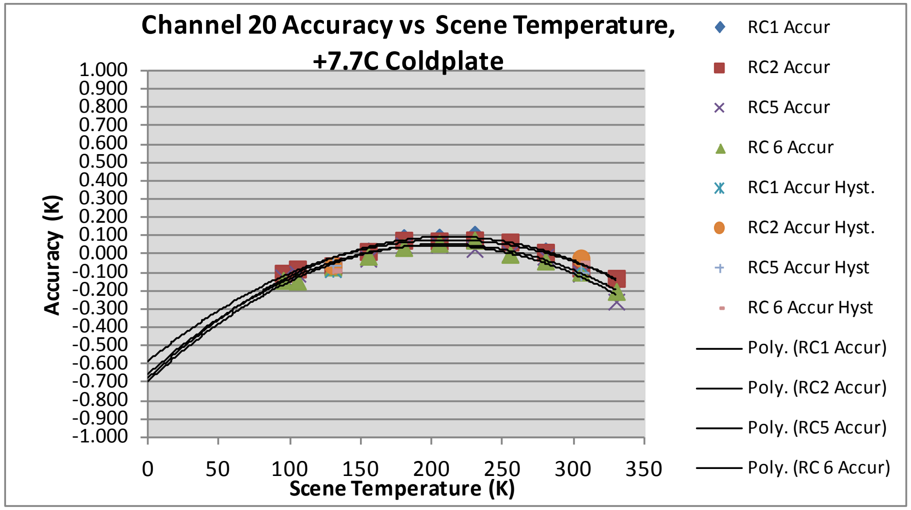

Radiometric Transfer Functions (cont.)

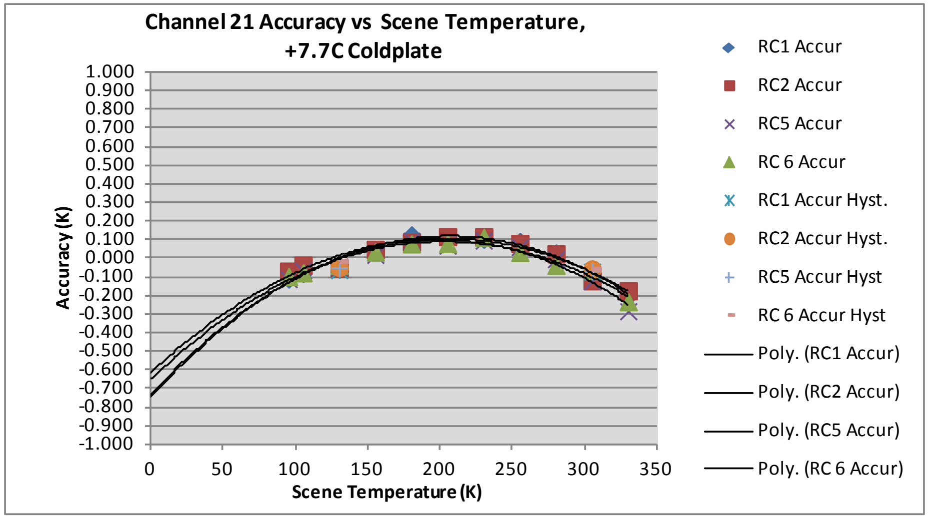

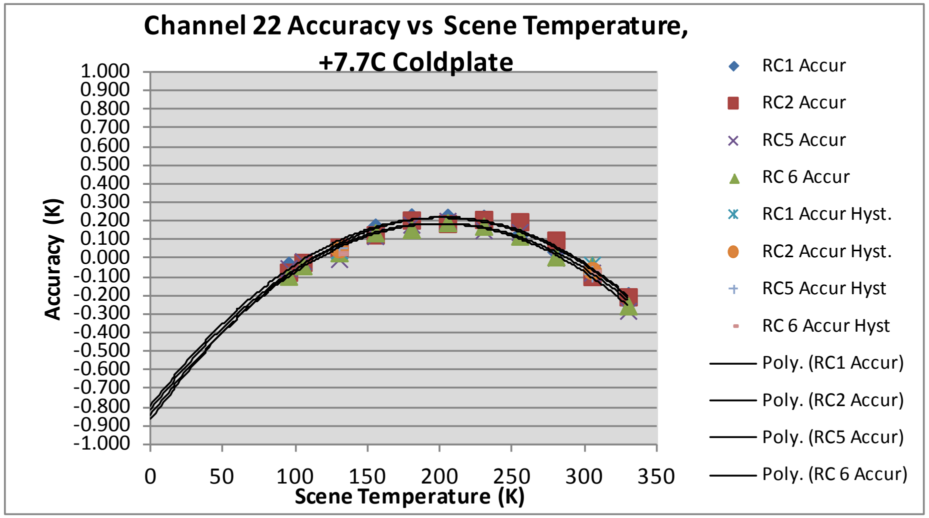

- Consistency between 4 redundancy configurations
  - Indicator of measurement repeatability
  - Feasible to use one set of curves for all 4 redundancy cases

Lunar Intrusion Alternate Scheme

Get *actual* cold space obs by changing to an uncontaminated scan profile (SP #1 ->#4) during LI. Example LI case below. The data outside the yellow ticks are good SV data. The dashed line is treated as previously good SV, which is adopted to replace the contaminated SV data. **Note the TB offset that could result unless gain variations can be predicted.**

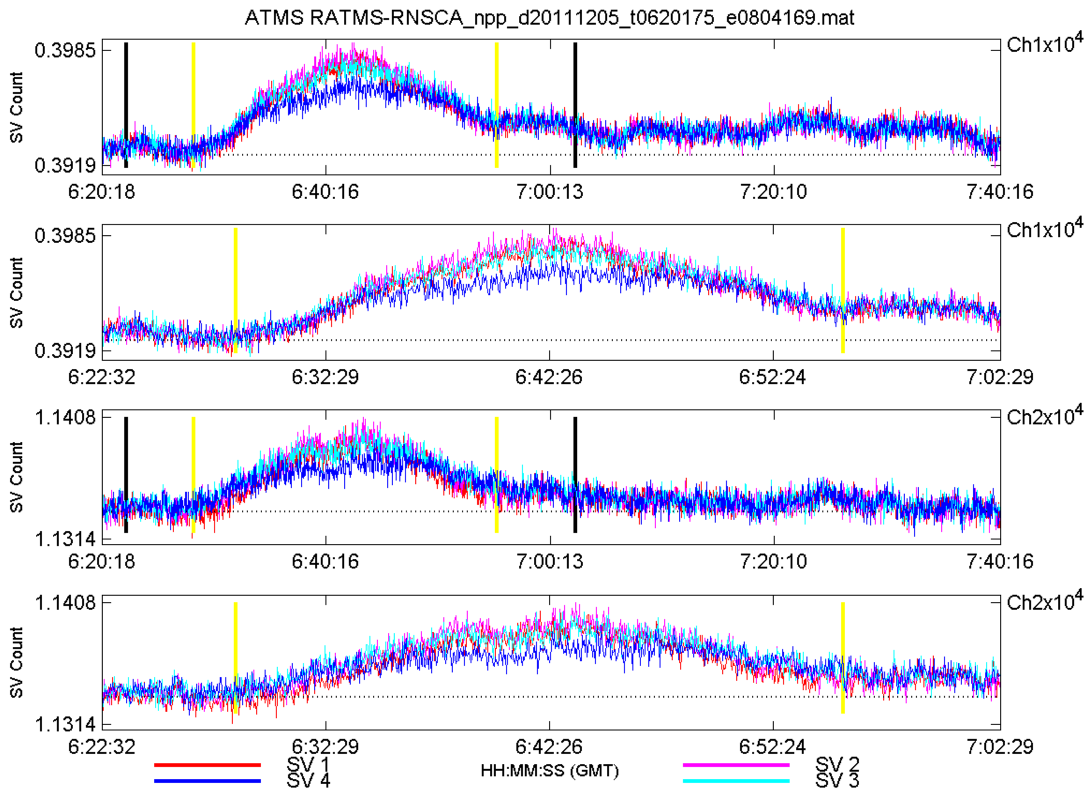

80 min

40 min

80 min

40 min

All 4 Ch 1 SV pixels are LI contaminated between yellow tick lines. Note that **the SV counts did not return to the level prior to LI (due to random gain changes).**

Remarks on Alternate LI Mitigation

- Switching scan profiles has already been done on orbit with S-NPP, and can be done over polar regions to minimize impact.
- Losing a few scans over the polar region is better than the worst LI correction cases, which could last for 25 min or longer.
- Since contaminated obs are replaced by un-contaminated actual obs, there should be no additional error.
- During commissioning, after switching between SP #1 and #4, no bias was found.
- This LI mitigation approach by switching between different SPs should work for all ATMS 22 channels. Namely, with proper SP selection (when applicable), there should be sufficient number of SV pixels that can be used for producing the SDR product uncontaminated by LI.

Inter-channel Correlation Coefficients

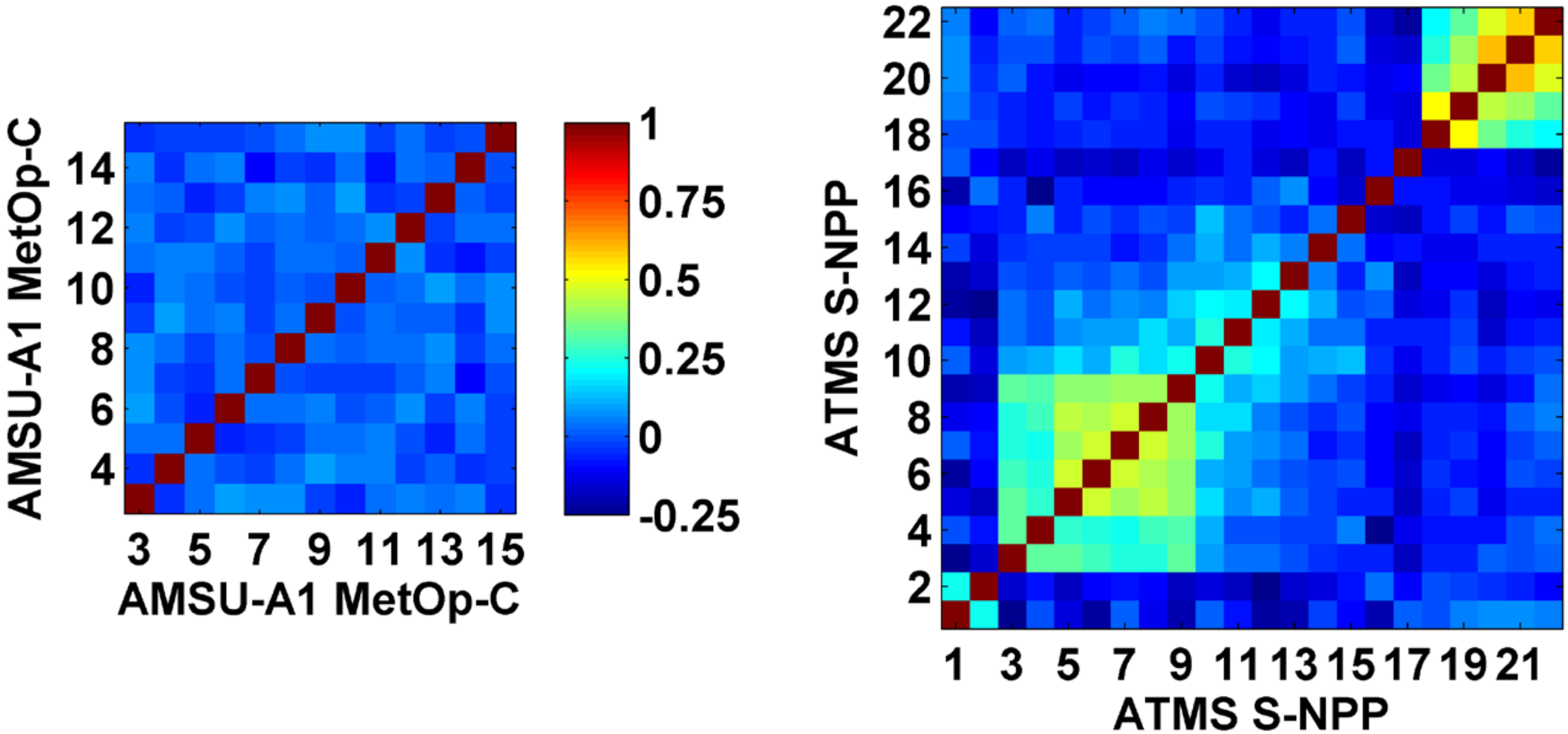

Correlation Coefficients of (left) AMSU-A1 and (right) ATMS Channel Gains.

NEDT for J-1 and NPP at Mid Cold Plate Temp Interpolated to 300K

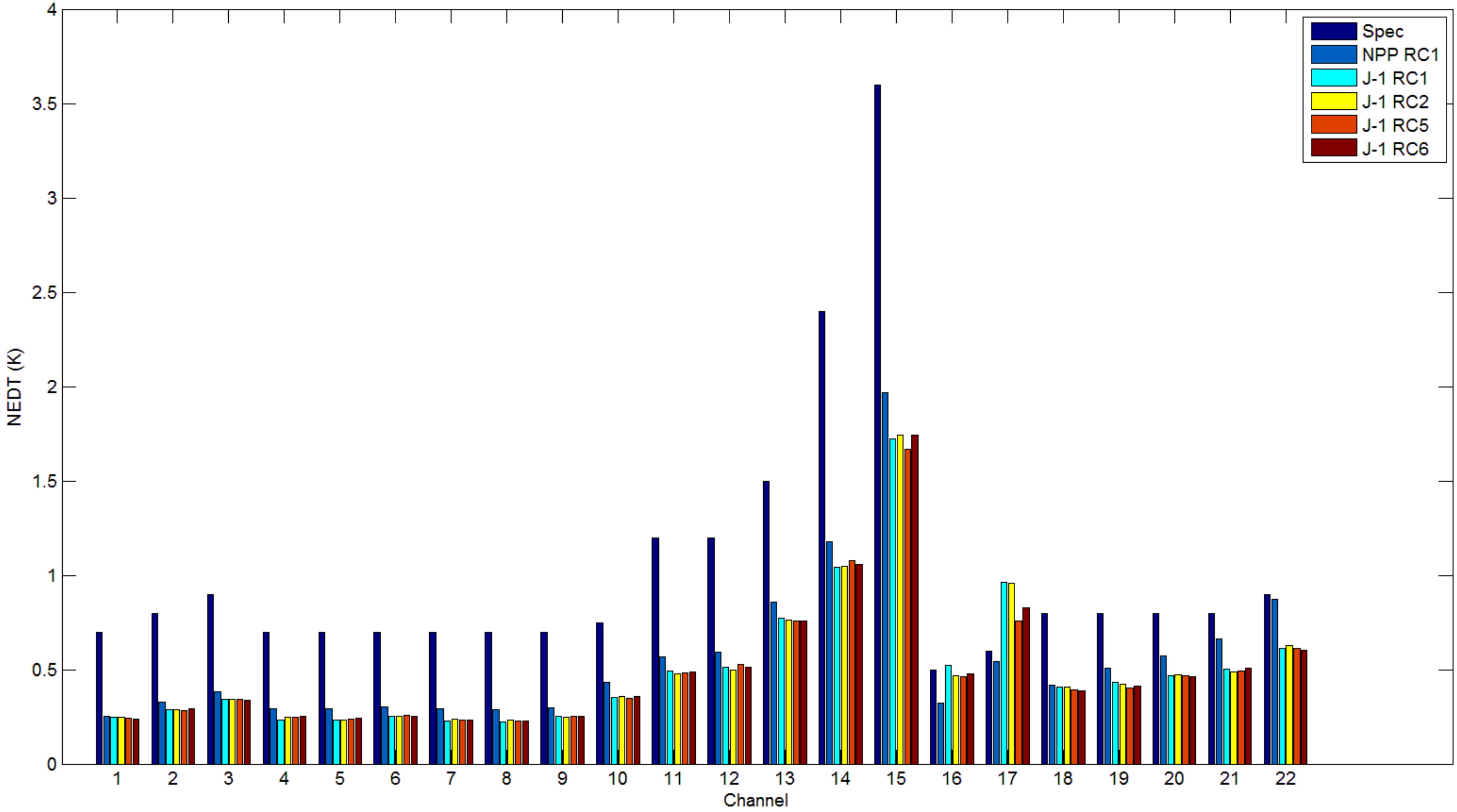

“Striping”

- All microwave imagers exhibit striping at some level—e.g., evidence is now being found of striping on AMSU, MHS, etc.—yet no NWP users saw striping-related issues with forecasts that used AMSU, MHS, etc data.

- The striping observed with S-NPP ATMS is not exceeding any hardware specs.

- Even so, ground processing changes (averaging) are being considered to somewhat reduce the existing striping. Such changes can be applied to S-NPP & J1-J3 ATMS without requiring any hardware changes.

- NWP users must therefore demonstrate the quantitative impact on forecasts from ATMS striping before any hardware changes can be considered. Even then the timeframe would be J4+.

NGAS Support to ATMS SDR CalVal

Degui Gu

May 13, 2014

Outline

- NGAS activities in support to ATMS SDR Cal/Val
- Lunar intrusion correction update and assessment of residual errors
- Striping error assessment and mitigation
- J-1 ATMS Channel 16 gain dropout waveform reconstruction
- Summary and future plan

NGAS Activities in Supporting ATMS CalVal

- Validation of ATMS SDR and Remap SDR data product quality performance
  - ATMS calibration accuracy and scan dependent biases
  - Remap SDR quality (B-G approach)
  - Geolocation
- DR investigations
- ATMS SDR algorithm code and LUT updates
  - Lunar intrusion detection and correction
  - G-ADA processing and testing
- Striping noise assessment, root cause analysis, and mitigation
- Support to J-1 sensor performance test and characterization
  - NEdT
  - Striping (gain stability)
  - Nonlinearity
  - Calibration accuracy
  - Anomaly identification and characterization

THE VALUE OF PERFORMANCE.

NORTHROP GRUMMAN

Lunar Intrusion Correction Code and LUT Update

Lunar Intrusion: Cold Counts Contaminated by Moon in Space View

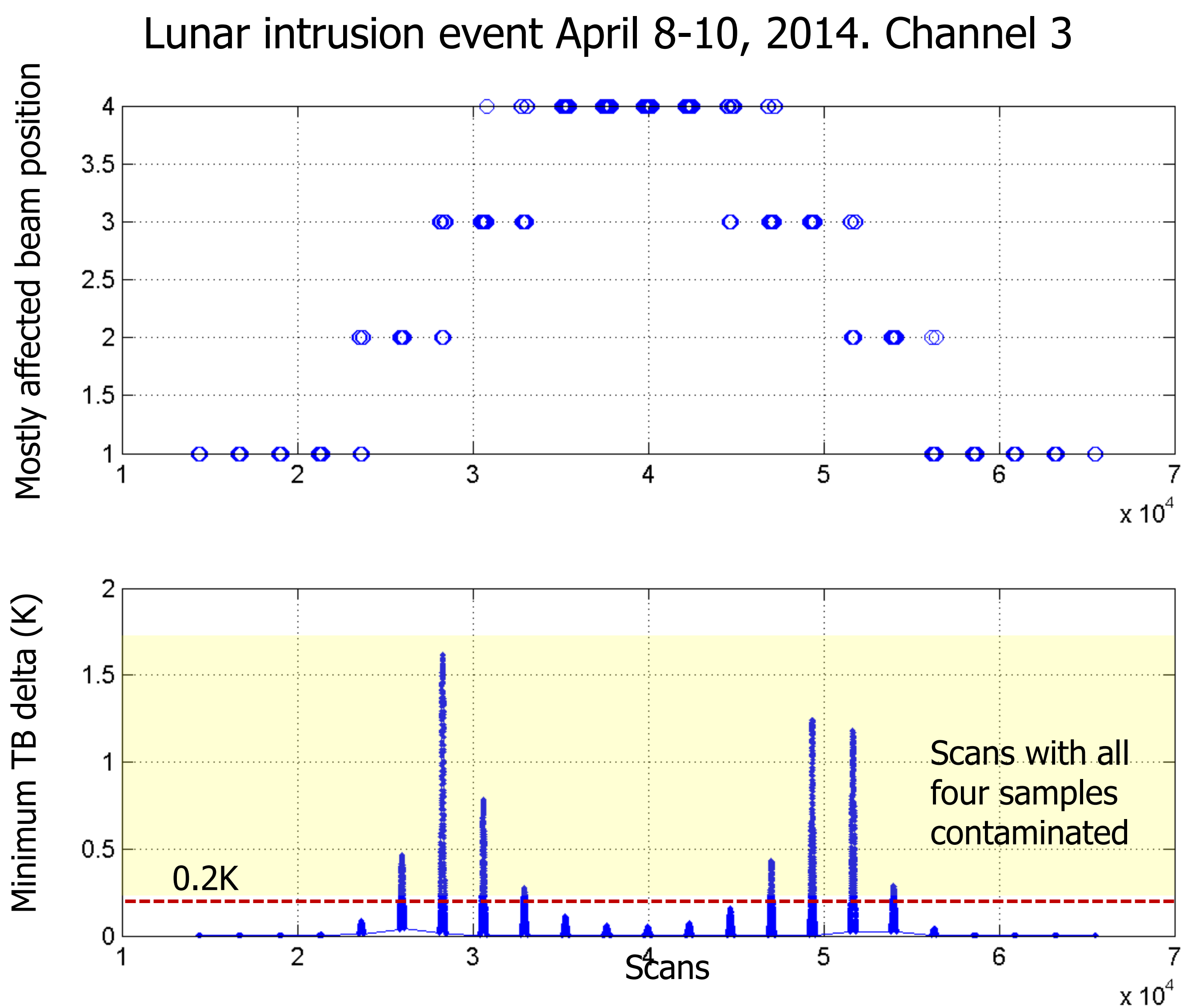

ATMS Lunar Intrusion Issues Before Code Updates

- NGAS found a coding error in ATMS operational algorithm software that caused the algorithm fail to correct for lunar intrusion, resulting up to ~1K errors in the affected ATMS SDR data products
- NGAS found the antenna beam size values in the PCT file are incorrect, causing lunar intrusion quality flags being triggered more extensive than needed to be
- ATMS SDR data gap could be produced if more than one space view samples are affected and the total number of “good” space view samples are less than 3
- Some other minor issues such as errors in NEdT calculation during lunar intrusion

Updated ATMS SDR Algorithm to Improve Lunar Intrusion Detection and Correction

NORTHROP GRUMMAN

- Fixed the software coding errors so that the lunar intrusion corrected space view counts are used to produce calibrated brightness temperatures
- Modified the algorithm to replace LI-contaminated space view samples with the uncontaminated good counts to avoid data gaps during lunar intrusion
  - If all four space views are affected by LI, good space view counts from the previous most recent scan are used
- Updated PCT file to use correct beam size values
- Code Update was implemented in MX8.3
  - Updated PCT implemented at a later time

Impact on ATMS SDR Data Product (1)

Before Update

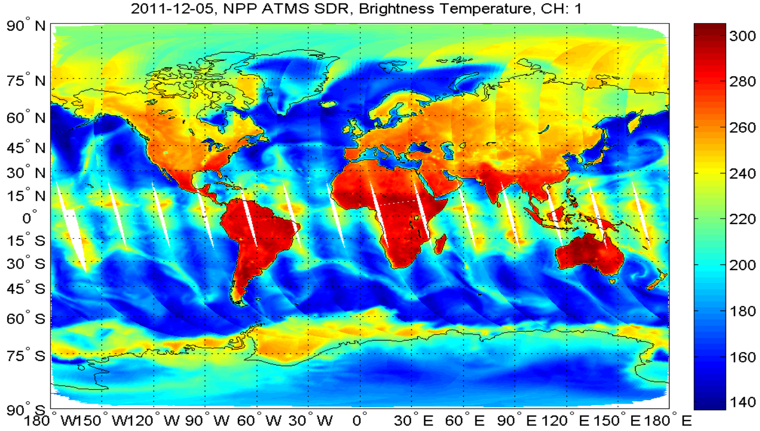

After Update

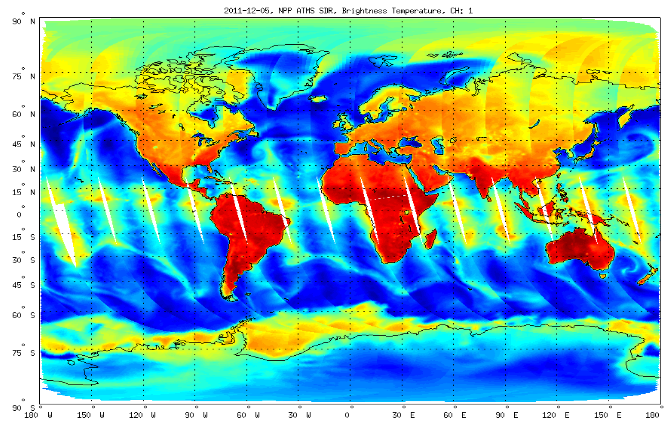

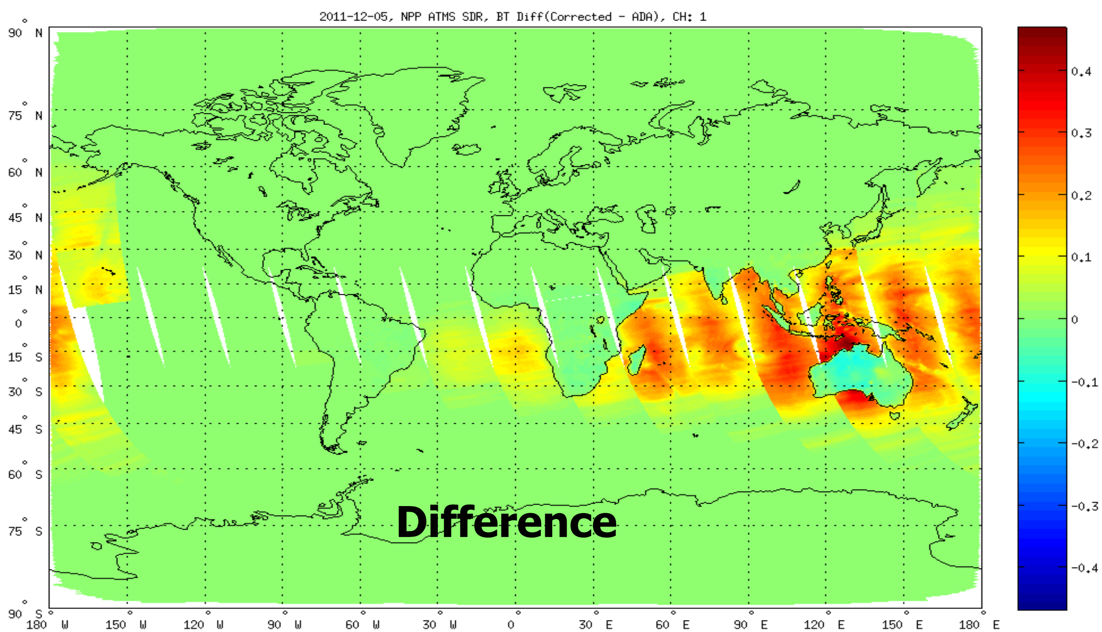

Impact on ATMS SDR Data Product (2)

Before Update

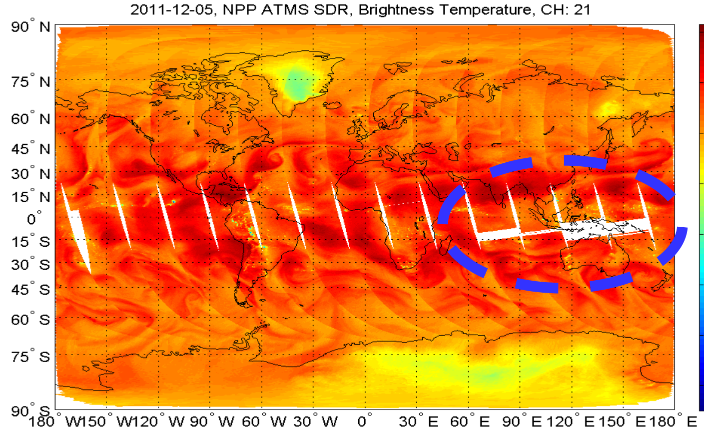

After Update

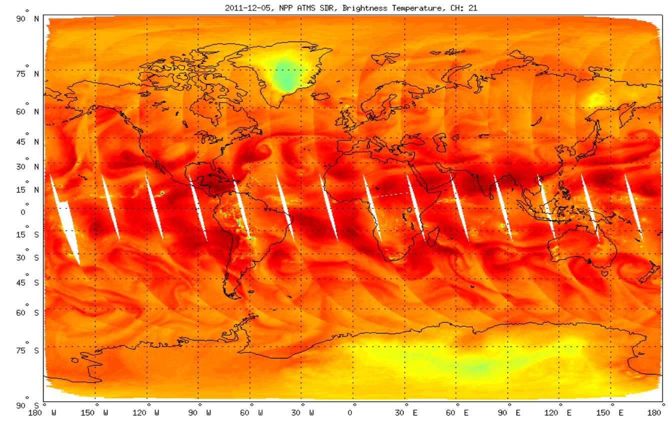

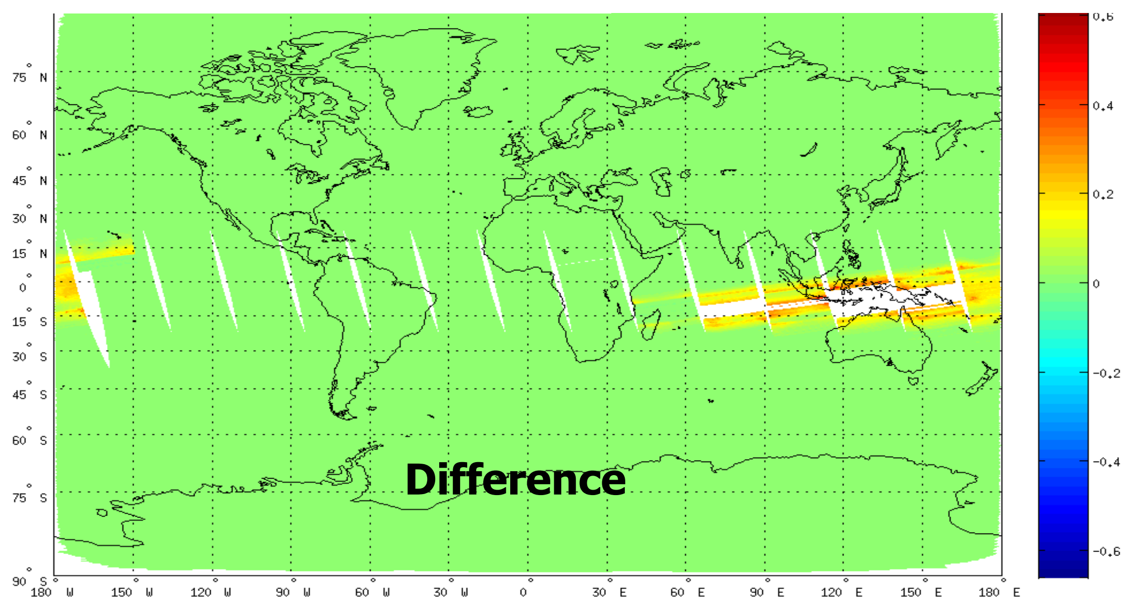

Assessment of Residual LI Correction Errors

- Residual LI correction errors can arise due to:
  - Uncorrected LI intrusion
    - LI affected cold counts not corrected if predicted TB increase < threshold of 0.2K (tunable)
  - Errors in the moon model
    - Simplified model for predicting space view temperature increases due to lunar intrusion
    - Moon position error (e.g., IDPS recently discovered code error)
  - Errors in the corrected cold counts
    - "Natural" changes in cold counts from last known uncontaminated sample to the current scan when all four samples are affected (duo to gain instability, orbital phase variation, etc.)
    - Reduced number of samples per scan (noisier calibration data)

On-orbit Cold Counts Variability

Estimated cold counts variability from autocorrelation analysis

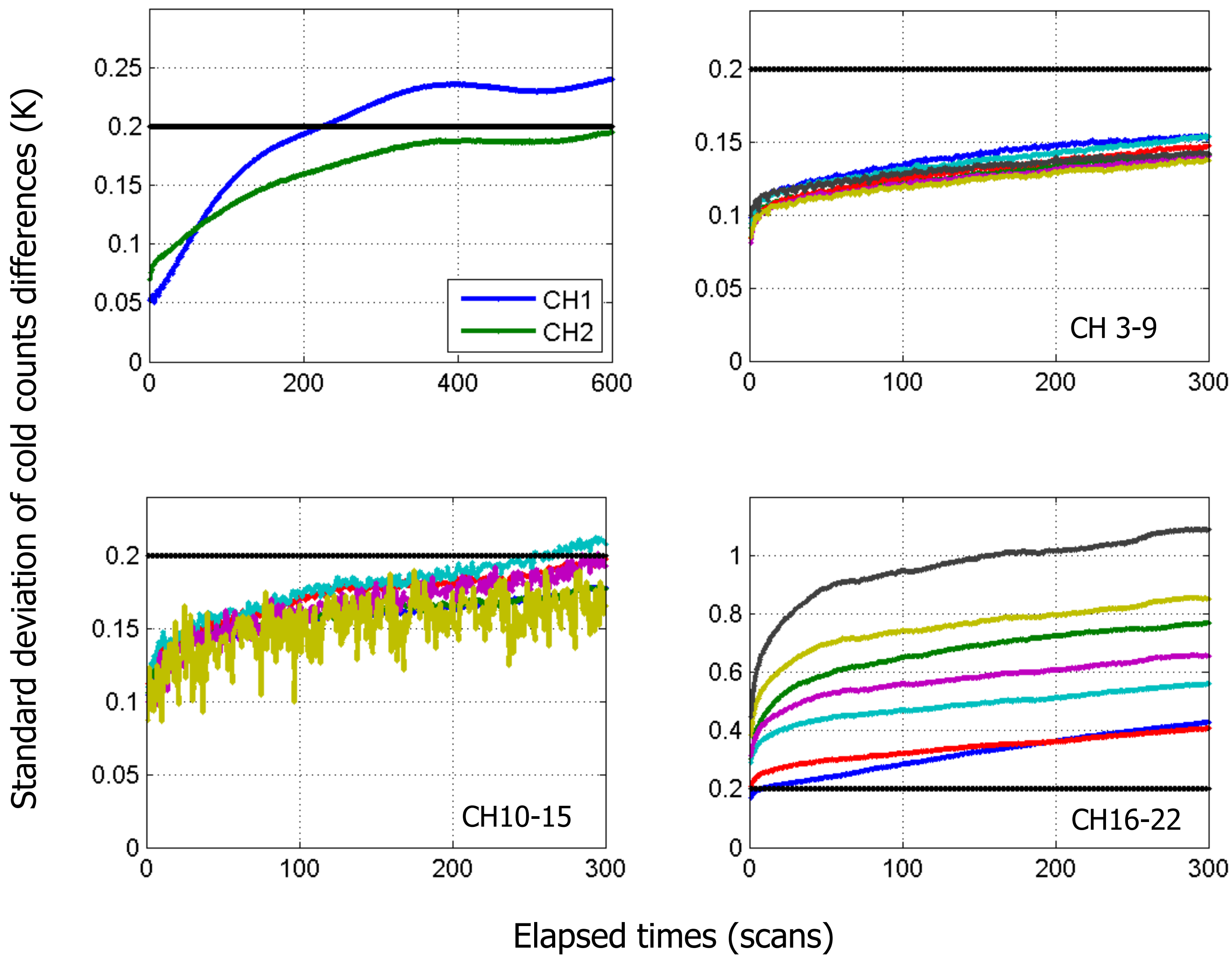

Estimated Residual LI Correction Errors due to Natural Cold Counts Variability

NORTHROP GRUMMAN

- Residual LI correction Errors will result only when all four space view samples are contaminated
- Nominal number of scans when all four space view samples are contaminated (dependent of FOV size)
  - 500 scans for CH1-2
  - 200 scans for V and W bands CH3-16
  - Not yet encountered for G band channels
- Estimated cold counts error from using history data
  - CH1-2: ~0.2K
  - CH3-15: ~0.15K
  - Ch16: ~0.35K
  - CH17-22: N/A
- When history data is used, the cold calibration data can be noisier due to fewer samples being averaged, causing additional (sometimes dominant) calibration errors (e.g., channel 15)

Residual LI Correction Errors due to Cold Counts Noises

Channel 15 cold counts variability and effect of averaging

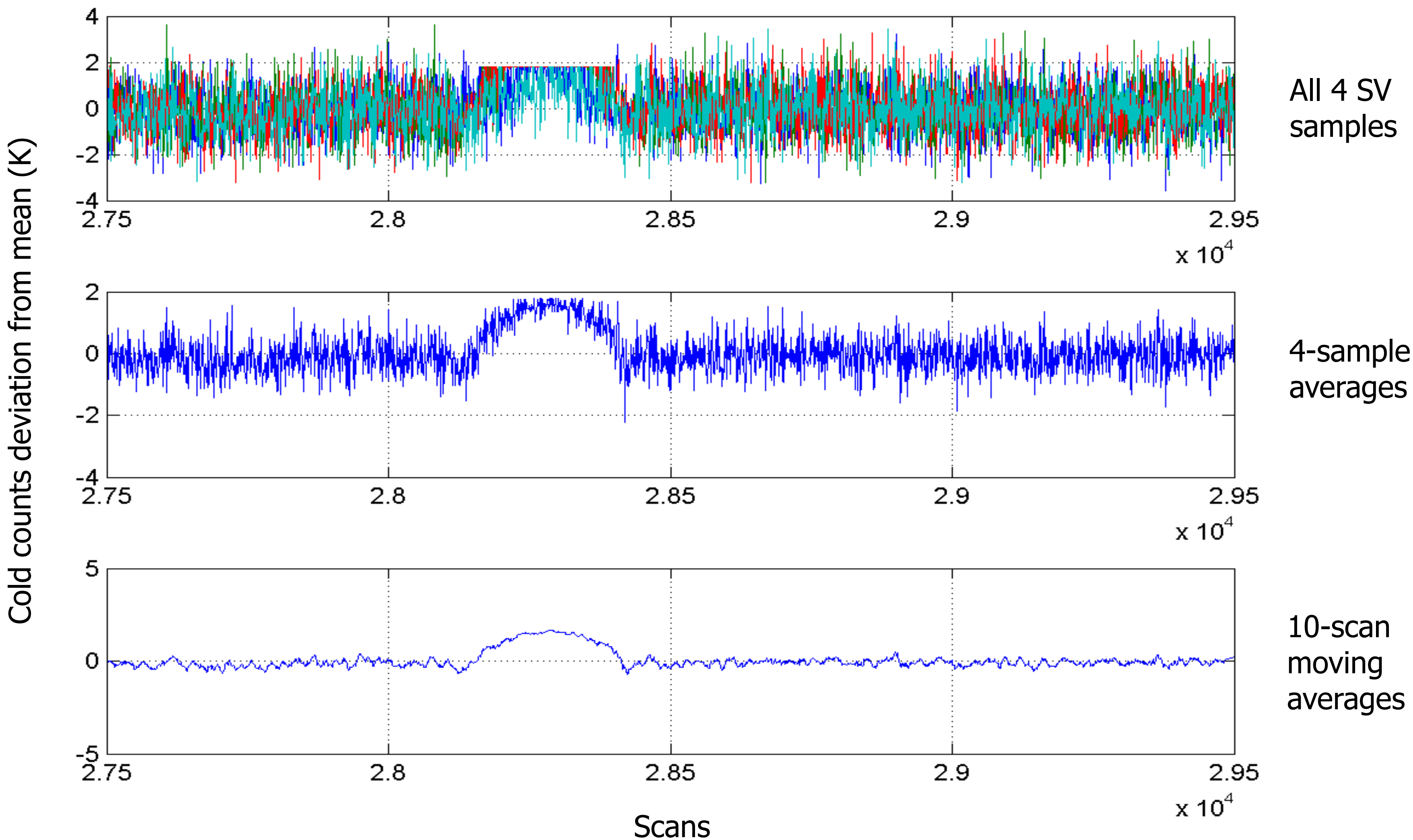

Channel 1 Residual Error Estimates

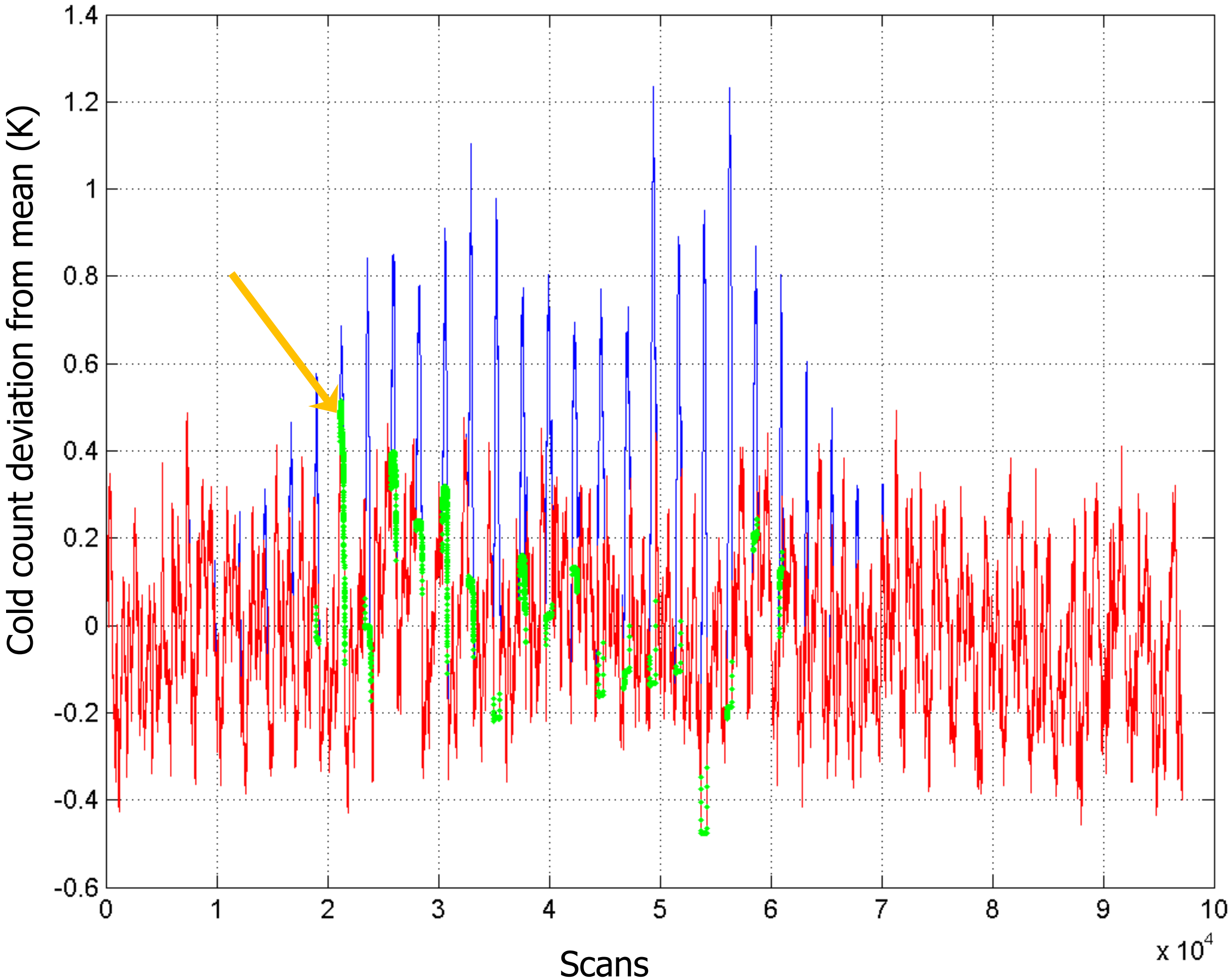

Blue: No LI correction
Red: After LI correction
Green: All four samples contaminated and history data used

Before LI Correction:
Worst cold count error: 1.2K
Median scene temp: 210K
Residual TB errors: 0.3K
Ocean: 180K, 0.45K

After LI Correction:
Worst cold count error: 0.5K
Median scene temp: 210K
Residual TB errors: 0.13K
Ocean: 180K, 0.18K

Channel 10 Residual Error Estimates

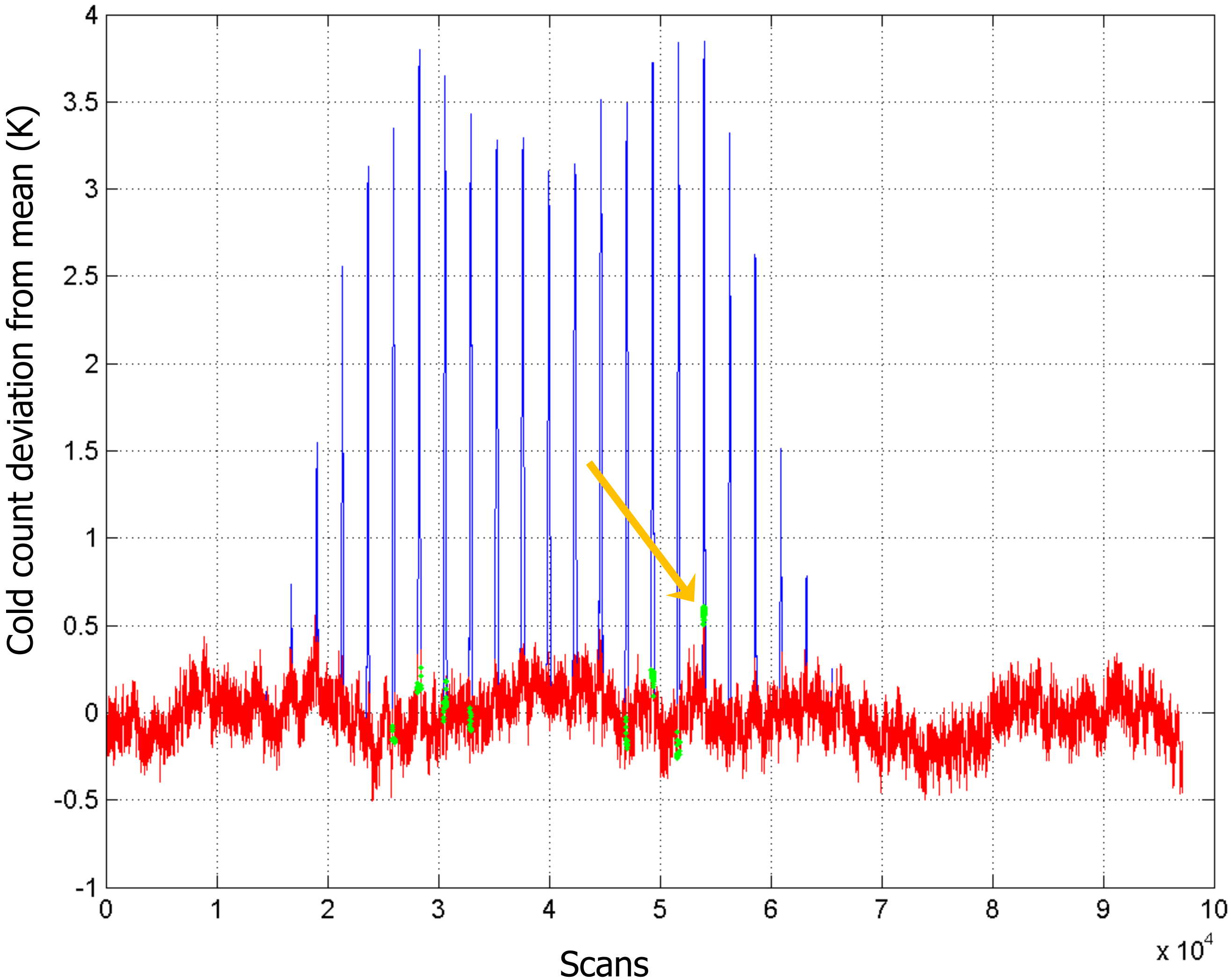

Blue: No LI correction
Red: After LI correction
Green: All four samples contaminated and history data used

Before LI Correction:
Worst cold count error: 3.5K
Median scene temp: 210K
Residual TB errors: 0.9K

After LI Correction:
Worst cold count error: 0.5K
Median scene temp: 210K
Residual TB errors: 0.13K

Channel 15 Residual Error Estimates

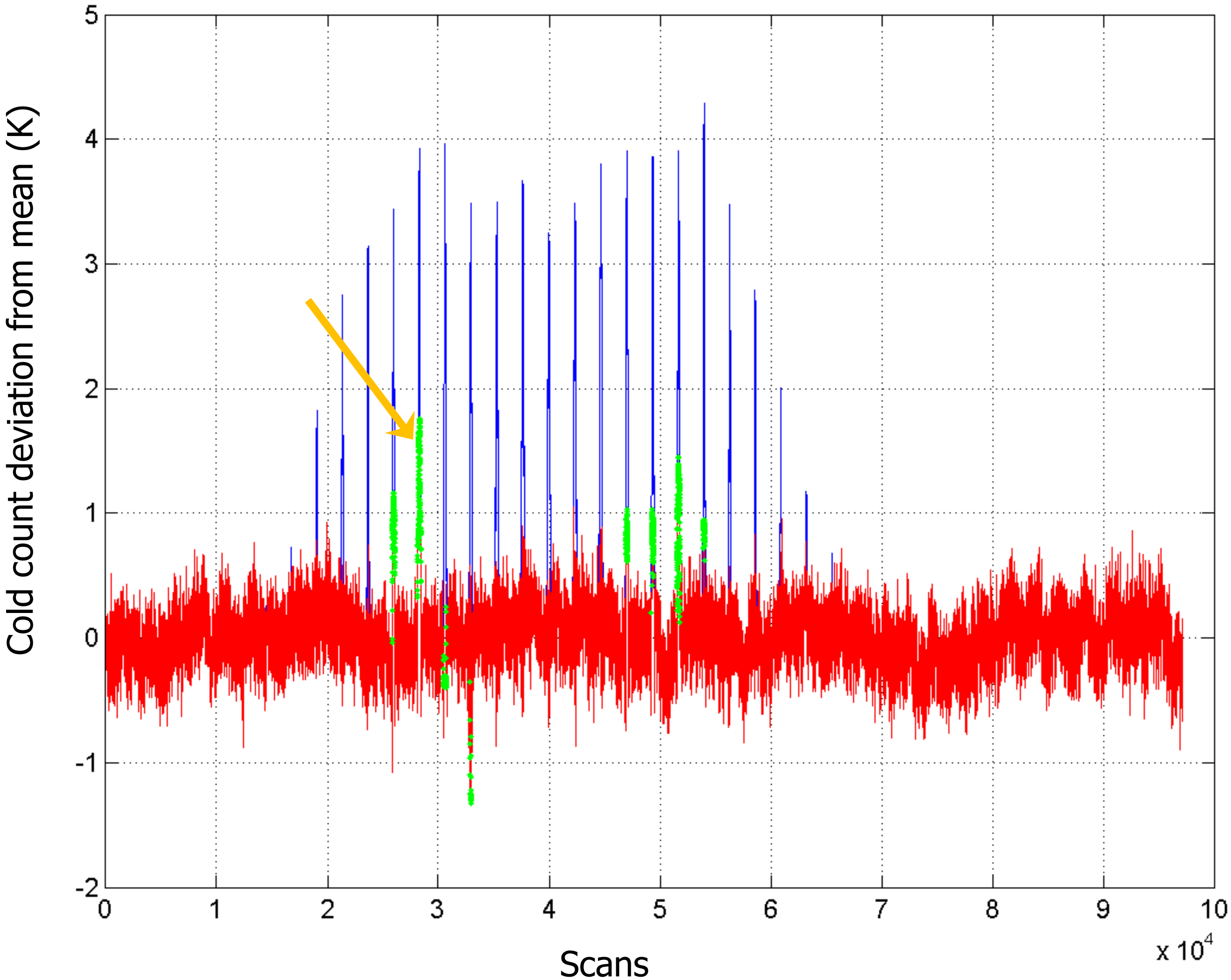

Blue: No LI correction
Red: After LI correction
Green: All four samples contaminated and history data used

Before LI Correction:
Worst cold count error: 4K
Median scene temp: 250K
Residual TB errors: 0.43K

After LI Correction:
Worst cold count error: 1.5K
Median scene temp: 250K
Residual TB errors: 0.17K

Channel 16 Residual Error Estimates

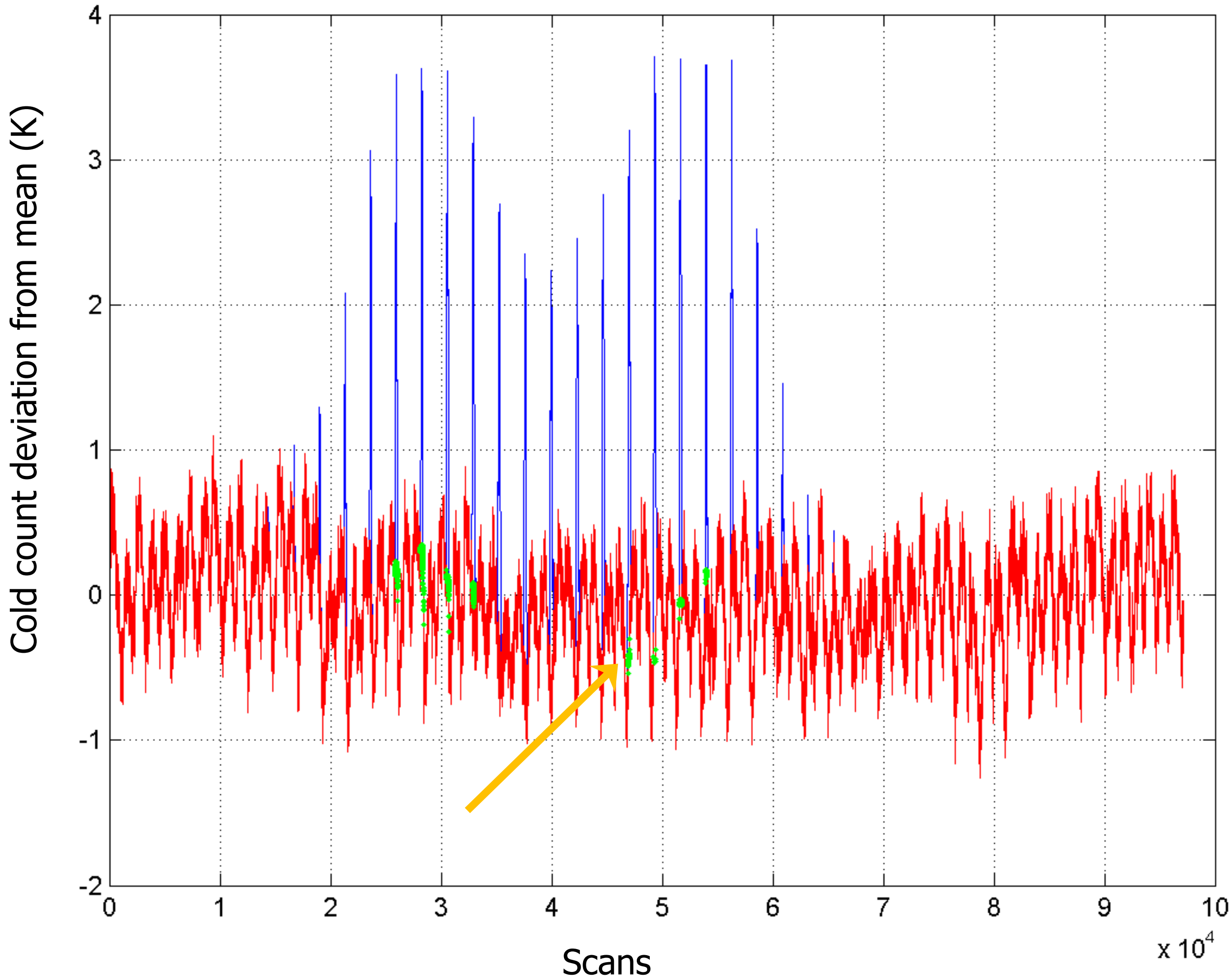

Blue: No LI correction
Red: After LI correction
Green: All four samples contaminated and history data used

Before LI Correction:
Worst cold count error: 3.5K
Median scene temp: 230K
Residual TB errors: 0.63K

After LI Correction:
Worst cold count error: 0.5K
Median scene temp: 230K
Residual TB errors: 0.1K

Channel 17 Residual Error Estimates

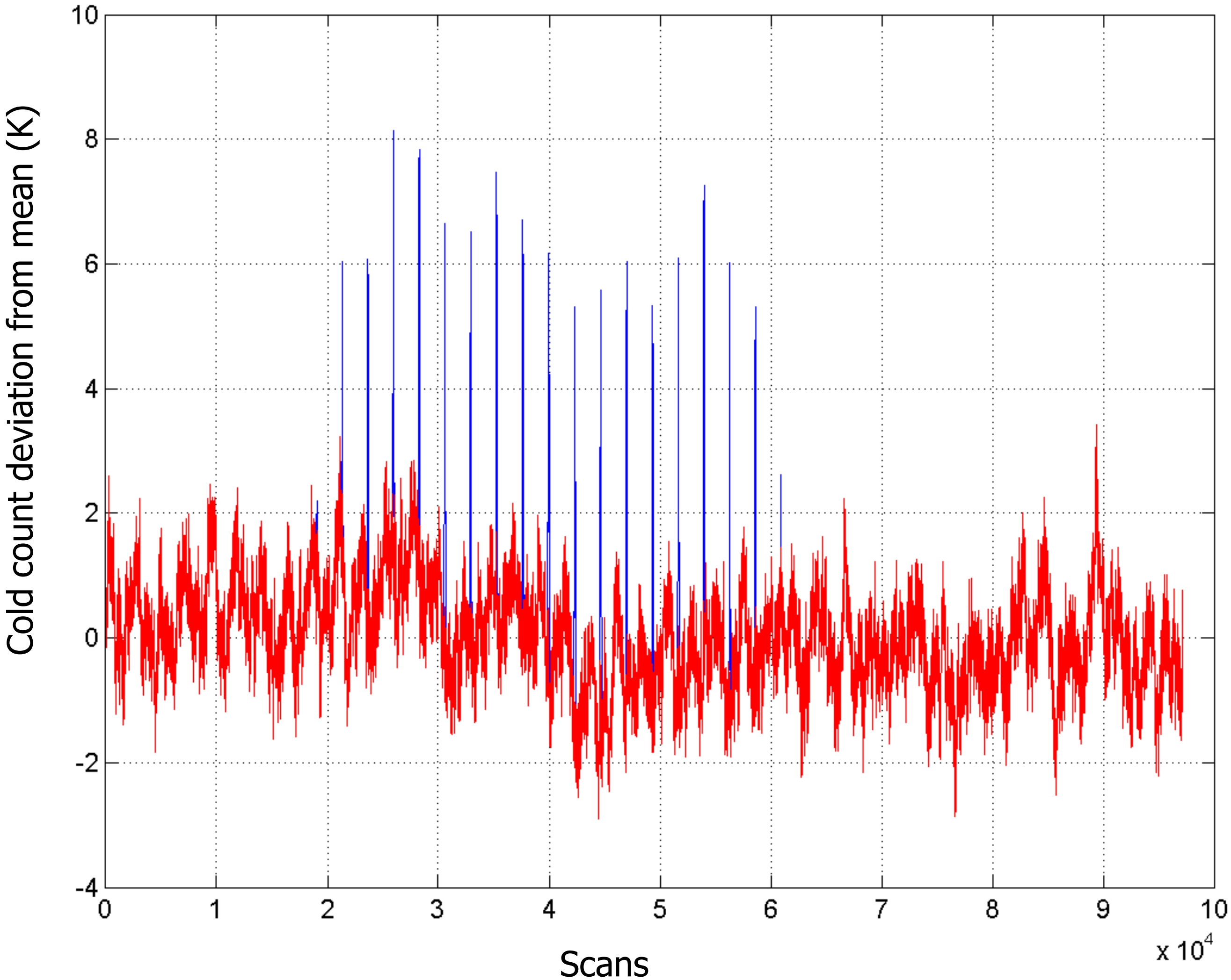

Blue: No LI correction
Red: After LI correction
Green: All four samples contaminated and history data used

Before LI Correction:
Worst cold count error: 8K
Median scene temp: 250K
Residual TB errors: 0.85K

After LI Correction:
Worst cold count error: 0.5K
Median scene temp: 250K
Residual TB errors: 0.05K

Assessment of Residual LI Correction Errors

- With MX8.3 code update and the PCT update, brightness temperature errors due to lunar intrusion have been reduced by a factor of 5-10 for most channels, except for channels 1, 2, and 15 which see reductions between 2-3 times
- Worst case residual errors are estimated to be ~0.2K for K/Ka/V band channels, ~0.1 K for the W band, and ~0.05K for the G band channels
  - Based on the analysis of April 8-10, 2014 lunar intrusion event
- Standard deviation of lunar intrusion correction residual errors should be much lower, estimated to be <0.1K for all channels

Striping Noise Assessment and Mitigation

THE VALUE OF PERFORMANCE.

NORTHROP GRUMMAN

NORTHROP GRUMMAN

Striping in S-NPP and J-1 Sensor Raw Data

Composite Image of normalized counts

J-1 TVAC Data (RC2, 230K)

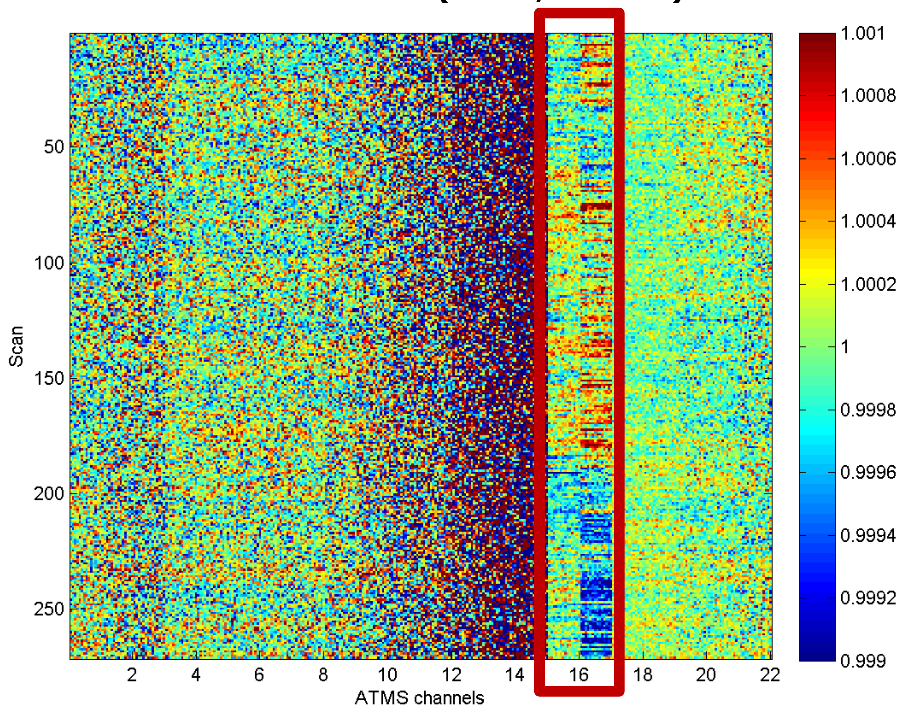

S-NPP TVAC Data (RC1, 230K)

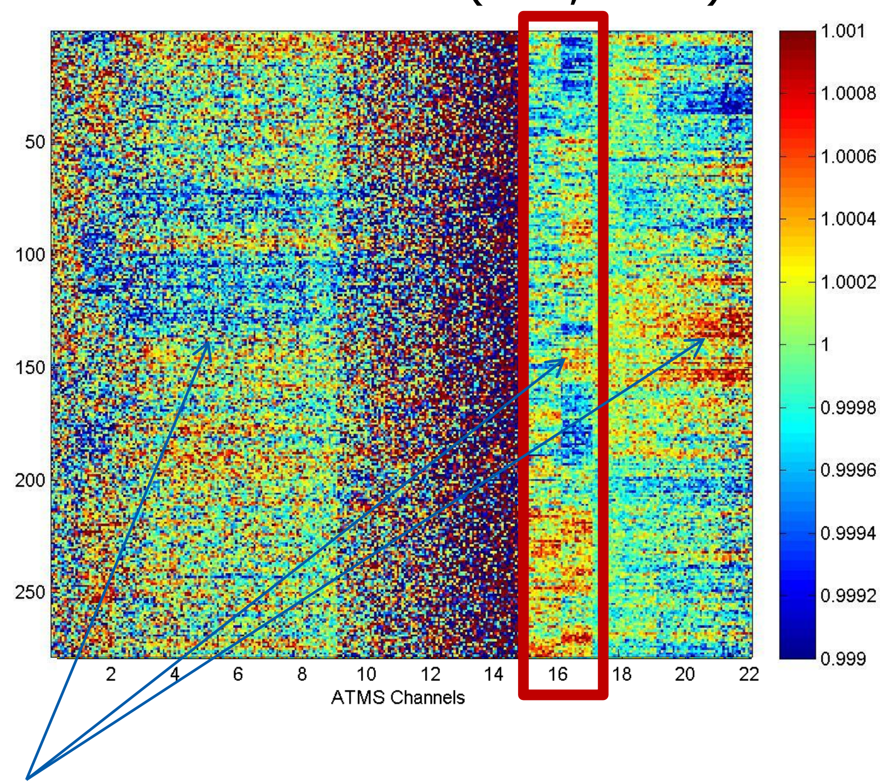

Striping on SNPP image, significantly reduced on J-1 image, except for channels 16 and 17

Residual Striping in S-NPP and J-1 Calibrated Brightness Temperatures

Composite Image of calibrated brightness temperatures

J-1 TVAC Data (RC2, 230K)

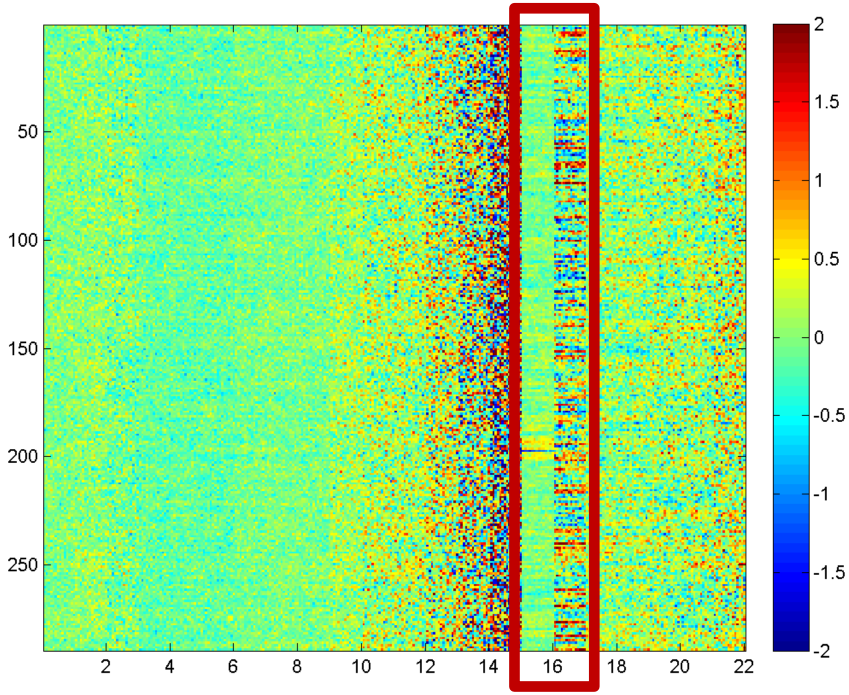

SNPP TVAC Data (RC1, 230K)

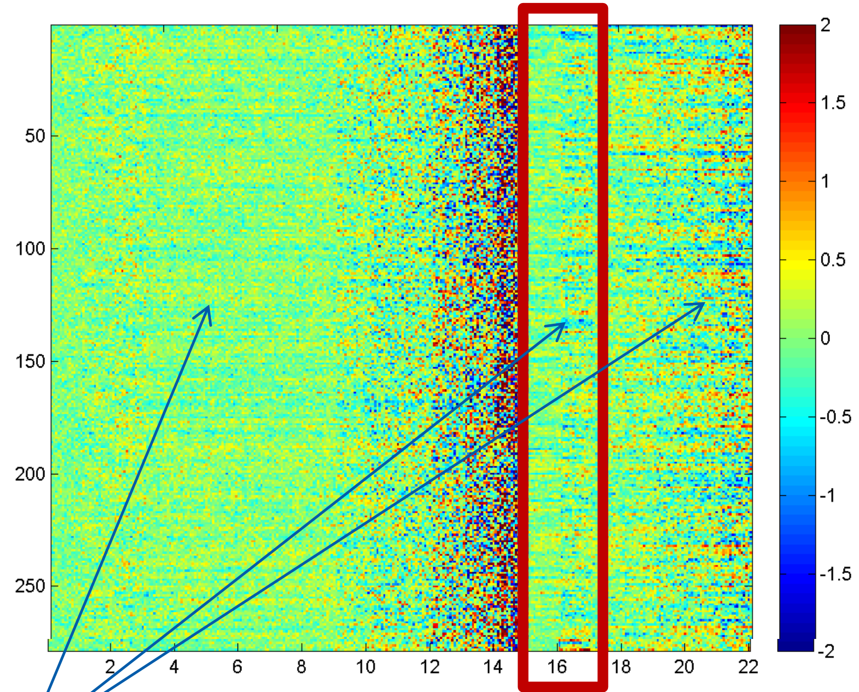

Striping on SNPP image, significantly reduced on J-1 image, except for channel 17

Striping Index to Quantify Striping Noise

Striping Index (SI) is defined as the ratio of along-track variance to cross-track variance of the observed brightness temperatures

$$SI = V_{AT} / V_{CT}$$

If this index is significantly larger than 1, it indicates additional scan-to-scan variability (striping)

This index can be used to inflate O-B error covariance for NWP assimilation to prevent over fit of data

This index can be computed using ground TVAC test data to verify sensor hardware performance before launch

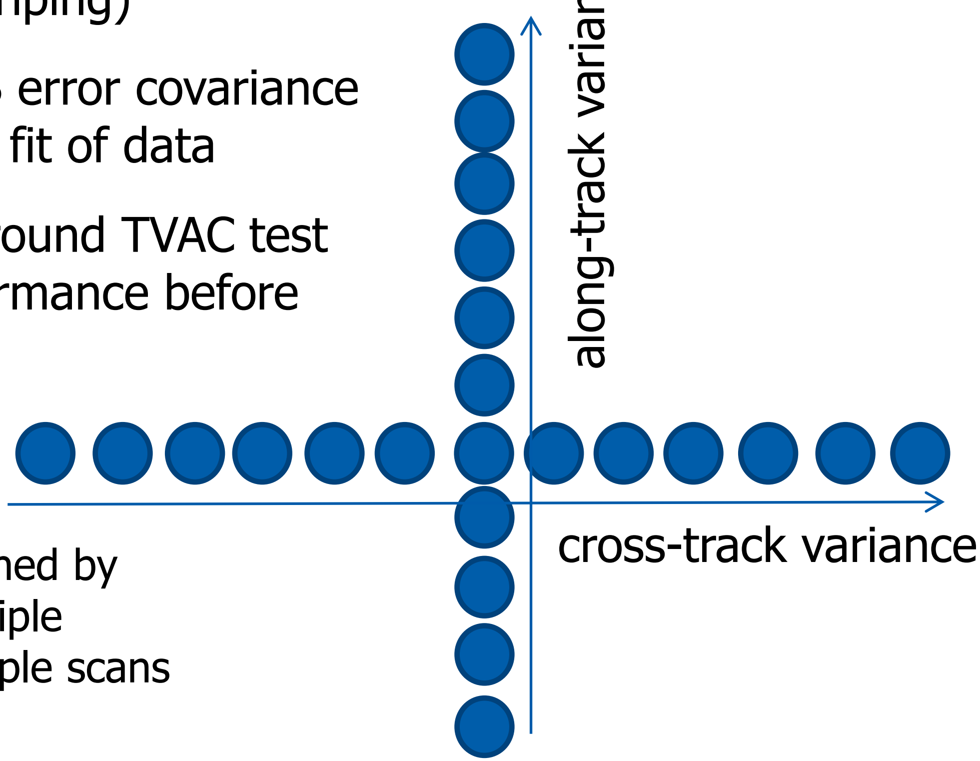

More precise estimate of SI can be obtained by averaging along-track variance over multiple FOVs and cross-track variance over multiple scans

Estimated J-1 Residual Striping Errors

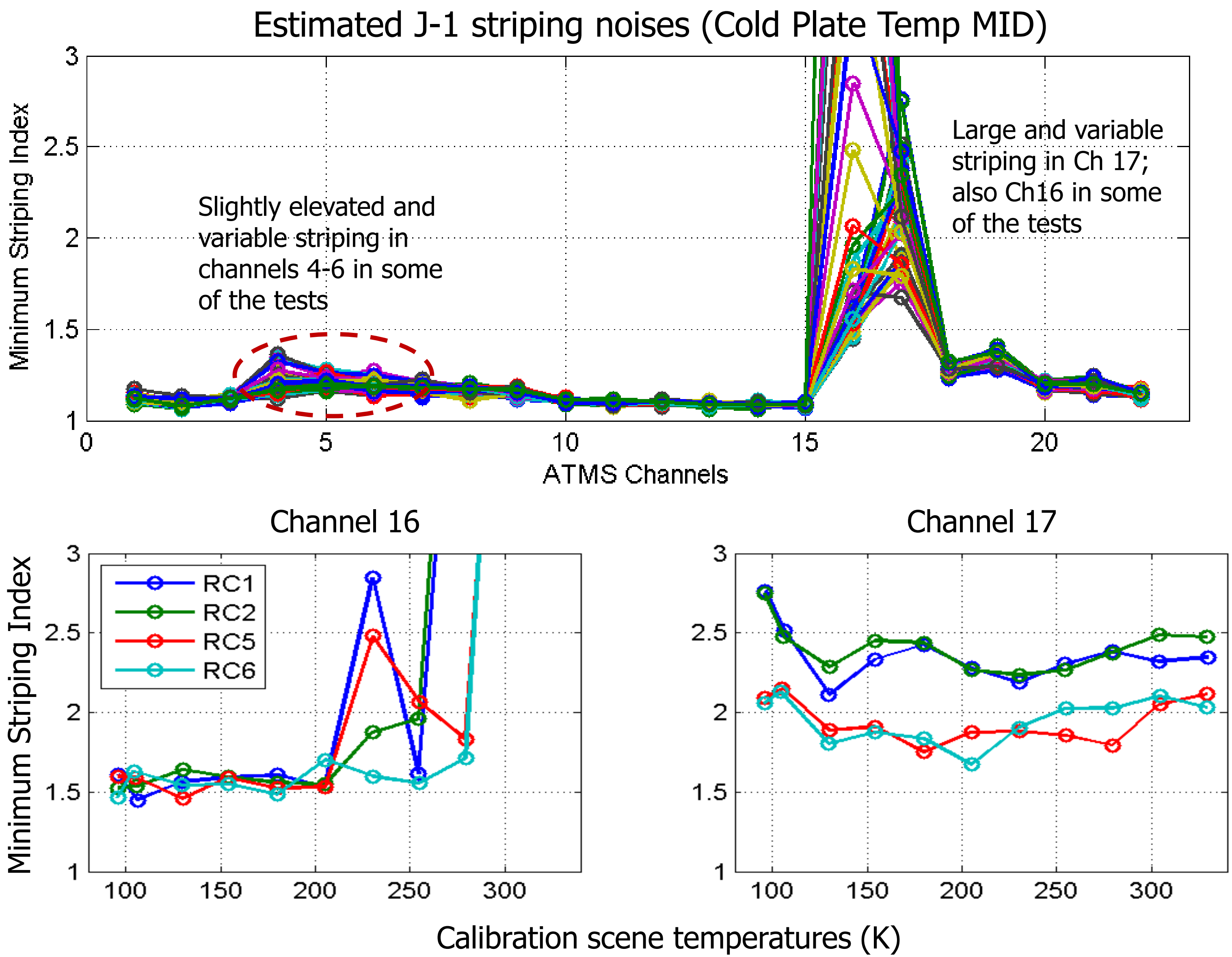

Comparison of J-1 and S-NPP Striping Noises

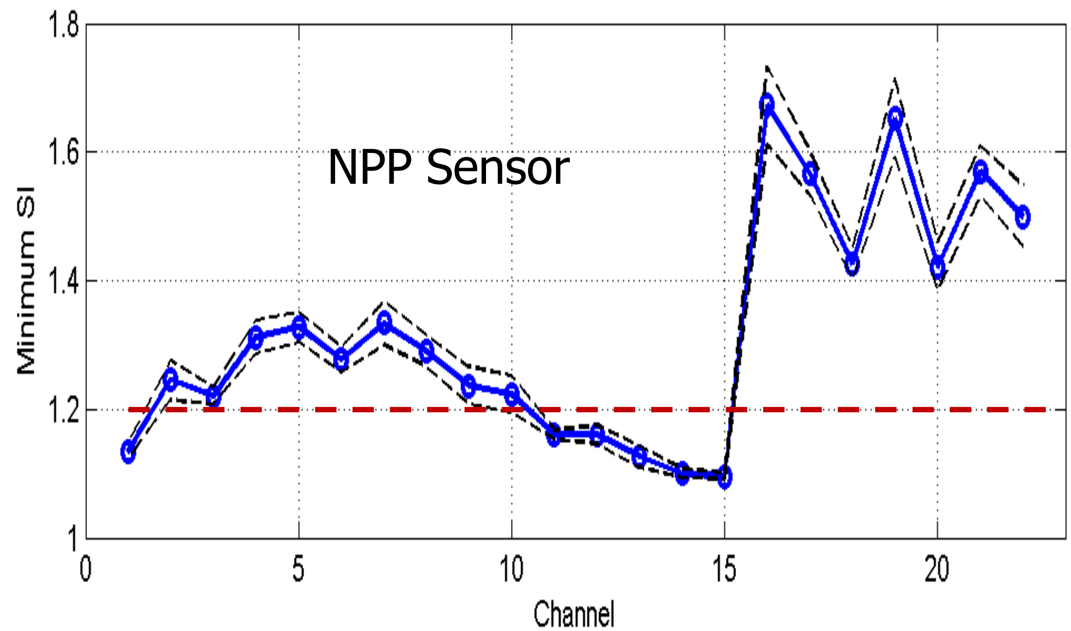

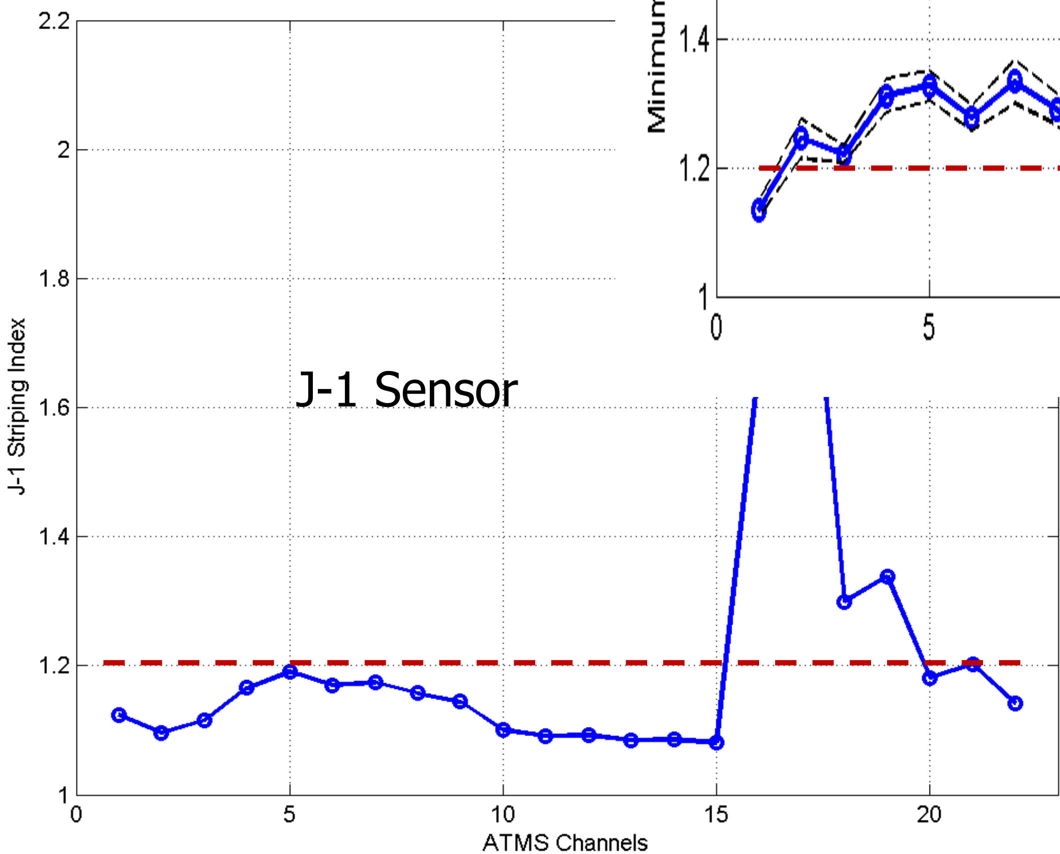

Estimated J-1 Sensor Gain Variability (1-sigma)

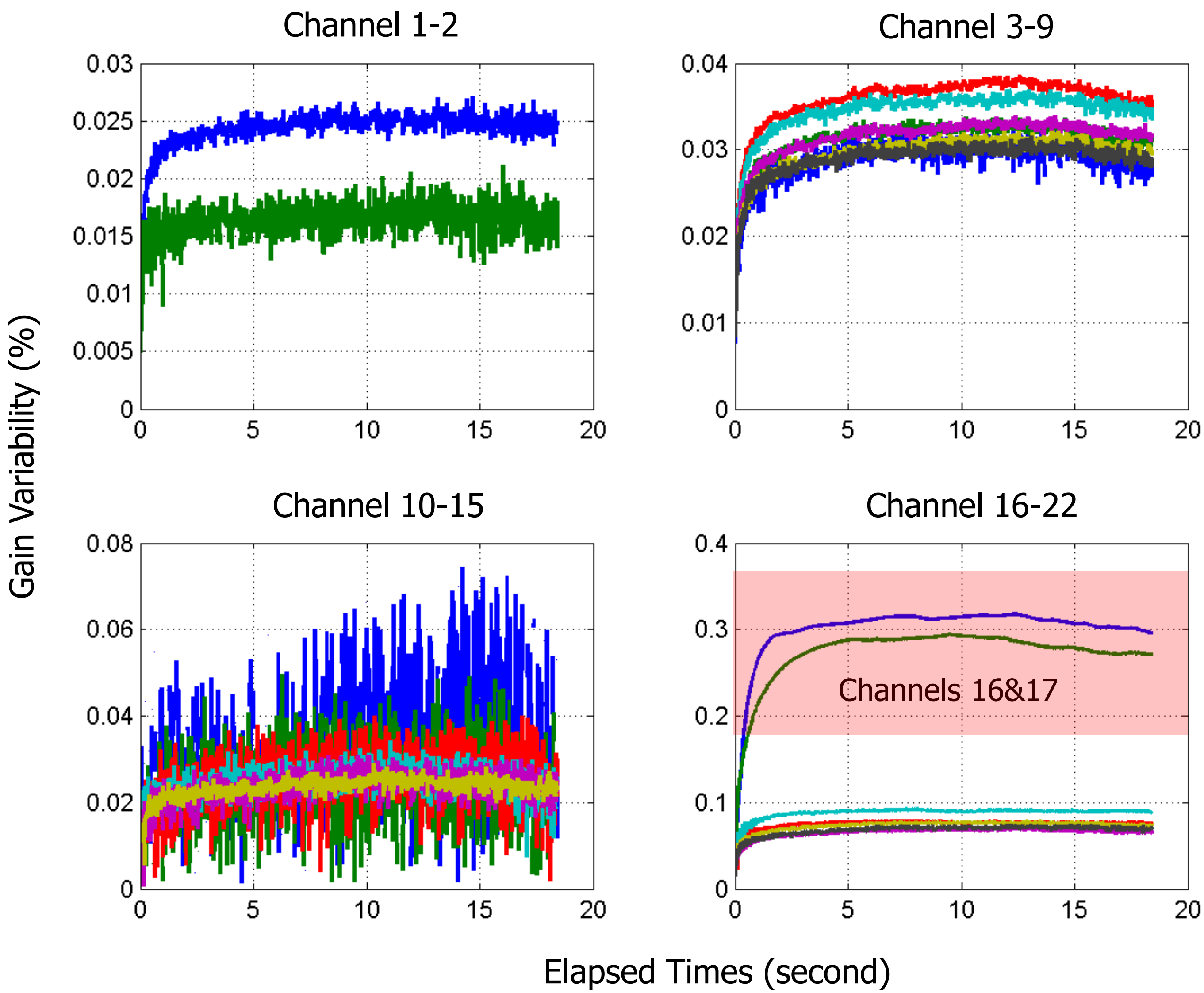

Gain Variability Data Analysis Results: CH 16

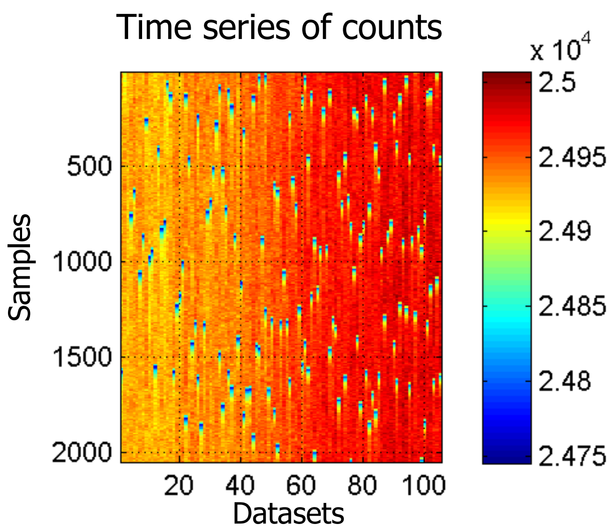

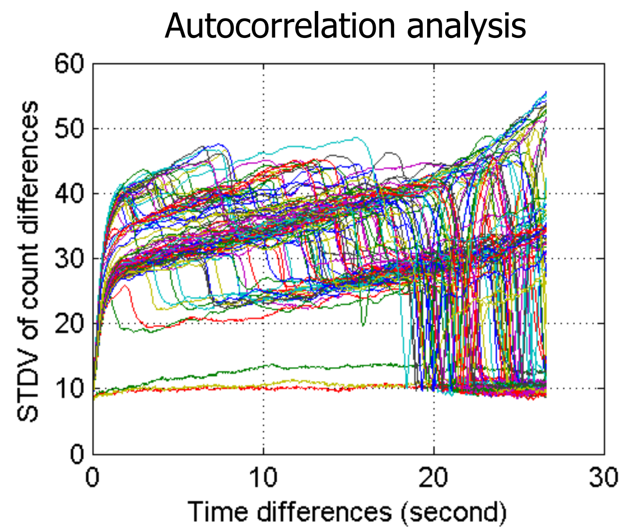

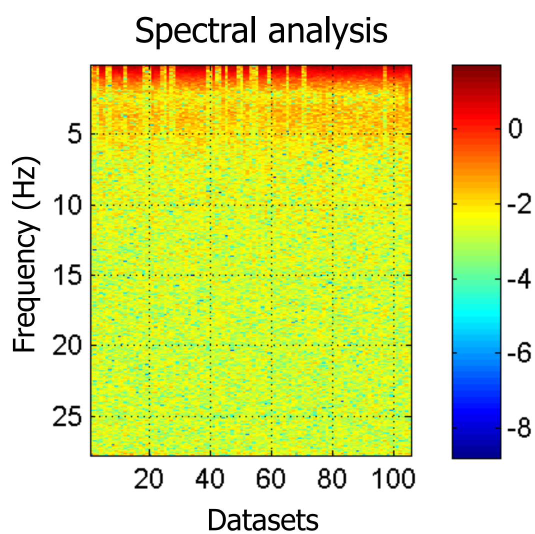

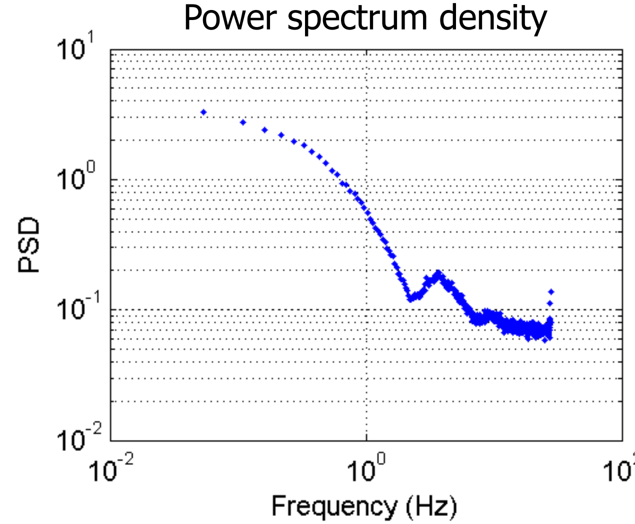

Gain Variability Data Analysis Results: CH 17

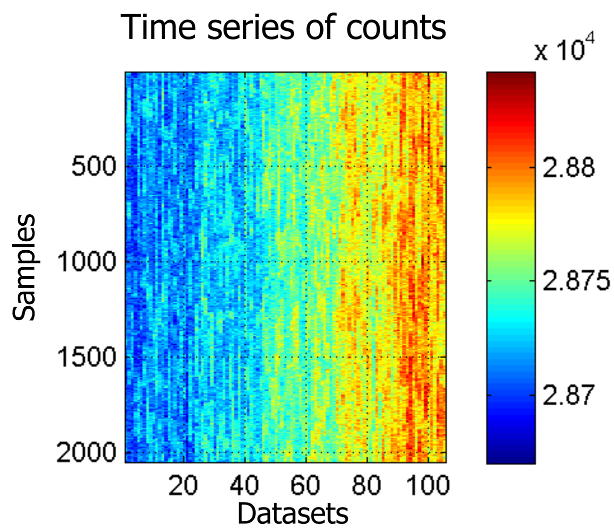

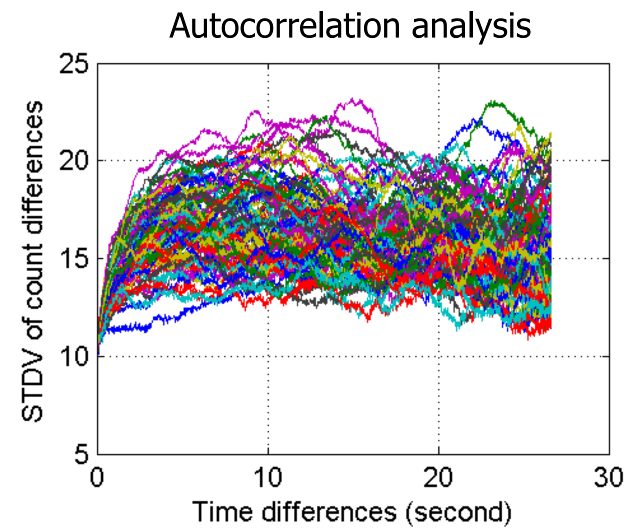

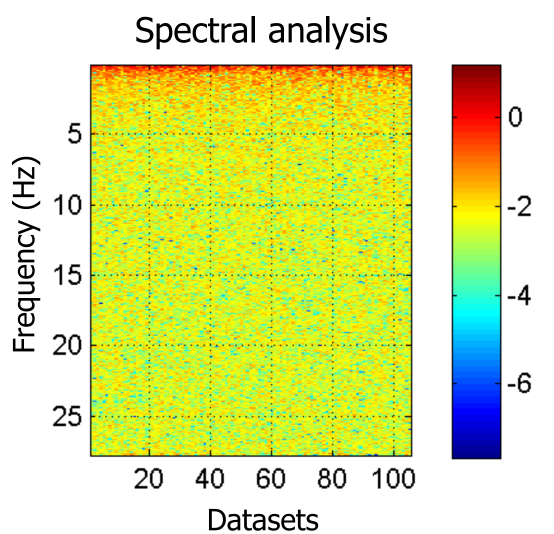

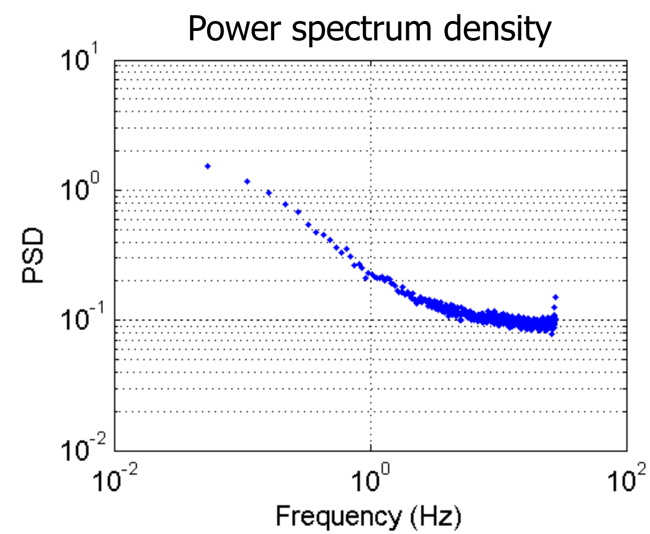

Gain Variability Data Analysis Results: CH 18

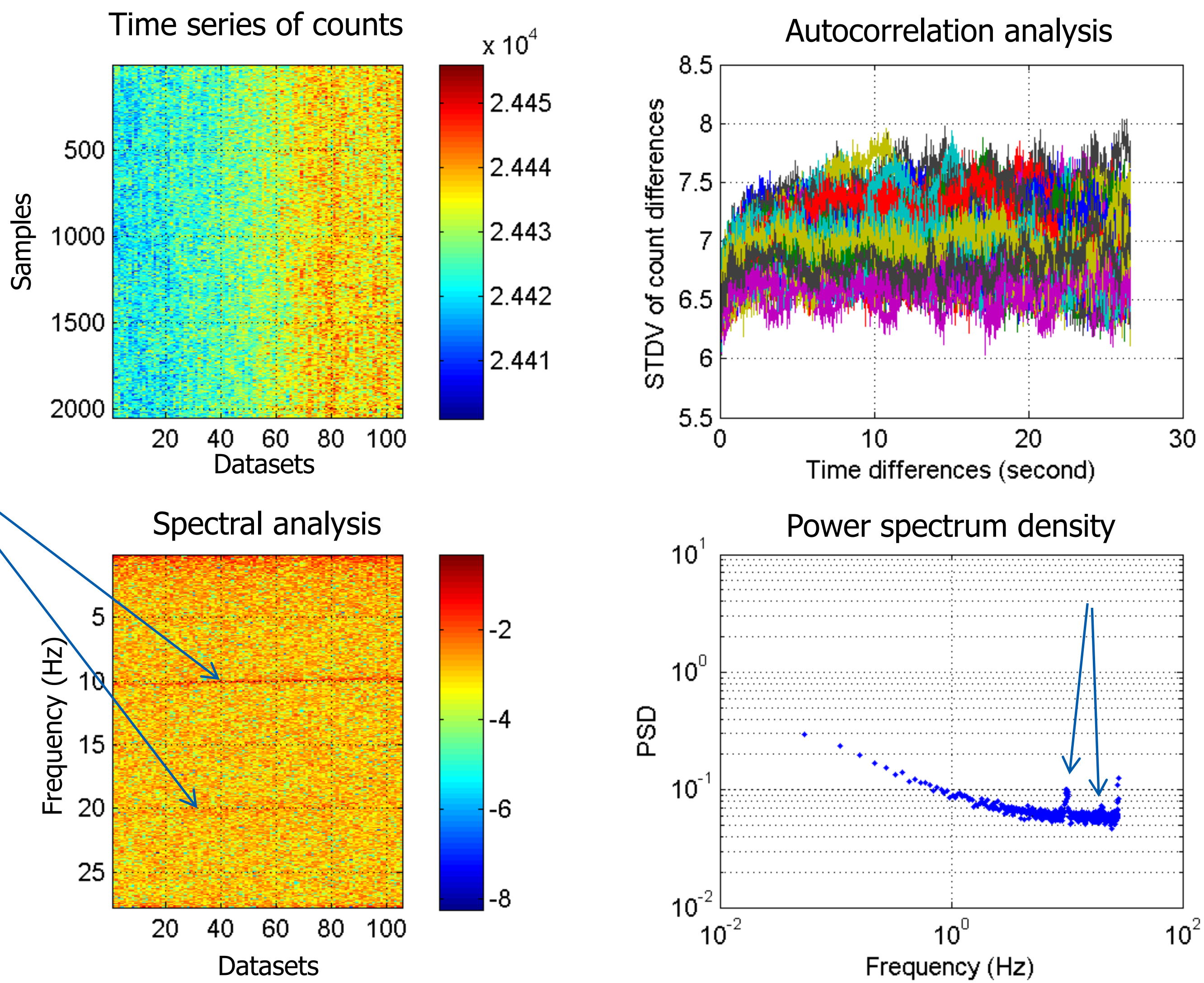

Mitigation of Striping Errors: PCA-EEMD Verification

- Simulated ATMS SDRs by adding random noise and striping noise to evaluate effectiveness of PCA-EEMD method in detecting and quantifying striping noises
  - Random noise added based on the simulated scene temperatures
  - Striping noise added based on scene temperatures and are correlated across scans
  - Magnitudes of random noise and striping noise are derived from previous analyses
- Performed PCA on simulated noisy brightness temperature images (200 scans)
- Extracted the EM's in the first PC scores using the EMD method
  - Special treatment at the edges to minimize ringing
- Assessment:
  - Reconstructed brightness temperature images with the striping-induced EM's removed to visually evaluate the effectiveness
  - Compared the estimated striping errors to the simulated errors to evaluate absolute accuracy

ECMWF Simulated SDR Channel 12

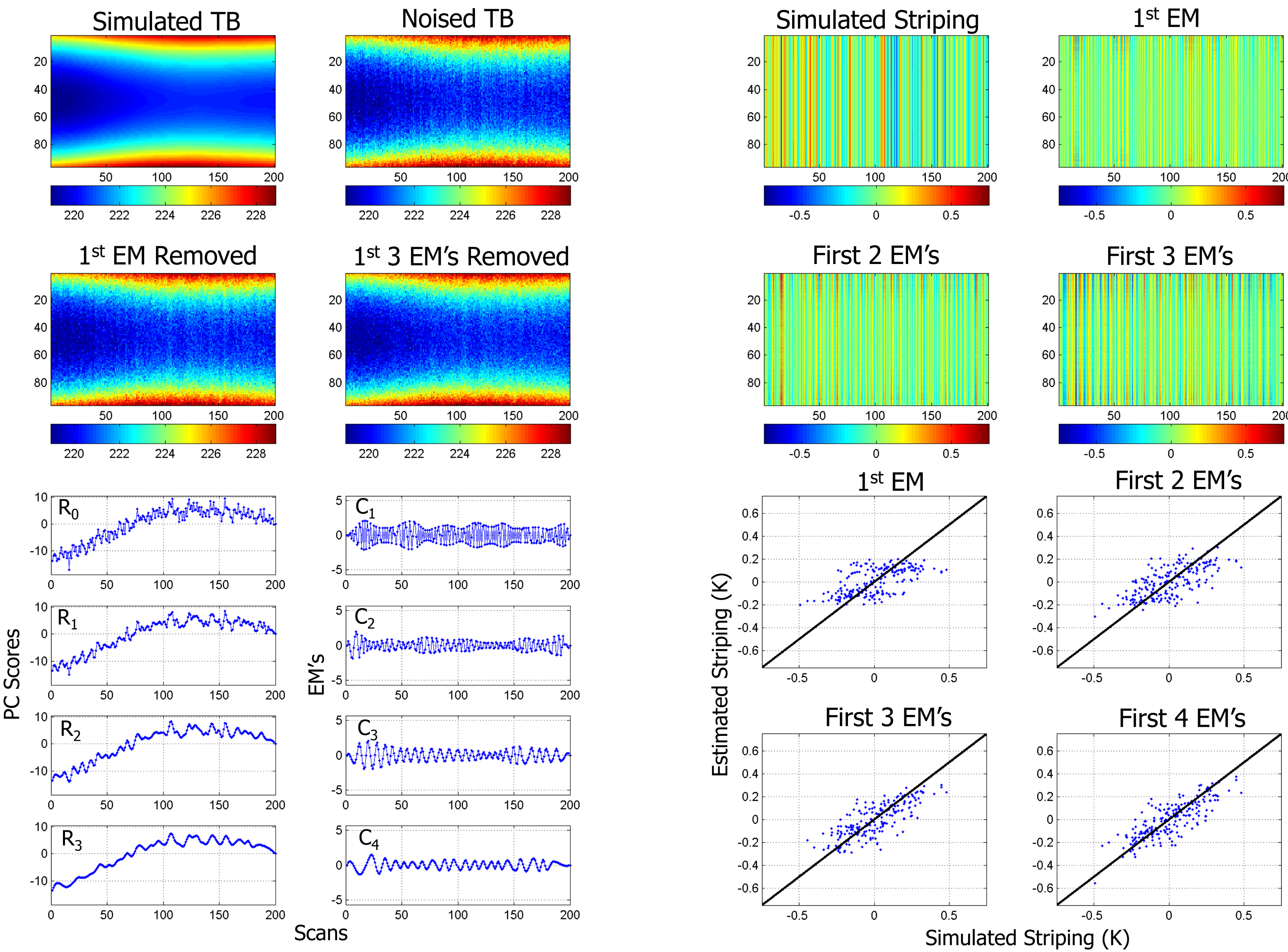

J-1 Channel 16 Gain Dropout Waveform Construction

Observed J-1 Sensor Channel 16 Gain Dropouts During Transition from CP LOW to CP MID

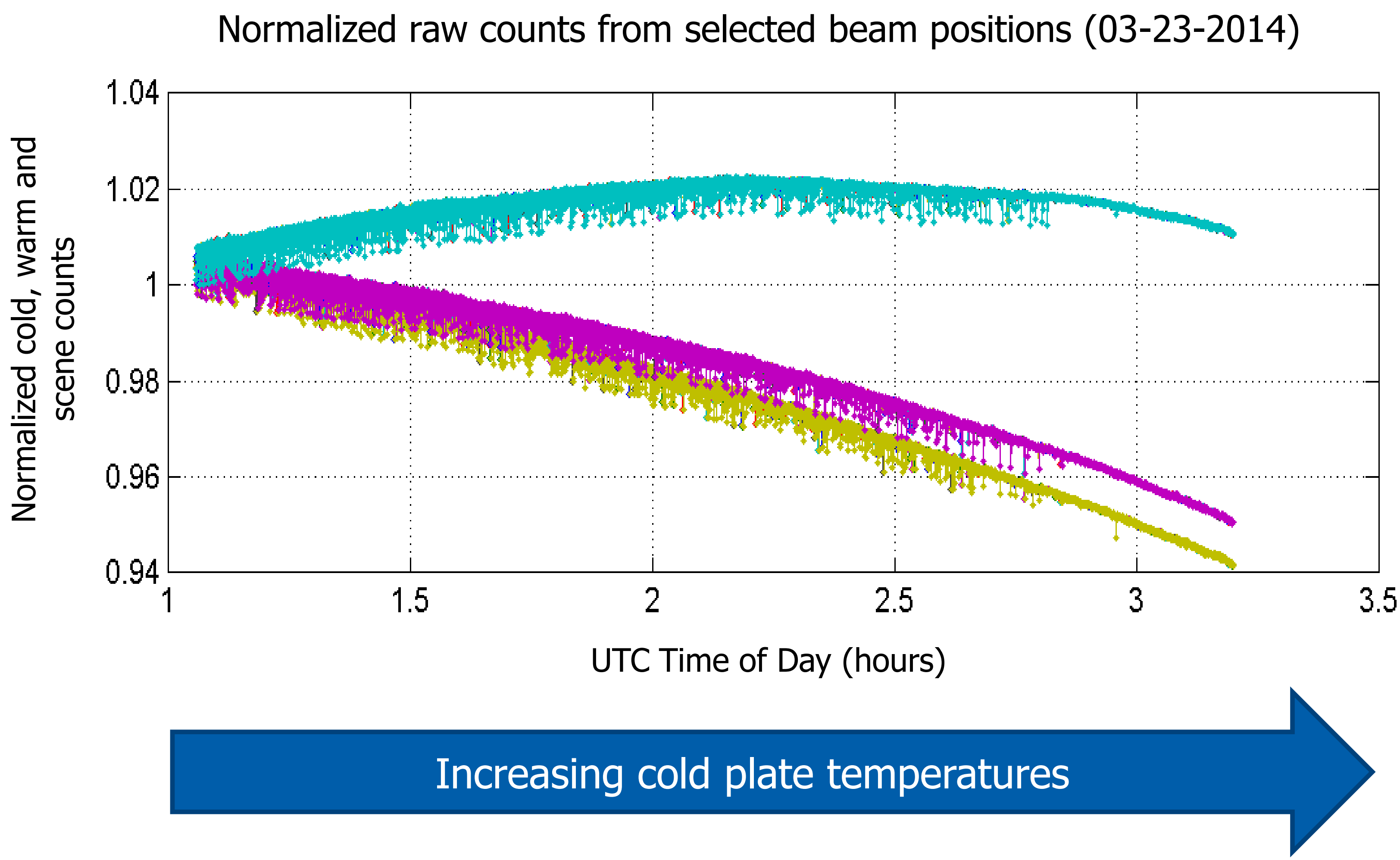

J-1 Channel 16 Gain Dropouts in Scan Data

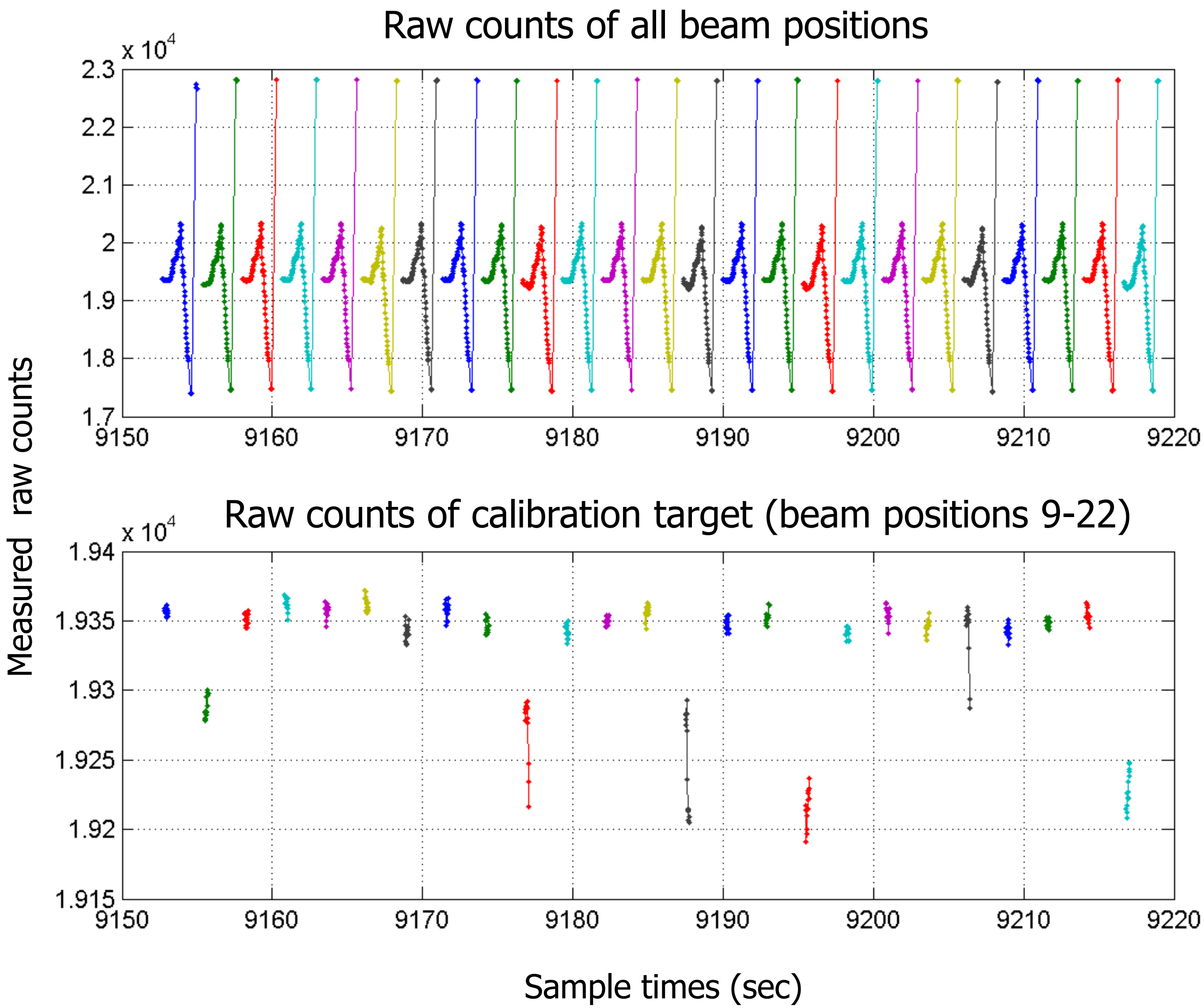

Reconstruction of Gain Dropouts from Thermal Cycle Test Datasets

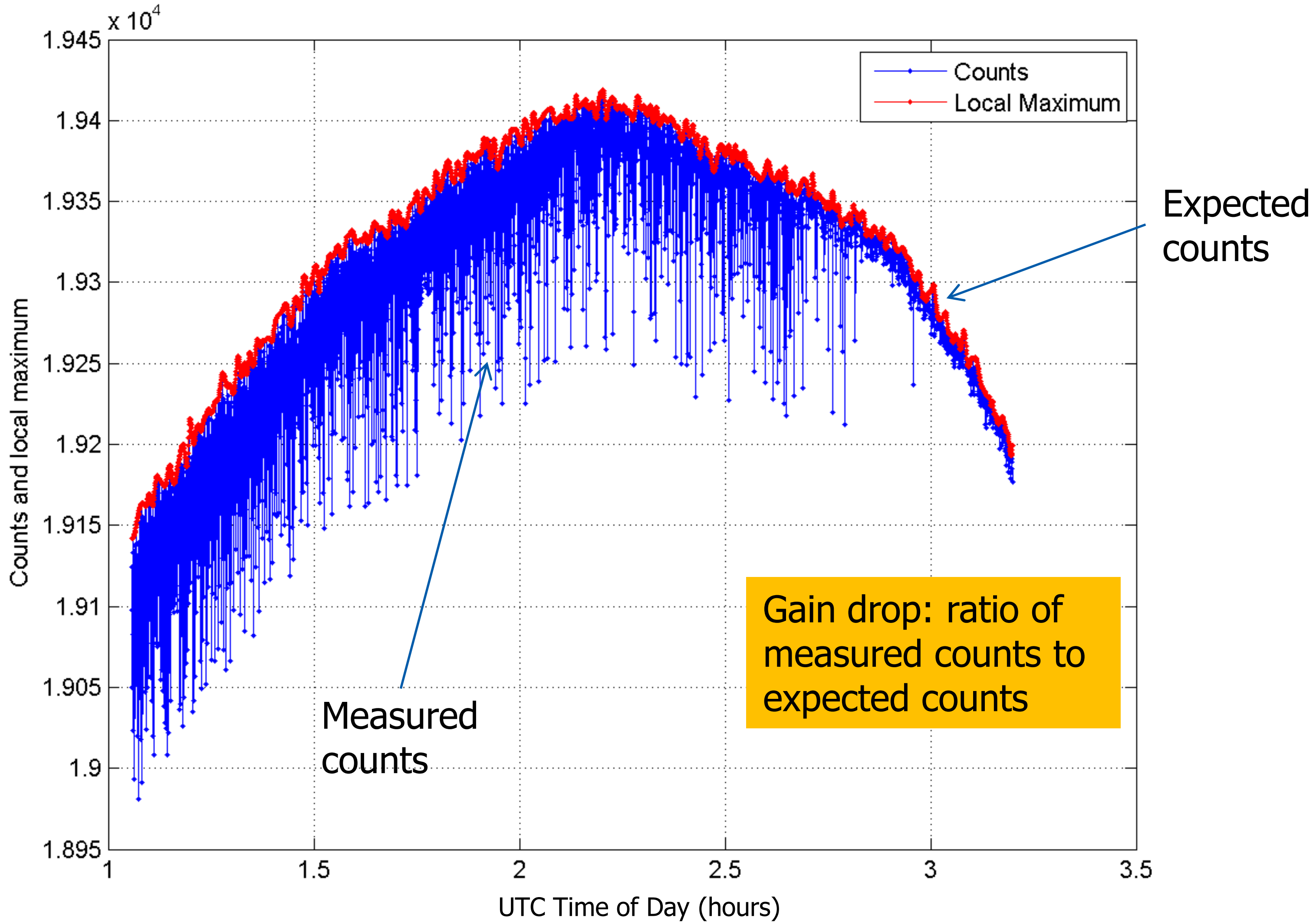

Reconstructed Gain Dropout Waveforms During Transition

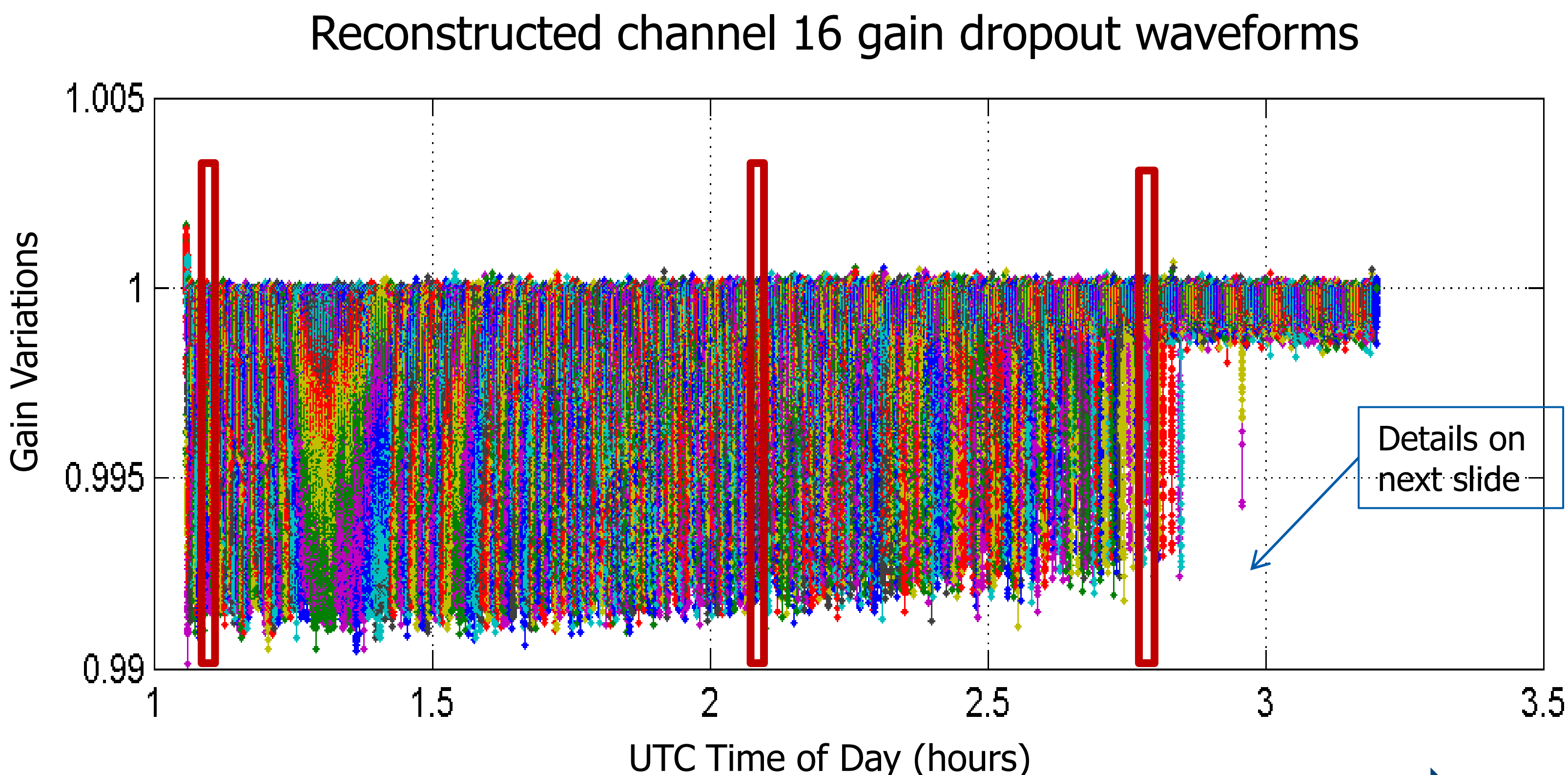

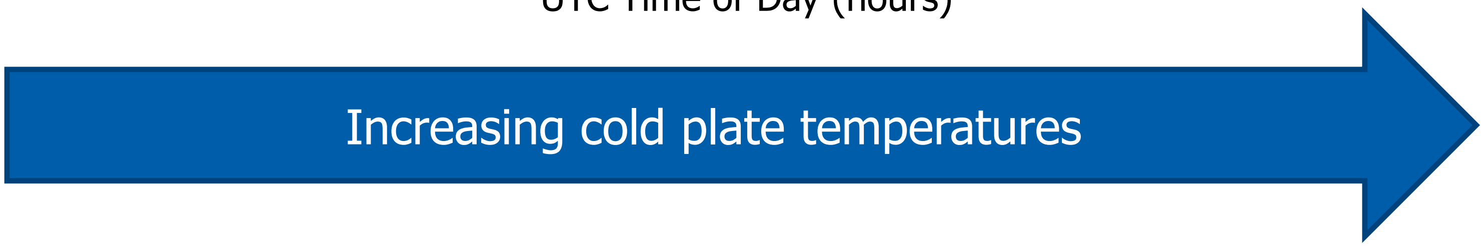

Reconstructed Gain Dropout Waveforms at Different Instrument Temperatures

Reconstructed gain dropout waveforms as cold plate temperature increases during transition from Cold #7 to Hot #8 at selected time windows. 2014-04-24 01:03-03:12 (UTC)

Continuous dropouts that takes ~3-4 scans to recover at Cold CP temp

Frequent dropouts that recovers in ~2 scans at transitional CP temp

Occasional dropouts that recovers in ~1 scan at near MID CP temp

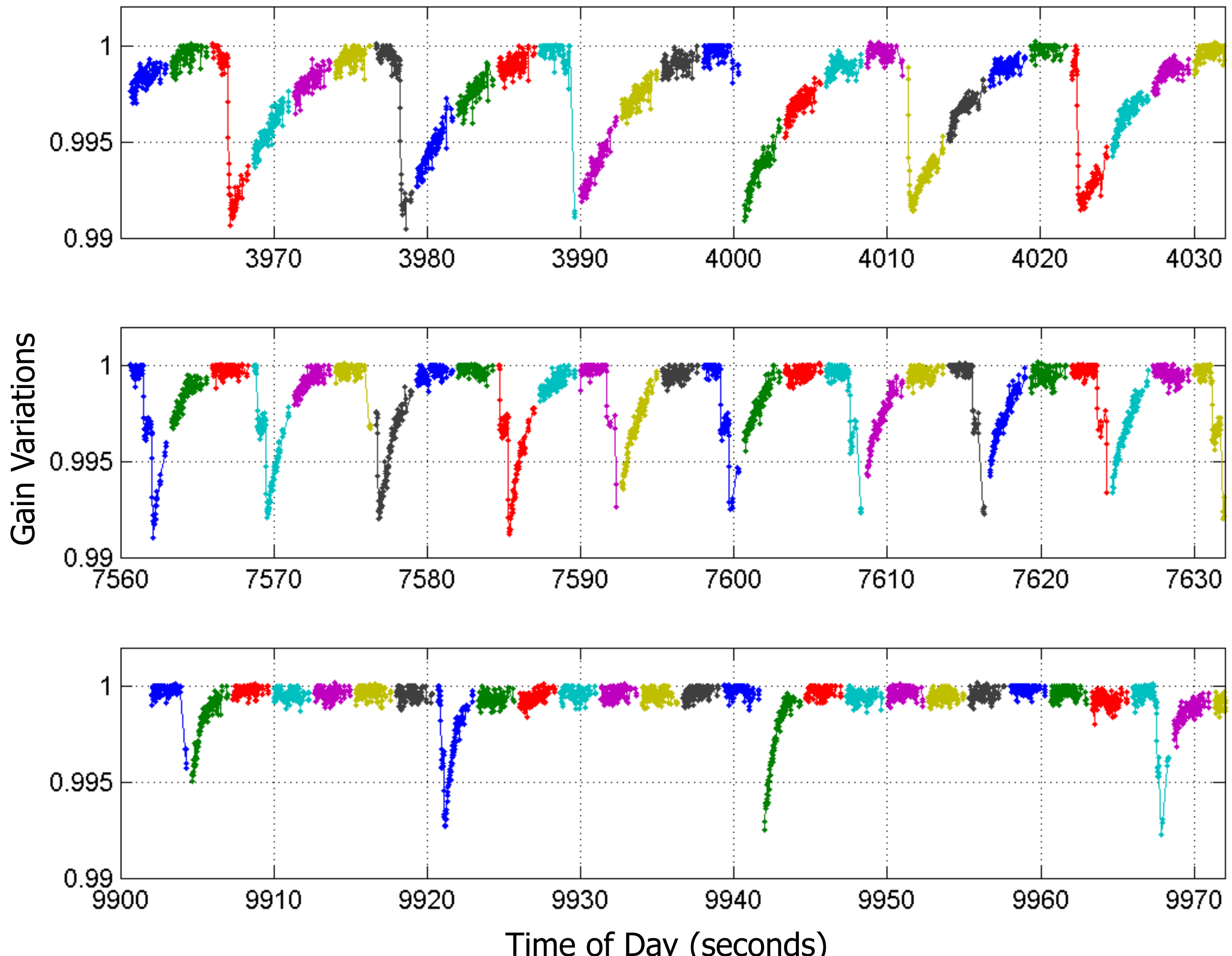

Increasing cold plate temperatures

(Degui Gu and Alex Foo, NGAS)

Verification of Reconstructed Waveforms against the Observed Waveforms

NORTHROP GRUMMAN

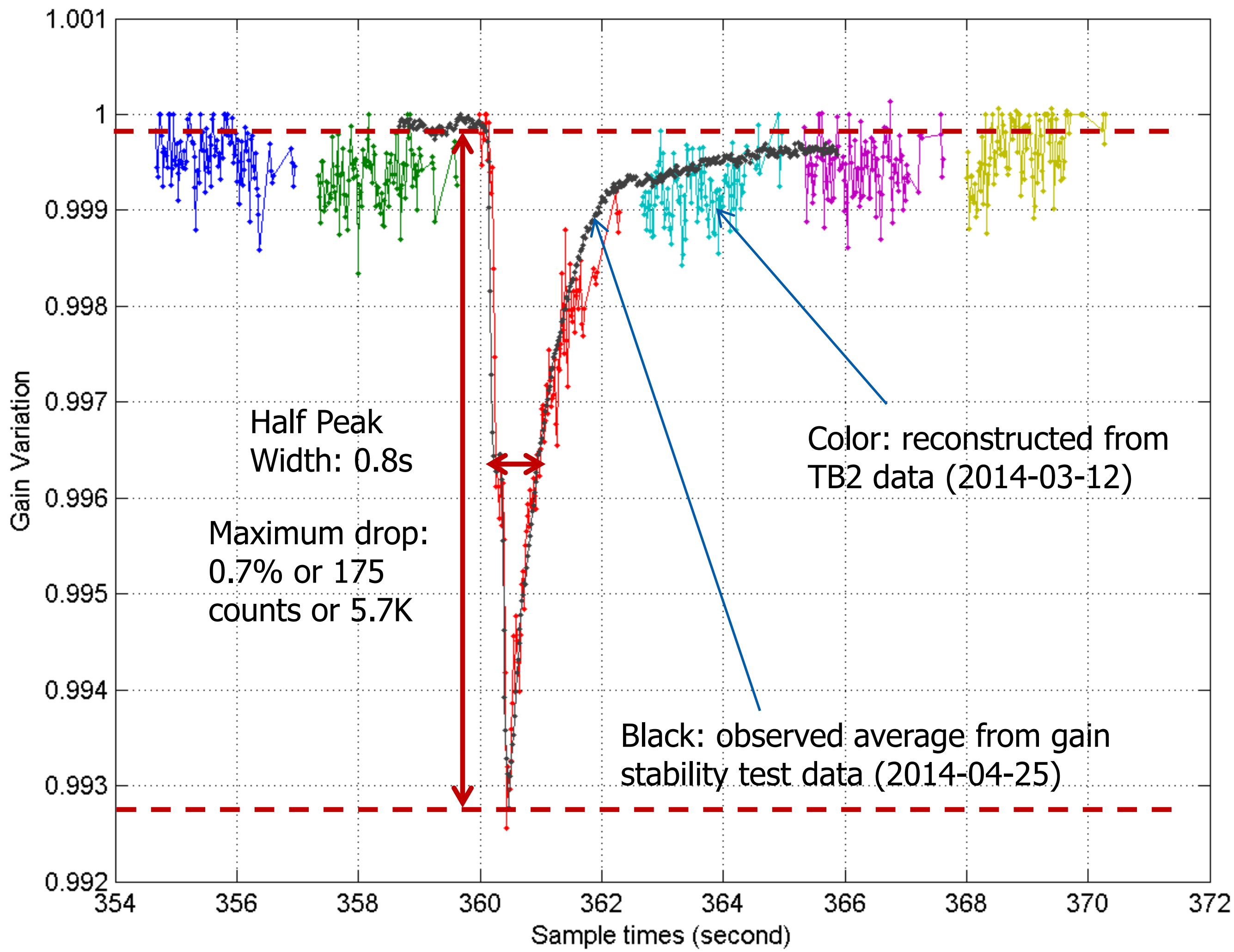

(Degui Gu and Alex Foo, NGAS)

Summary and Future Work

- NGAS ATMS team will continue to support S-NPP ATMS SDR CalVal activities as the focus transitioning to LTM
- We plan to continue to support J-1 ATMS sensor testing and characterization
  - Support to sensor sell off
  - Support to J-1 algorithm development and improvement
  - Support to J-1 algorithm LUT/PCT coefficients derivation and verification
    - Calibration coefficients and nonlinearity correction
    - Beam efficiency correction coefficients
    - Striping noise mitigation by filtering
    - Geolocation LUT (sensor pointing and mounting data verification)

STAR Independent Assessment of J1 ATMS Thermal Vacuum Test CP-Mid and CP-High Data Analysis

STAR ATMS SDR Team

May 13, 2014

Introduction

Analyzing TVAC calibration data provides instrument performance assessment:

- Calibration Accuracy
- Nonlinearity
- Sensitivity (i.e., NEΔT)
- Dynamic Range
- Striping

J1 ATMS TVAC Test

- Data is updated till May 9, 2014
- TVAC calibration: ST95, 105, 130, 155, 180, 205, 230, 255, 280, 305, 330 in CP_Mid and CP_High

Software

- Log file reader is provided by MIT-LL (version 1.7)
- Programs mainly prepared for TVAC calibration test

Date: May 13, 2014

J1 ATMS TVAC Redundancy Configuration

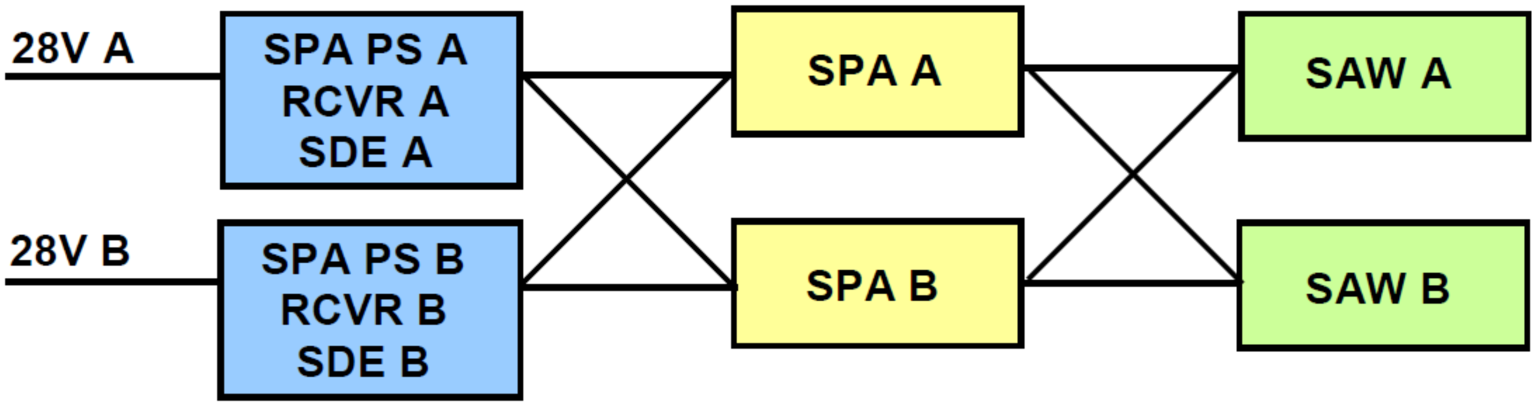

CONFIG.	SPA PS	RECEIVER SELECT	SDE SELECT	SPA CROSS	SAW CROSS
1	A	REC A - PLO, CSO, GDO, RPS	SDE A	SPA A	SAW A
2					SAW B
3				SPA B	SAW B
4					SAW A
5	B	REC B - PLO, CSO, GDO, RPS	SDE B	SPA B	SAW B
6					SAW A
7				SPA A	SAW A
8					SAW B

Cold Plate Temperature at CP_Mid ST-330

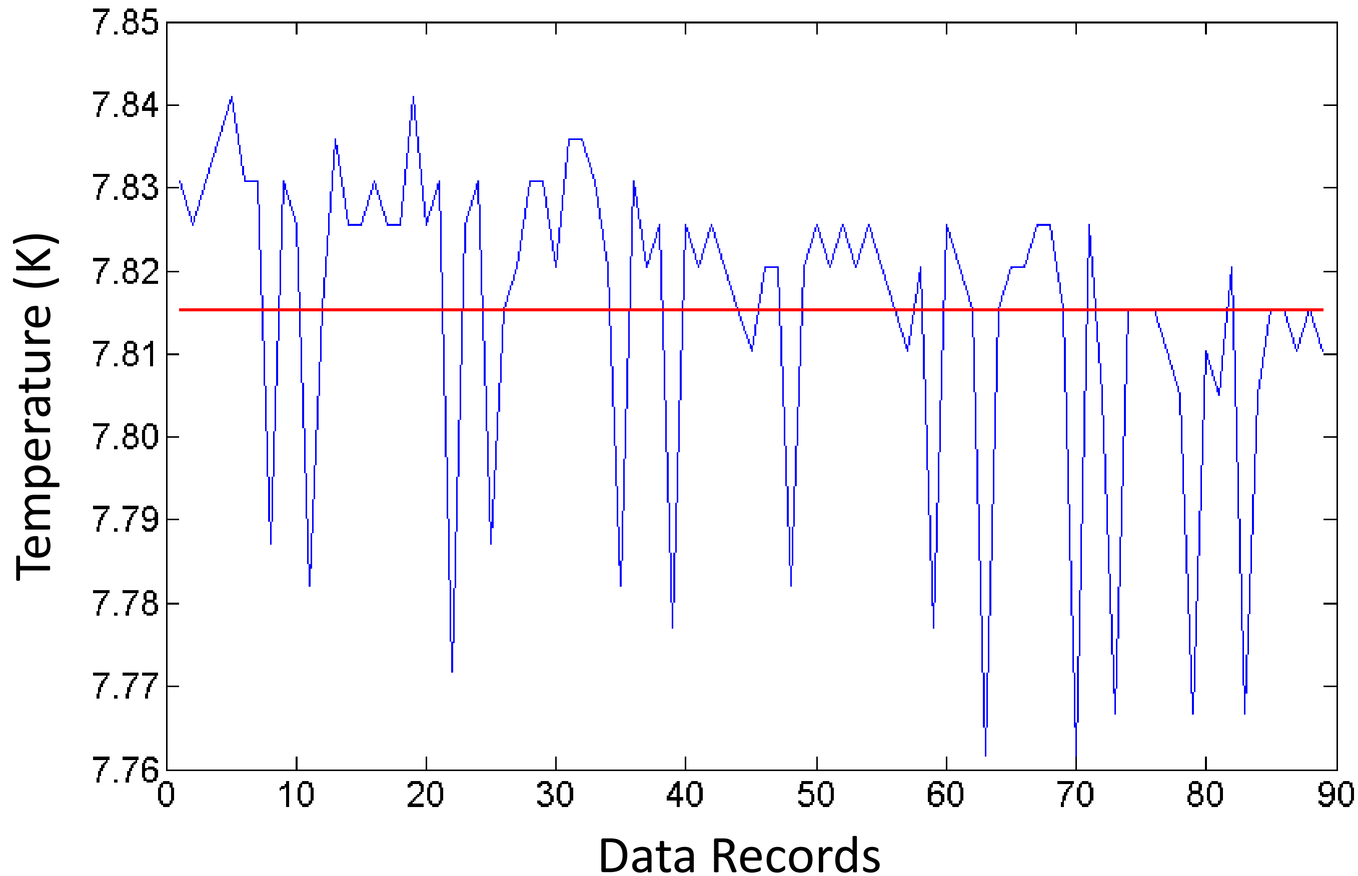

Mean: 7.8152K ; Std. Dev: 0.0189K

NEΔT at CP_Mid

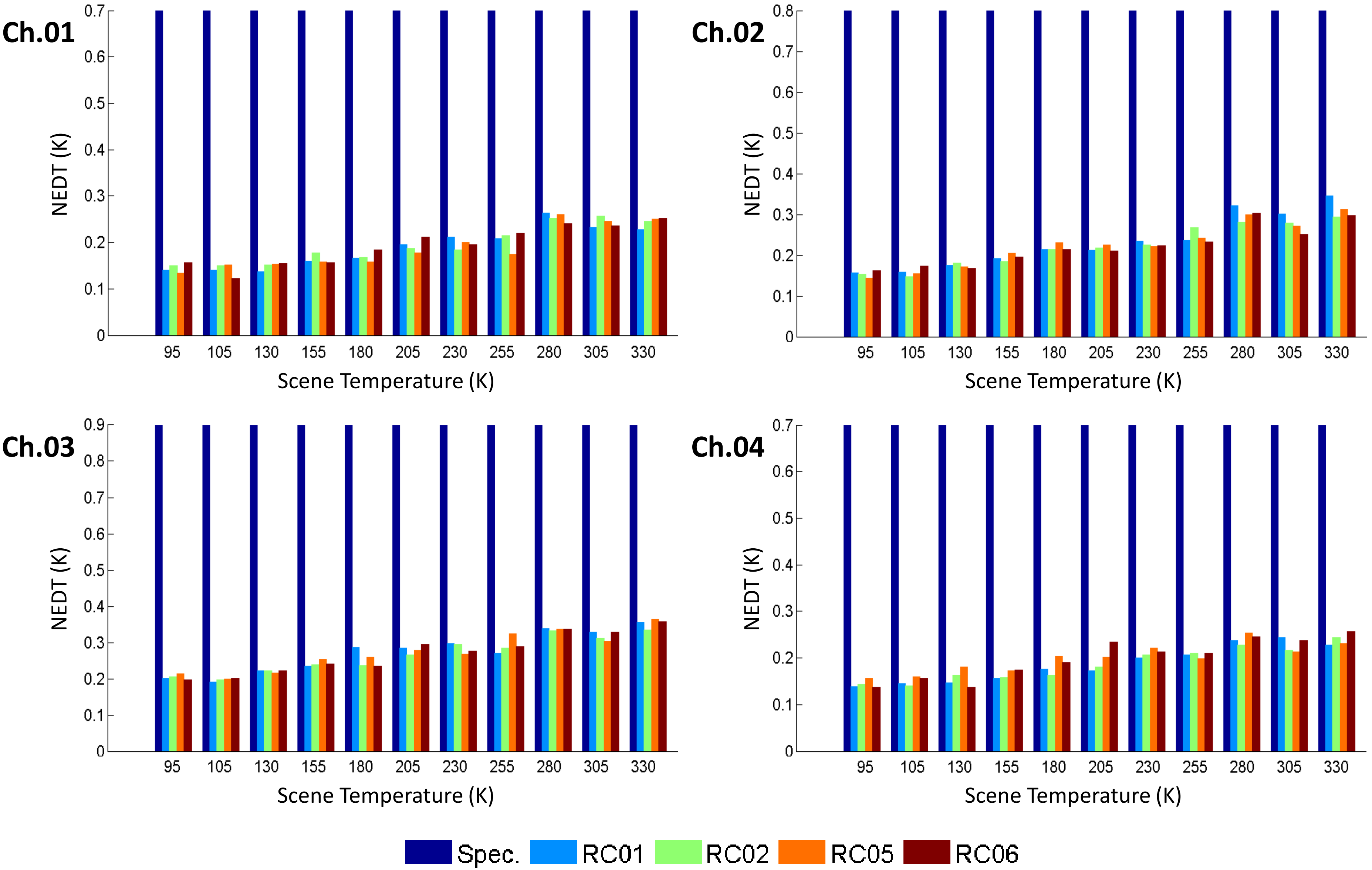

NEΔT at CP_Mid

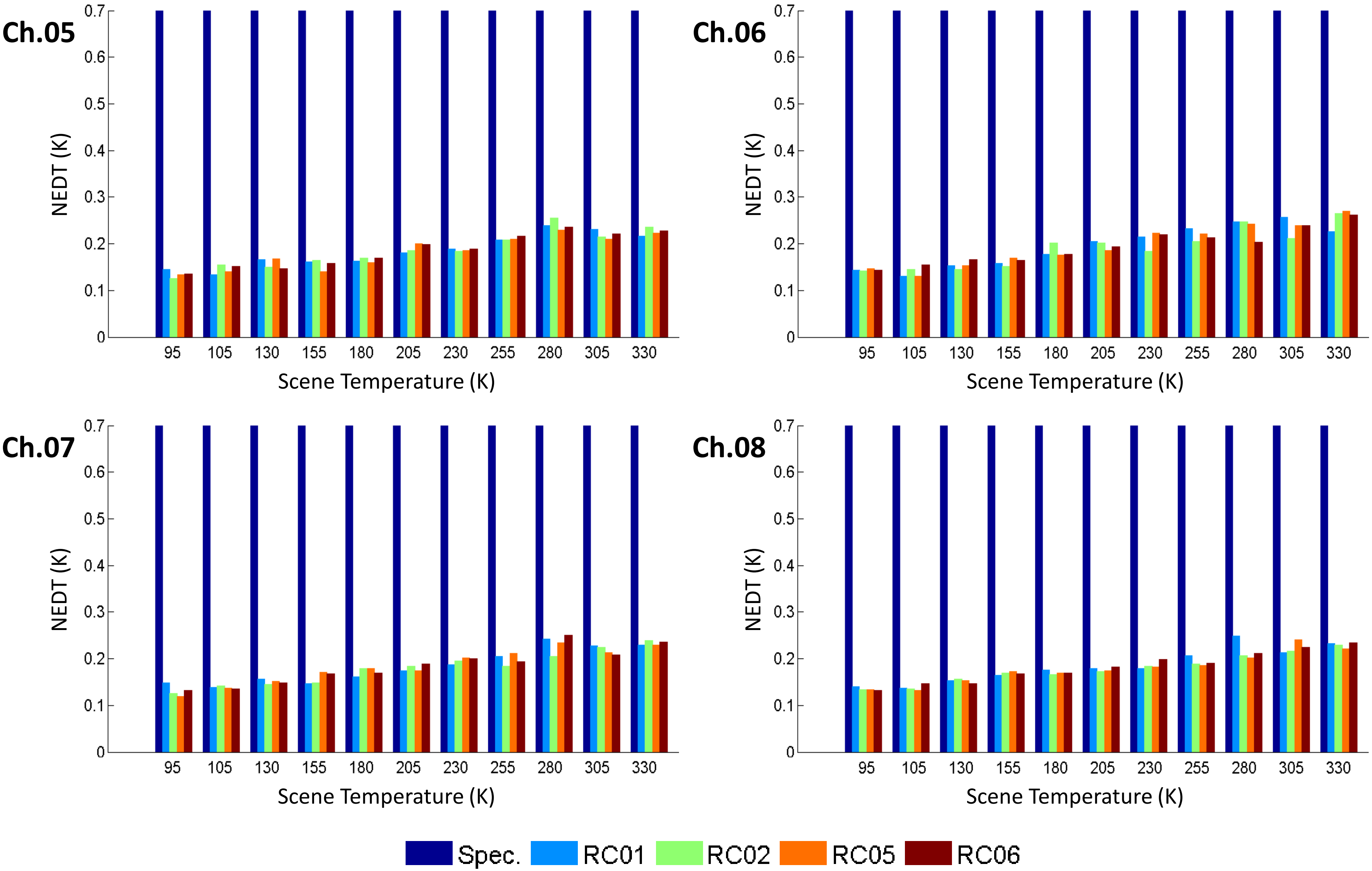

NEΔT at CP_Mid

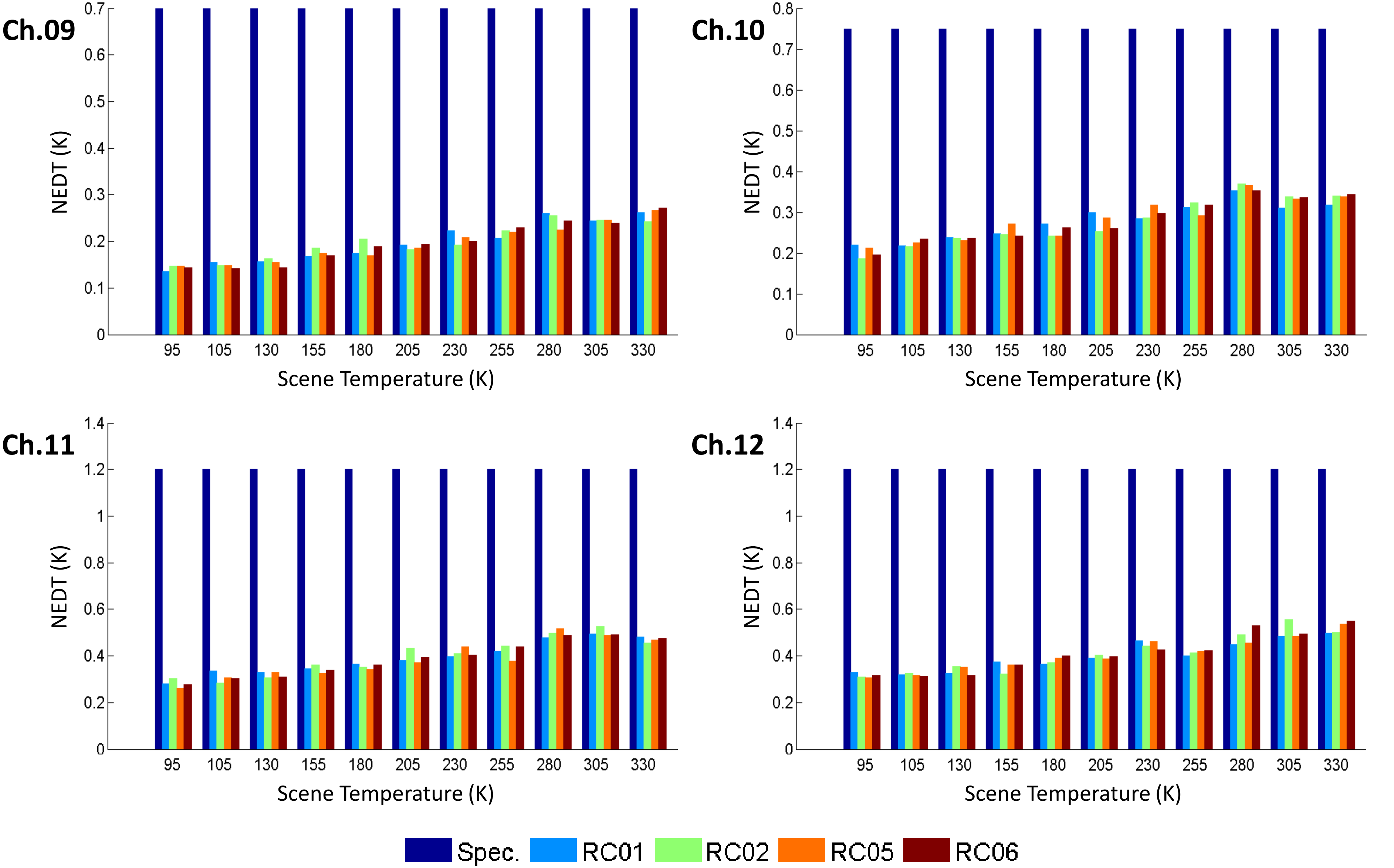

NEΔT at CP_Mid

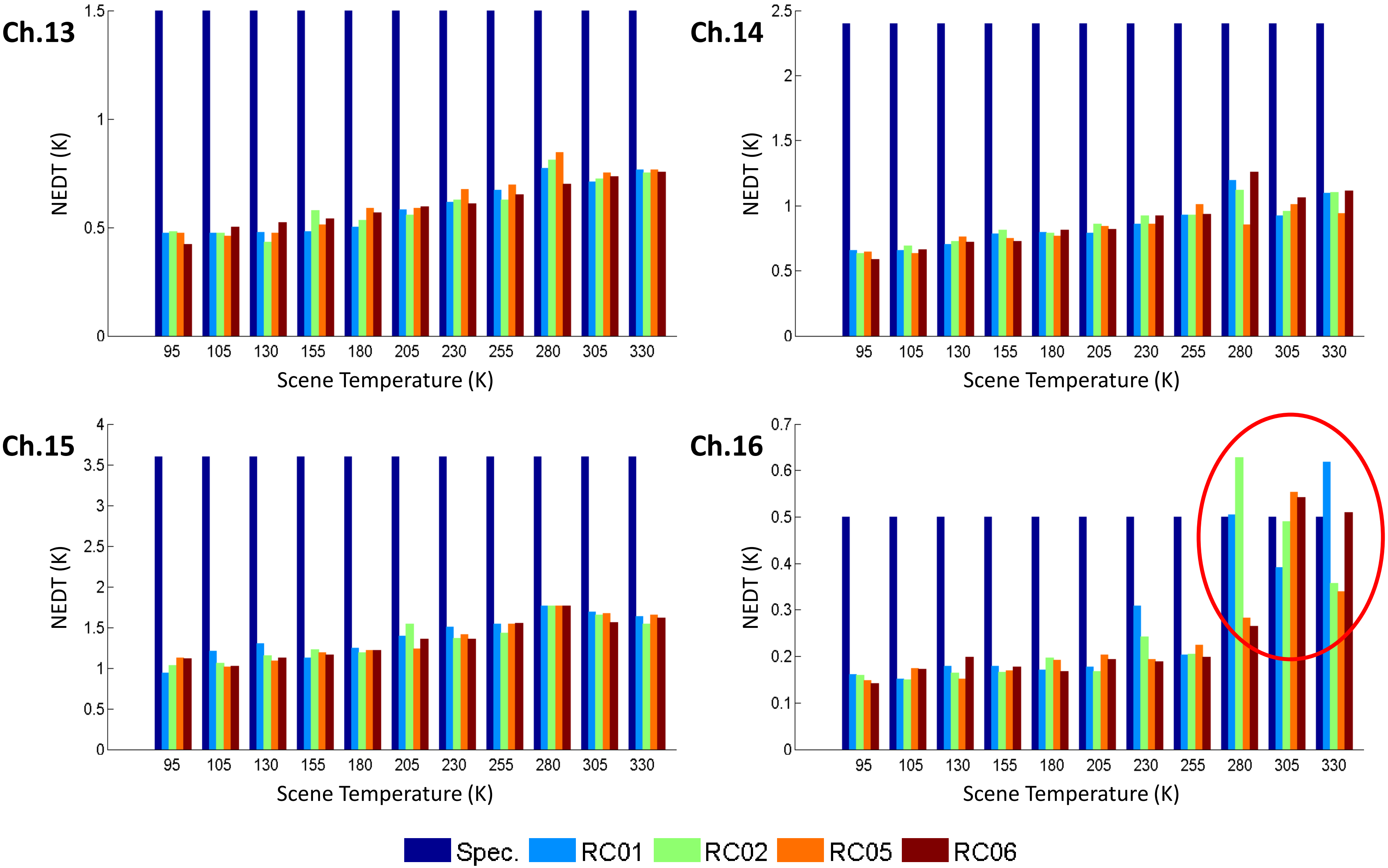

NEΔT at CP_Mid

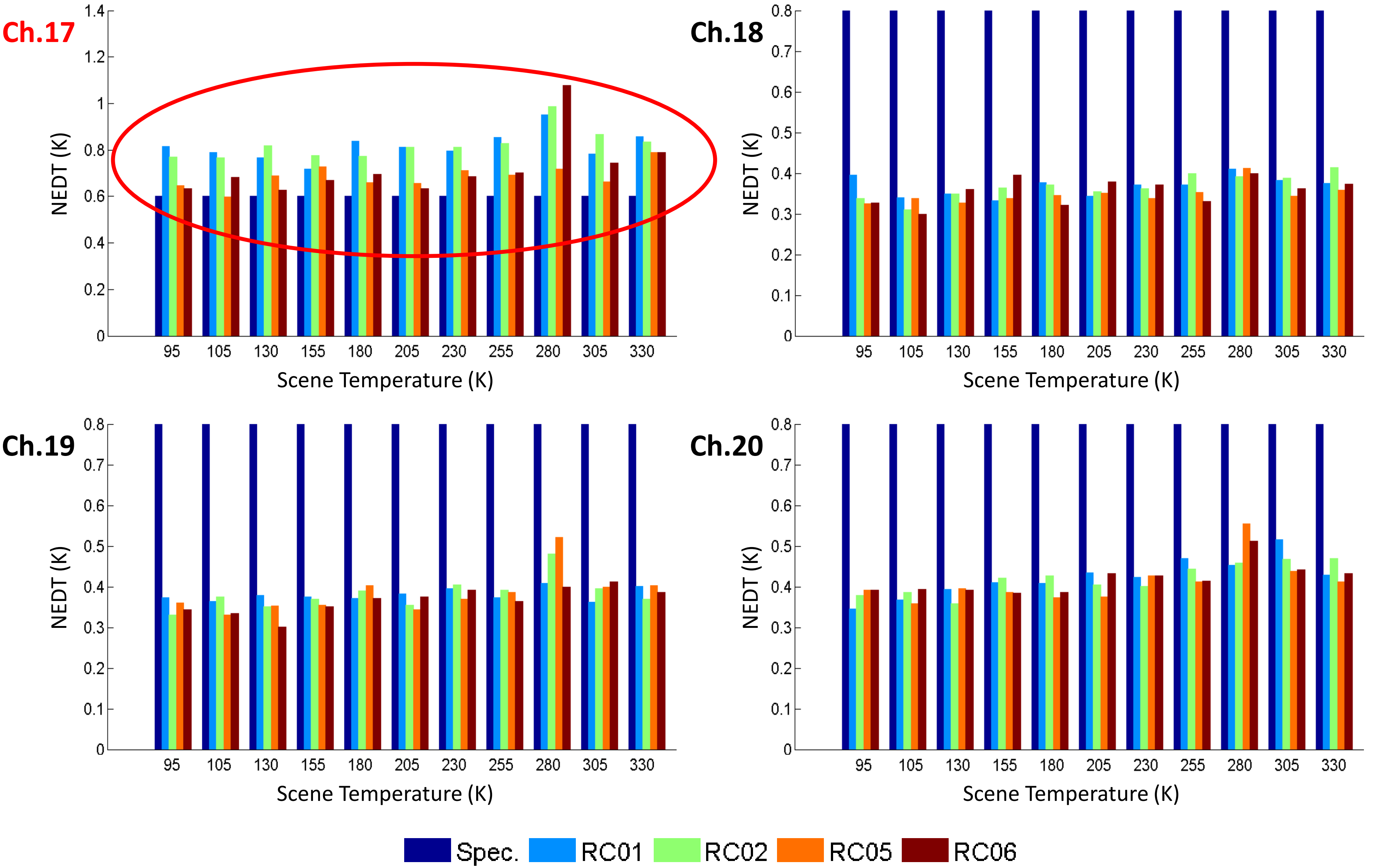

NEΔT at CP_Mid

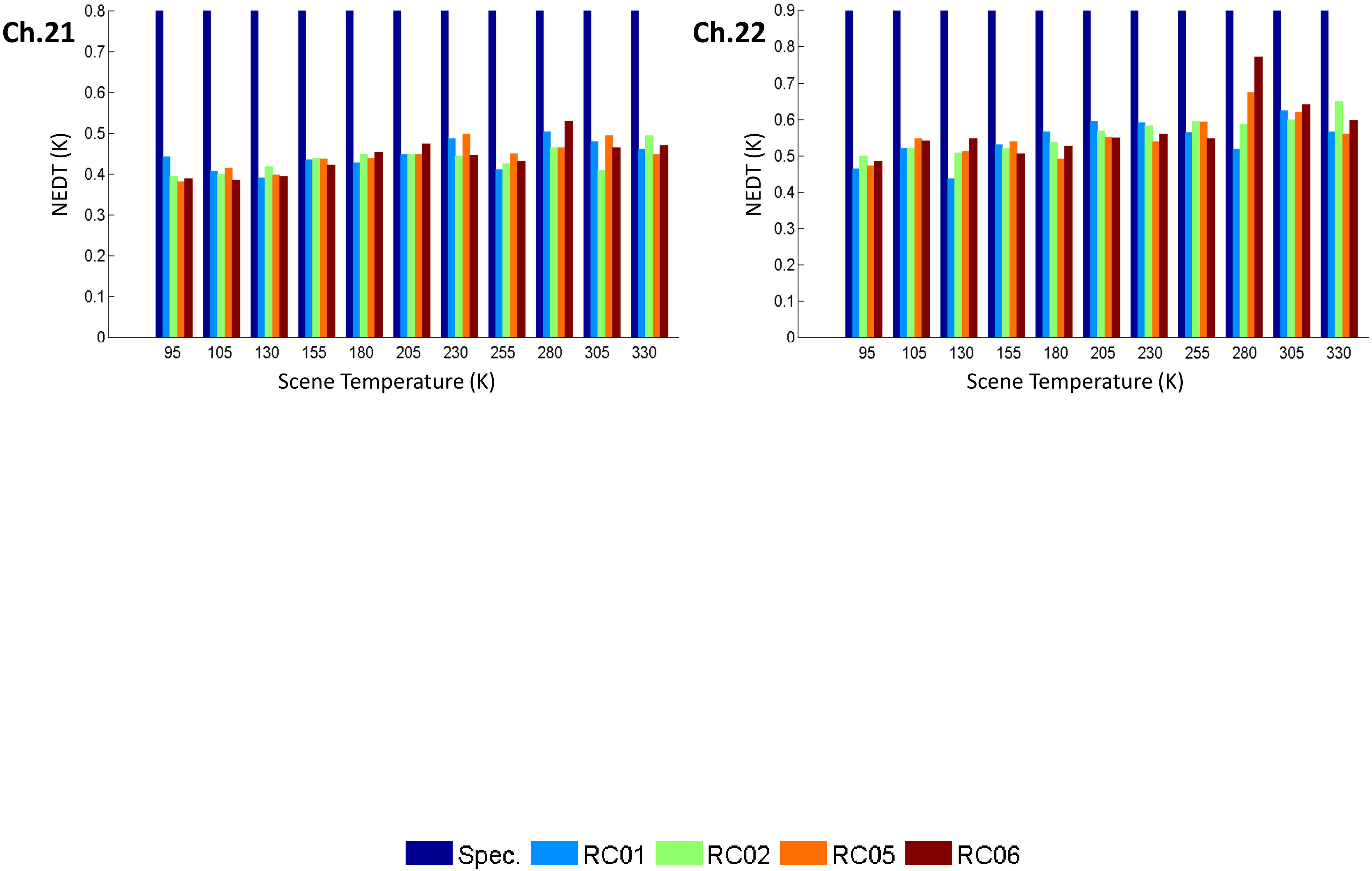

Ch.16 and 17 NEΔT at CP_Mid&CP_High

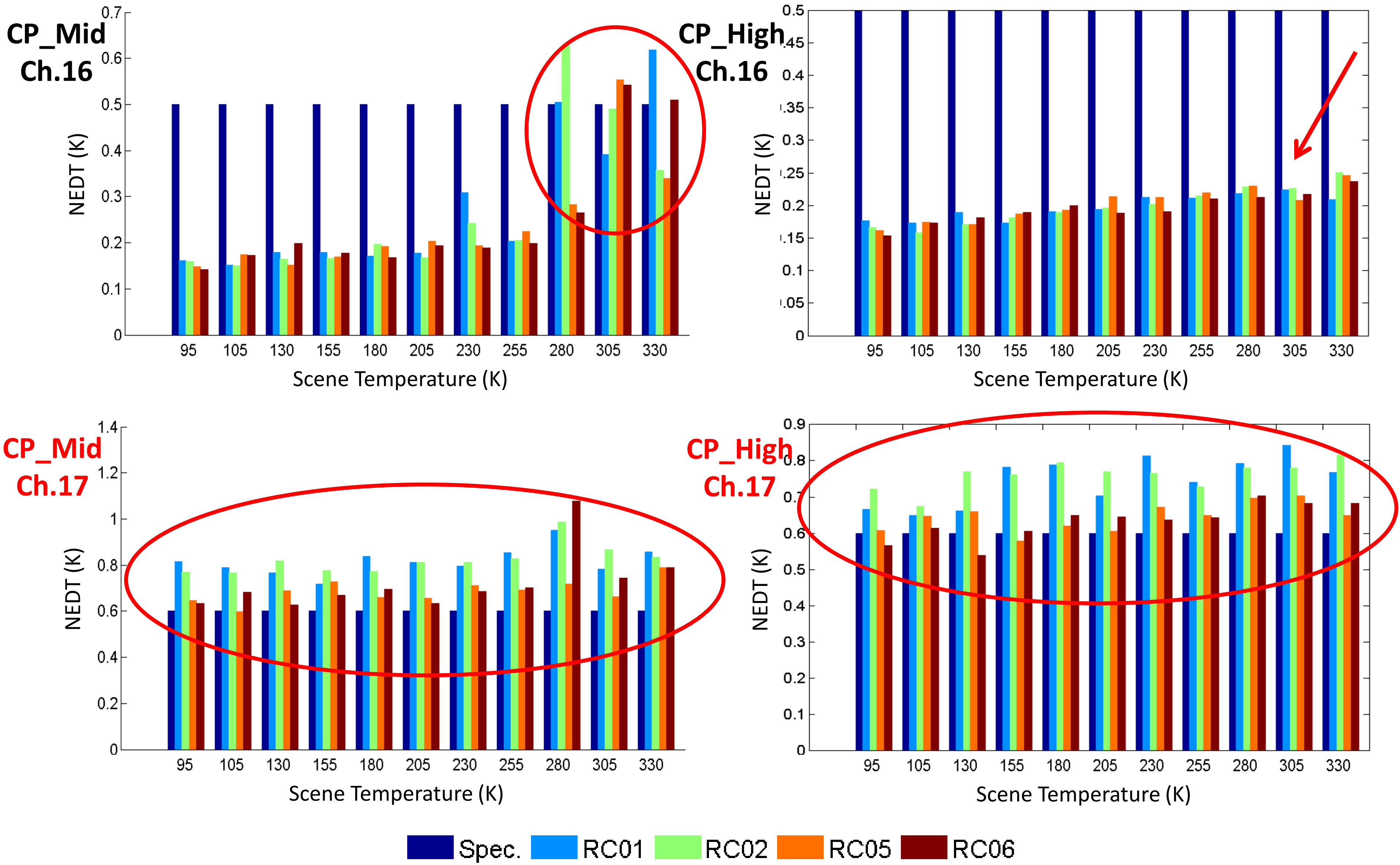

NEΔT at 300K CP_Mid vs. CP_High

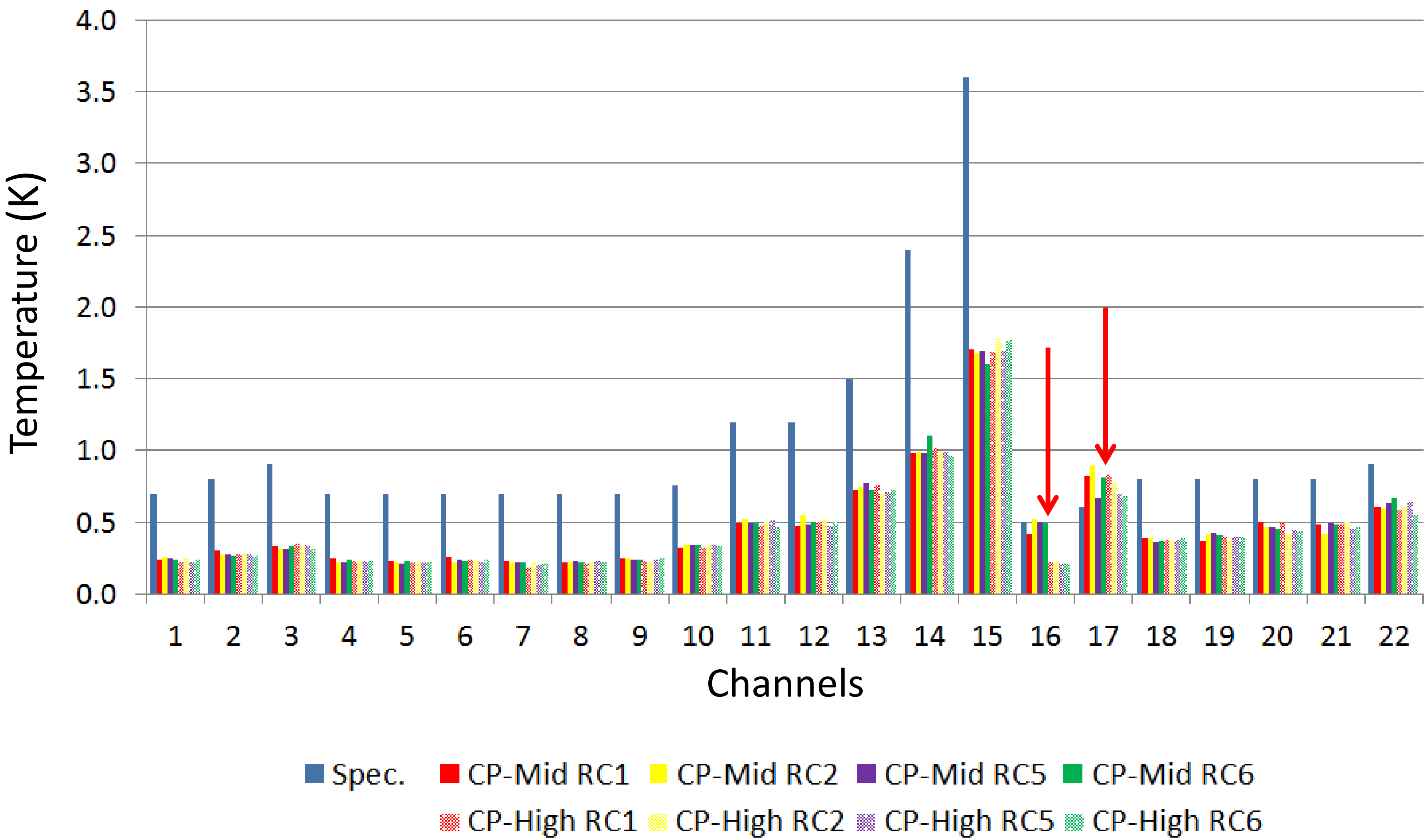

NEΔT at 300K S-NPP vs. J1

NPP	Req.	RC 01	RC 02	RC 05	RC 06
Ch. 01	0.7	0.2472	0.2487	0.2523	0.2465
Ch. 02	0.8	0.3113	0.3104	0.3138	0.3123
Ch. 03	0.9	0.3654	0.3653	0.3647	0.3619
Ch. 04	0.7	0.2789	0.2763	0.2810	0.2784
Ch. 05	0.7	0.2783	0.2688	0.2791	0.2805
Ch. 06	0.7	0.2885	0.2743	0.2847	0.2849
Ch. 07	0.7	0.2712	0.2625	0.2723	0.2680
Ch. 08	0.7	0.2667	0.2584	0.2708	0.2642
Ch. 09	0.7	0.2907	0.2877	0.2869	0.2896
Ch. 10	0.75	0.4179	0.4168	0.4192	0.416
Ch. 11	1.2	0.5547	0.5493	0.5508	0.556
Ch. 12	1.2	0.5744	0.5846	0.5892	0.5819
Ch. 13	1.5	0.8454	0.8473	0.8562	0.8522
Ch. 14	2.4	1.1819	1.2050	1.2334	1.1977
Ch. 15	3.6	1.9266	1.9452	1.9216	1.915
Ch. 16	0.5	0.2848	0.2813	0.2887	0.2771
Ch. 17	0.6	0.4323	0.4507	0.4441	0.4393
Ch. 18	0.8	0.3711	0.3772	0.3546	0.3511
Ch. 19	0.8	0.4318	0.4521	0.4291	0.4179
Ch. 20	0.8	0.5014	0.5346	0.4990	0.4865
Ch. 21	0.8	0.5596	0.5734	0.5362	0.5180
Ch. 22	0.9	0.7119	0.7255	0.6838	0.6817

J1	RC 01	RC 02	RC 05	RC 06	RC 01	RC 02	RC 05	RC 06
Ch. 01	0.2390	0.2562	0.2482	0.2371	0.2298	0.2512	0.2252	0.2441
Ch. 02	0.3047	0.2797	0.2765	0.2620	0.2832	0.2900	0.2857	0.2706
Ch. 03	0.3301	0.3149	0.3106	0.3303	0.3580	0.3360	0.3474	0.3212
Ch. 04	0.2428	0.2188	0.2210	0.2386	0.2305	0.2333	0.2301	0.2363
Ch. 05	0.2323	0.2232	0.2137	0.2242	0.2206	0.2281	0.2265	0.2212
Ch. 06	0.2548	0.2193	0.2402	0.2325	0.2414	0.2440	0.2246	0.2393
Ch. 07	0.2307	0.2201	0.2169	0.2168	0.1916	0.2262	0.2080	0.2151
Ch. 08	0.2207	0.2146	0.2324	0.2215	0.2130	0.2248	0.2346	0.2253
Ch. 09	0.2472	0.2469	0.2407	0.2398	0.2367	0.2284	0.2477	0.2492
Ch. 10	0.3190	0.3440	0.3392	0.3400	0.3294	0.3509	0.3506	0.3407
Ch. 11	0.4910	0.5199	0.4942	0.4899	0.4816	0.5063	0.5139	0.4685
Ch. 12	0.4765	0.5431	0.4794	0.5023	0.5066	0.5233	0.4743	0.5068
Ch. 13	0.7241	0.7426	0.7703	0.7282	0.7581	0.6994	0.7180	0.7299
Ch. 14	0.9773	0.9877	0.9789	1.1020	1.0217	1.0030	0.9990	0.9653
Ch. 15	1.7068	1.6756	1.6909	1.6007	1.6940	1.7809	1.7025	1.7734
Ch. 16	0.4142	0.5182	0.4987	0.4865	0.2225	0.2270	0.2124	0.2159
Ch. 17	0.8167	0.8902	0.6734	0.8094	0.8328	0.7797	0.7014	0.6857
Ch. 18	0.3881	0.3885	0.3569	0.3697	0.3837	0.3862	0.3835	0.3903
Ch. 19	0.3711	0.4120	0.4235	0.4101	0.4032	0.3894	0.3989	0.4058
Ch. 20	0.5035	0.4660	0.4611	0.4555	0.4948	0.4225	0.4482	0.4404
Ch. 21	0.4833	0.4194	0.4868	0.4776	0.4882	0.5108	0.4600	0.4727
Ch. 22	0.6022	0.5970	0.6311	0.6674	0.5940	0.6081	0.6469	0.5506

NEΔT vs. Allan Variance at 300K (CP_Mid)

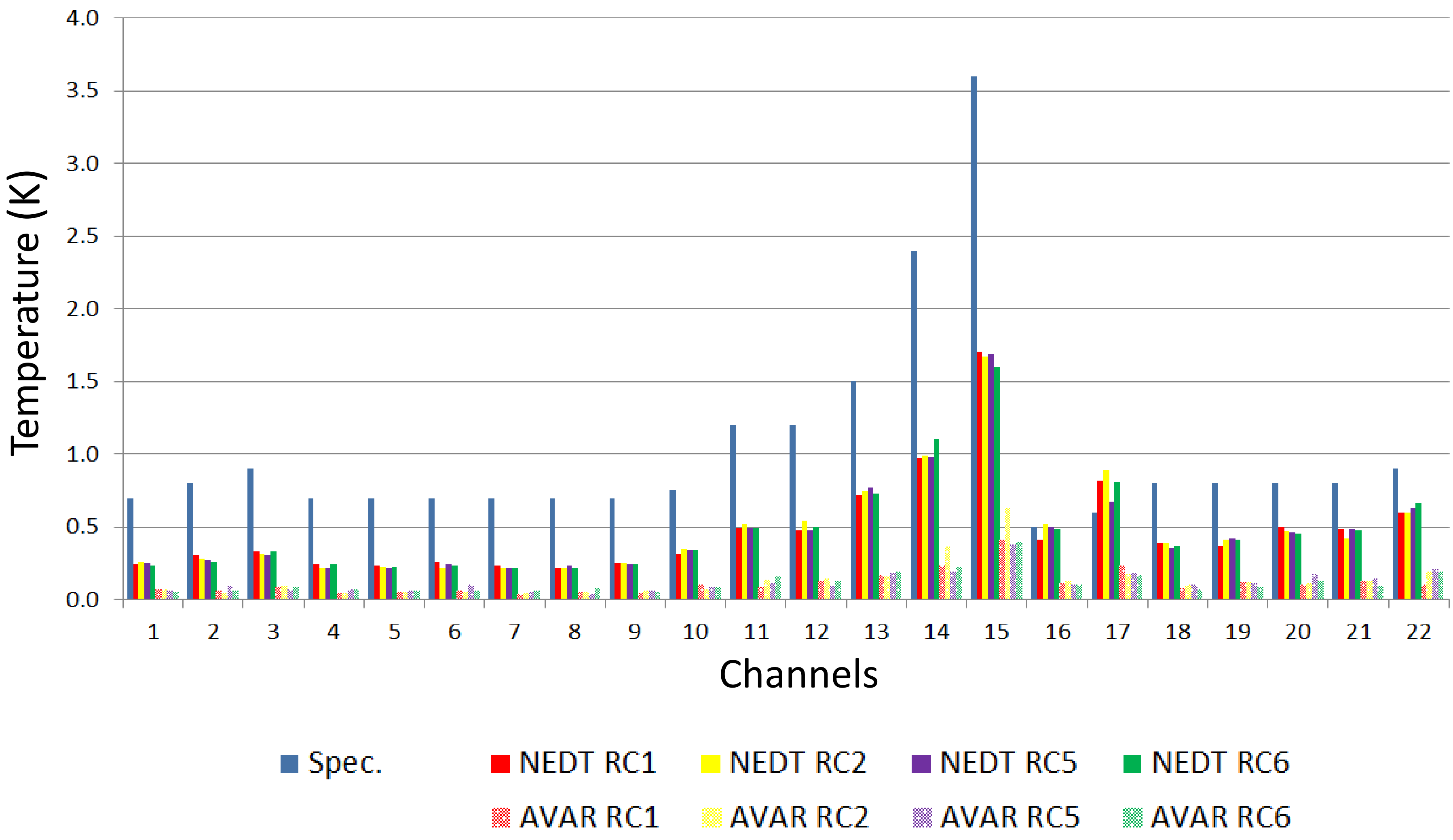

Radiometric Accuracy at CP_Mid ST-95

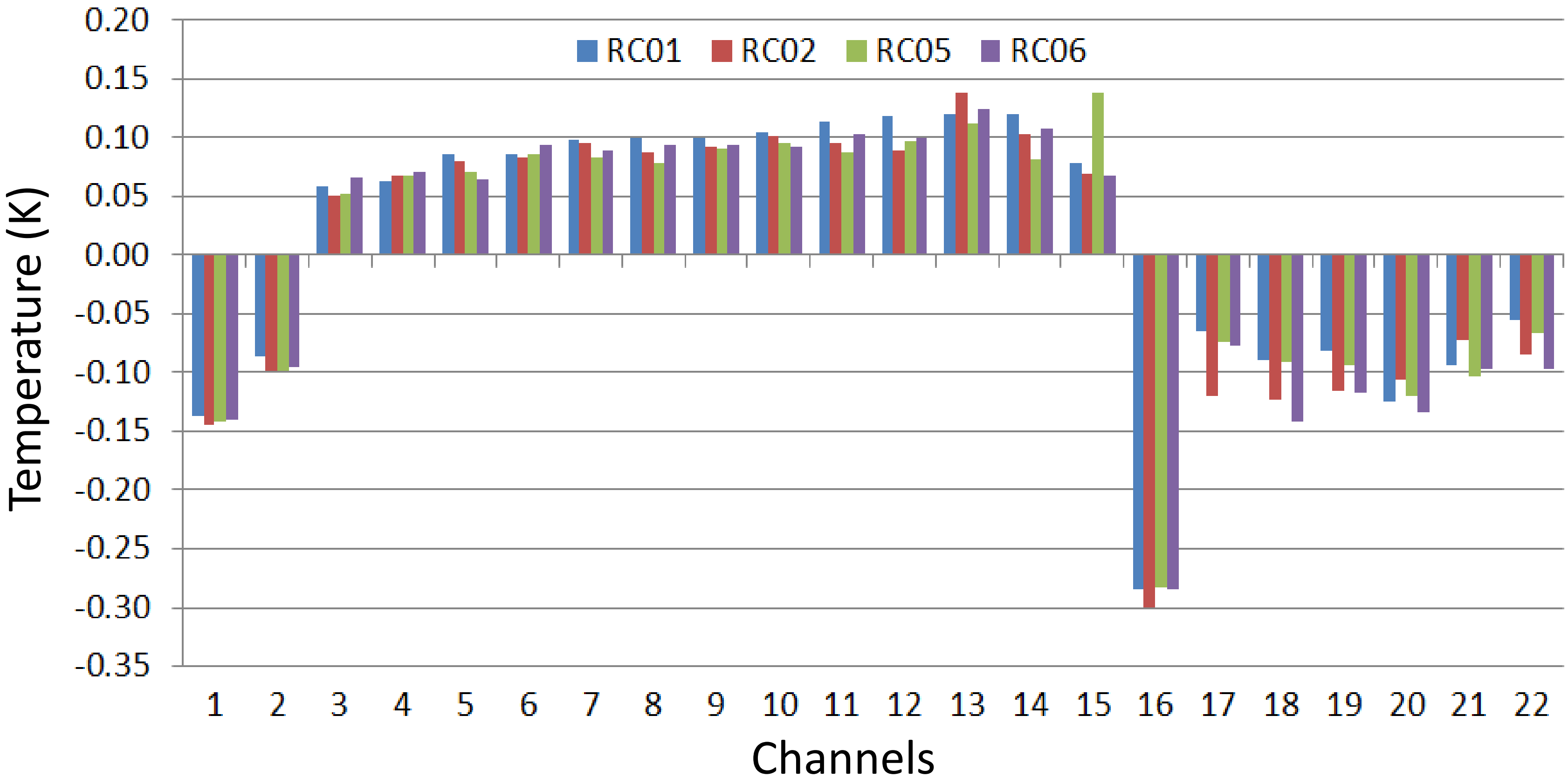

Note: Accuracy is computed by subtracting the inferred scene brightness temperature using two-point linear calibration equation with corresponding measured scene brightness temperature. FOV# 9 to 22 are used.

Radiometric Accuracy at CP_Mid ST-105

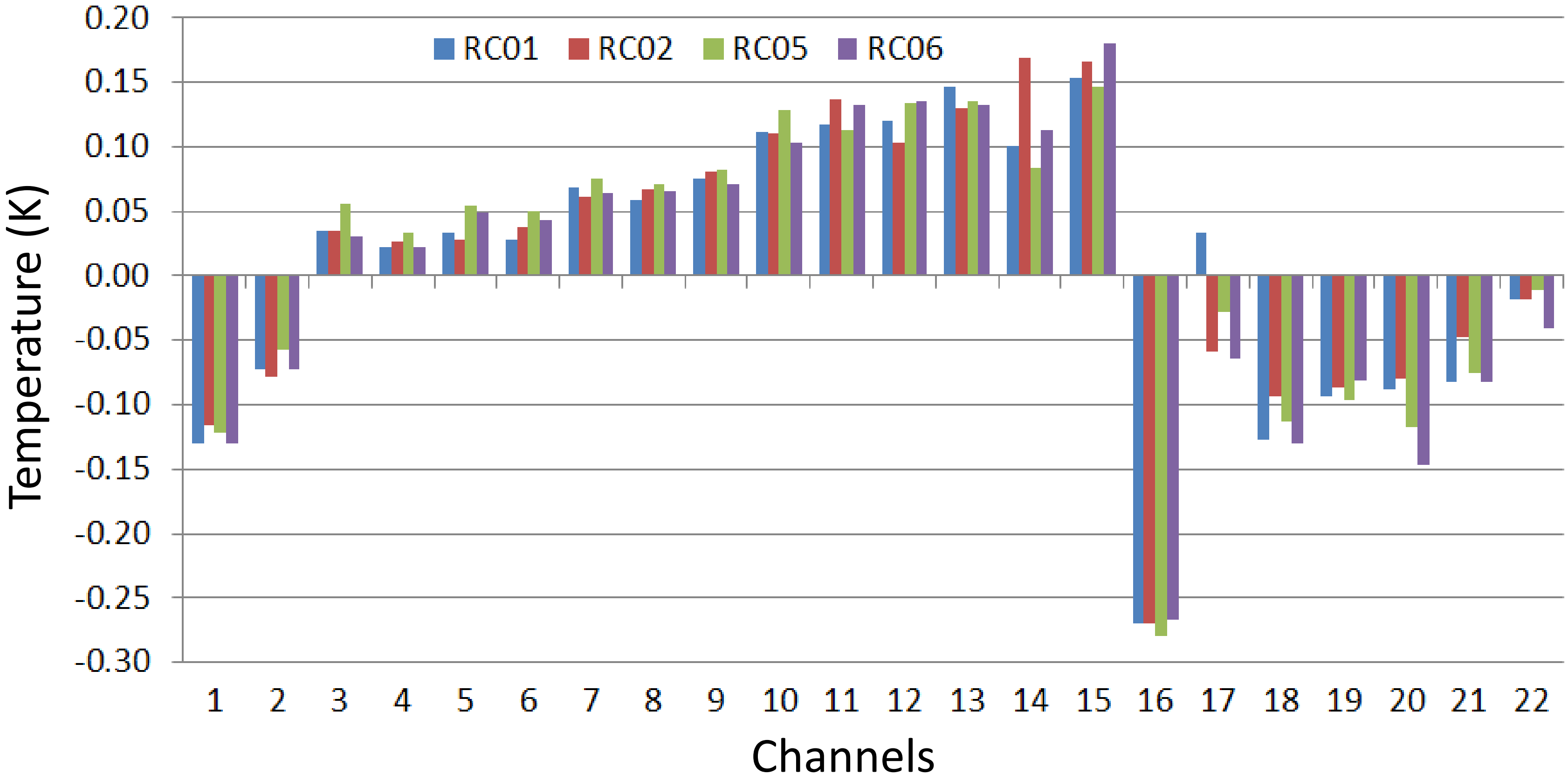

Radiometric Accuracy at CP_Mid ST-130

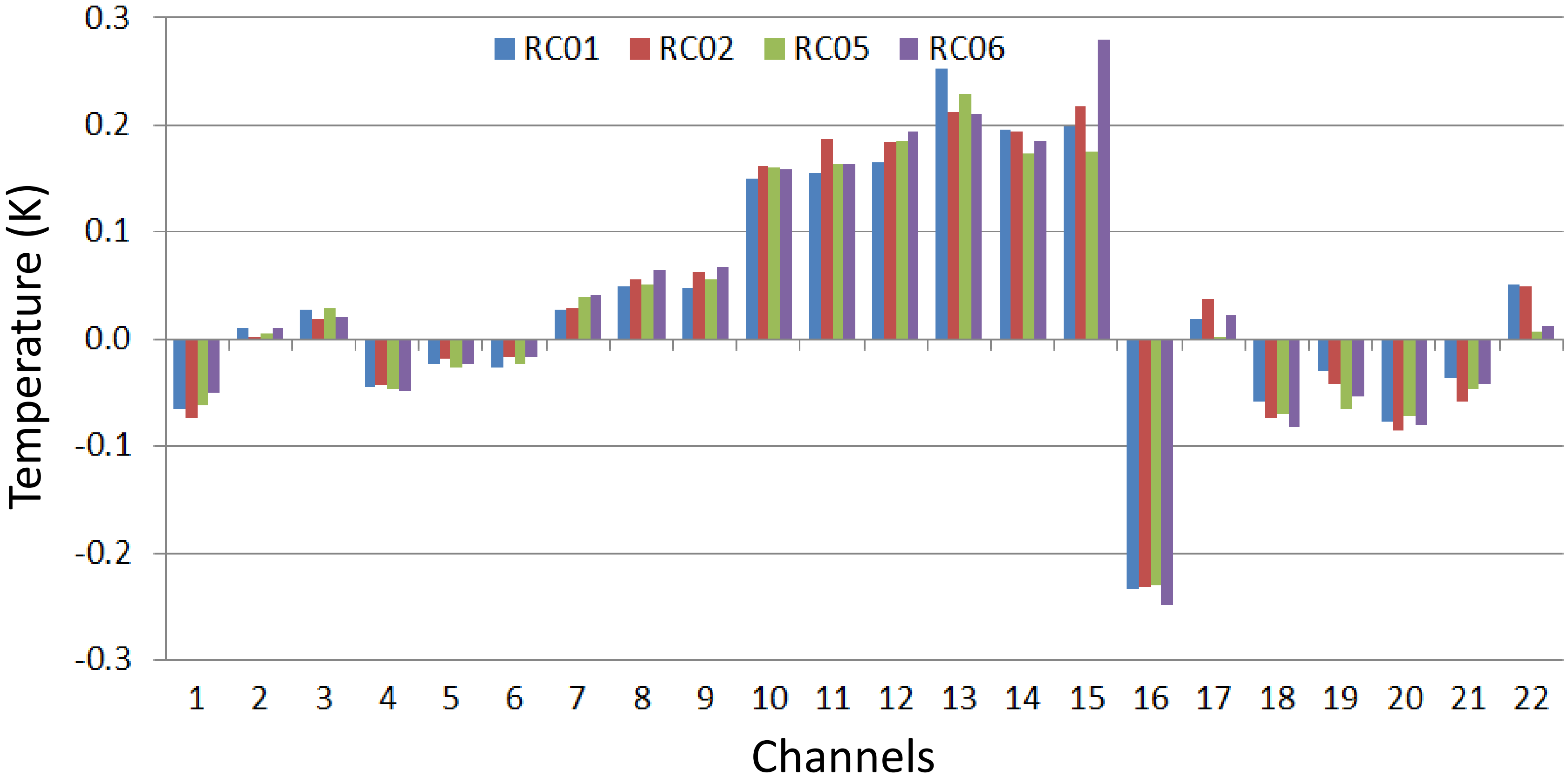

Radiometric Accuracy at CP_Mid ST-155

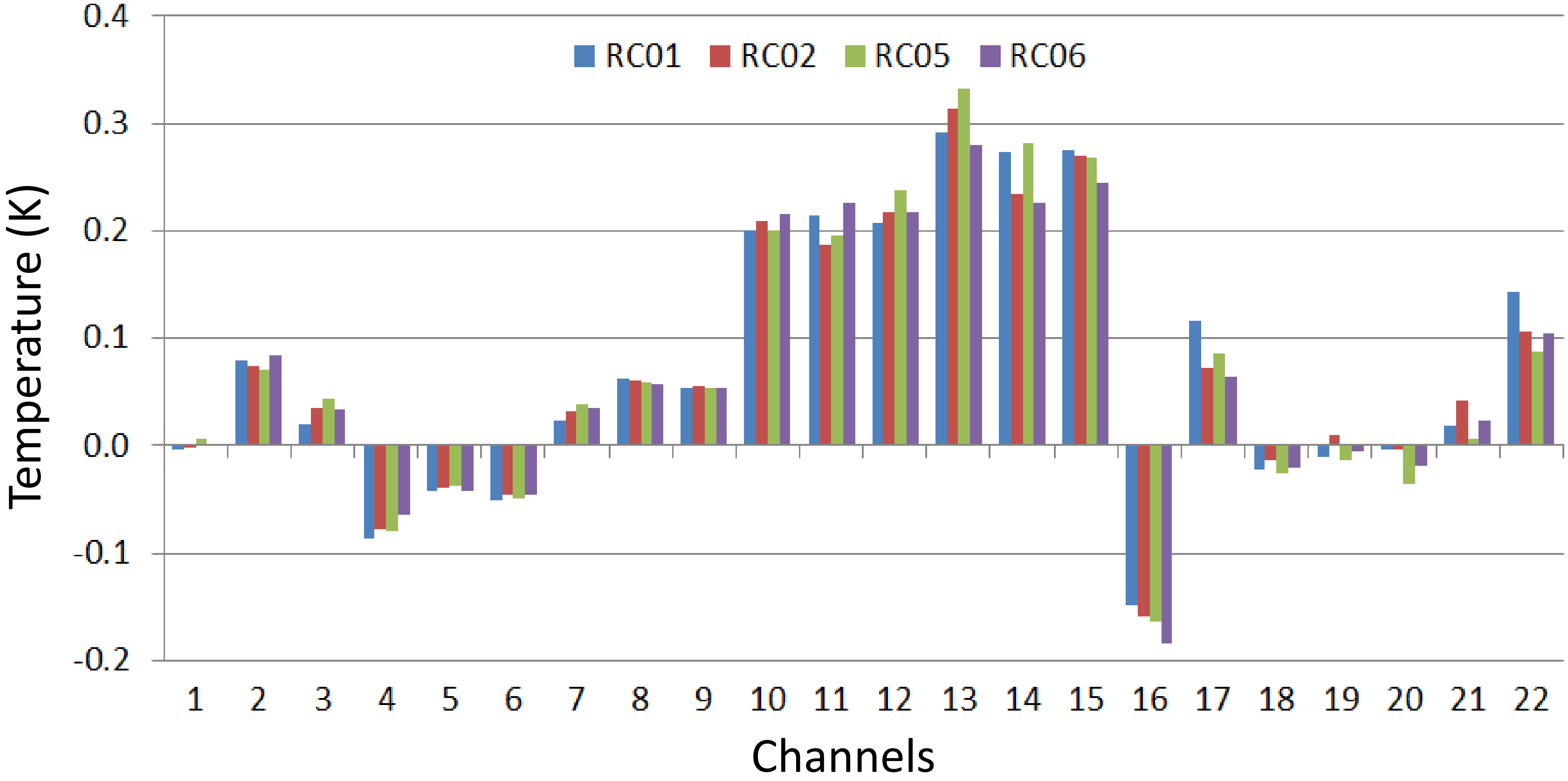

Radiometric Accuracy at CP_Mid ST-180

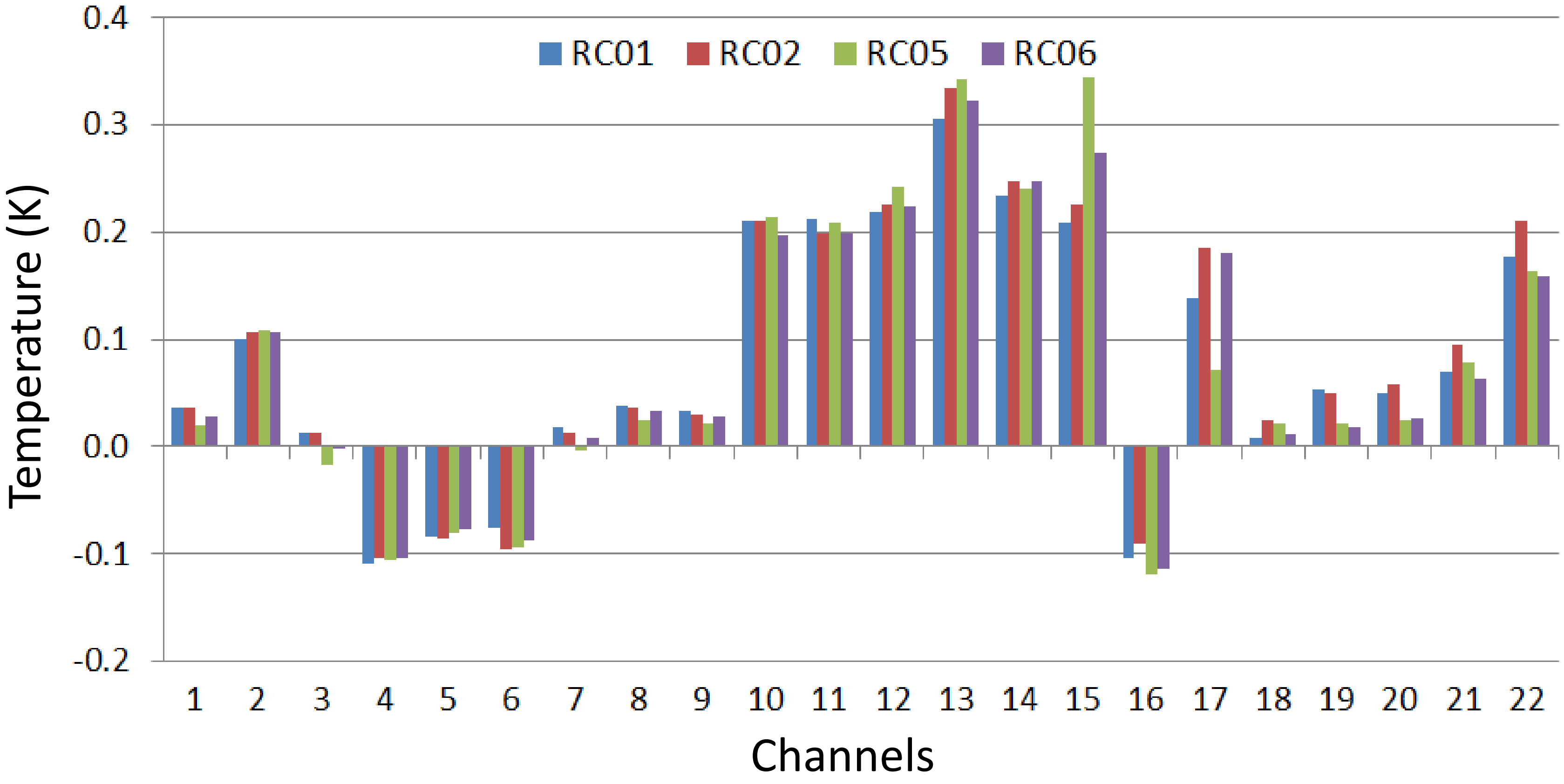

Radiometric Accuracy at CP_Mid ST-205

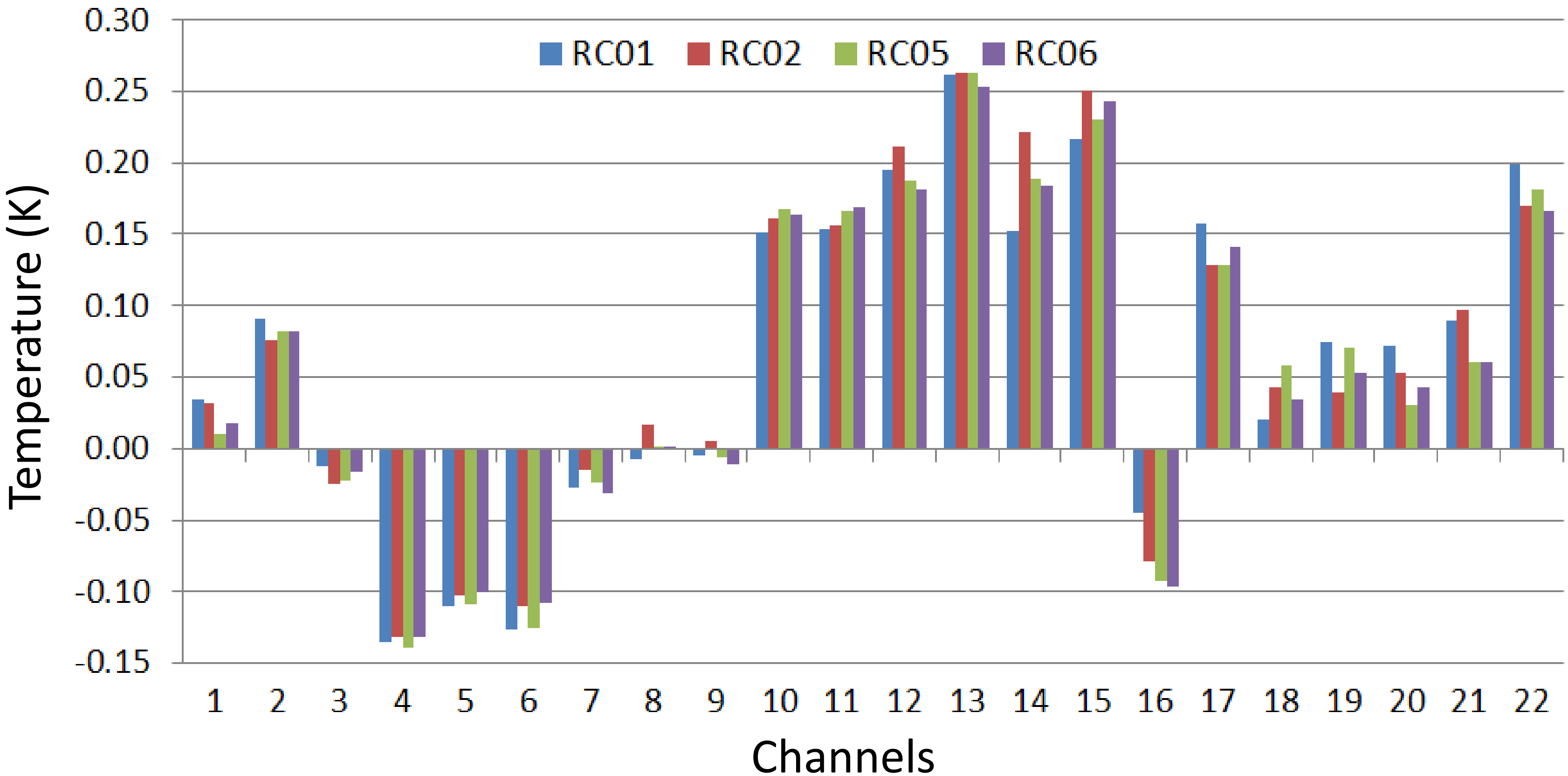

Radiometric Accuracy at CP_Mid ST-230

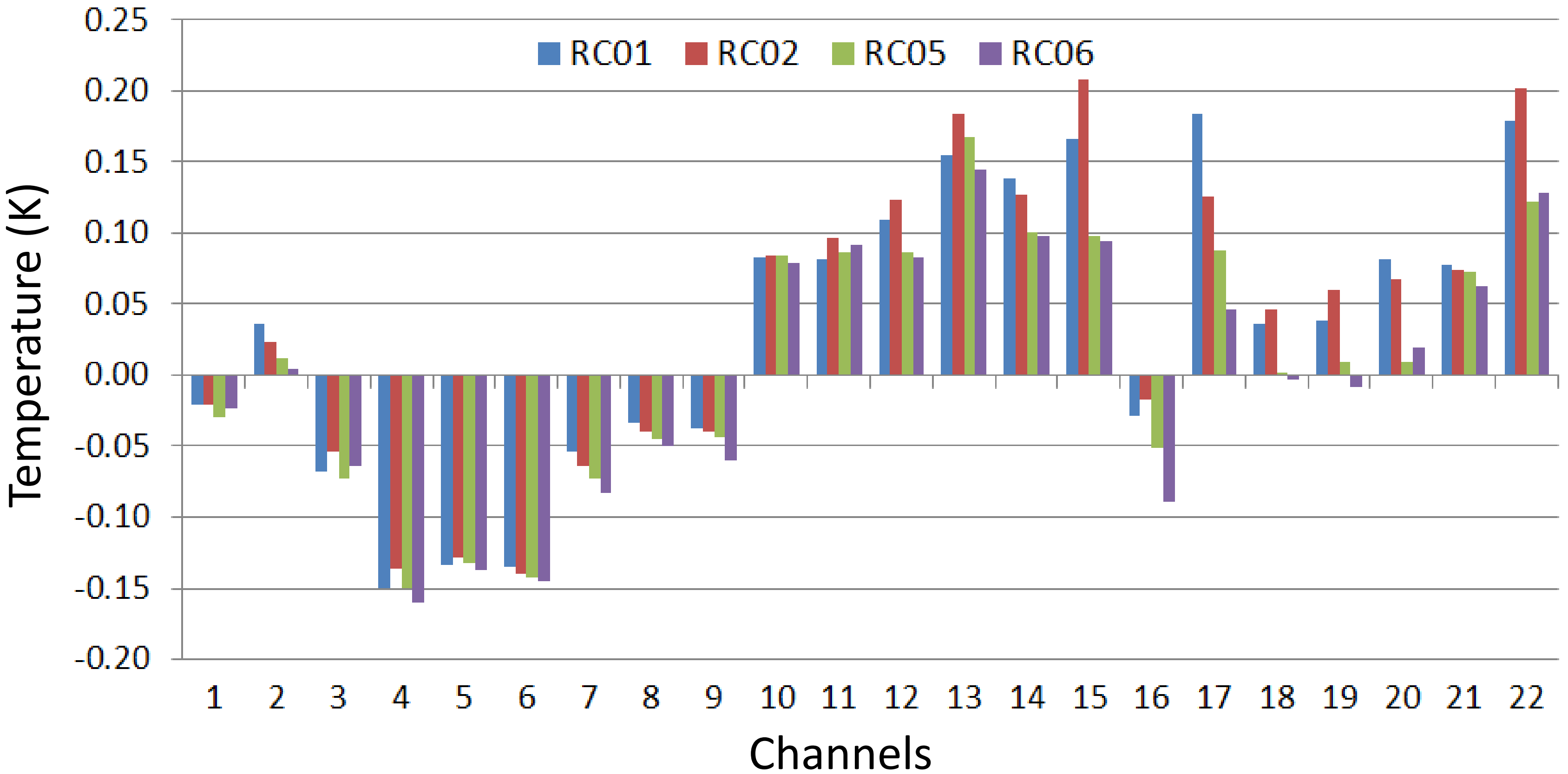

Radiometric Accuracy at CP_Mid ST-255

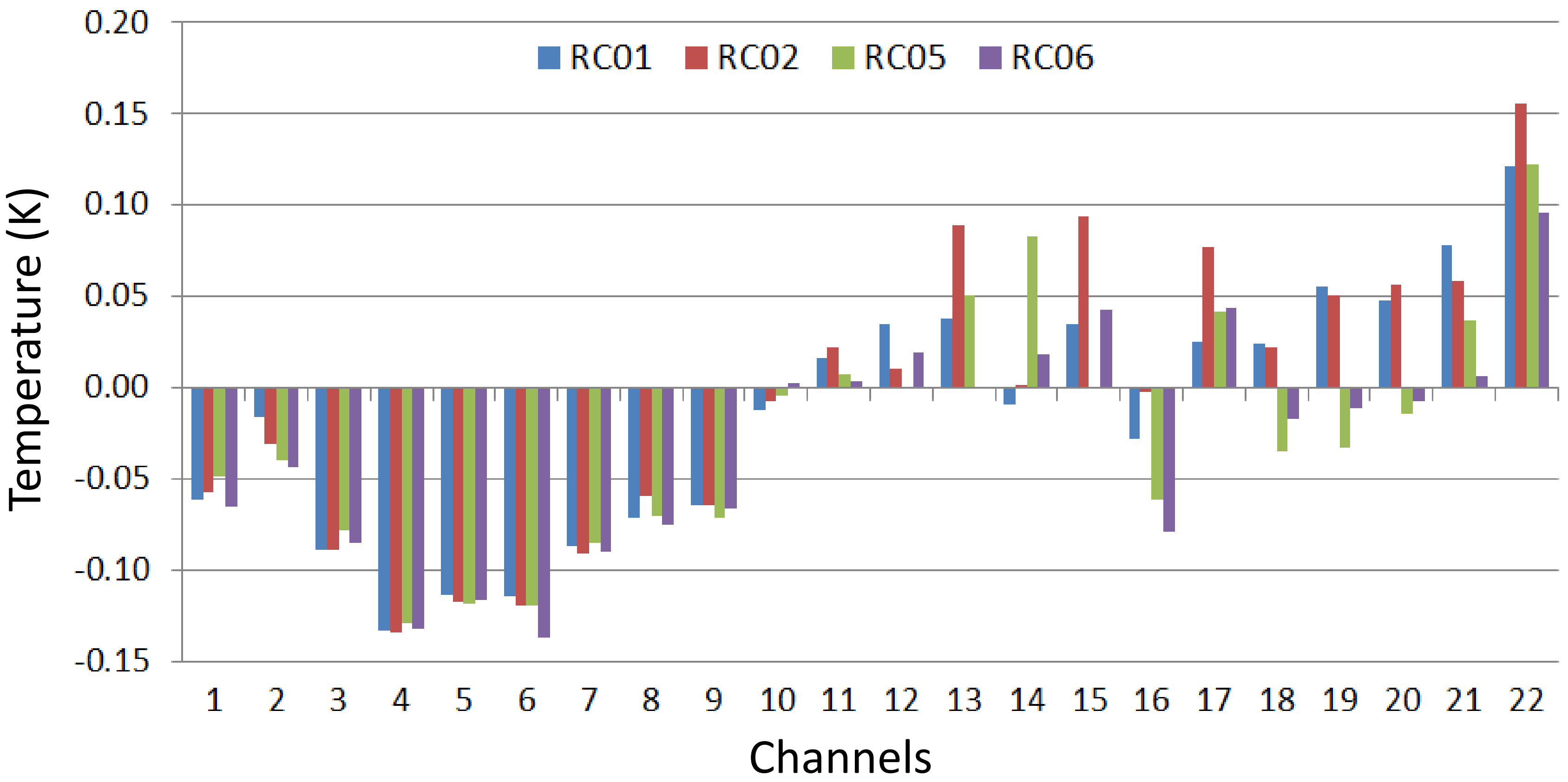

Radiometric Accuracy at CP_Mid ST-280

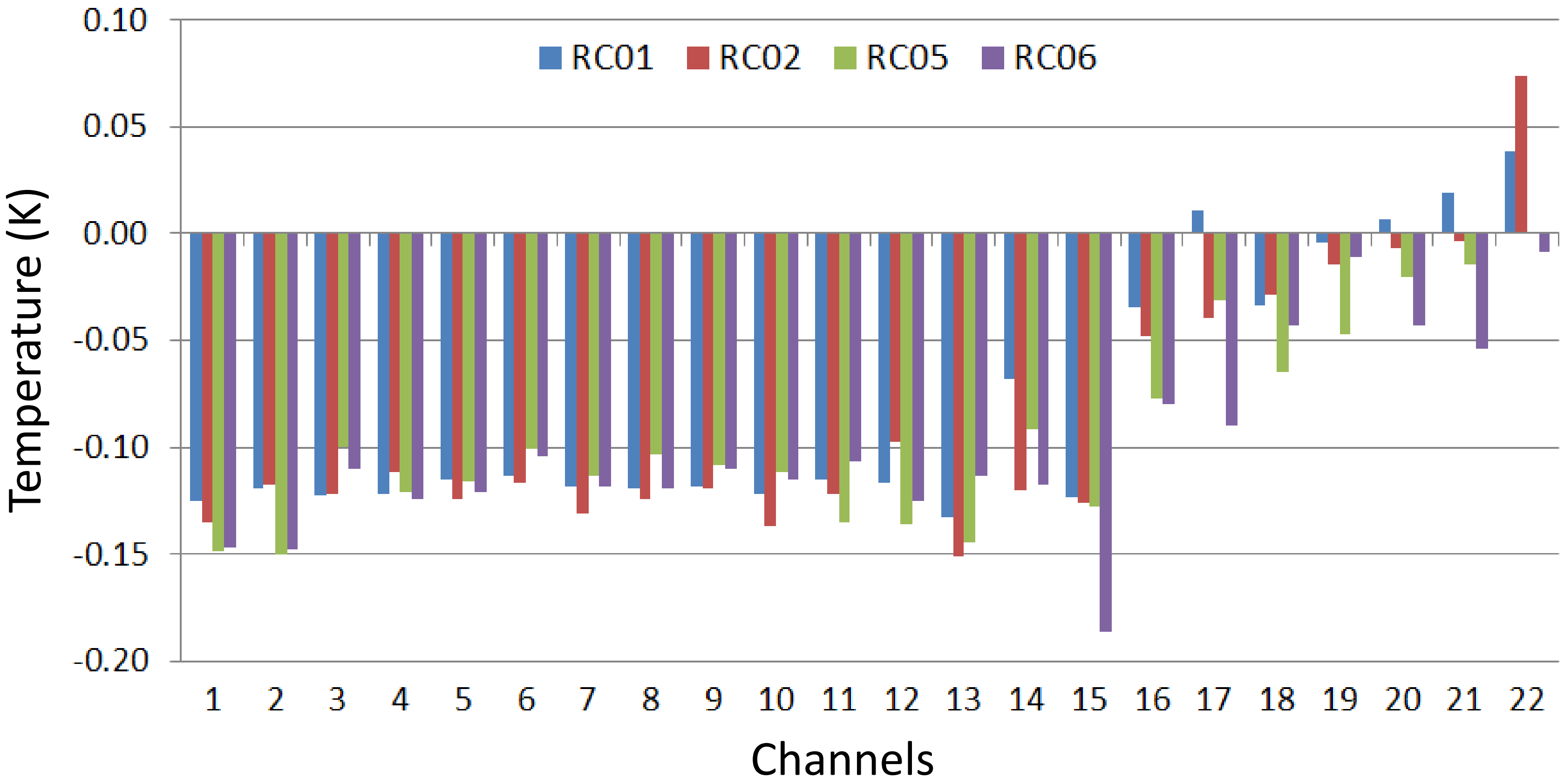

Radiometric Accuracy at CP_Mid ST-305

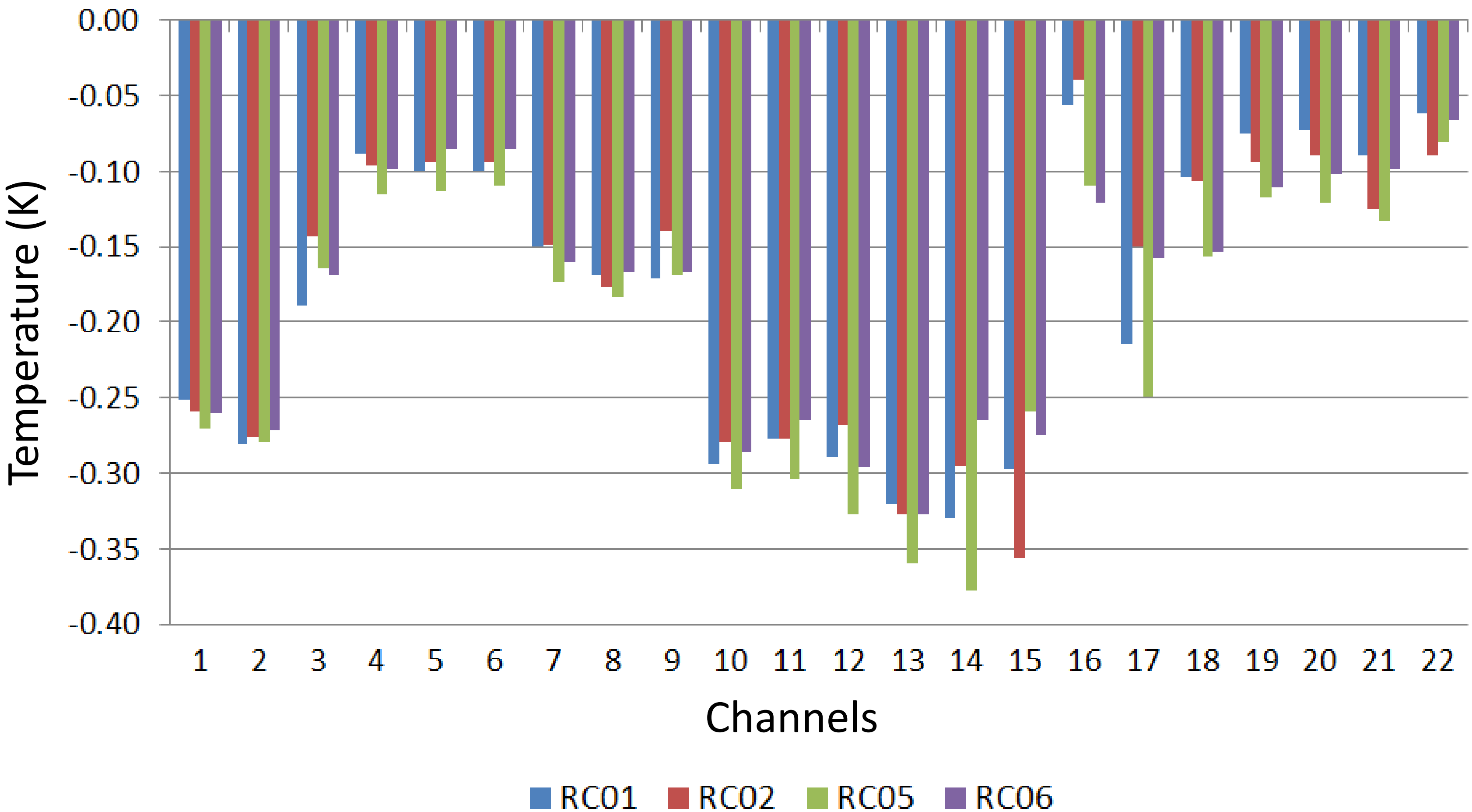

Radiometric Accuracy at CP_Mid ST-330

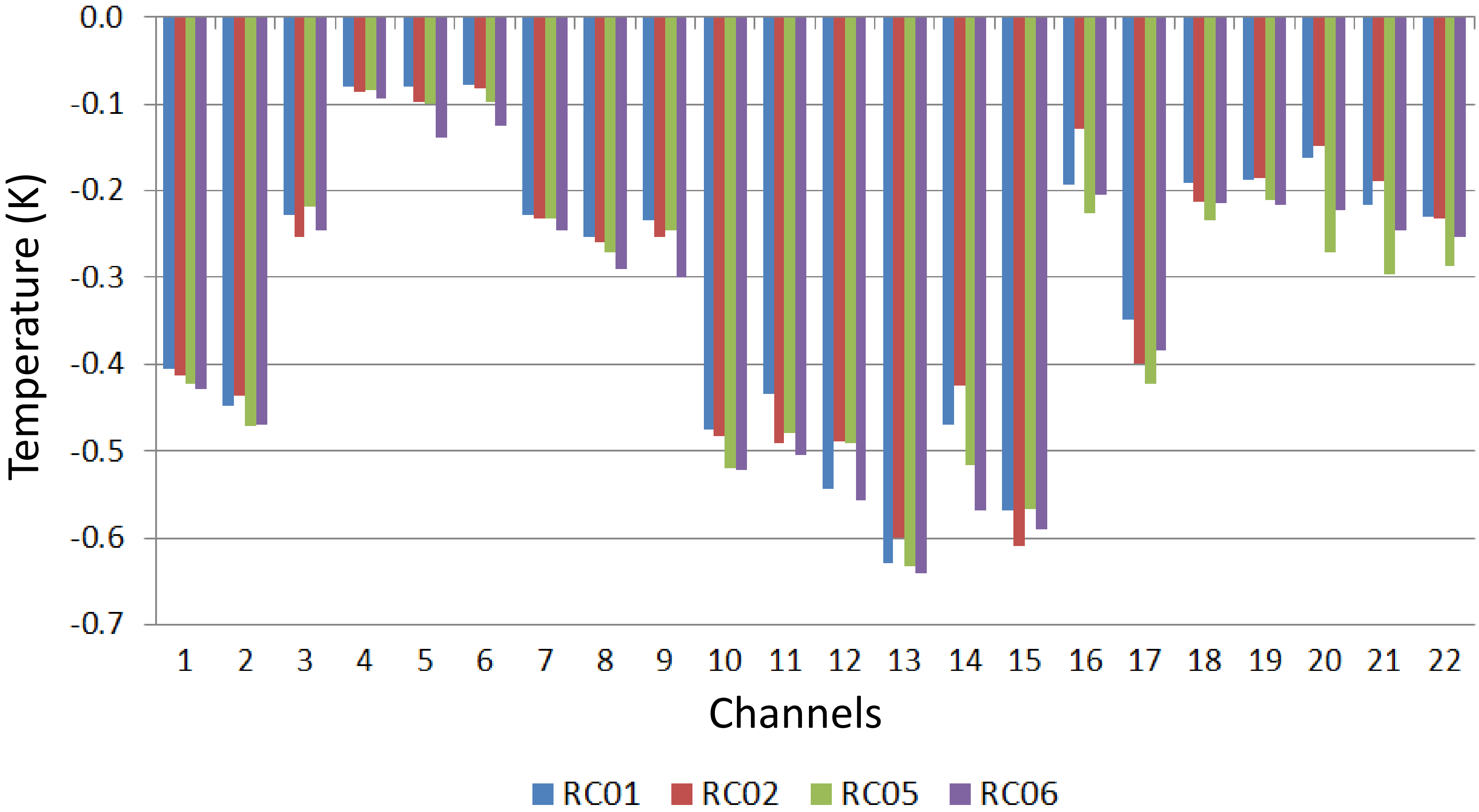

Radiometric Accuracy at CP_Mid RC1

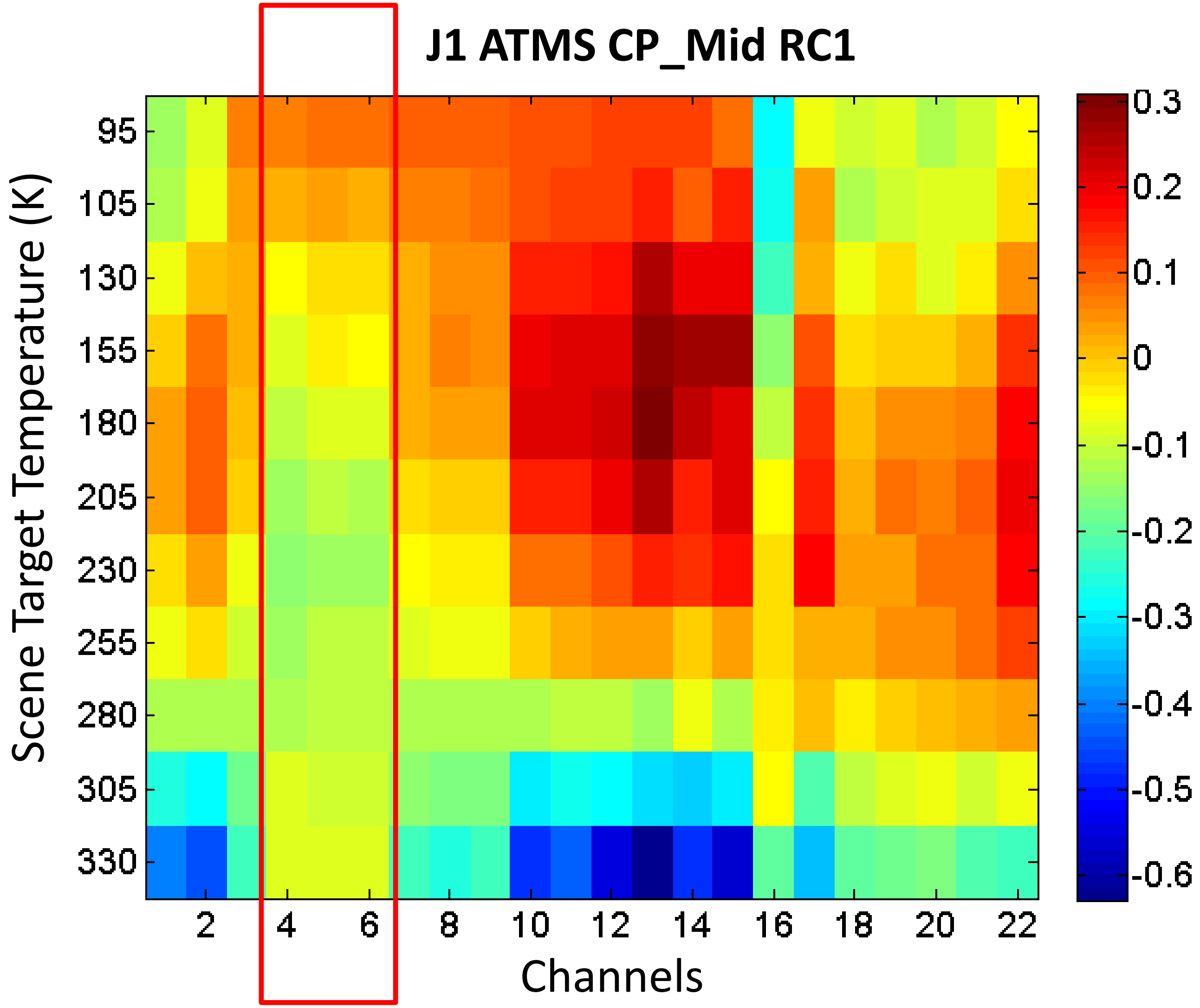

Nonlinearity Fitting for CP_Mid RC1 vs. S-NPP

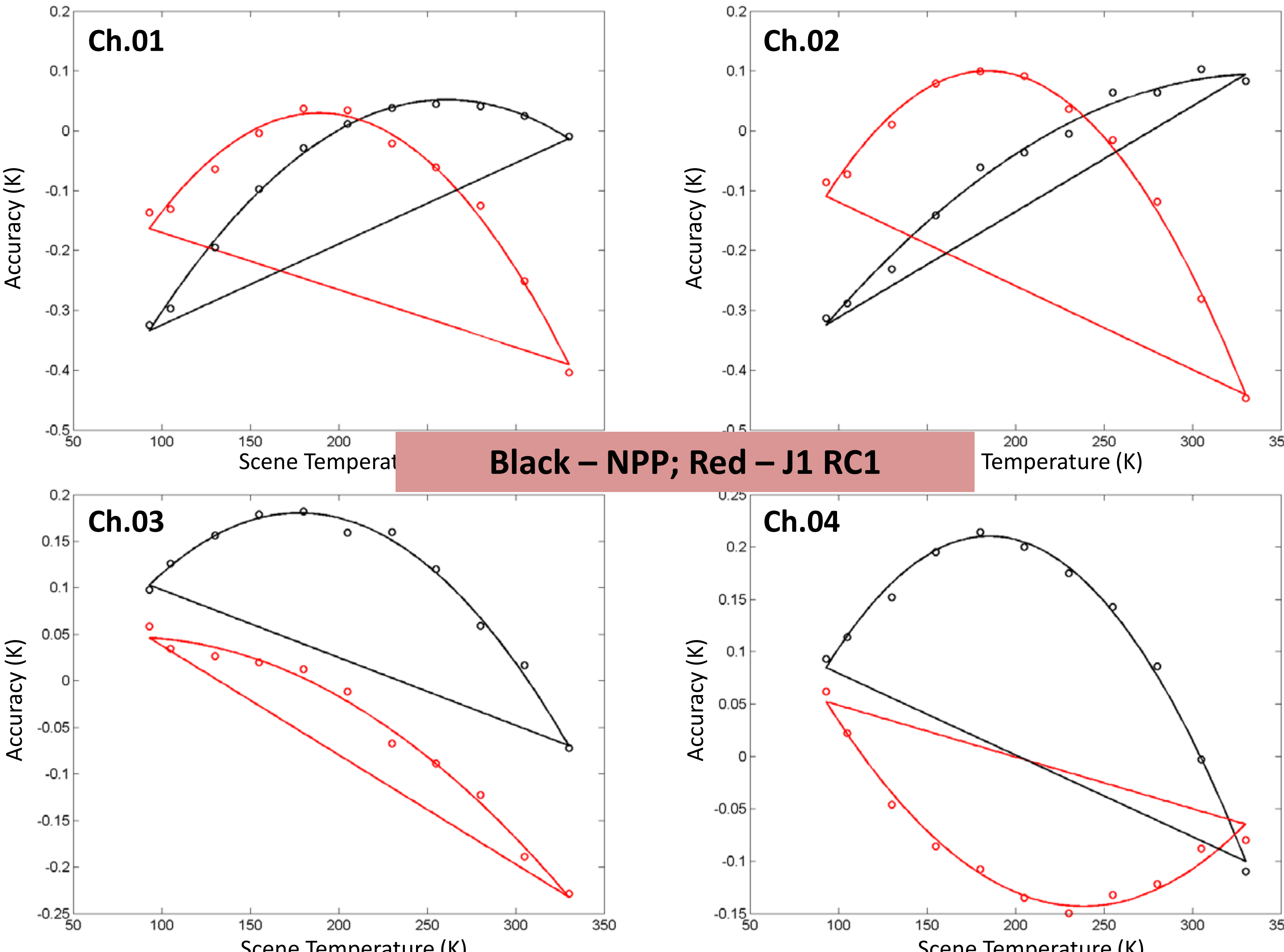

Nonlinearity Fitting for CP_Mid RC1 vs. S-NPP

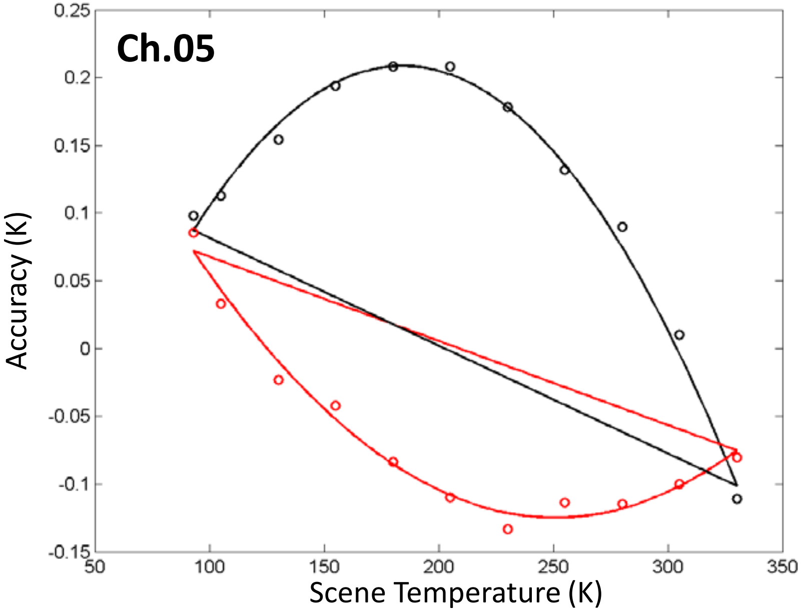

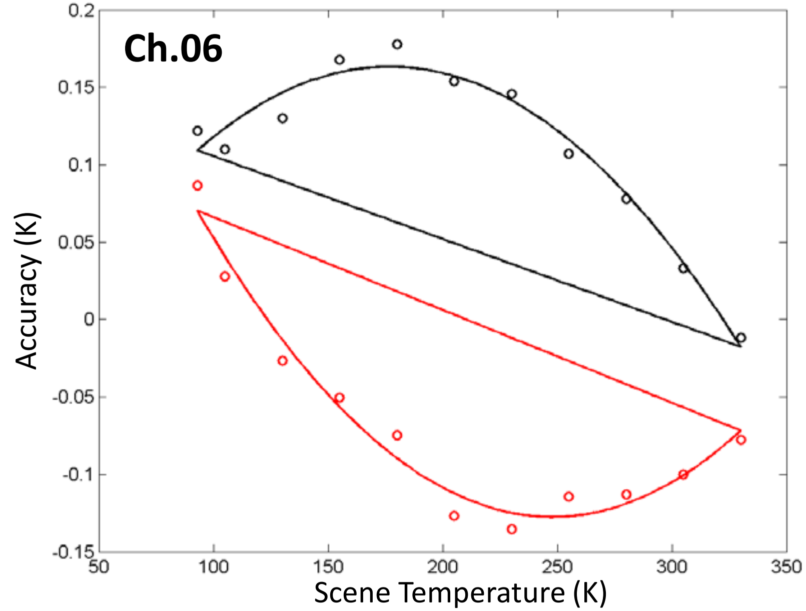

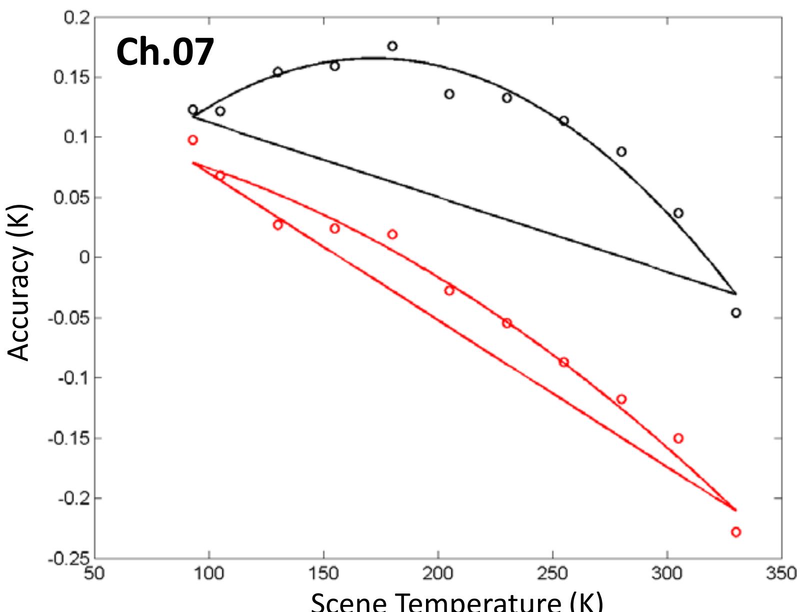

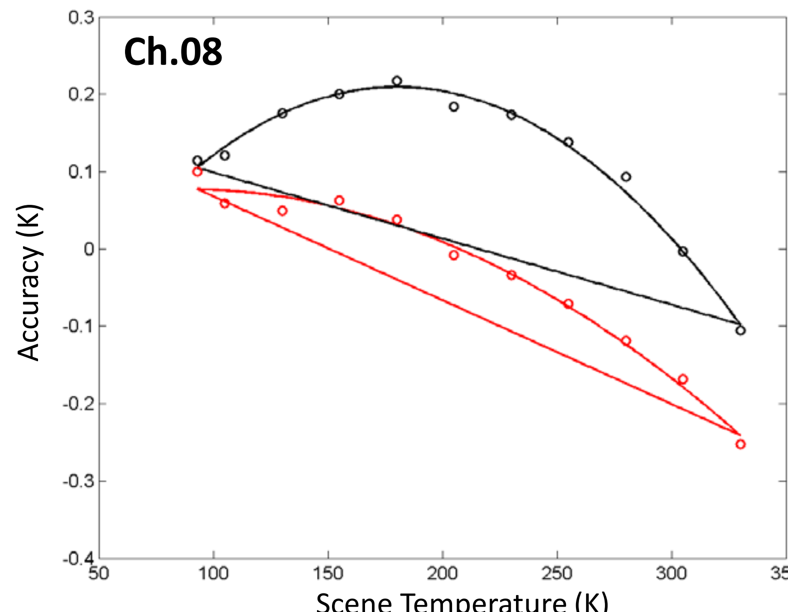

Nonlinearity Fitting for CP_Mid RC1 vs. S-NPP

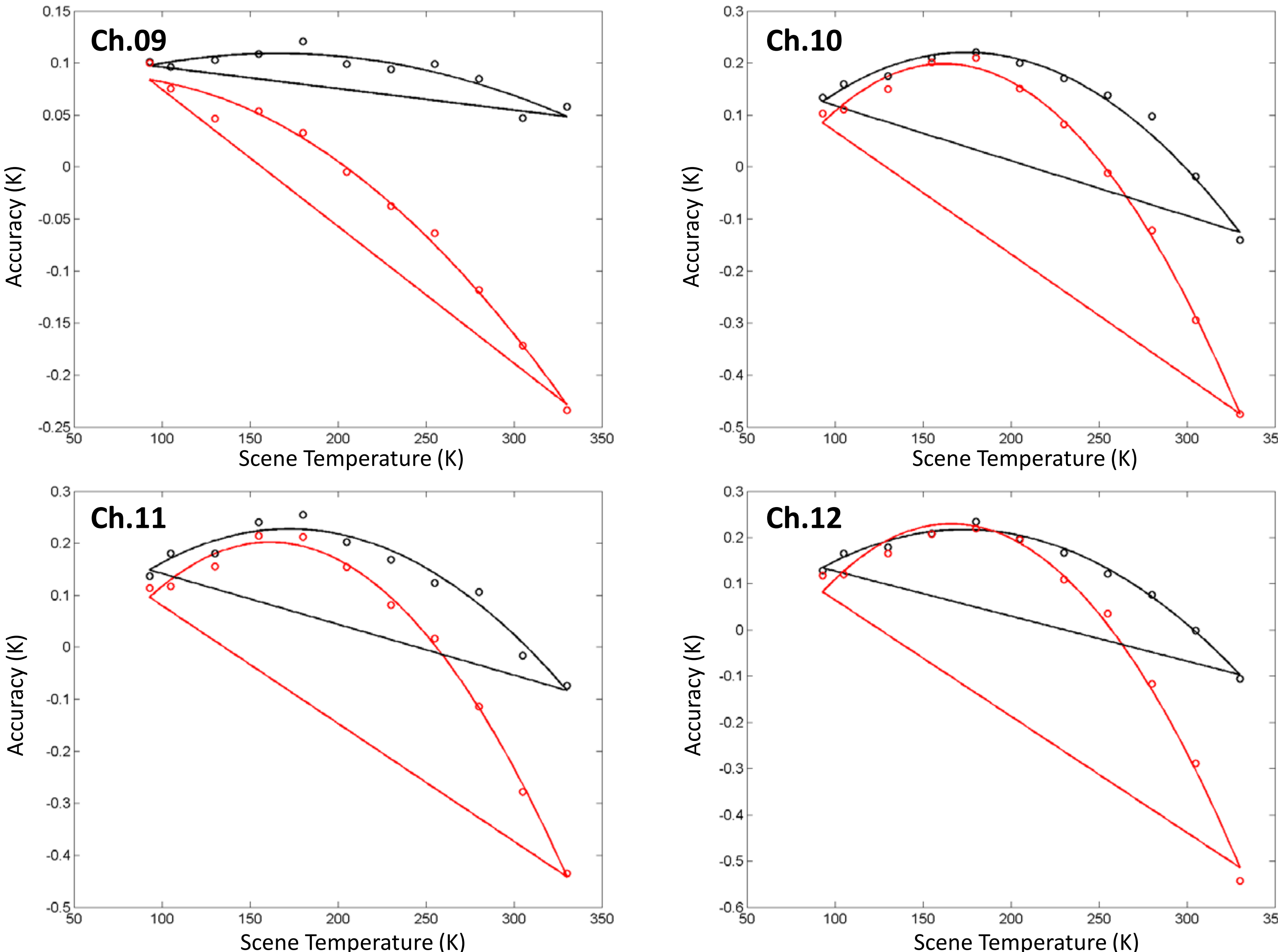

Nonlinearity Fitting for CP_Mid RC1 vs. S-NPP

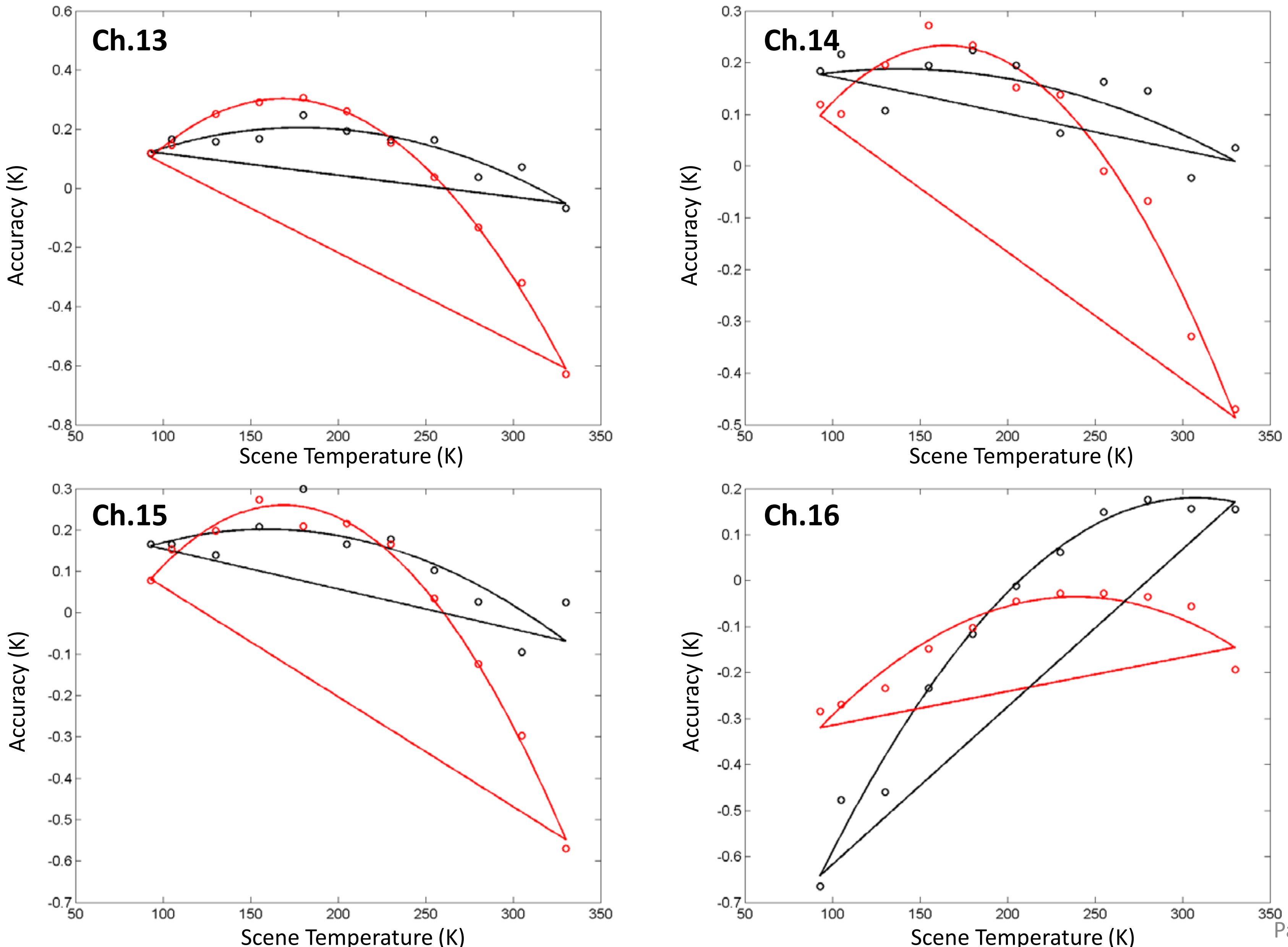

Nonlinearity Fitting for CP_Mid RC1 vs. S-NPP

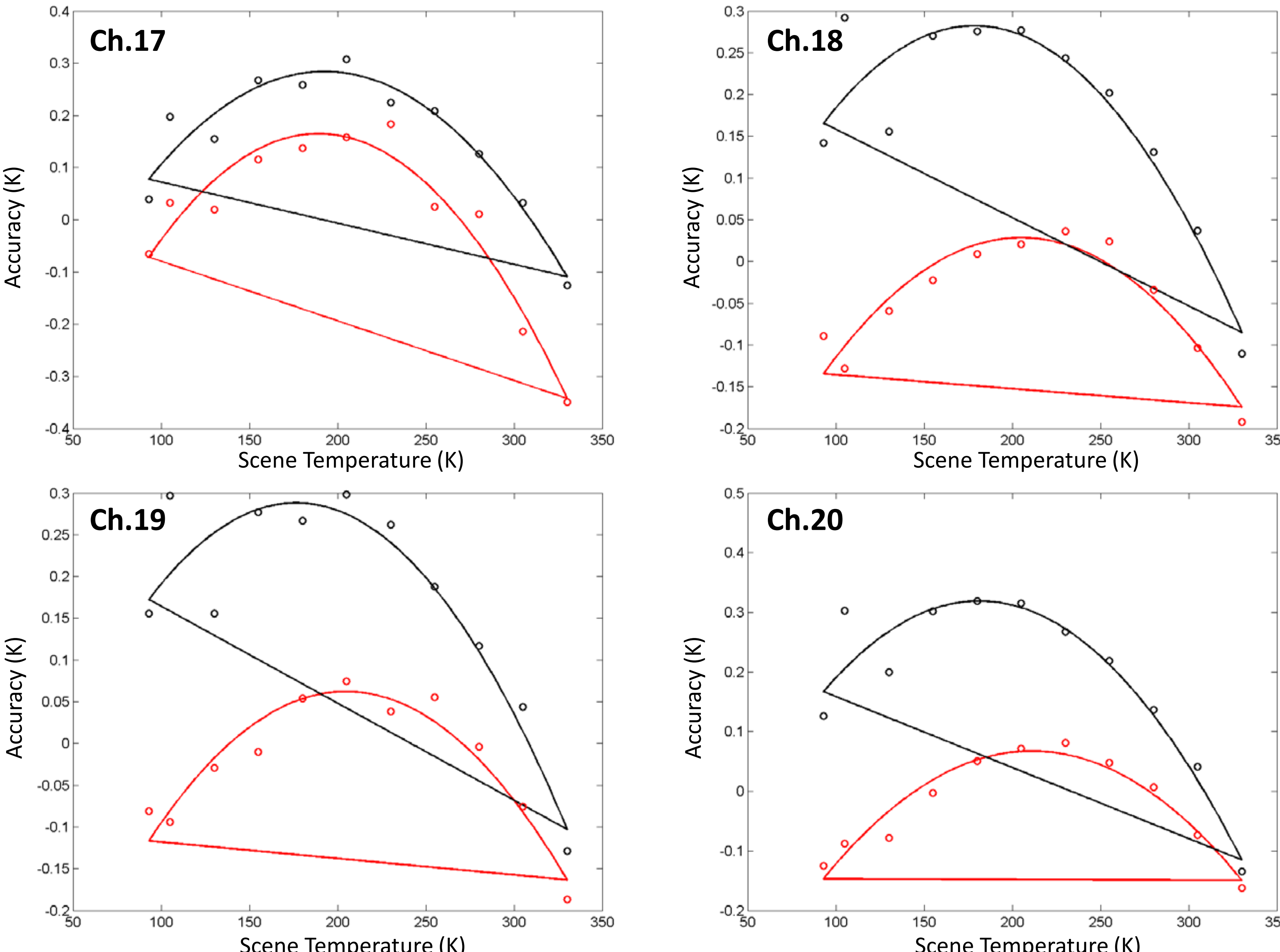

Nonlinearity Fitting for CP_Mid RC1 vs. S-NPP

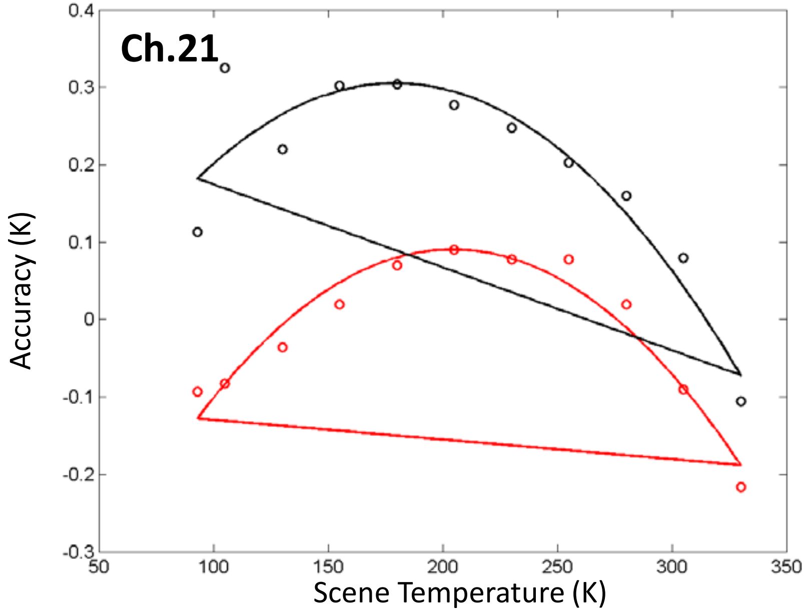

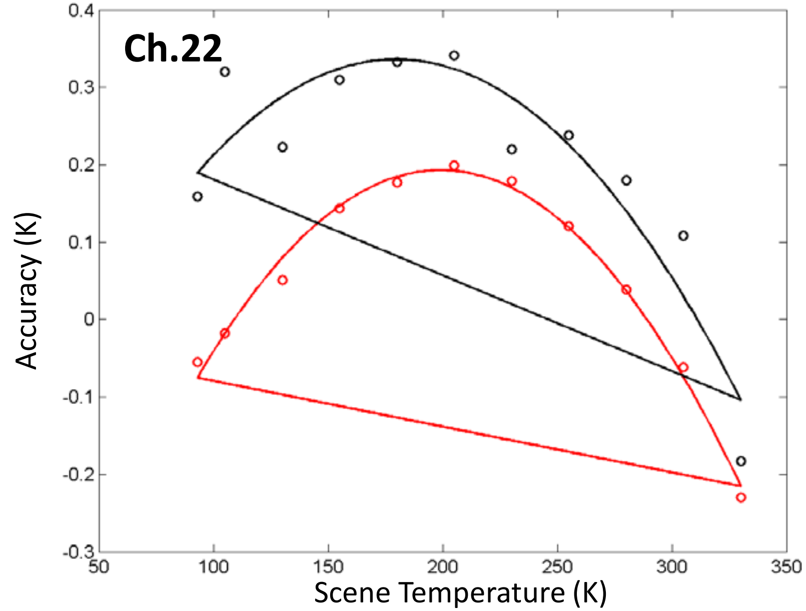

Peak Nonlinearity CP_Mid vs. CP_High vs. S-NPP

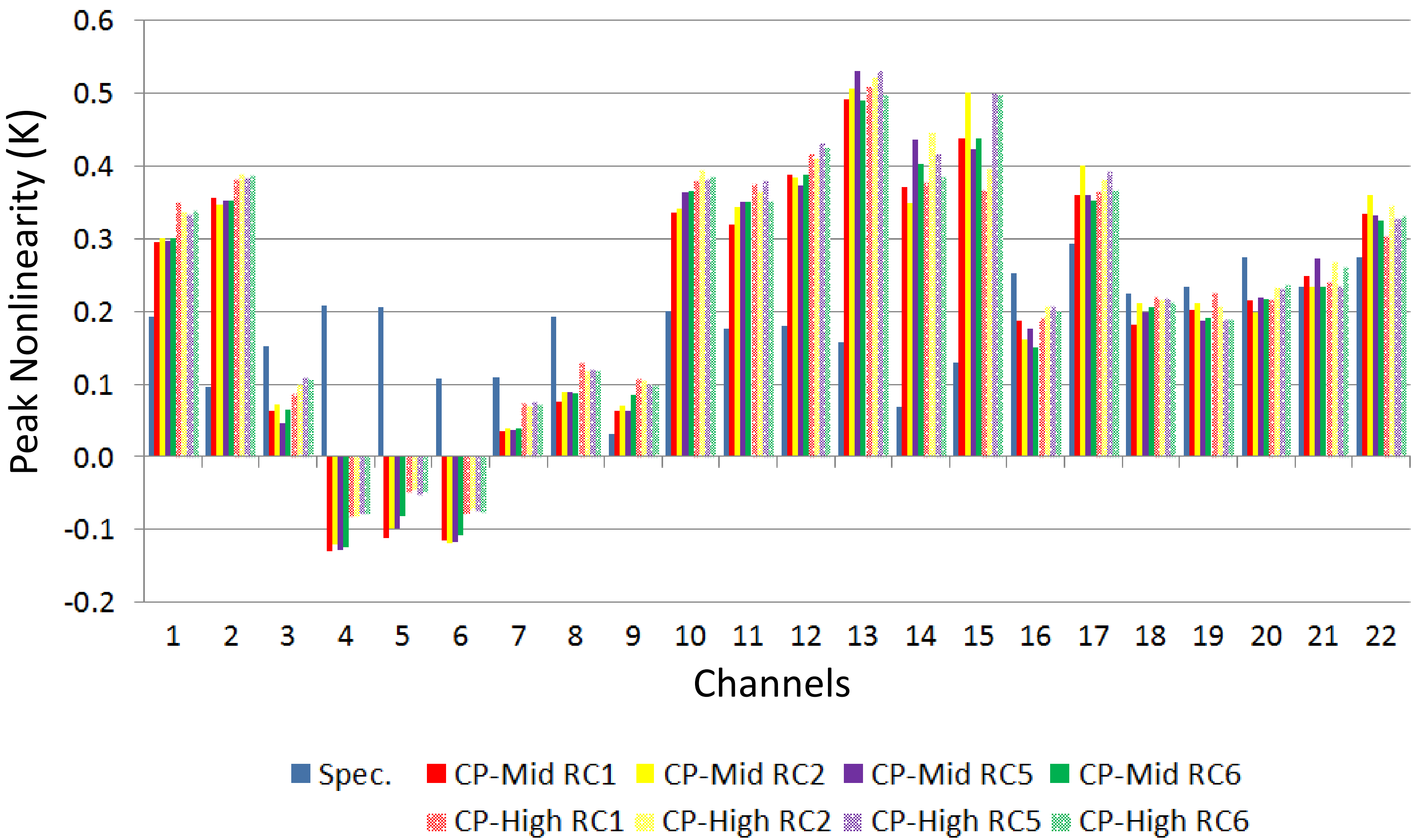

Peak Nonlinearity CP_Mid vs. CP_High vs. S-NPP

	Req.	NPP	RC 01	RC 02	RC 05	RC 06	RC 01	RC 02	RC 05	RC 06
Ch. 01	0.3	0.192375	0.295533	0.300354	0.295683	0.300126	0.350545	0.335861	0.332529	0.338800
Ch. 02	0.4	0.097030	0.356295	0.347214	0.352813	0.352103	0.381823	0.388844	0.382640	0.386258
Ch. 03	0.4	0.151654	0.063326	0.071473	0.046543	0.065086	0.087422	0.100421	0.107853	0.107398
Ch. 04	0.4	0.207822	-0.13045	-0.12117	-0.12731	-0.12330	-0.081500	-0.082200	-0.078464	-0.079056
Ch. 05	0.4	0.205013	-0.11092	-0.09897	-0.09844	-0.08080	-0.049000	-0.045700	-0.052999	-0.048141
Ch. 06	0.4	0.108404	-0.11574	-0.11833	-0.11686	-0.10726	-0.077700	-0.073500	-0.073962	-0.076087
Ch. 07	0.4	0.110230	0.036040	0.039193	0.037443	0.038843	0.072957	0.069023	0.076008	0.071417
Ch. 08	0.4	0.192375	0.076095	0.089287	0.088286	0.087903	0.128727	0.118902	0.120489	0.117619
Ch. 09	0.4	0.031454	0.063095	0.069742	0.063940	0.084724	0.107218	0.104286	0.100277	0.096756
Ch. 10	0.4	0.200801	0.334665	0.341480	0.363272	0.364838	0.379554	0.393401	0.381613	0.385252
Ch. 11	0.4	0.175525	0.317945	0.342248	0.350390	0.349432	0.376068	0.364571	0.380200	0.351793
Ch. 12	0.4	0.179738	0.388312	0.383448	0.371666	0.386639	0.416540	0.410095	0.432229	0.425297
Ch. 13	0.4	0.157270	0.490847	0.505495	0.530009	0.489683	0.509692	0.522424	0.532068	0.497168
Ch. 14	0.4	0.068104	0.369805	0.348896	0.436279	0.401462	0.378473	0.445803	0.415863	0.384177
Ch. 15	0.4	0.129748	0.436805	0.500044	0.422272	0.437745	0.366713	0.396972	0.499259	0.497620
Ch. 16	0.4	0.251352	0.187002	0.160974	0.176309	0.149825	0.189948	0.206867	0.206306	0.199304
Ch. 17	0.4	0.292074	0.359176	0.400952	0.359268	0.351730	0.364226	0.381516	0.393170	0.366368
Ch. 18	0.4	0.224672	0.182350	0.210731	0.198731	0.206451	0.220616	0.216834	0.218325	0.211934
Ch. 19	0.4	0.233097	0.201559	0.211713	0.187876	0.190328	0.225926	0.206616	0.187707	0.188110
Ch. 20	0.4	0.275223	0.215399	0.198030	0.219165	0.216822	0.215823	0.232860	0.231878	0.237326
Ch. 21	0.4	0.233097	0.247567	0.232987	0.272747	0.232993	0.239922	0.267539	0.235167	0.261524
Ch. 22	0.4	0.273819	0.334551	0.359397	0.330968	0.325268	0.303348	0.345271	0.327134	0.331810

Striping in RC1 at CP_Mid ST-95 vs. ST-330

ST-95 Scene Counts

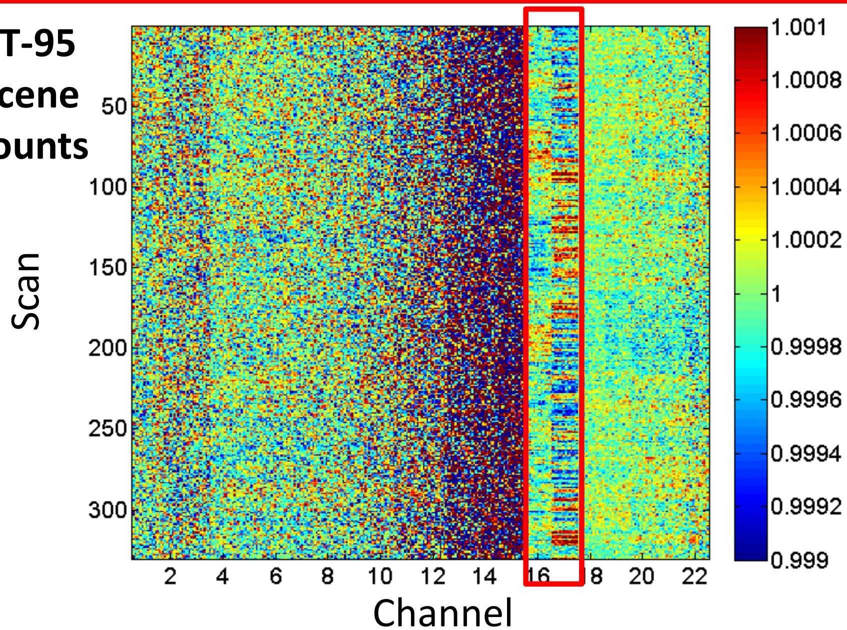

ST-95 Scene TB

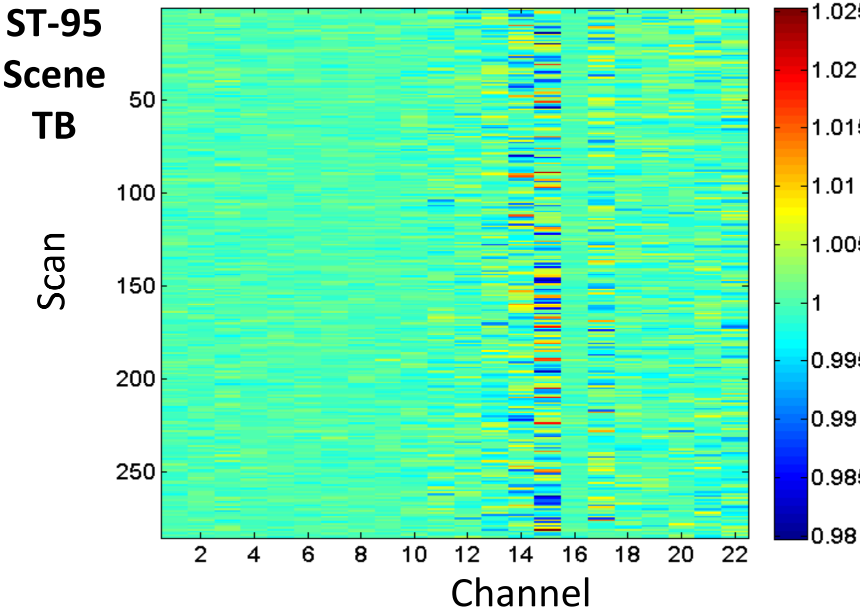

ST-330 Scene Counts

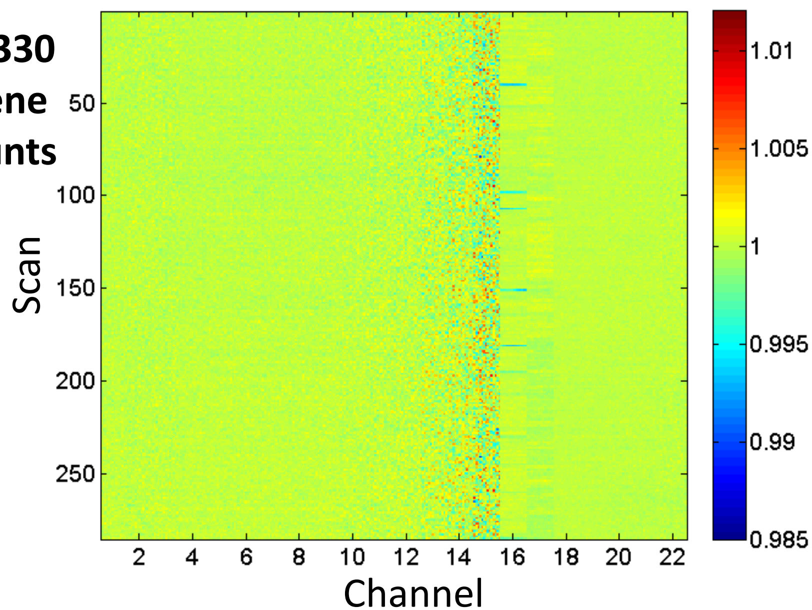

ST-330 Scene TB

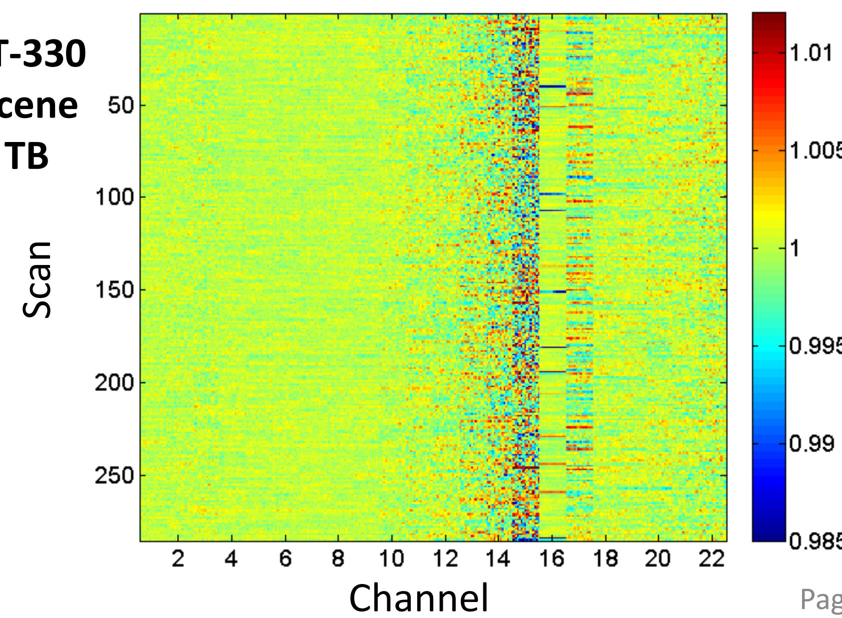

Striping Index at CP_Mid ST-330

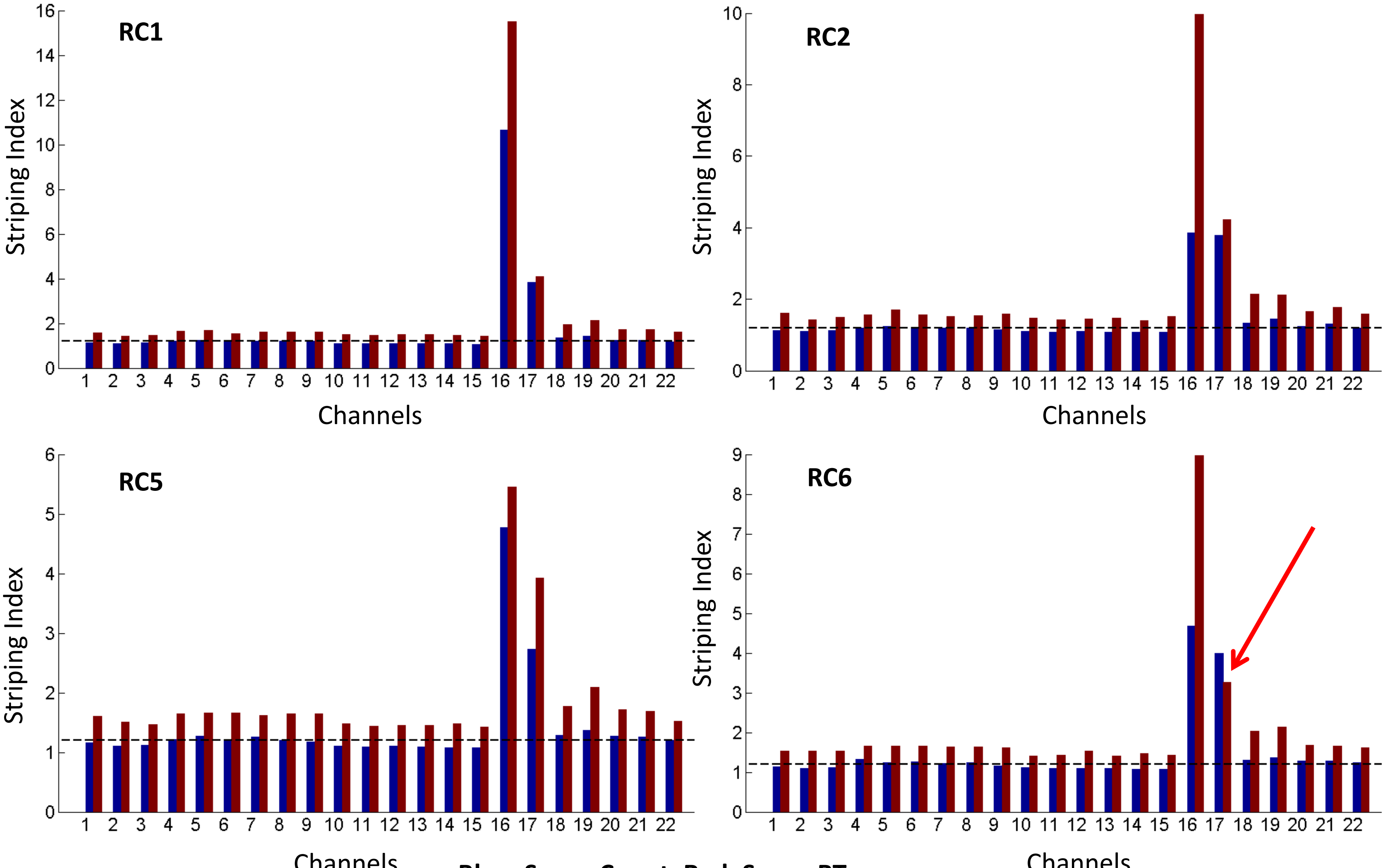

Blue: Scene Count; Red: Scene BT

Striping Index at ST-230 CP_Mid vs. CP_High

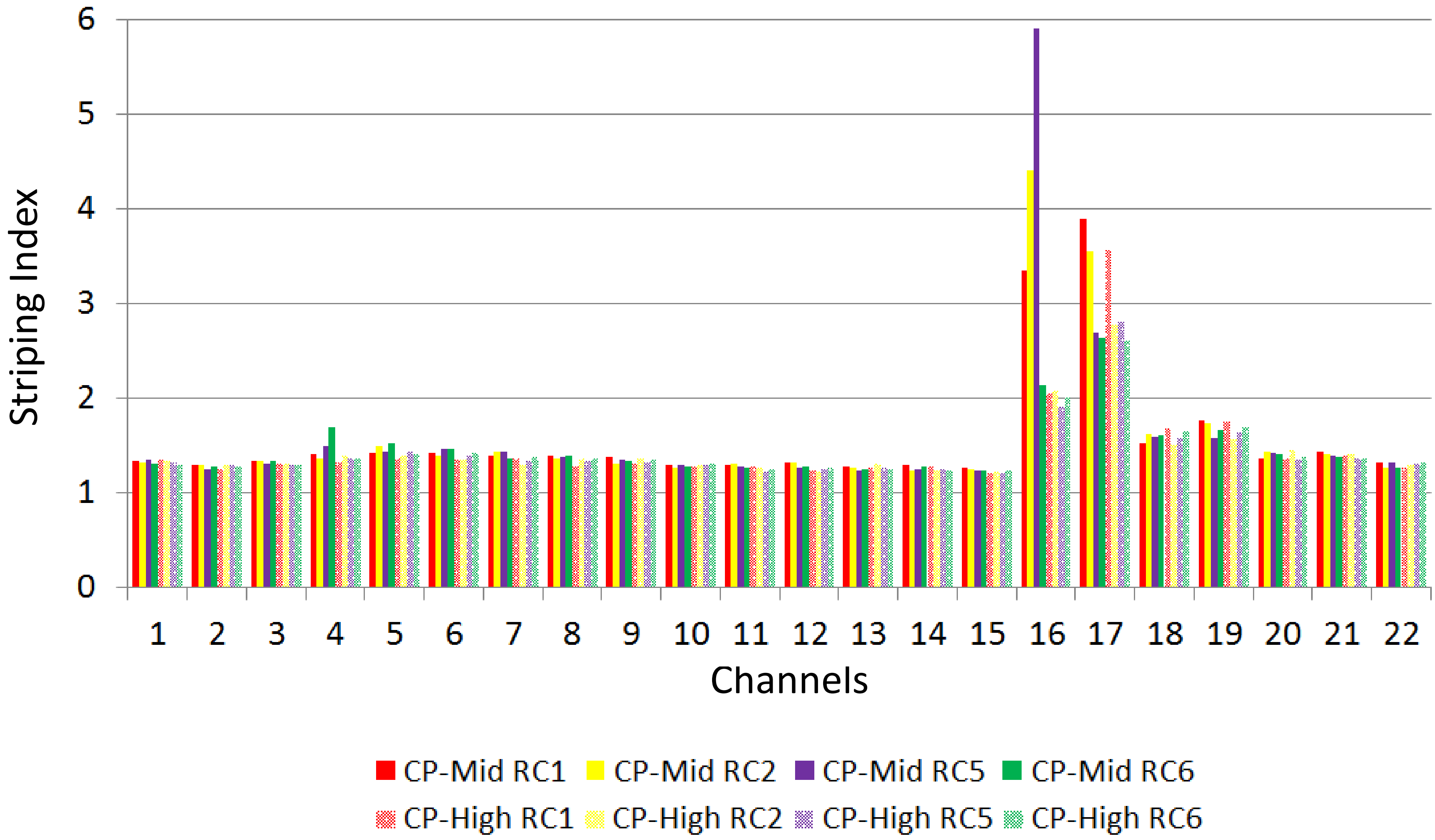

Striping Index at ST-255 CP_Mid vs. CP_High

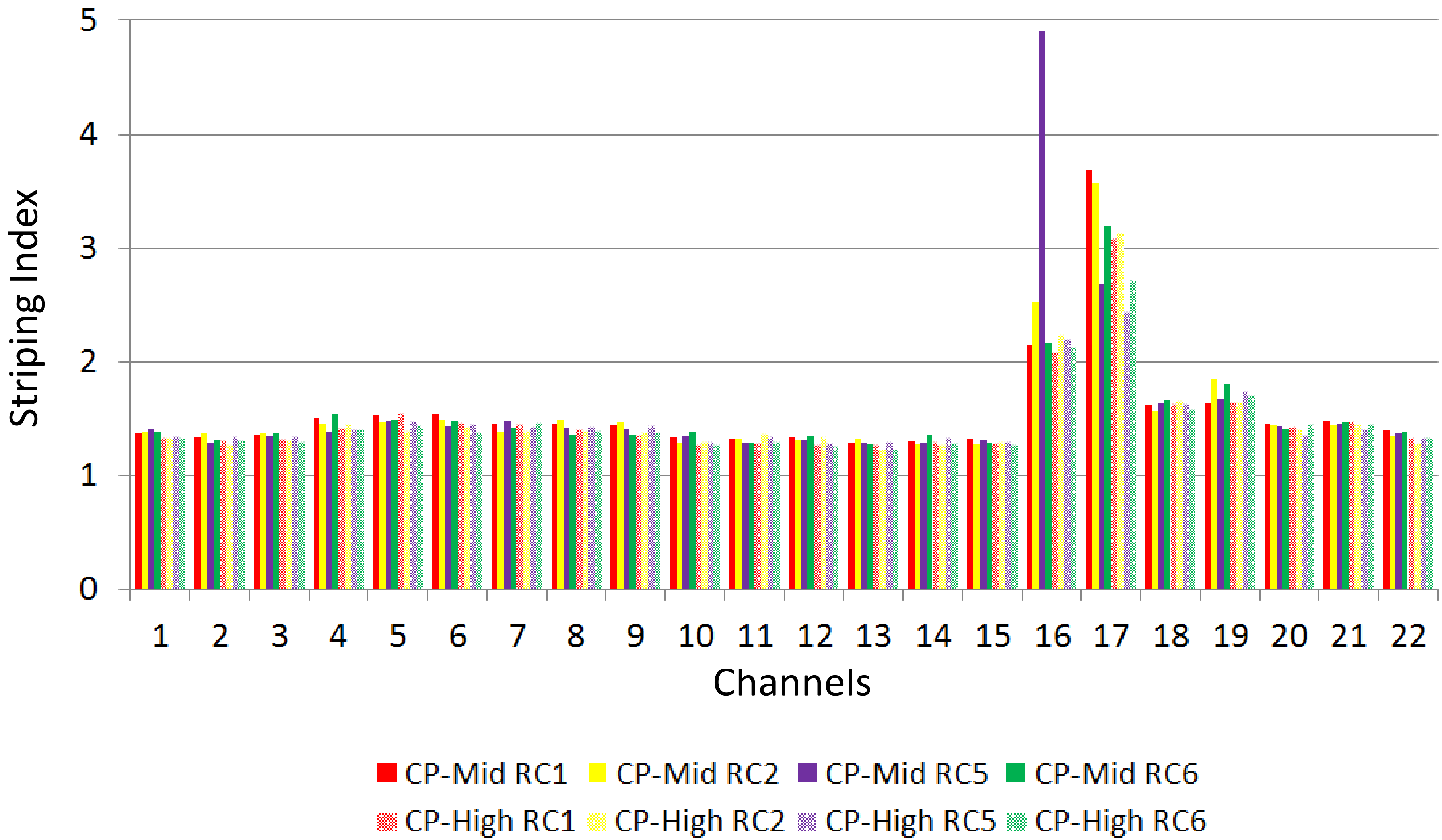

Striping Index at ST-280 CP_Mid vs. CP_High

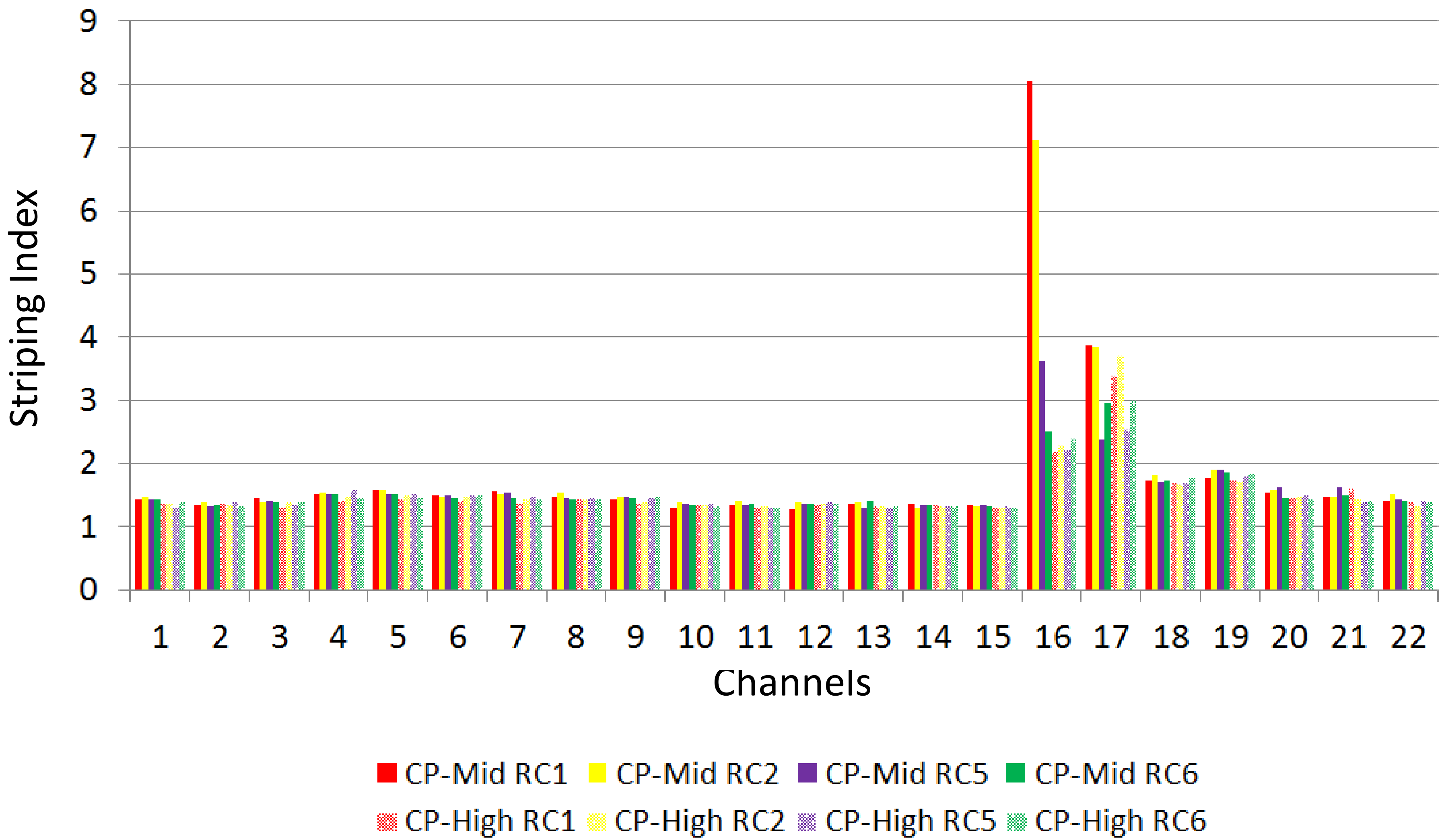

Striping Index at ST-305 CP_Mid vs. CP_High

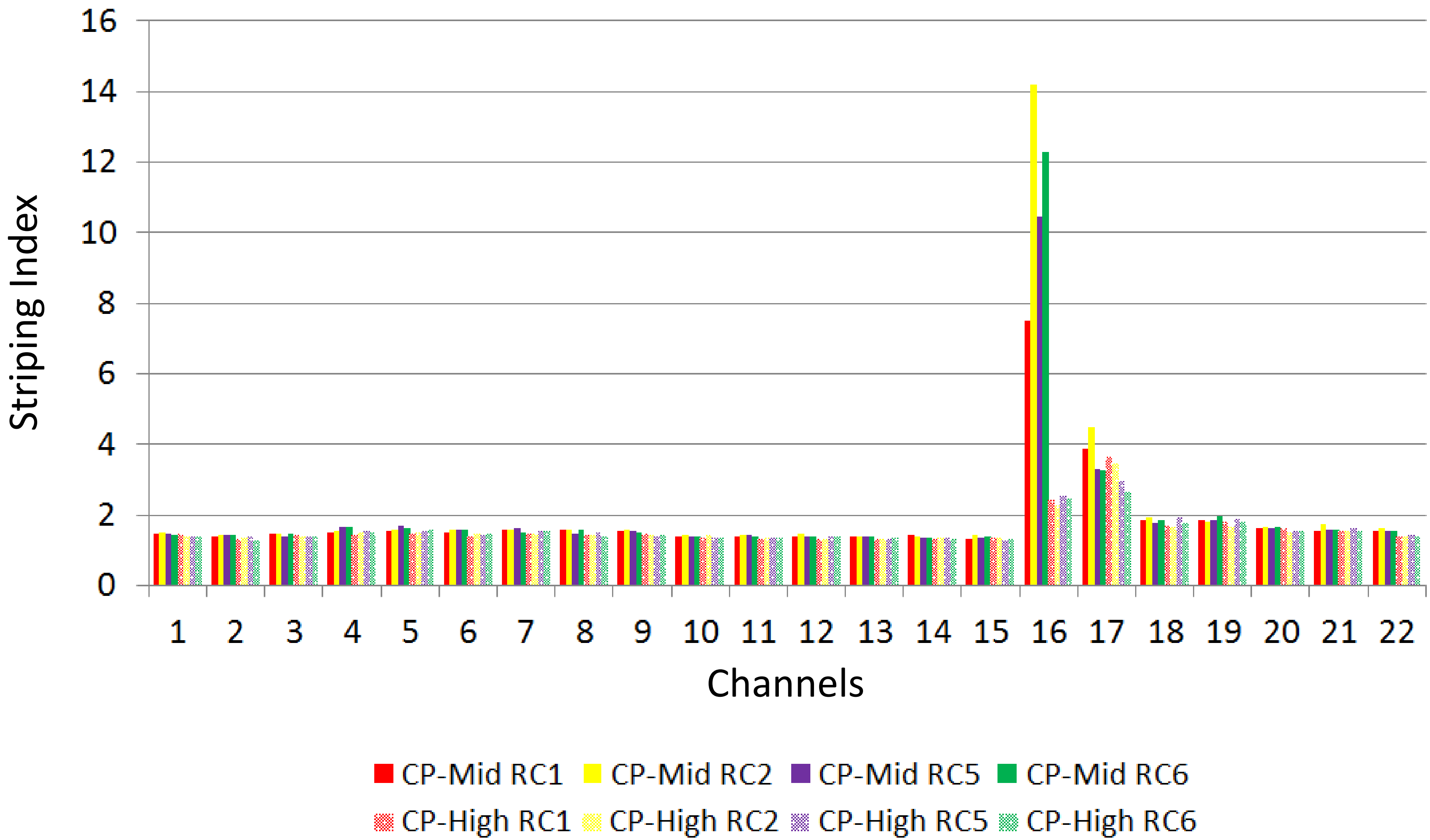

Striping Index at ST-330 CP_Mid vs. CP_High

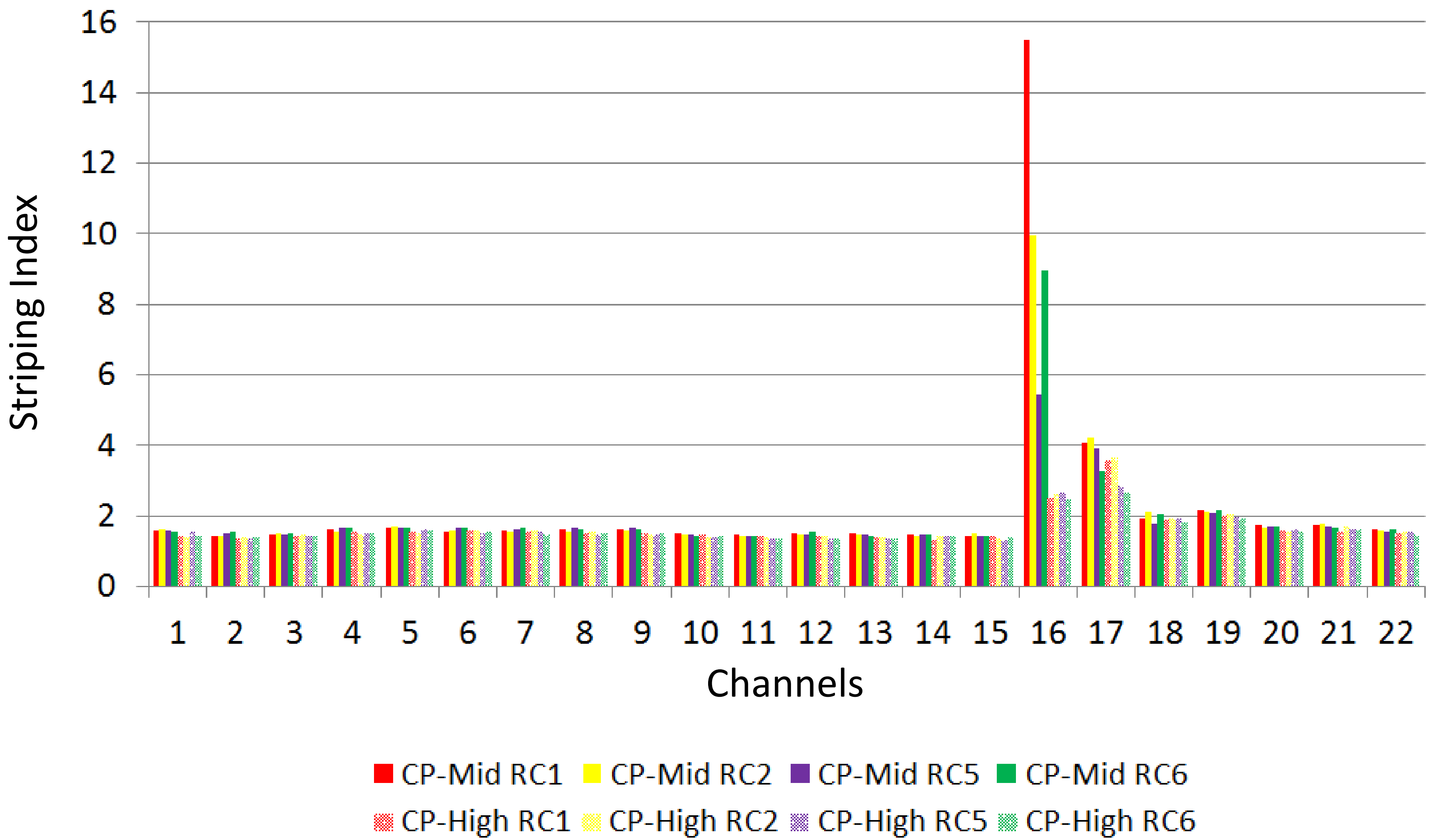

Ch.15 Counts Anomaly at CP_Mid ST-180

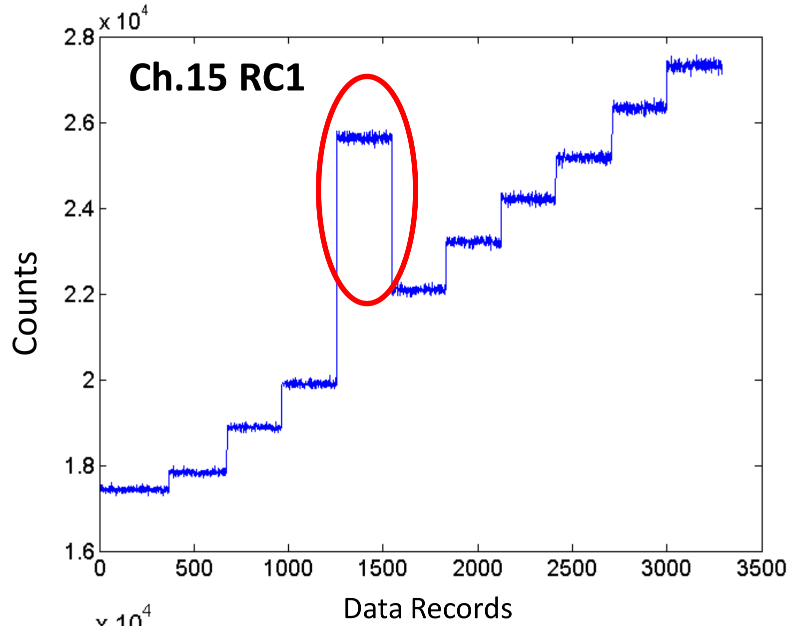

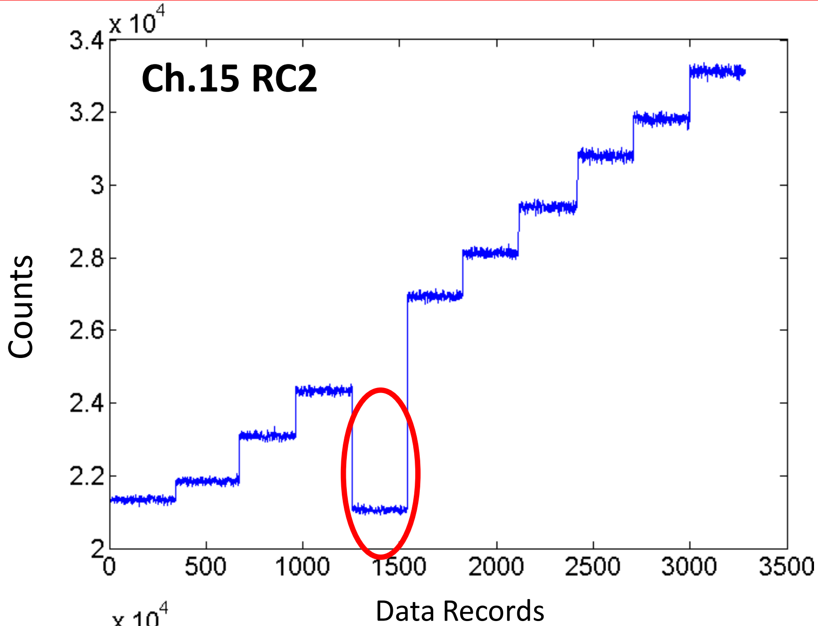

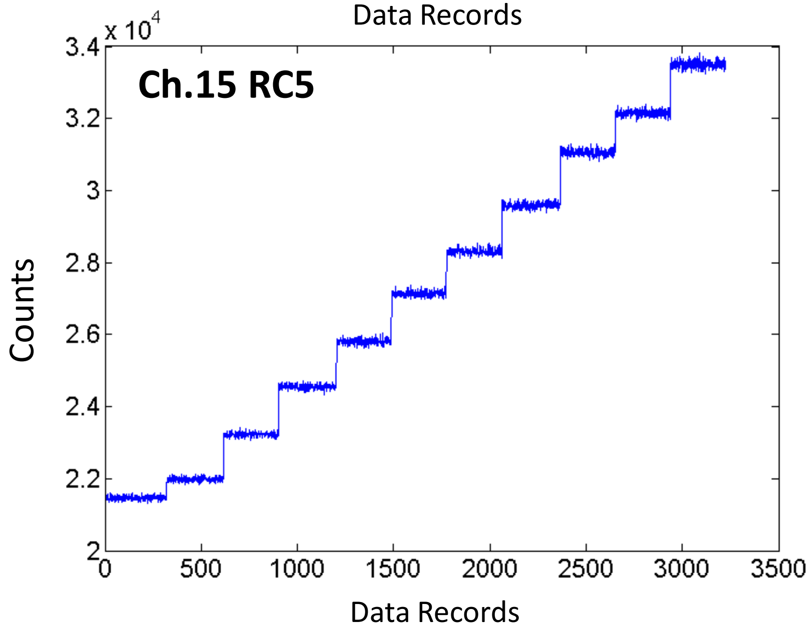

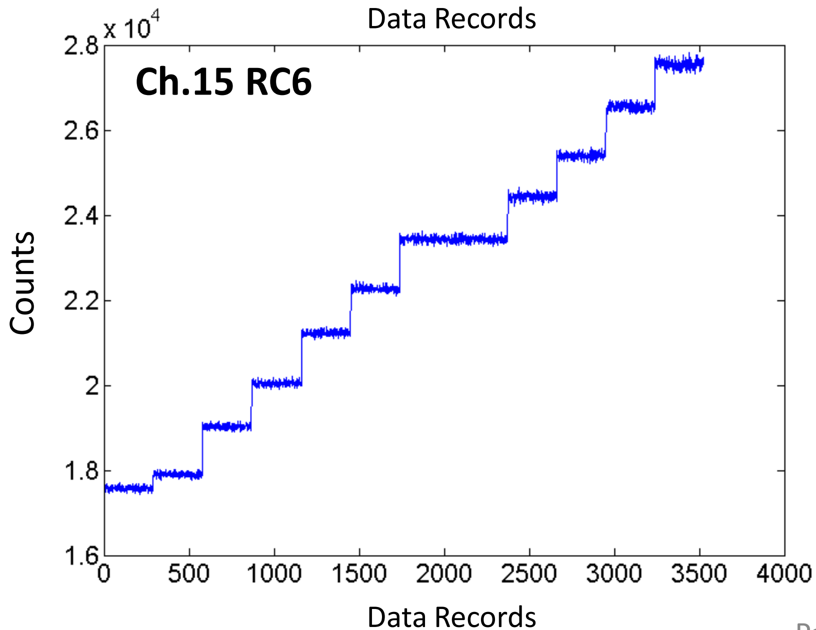

Ch.15 Counts Anomaly at CP_Mid ST-180

Ch.15 RC1

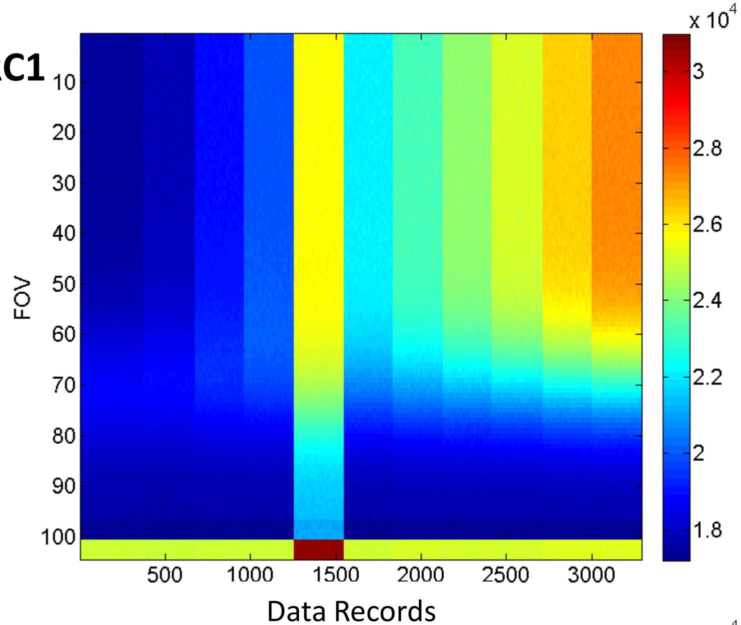

Ch.15 RC2

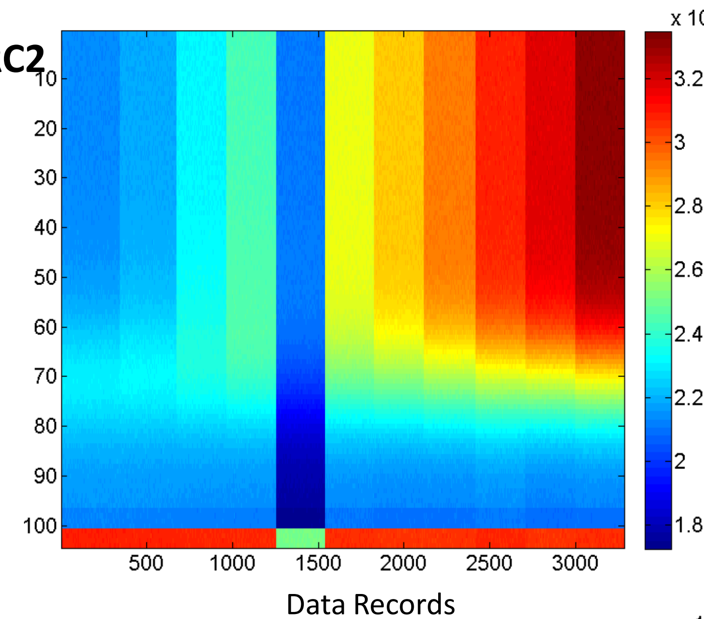

Ch.15 RC5

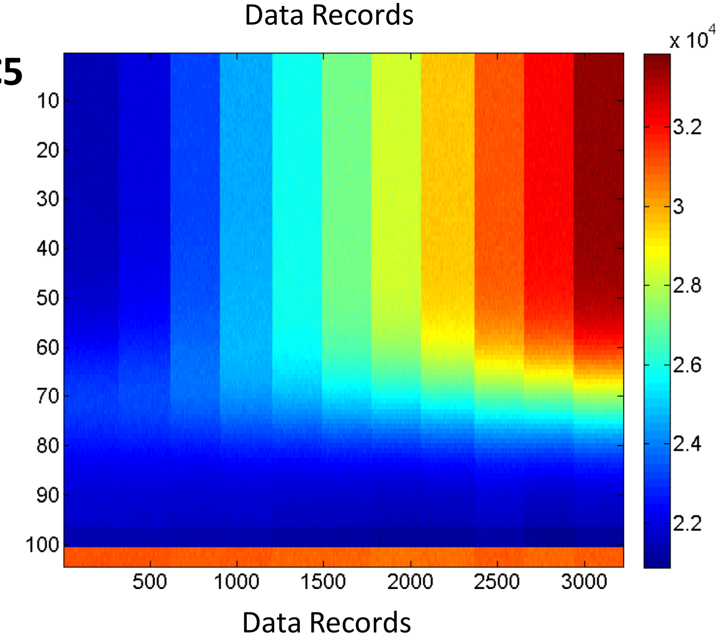

Ch.15 RC6

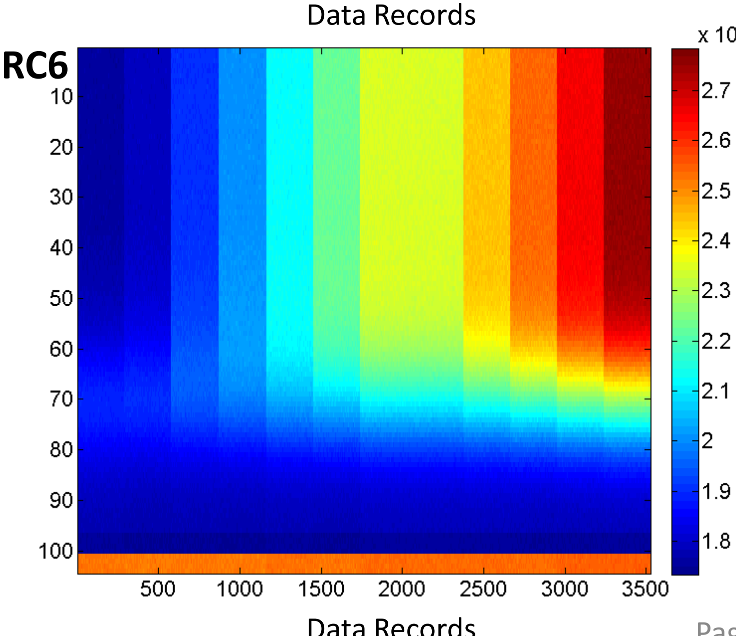

Summary

- J1 ATMS all channels' NEΔT, except channel 17, meet the mission requirements
- Channel 16 demonstrates large temperature dependent noise
- Radiometric accuracy at channel 4 to 6 present reversed pattern compared to S-NPP
- Radiometric accuracy residuals exist at ST-95 and large difference is found between S-NPP and J1
- Several V-band channels' peak nonlinearity are out of specifications
- SDR algorithm introduces additional striping affects

CrIS Radiometric Uncertainty (RU) Estimates

Dave Tobin, Hank Revercomb, Joe Taylor, Bob Knuteson, Dan DeSlover, Lori Borg, Graeme Martin
Space Science and Engineering Center, University of Wisconsin-Madison

2014 JPSS Science Teams Annual Meeting
NOAA Center for Weather and Climate Prediction, College Park, MD
13 May 2014

RU estimates are useful for understanding the size and dependencies of the primary contributors to the CrIS SDR uncertainties, for calibration improvements, and for weather, process, trend, and inter-calibration applications.

1. Perturbation of Calibration Equation and Parameter uncertainties
2. On-orbit RU estimates for Suomi-NPP CrIS
3. Changes for JPSS-1 (2017 launch), JPSS-2 (2022 launch) and CrIS-NG (TBD ~2027)

RU estimates for AIRS, IASI, and CrIS

- A) Observation intercomparisons and other Cal/Val approaches versus B) RU estimation via calibration equation perturbation. Synergy between these two.

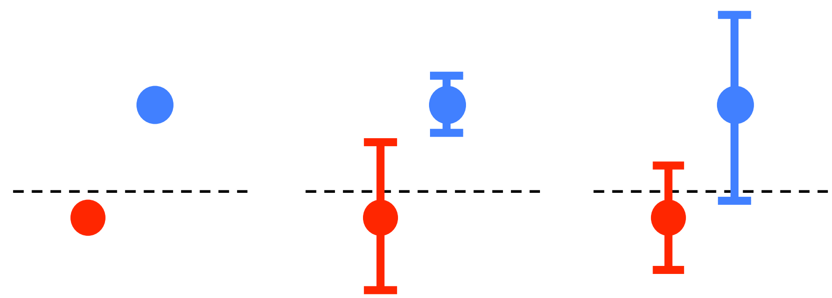

- RU estimates for AIRS, IASI, and CrIS:
  - Standard RU methodology and terminology needed
  - AIRS: *Pagano et al., Lessons learned from the AIRS pre-flight radiometric calibration. Proc. SPIE 8866, Earth Observing Systems XVIII, 88660U (September 23, 2013); doi: 10.1117/12.2023810.*
  - CrIS: *Tobin et al., (2013), Suomi-NPP CrIS radiometric calibration uncertainty, J. Geophys. Res. Atmos., 118, 10,589–10,600, doi:10.1002/jgrd.50809.*
  - IASI: CNES team is currently working to produce RU estimates for IASI-A and IASI-B.

Achieving Climate Change Absolute Accuracy in Orbit

Wielicki et al., BAMS, 2013

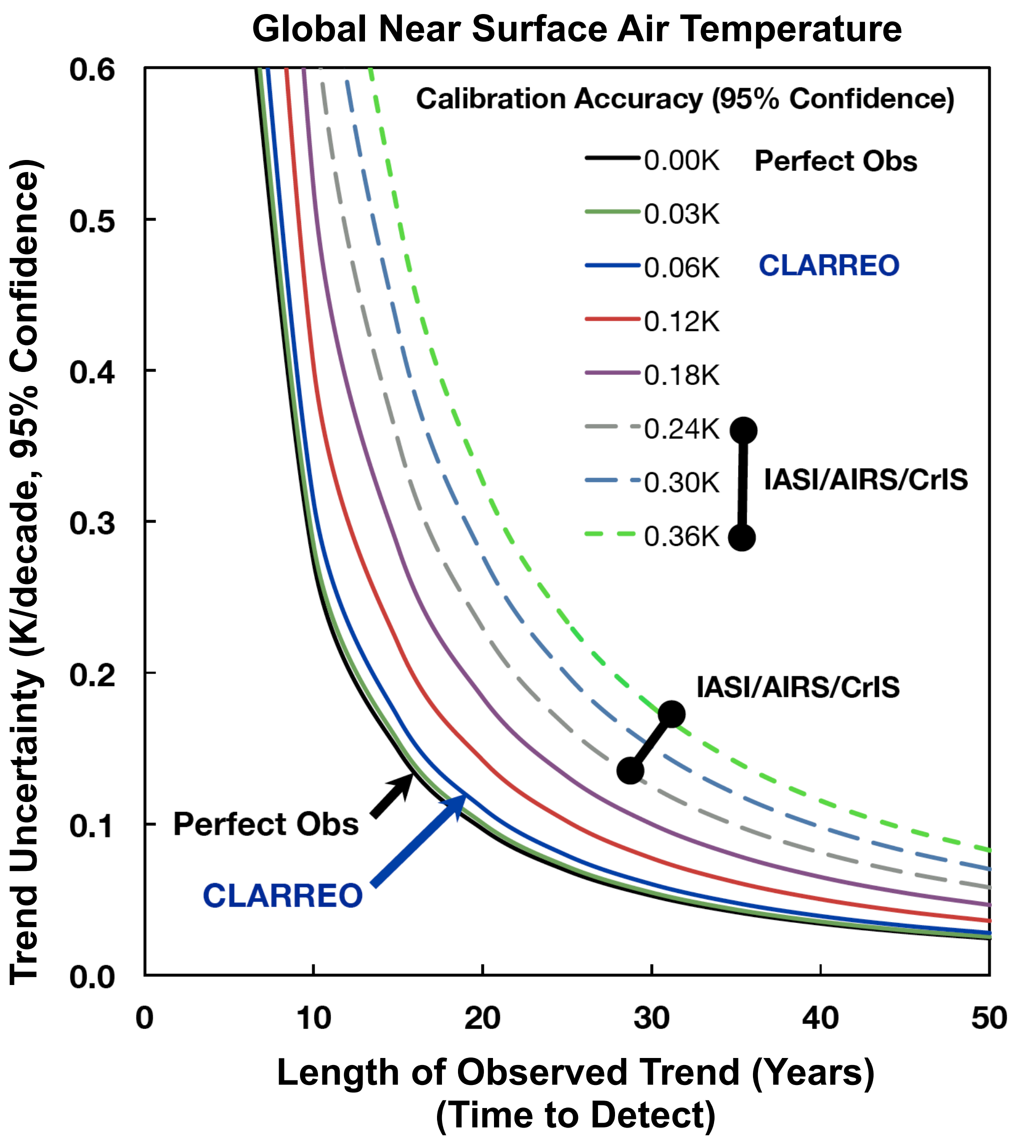

- CLARREO prototypes developed and performance recently demonstrated, but mission TBD.
- Emphasizes the benefit of characterizing AIRS/IASI/CrIS as well as possible, and improving if possible.

Suomi-NPP CrIS Radiometric Uncertainty Estimates

Simplified On-Orbit Radiometric Calibration Equation:

$$R_{scene} = \mathcal{Re}\{(C'_{scene} - C'_{SP}) / (C'_{ICT} - C'_{SP})\} R_{ICT} \quad \text{with:}$$

Nonlinearity Correction: $C' = C \cdot (1 + 2\, a_2\, V_{DC})$

ICT Predicted Radiance: $R_{ICT} = \varepsilon_{ICT}\, B(T_{ICT}) + (1-\varepsilon_{ICT})\, [\, 0.5\, B(T_{ICT,\ Refl,\ Measured}) + 0.5\, B(T_{ICT,\ Refl,\ Modeled})]$

Parameter Uncertainties:

Parameter	Nominal Values	3-σ Uncertainty
T_{ICT}	280K	112.5 mK*
ε_{ICT}	0.974-0.996	0.03
$T_{ICT,\ Refl,\ Measured}$	280K	1.5 K
$T_{ICT,\ Refl,\ Modeled}$	280K	3 K
a_2 LW band	0.01 – 0.03 V^{-1}	0.00403 V^{-1}
a_2 MW band	0.001 – 0.12 V^{-1}	0.00128 – 0.00168 V^{-1}

**Exelis at-launch estimate*

Suomi-NPP CrIS, example 3-sigma RU estimates

For a typical warm, ~clear sky spectrum

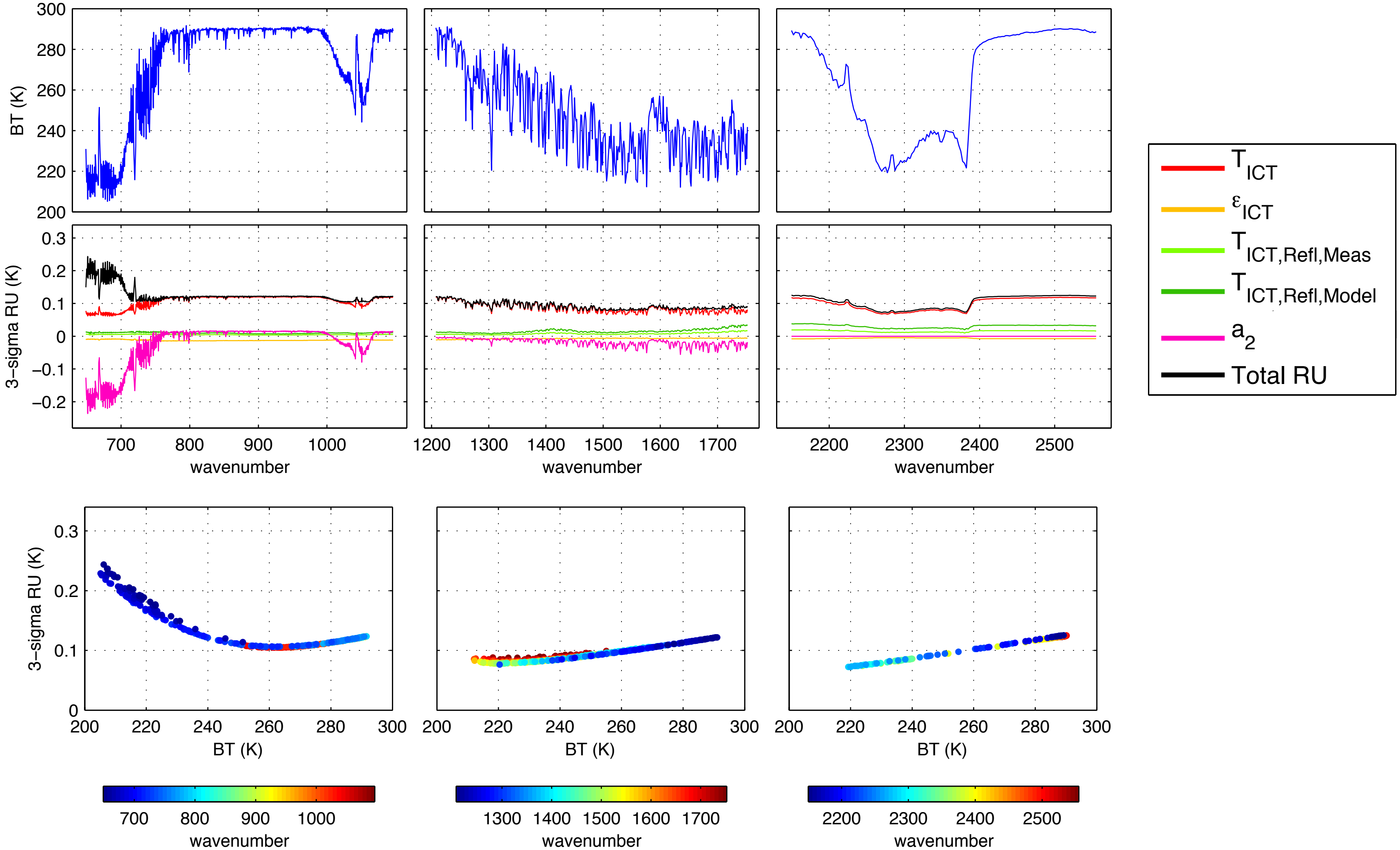

Suomi-NPP CrIS, example 3-sigma RU estimates

For a cold, high cloud spectrum

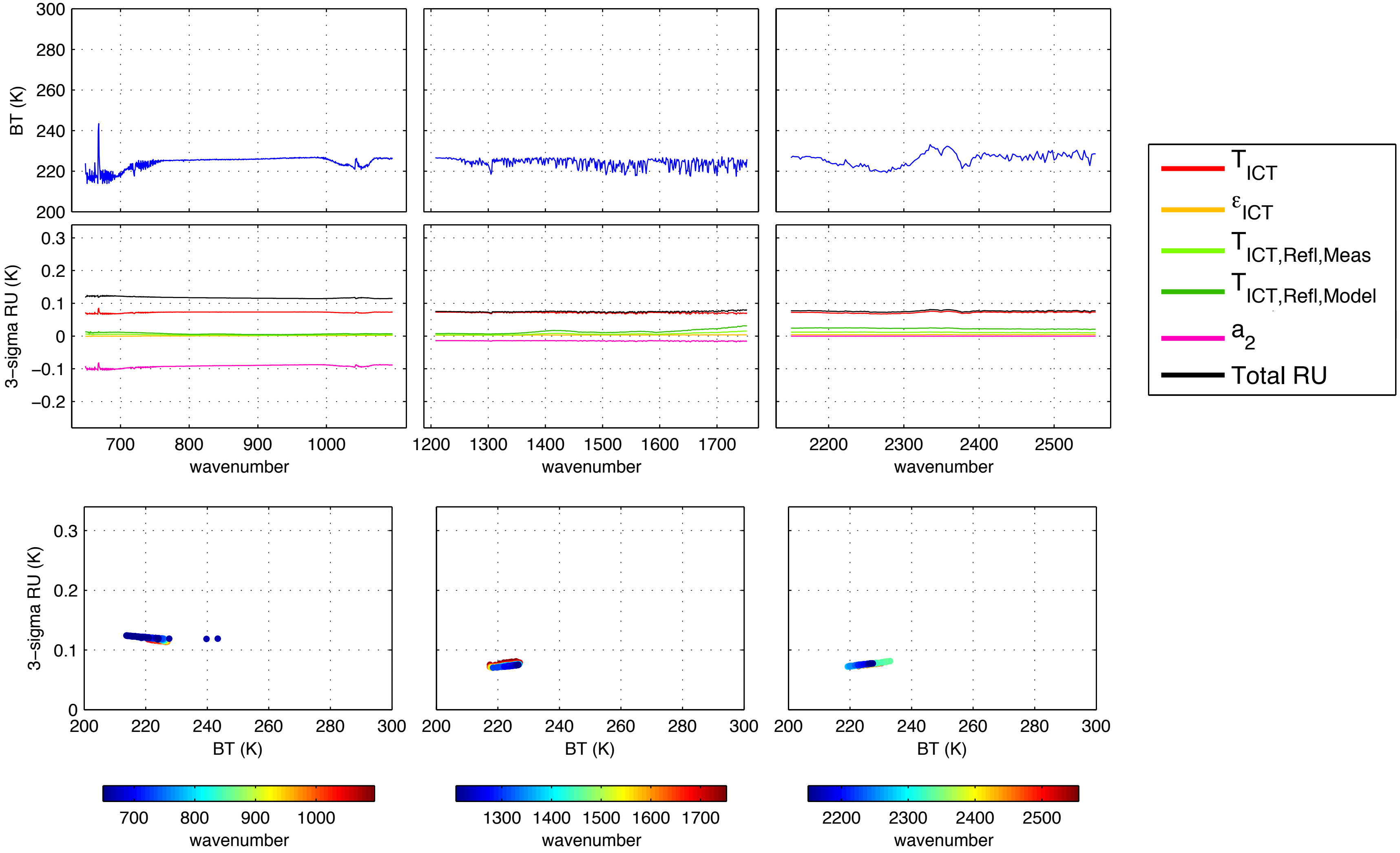

ICT Emissivity and Reflected terms

- **Despite relatively low ICT emissivity and greater sensitivity to the reflected terms, cal/val has not shown radiometric artifacts related to these contributions. This is not unexpected due to the ambient temperature design of CrIS and the relative size of these RU contributions compared to other terms.**

- **The redesigned ICT for J1 and J2 CrIS has emissivity requirements of >0.995 emissivity and uncertainty <0.0015 1-sigma. Modeling and testing to date shows the expected performance meets these requirements and the corresponding RU contributions should be much smaller (~negligible) compared to those for Suomi-NPP.**

ICT Temperature

- **Suomi-NPP CrIS has BOL uncertainty of 112 mK 3-sigma, and significant BOL to EOL contributions.**

- **J1 CrIS has BOL uncertainties similar to Suomi-NPP CrIS but reduced BOL to EOL contributions.**

- **Phase change cells on the ICT are being considered for J2 CrIS which would further reduce BOL to EOL contributions and allow performance to be verified on-orbit.**

Nonlinearity

- **On-orbit Nonlinearity RU contributions for J1 CrIS should be similar to those for Suomi-NPP.**
  – Preliminary DM results for J1 are qualitatively similar to FM1 (SW is linear, some linear MW FOVs, all LW FOVs are nonlinear) and the same type of NL correction and TVAC and on-orbit a_2 analysis techniques will be needed for J1.
  – Compared to S-NPP, the J1 LW FOVs are more linear (except FOV5), and 8 of the J1 MW FOVs are very linear.

- **LW and MW detectors are being selected for J2 CrIS. An accurate measure of nonlinearity should be assessed as part of this selection, with an FTS for example.**

Other RU Terms

Smaller contributors not currently accounted for in the calibration algorithm or included in current RU estimates:

- Spectral Ringing
- Polarization
- Possible SW Nonlinearity
- Other smaller/negligible terms:
  - Detector temperature changes, Changes in DA Bias tilt over 4 minutes, Changes in optical flatness, OPD sample rate drift over 4 minutes, Electronic gain drift over 4 minutes, Electronic delay drift over 4 minutes, FOV to FOV crosstalk in same band, FOV to FOV crosstalk between bands, Stray light, Optics temperature change during cal, Changes in channel spectra

Error from Scene Mirror Induced Polarization

- CrIS uses a 45° gold scene mirror that provides low sensitivity to polarization; no correction is included in the SDR algorithm/processing.
- However, it seems almost certain that CrIS should have polarization effects of ~50 mK for especially warm and cold brightness temperatures in some spectral regions.
- Radiance error dependence $\sim 2p_r p_t\,(N - B_{ICT})$
- A correction should be developed based on CrIS characterization tests yet to be conducted (measurements of scene mirror degree of polarization, p_r, and interferometer polarization sensitivity, p_t)

SW Band Biases

- FOV-2-FOV analyses and differences with respect to other sensors suggest small artifacts in the SW band, both in Mean biases and FOV-2-FOV differences.

  E.g. Differences with respect to IASI

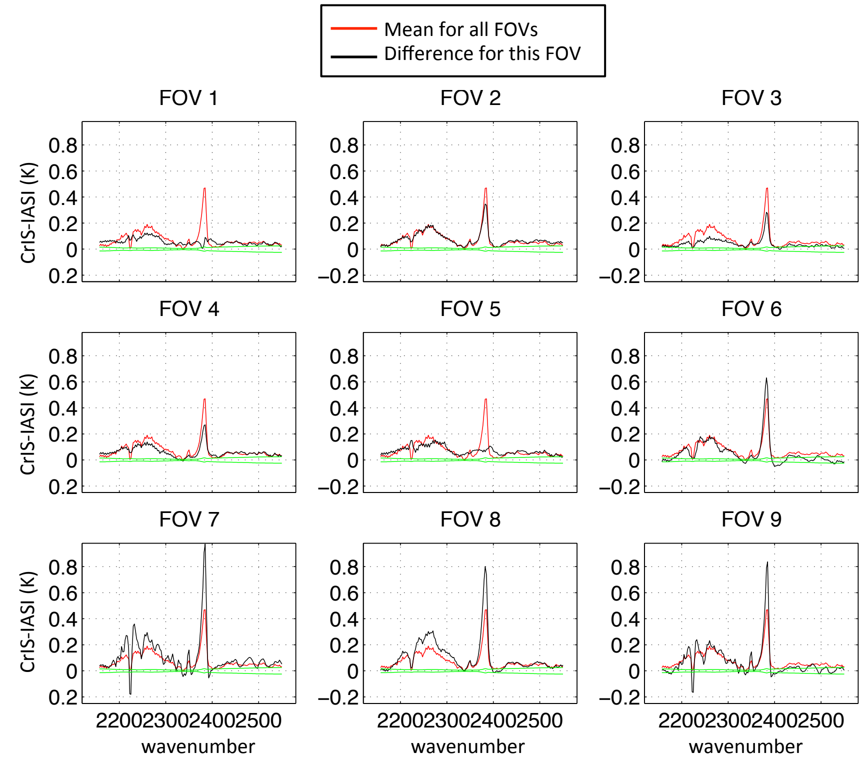

- Mechanisms investigated:
  - Spectral shift
  - Thermal SP view contamination
  - Solar SP view contamination
  - Polarization
  - ➢ Low level Nonlinearity
    - Displays FOV dependent behavior
    - Has plausible spectral and scene level dependencies
  - ➢ Low SNR Radiometric Calibration

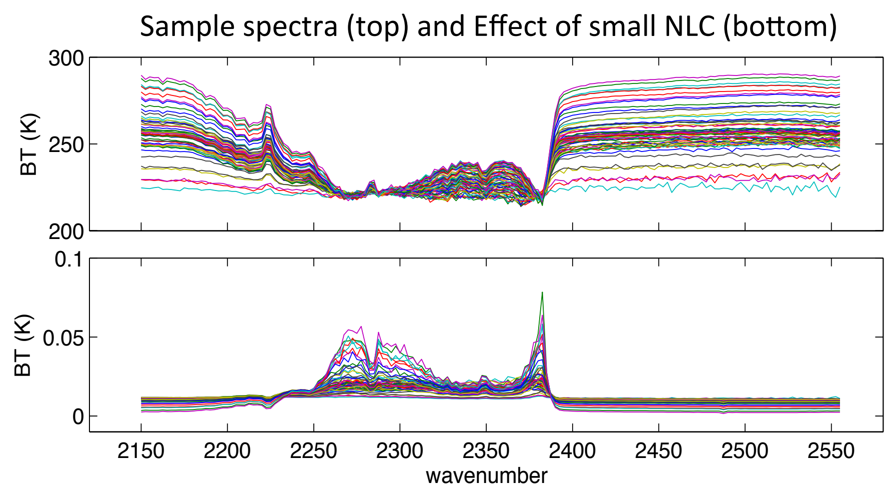

Other Potential Changes for CrIS

1. **Remove spectral gaps**
   – **J2 baseline design does not remove gaps, but a cost study is underway and if successful will be proposed to NOAA as a design mod.**
2. **Smaller and more numerous footprints**
   – **Not included in J1 or J2 design**

- **There are compelling scientific reasons for both, and feasible concepts presented for implementing both.**
- **Both require efforts/funding to perform further design/costing studies, and both likely require higher data rate for DB downlink.**

Summary

J1: RU should be similar to S-NPP CrIS

J2: Possibly reduced RU pending detector selection and associated nonlinearity behavior, and addition of ICT phase change cells.

Polarization measurements

Additional changes (remove spectral gaps, smaller footprints) require efforts/funding to perform further design/costing studies, and both likely require higher data rate for DB downlink.

- **Need clear and efficient communication between users, Flight and JPSS project offices, and DB users in order to make progress.**

SDR algorithm testing

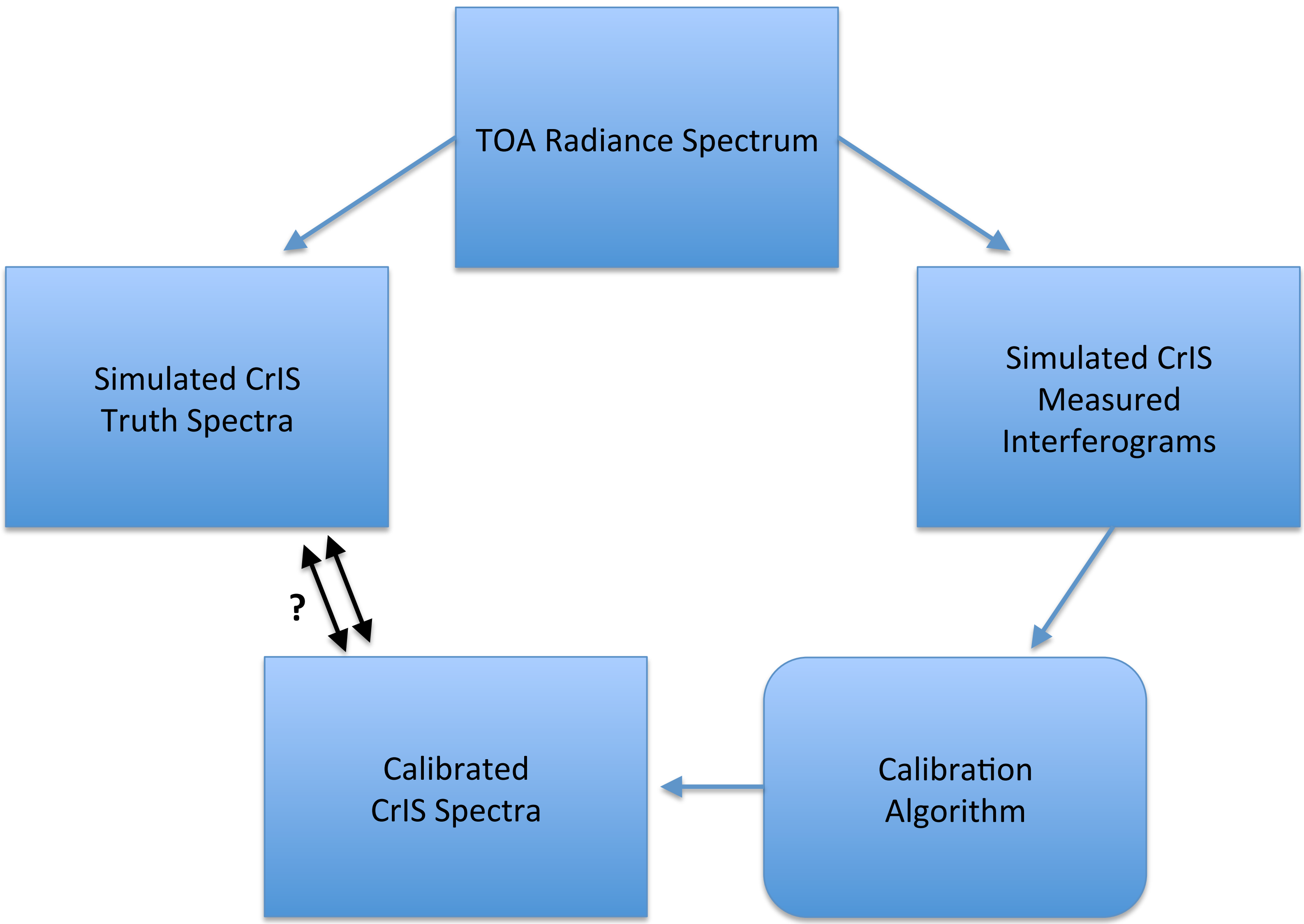

backup slides

Intercomparison of IASI-A, IASI-B, and CrIS

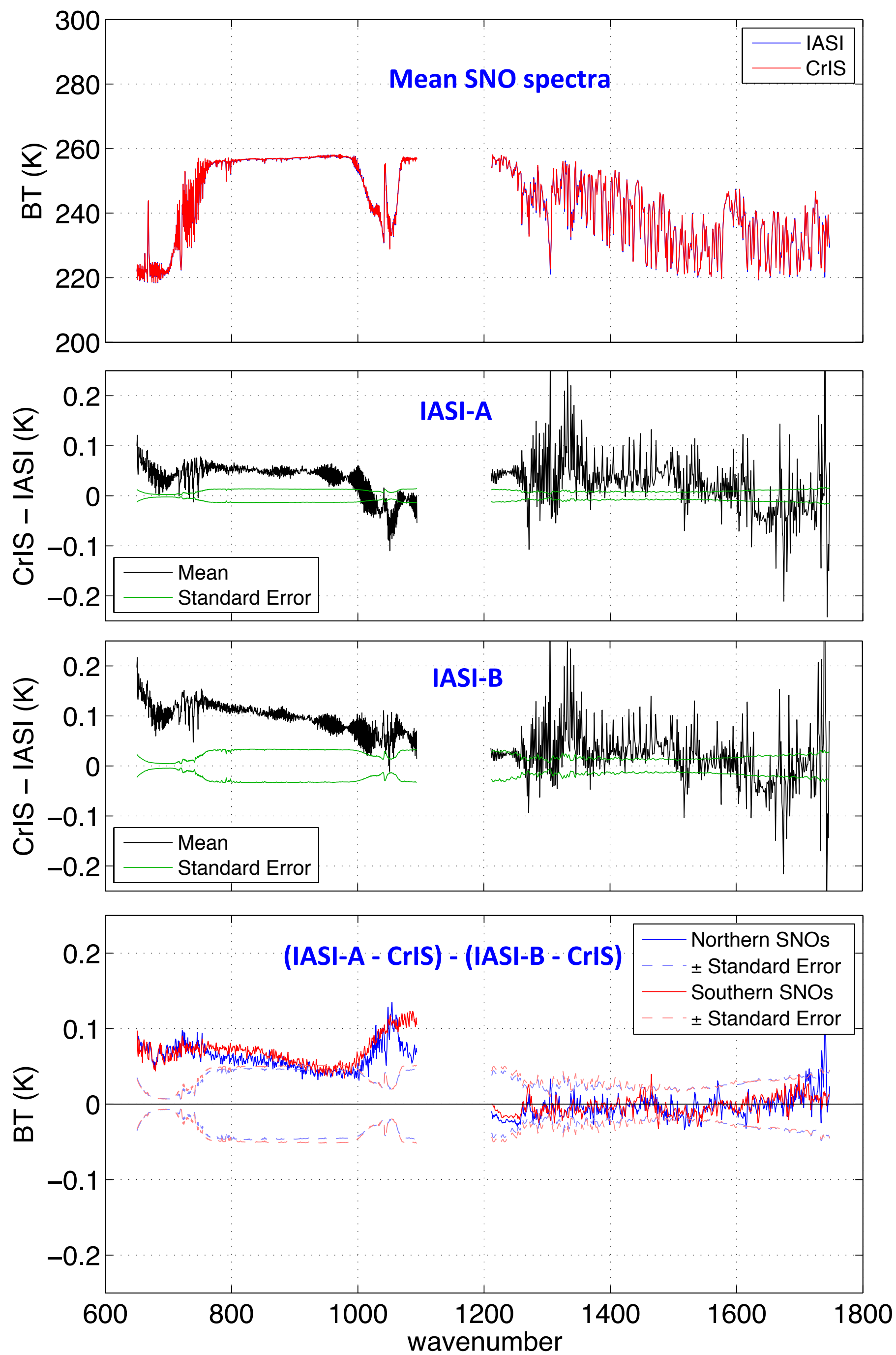

Intercomparison of CrIS and VIIRS; Daily Mean Differences

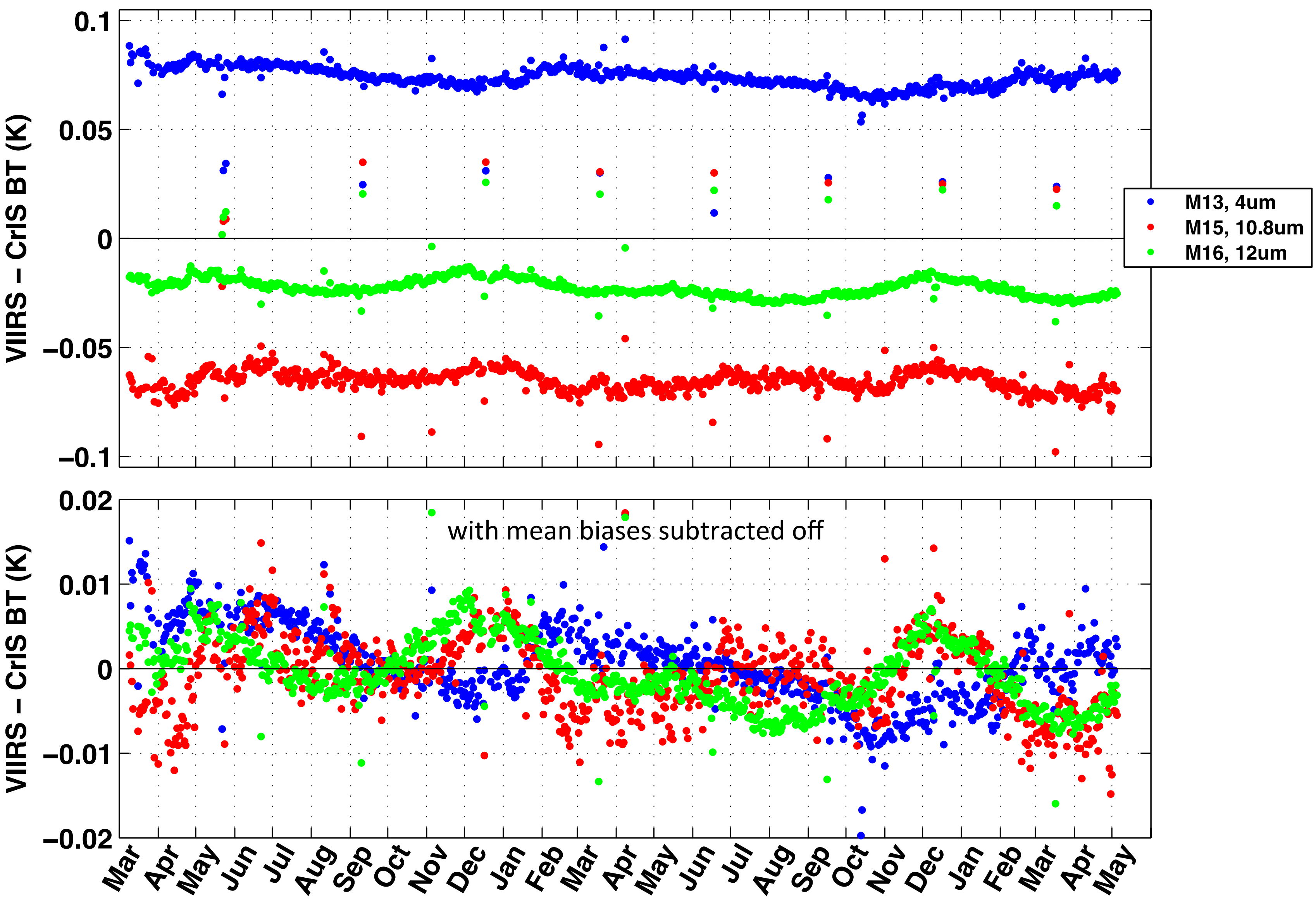

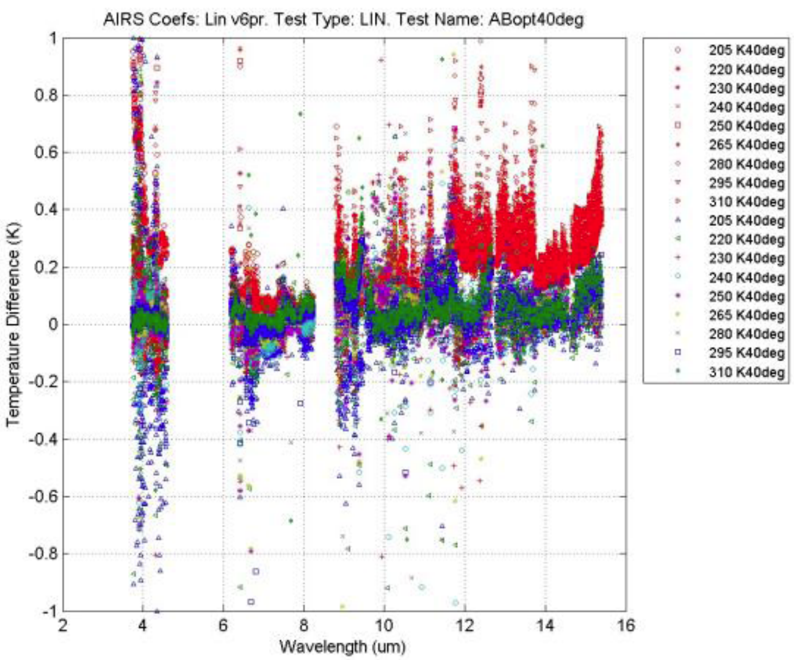

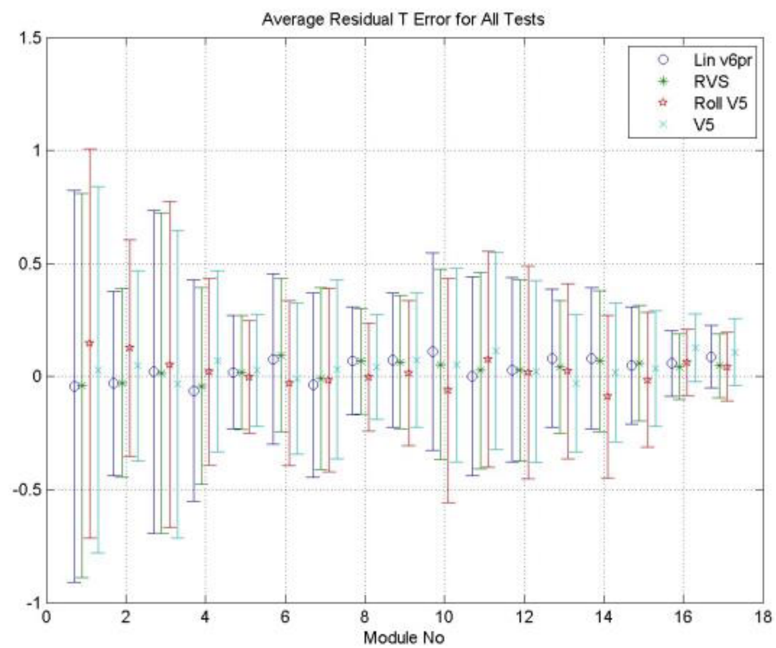

Figure 9a (left). Residual Differences (retrieved vs LABB measured) for ABopt Linearity test at 40 degree scan angle. Red curves are predicted temperature error from the radiometric uncertainty model for each LABB temperature. Figure 9b (right) Average residual error over all tests by module for each of the different polarization coefficient types (legend). Residual errors are similar for most coefficient types.

Pagano, T. S., H. H. Aumann, M. Weiler; Lessons learned from the AIRS pre-flight radiometric calibration. Proc. SPIE 8866, Earth Observing Systems XVIII, 88660U (September 23, 2013); doi:10.1117/12.2023810.

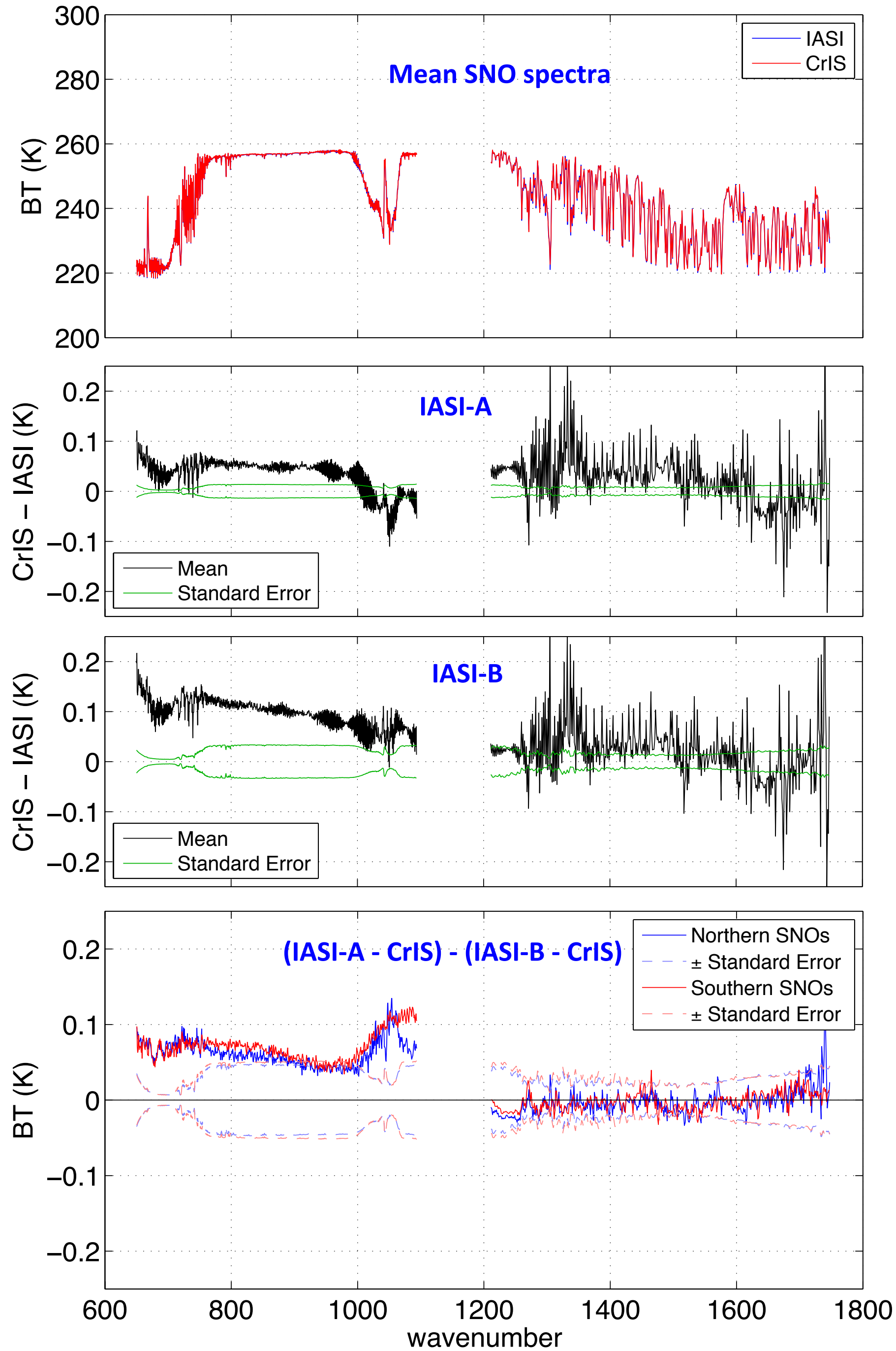

Mean SNO spectra
IASI
CrIS
BT (K)
300
280
260
240
220
200
IASI-A
CrIS – IASI (K)
Mean
Standard Error
IASI-B
CrIS – IASI (K)
Mean
Standard Error
(IASI-A - CrIS) - (IASI-B - CrIS)
Northern SNOs
± Standard Error
Southern SNOs
± Standard Error
BT (K)
0.2
0.1
0
−0.1
−0.2
600
800
1000
1200
1400
1600
1800
wavenumber

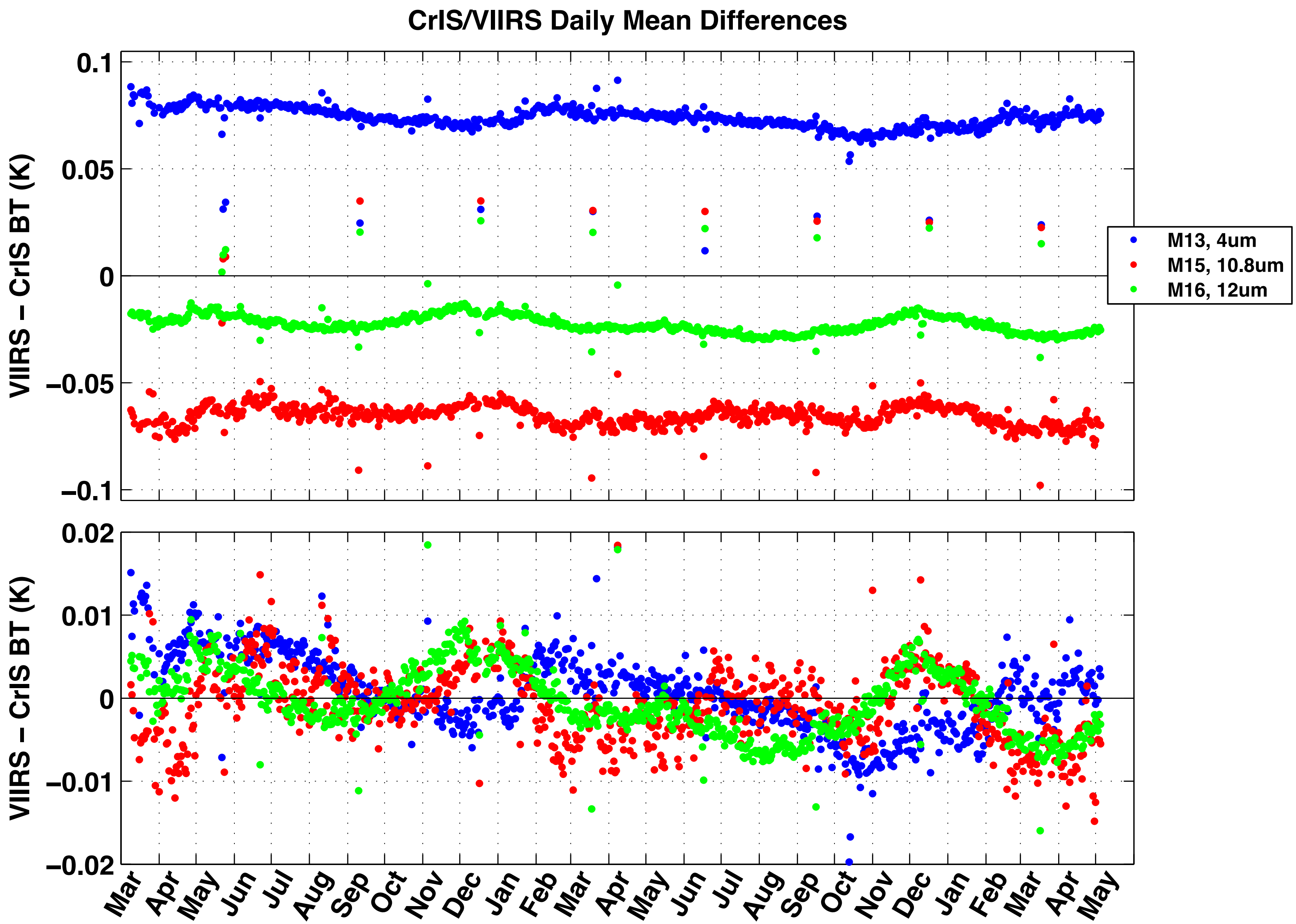

CrIS/VIIRS Daily Mean Differences
VIIRS – CrIS BT (K)
0.1
0.05
0
−0.05
−0.1
M13, 4um
M15, 10.8um
M16, 12um
VIIRS – CrIS BT (K)
0.02
0.01
0
−0.01
−0.02
Mar Apr May Jun Jul Aug Sep Oct Nov Dec Jan Feb Mar Apr May Jun Jul Aug Sep Oct Nov Dec Jan Feb Mar Apr May

QA & Latency Trending, IDPS

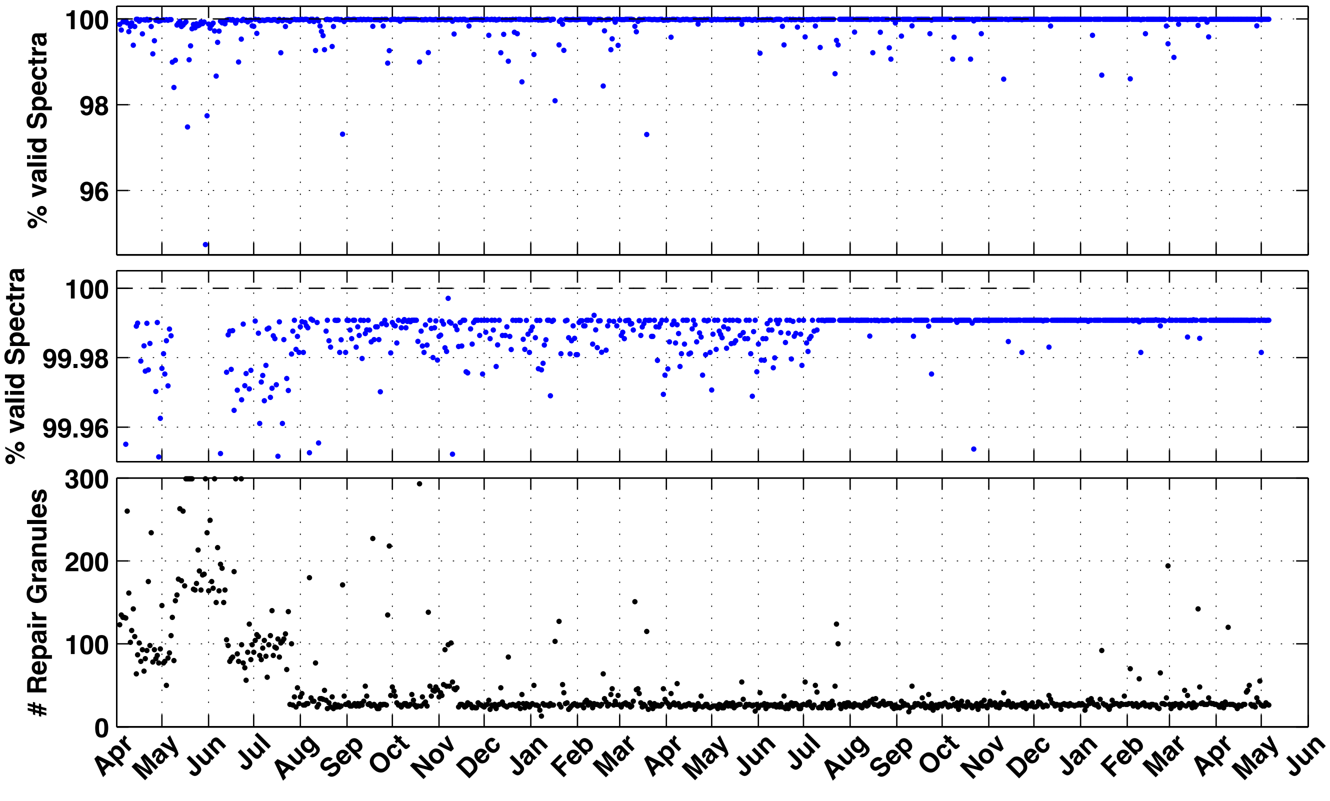

QA & Latency Trending, CSPP

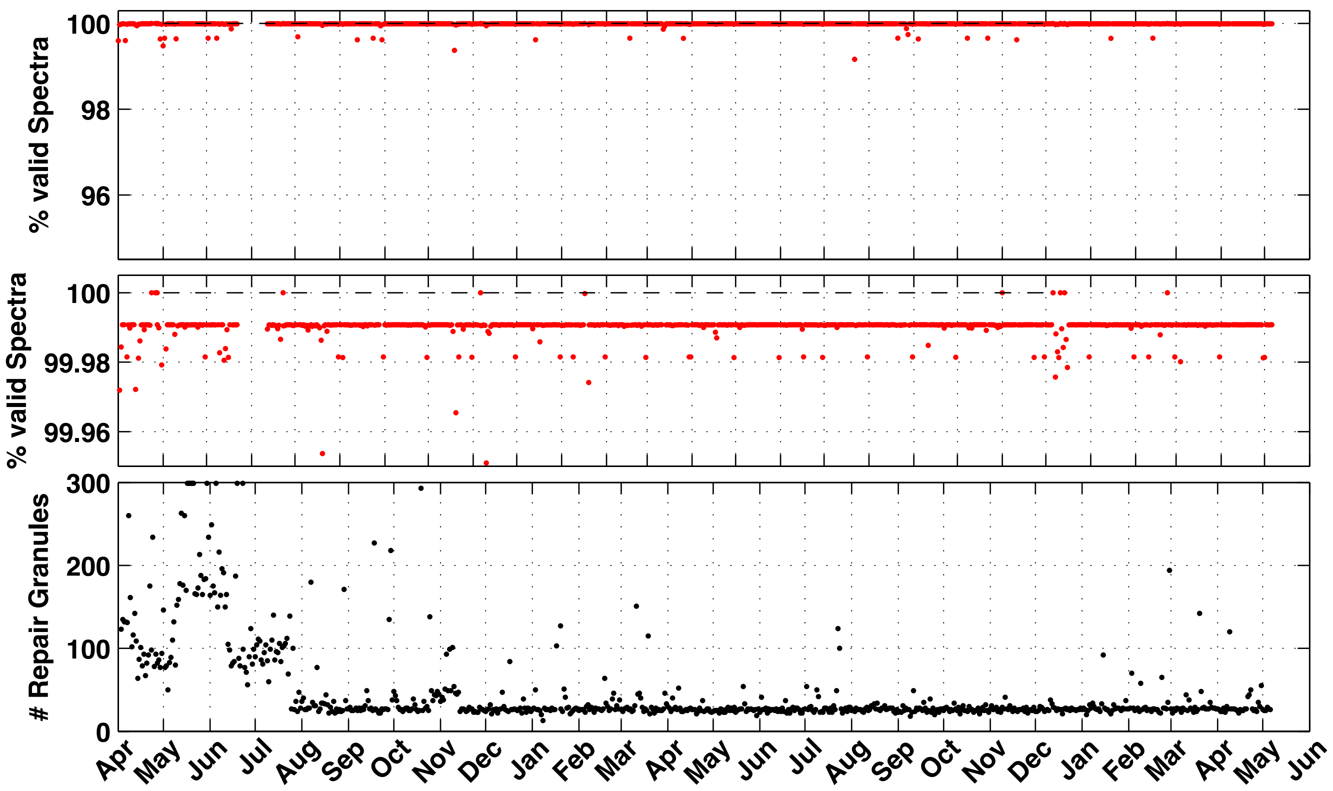

Low SNR Radiometric Calibration

- Rowe et al., 2011: A responsivity-based criterion for accurate calibration of FTIR emission spectra: Theoretical development and bandwidth estimation, *Optics Express*, **19**(7), 5930-5941.
- Rowe et al., 2011: A responsivity-based criterion for accurate calibration of FTIR emission spectra: Identification of in-band low-responsivity wavenumbers, *Optics Express*, **19**(6), 5451-5463.
- Sromovsky, 2003: Radiometric Errors in Complex Fourier Transform Spectrometry," Appl. Opt. **42**, 1779-1787.

CrIS Spectral Calibration

L. Larrabee Strow, Howard Motteler, Chris Hepplewhite, Sergio De-Souza Machado, and Breno Imbiriba

Department of Physics, JCET
University of Maryland Baltimore County (UMBC)

STAR JPSS Science Team Annual Meeting
May 2014
College Park, MD

Overview

- Spectral calibration performance: Neon stability
- High-resolution spectral improvements: Period Sinc basis
- Full spectral comparison with AIRS via SNOs

Absolute ν Calibration: IDPS SDRs

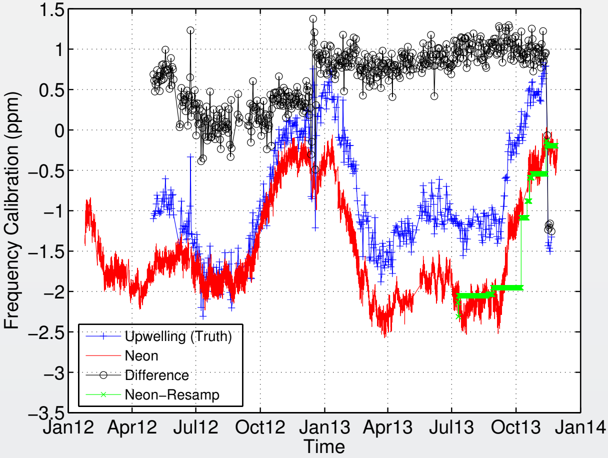

- Data using IDPS long-wave SDRs; Very few updates due to 2 ppm threshold
- SDR's exhibit ~3 ppm variability
- Correct operation of CMO generation started in Nov. 2013

2-Year Neon Calibration Record

Metrology Laser Wavelength Follows Thermal Environment?

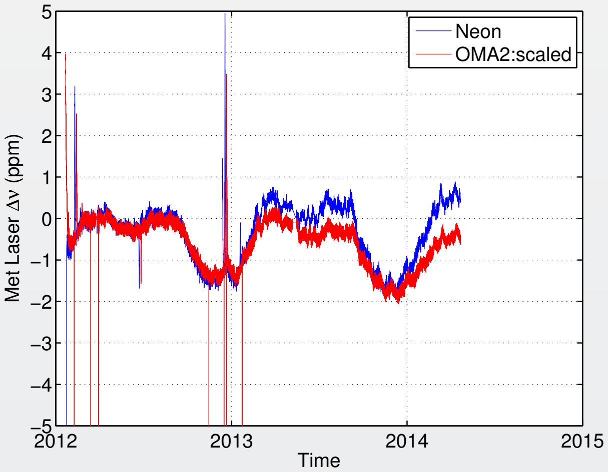

- Question: Is any of this drift due to the Neon lamp? Original plans were to update the Neon calibration via up-welling radiances 1/month.
- Difficult to use IDPS SDR record for this since Neon cal used in IDPS uncertain until Nov. 2013.

2-Year Neon Calibration from CCAST

CCAST: UW/UMBC SDR Testbed Code

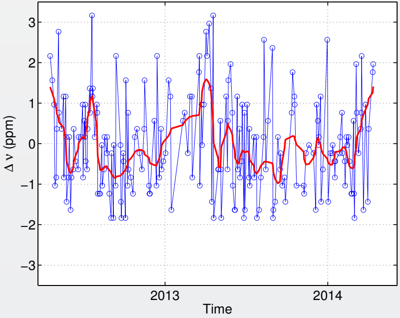

- Reprocess 2 years of SDRs with CCAST using metrology laser that follows Neon calibration exactly.
- Normal ν-cal compares observed to NWP simulated radiances: not yet finished.
- Here: compare (via cross-correlation) April 2012 scene radiances to time series of a small clear subset of CCAST output.
- Regression of drift over 2 years: -0.07 ppm $\pm$ 0.54 ppm
- Excellent long-term stability

This approach introduces noise, we will soon finish matching 2-years of CCAST output to NWP (ECMWF) and will have a much lower noise Neon calibration to determine if it is drifting and needs any updates.

The results shown here suggest no long-term drifts, but possibly a small seasonal drift with solar heating of the instrument.

CCAST SDR Cal Approach for This Work

$$r_{\mathrm{OBS}} = F \cdot r_{\mathrm{ICT}} \cdot f \cdot \mathrm{SA}^{-1} \cdot f \cdot \frac{\mathrm{ES} - \mathrm{SP}}{\mathrm{IT} - \mathrm{SP}}$$

- r_{OBS} is calibrated radiance at the user grid
- F is Fourier interpolation from sensor to user grid
- f is a raised-cosine bandpass filter
- r_{ICT} is expected ICT radiance at the sensor grid
- SA^{-1} is the inverse of the ILS matrix
- ES is earth-scene count spectra
- IT is calibration target count spectra
- SP is space-look count spectra

Periodic Sinc Applied to High-Resolution Spectra

- Periodic sinc (psinc) is the correct basis for the instrument line shape (ILS)
- Thanks to Dan Mooney, see next talk
- IDPS and previously CCAST used sinc, not psinc

Two metrics for spectral performance

Observed - Computed (NWP)
100 Clear Ocean Scenes

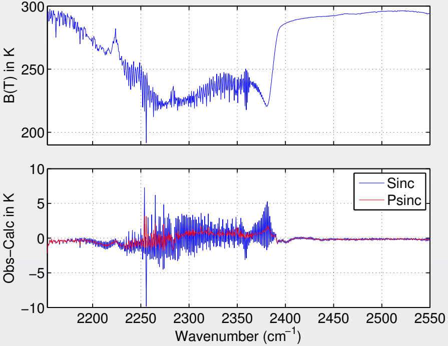

Standard Deviation of FOV5-FOV*n*
Large global dataset FORS=15,16

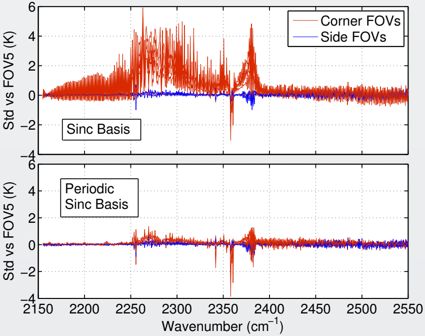

Periodic Sinc: Details

Bias Psinc/sinc - Bias Hamming
A clean metric for excess ringing

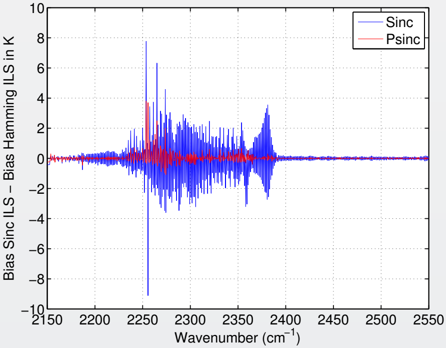

Observed - Computed (NWP)
Psinc apodized to Hamming

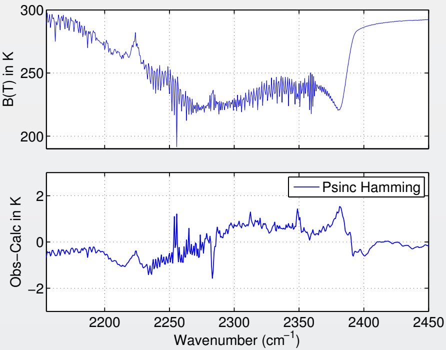

- This is a major improvement to the high-resolution short-wave data
- Periodic sinc mostly improves corner FOVS, where the self-apodization correction is largest, SA matrix is more poorly conditioned.
- Should help improve absolute spectral calibration once CrIS is in high-resolution mode

FOV7 Non-Linearity in High-Resolution Data

- High-res mid-wave water vapor line centers very cold
- Below: Std. Dev. of FOV5-FOV*n* for global data set. IDPS non-linear coefficients (Feb. 20, 2014 +).
- FOV7 non-linearity may need a more refined correction

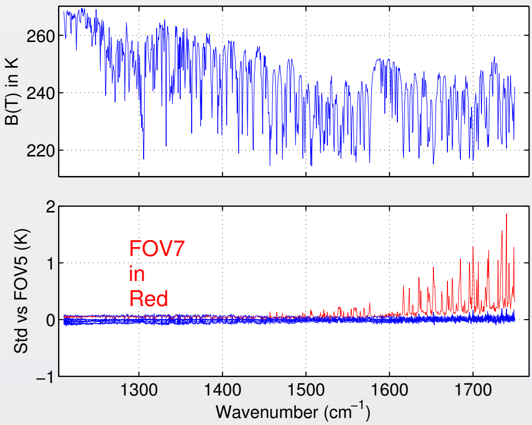

Periodic Sinc Applied to Normal Resolution SDRs

Bias Psinc/sinc - Bias Hamming
(ringing metric)

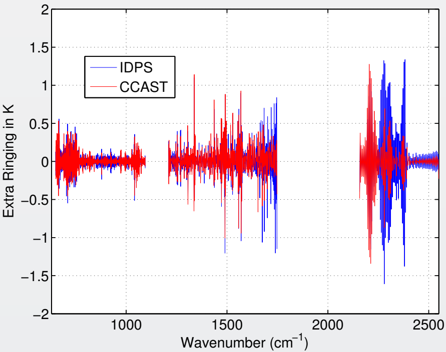

Difference of abs(ringing metric)
(IDPS minus CCAST)

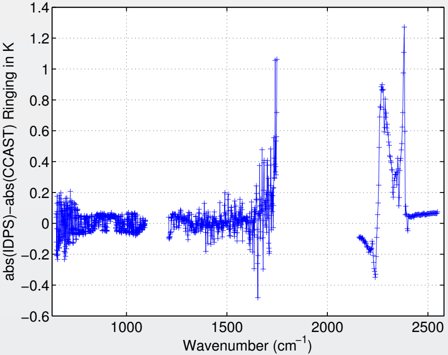

- Periodic sinc only clearly better at high wavenumber end of mid-wave band and most of short-wave band.
- Other contributors to non-sinc ringing dominate

CrIS/AIRS SNOs using Native CrIS ILS

- Intercalibration of AIRS and CrIS can only be done with L1b data in winow regions.
- ILS (Instrument Line Shape) differences cause large (4+K) differences between AIRS and CrIS for
- We convert AIRS (L1c) radiances using a deconvolution, reconvolution approach.
- The AIRS$\longrightarrow$CrIS data may provide the best approach for building a seamless AIRS + CrIS L2 time series.

AIRS L1c: Mismatch due to ILS Differences

Sampling of AIRS vs CrIS ILS

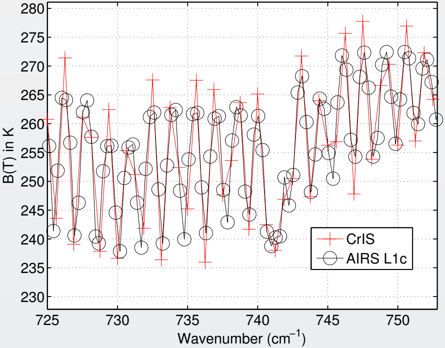

B(T) error using just ν interpolation

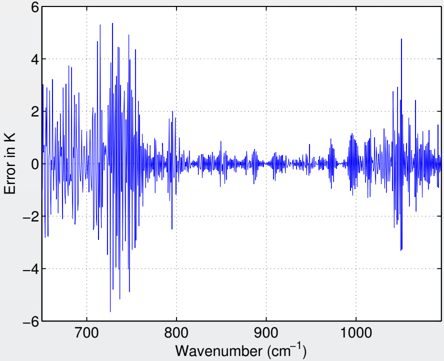

AIRS $\longrightarrow$ CrIS Conversion

This topic is beyond the scope of this talk, so just a summary.

Basic methodology

Let S_a be a matrix whose rows are AIRS SRFs on a 0.1 cm^{-1} grid, c AIRS channel radiances, and r radiances on the same 0.1 cm^{-1} grid. Then we can write

$$c = S_a r,$$

expressing the channel radiances as the convolution of observed radiance. In practice we have c and don't know r, but we can approximate it by taking the pseudo-inverse S_a^{-1} and applying it to c,

$$r = S_a^{-1} c.$$

This is the deconvolution. This regularly spaced r can then be convolved to CrIS radiances at the user grid, taking into account band differences. The key in practice is that the L1c channel set gives a relatively well-conditioned S_a.

Example of De-convolved AIRS Spectrum

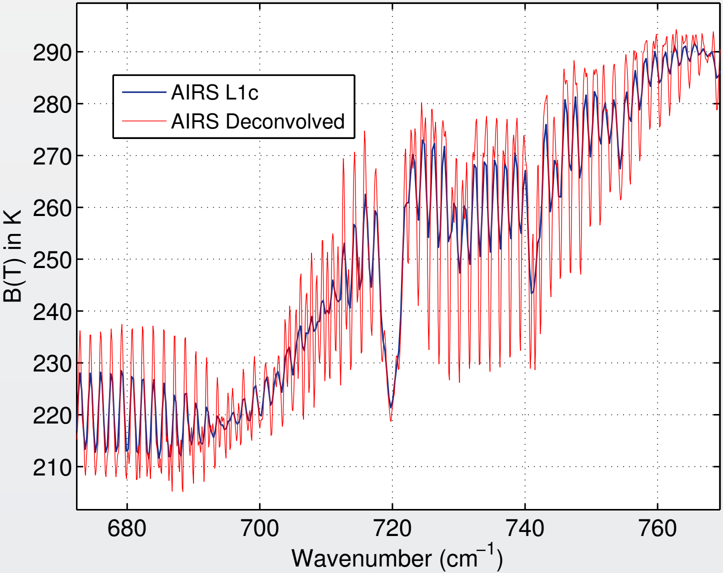

Example of AIRS L1c and Conversion to CrIS

L1b

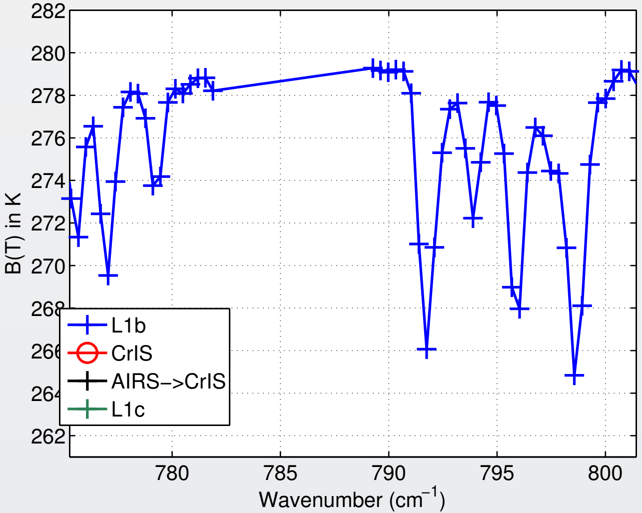

Example of AIRS L1c and Conversion to CrIS

L1b + L1c

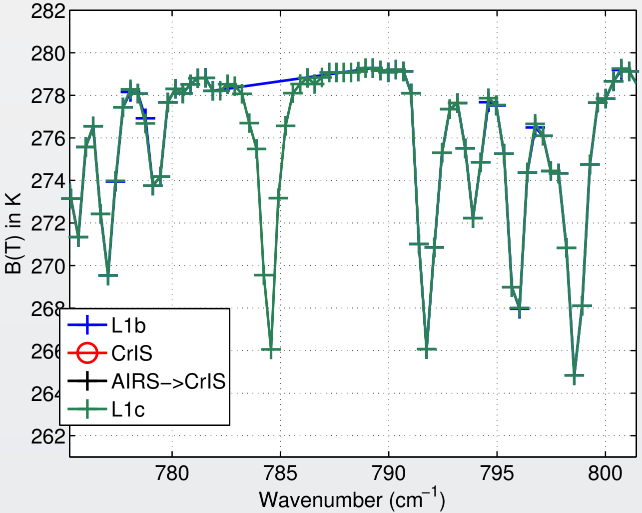

Example of AIRS L1c and Conversion to CrIS

L1b + L1c + L1c⟶CrIS

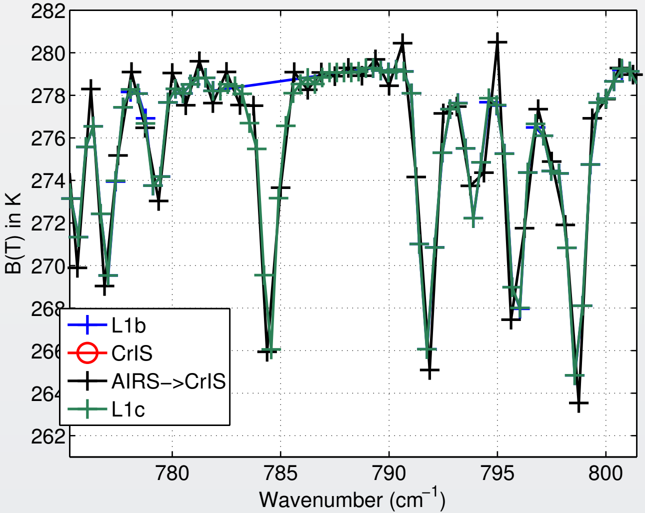

Example of AIRS L1c and Conversion to CrIS

L1b + L1c + L1c⟶CrIS + CrIS

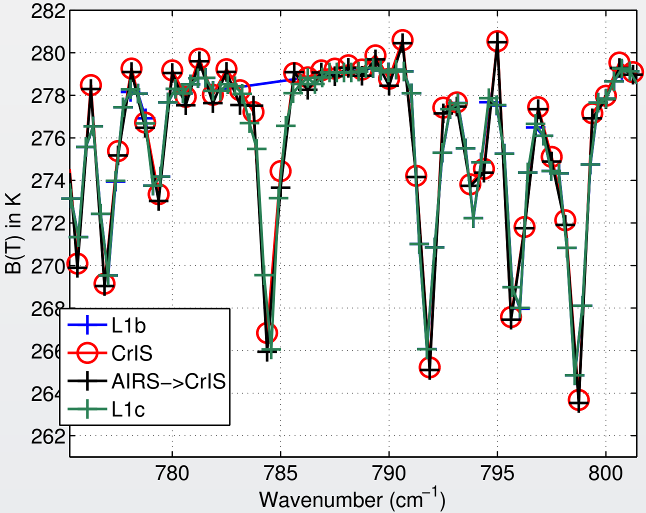

Example of AIRS L1c and Conversion to CrIS

L1c ⟶ CrIS + CrIS

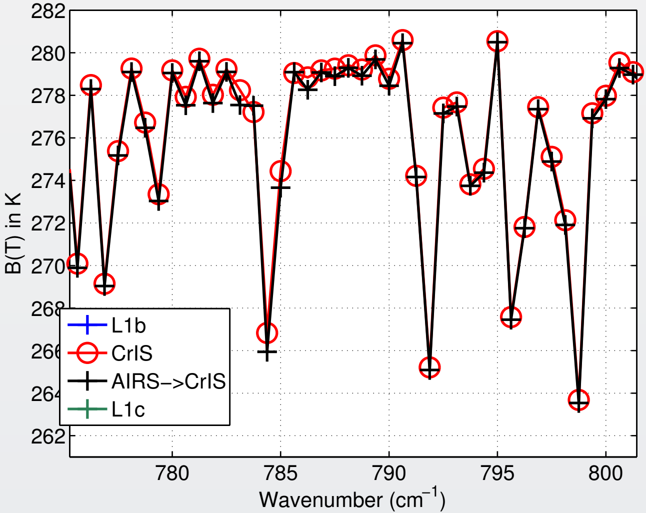

Full Spectrum Differences (Pre-Feb. 2014 Non-Linearity)

Hamming Apodization

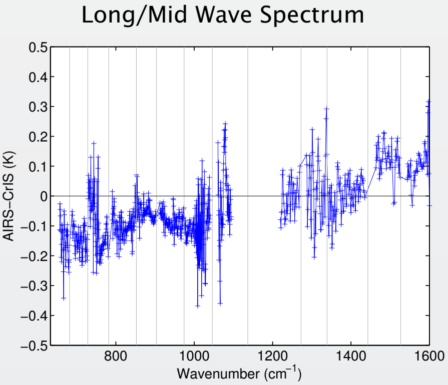

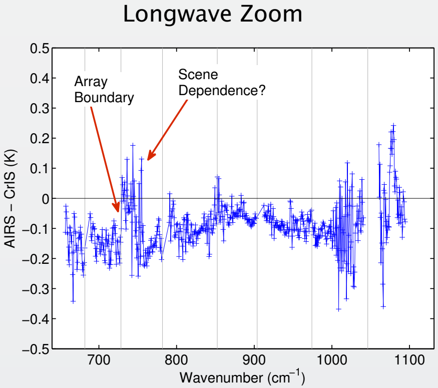

0.2K “ringing” may be due to lack of frequency calibration

The standard error is extremely small. ±50°latitude SNOs, 2 million+ samples.

Full Spectrum Differences (Post-Feb. 2014 Non-Linearity)

Day versus Night

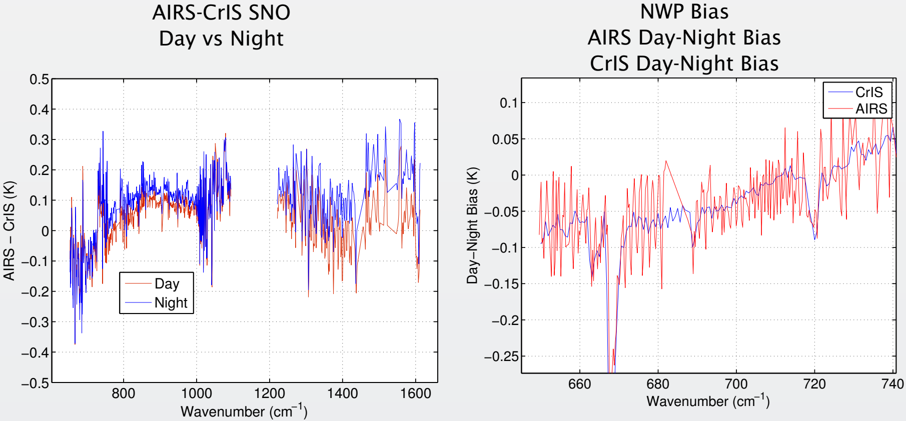

- Differences between CrIS vs AIRS day/night larger than statistical errors
- Thermal issues on one of these instruments?
- NWP day vs night biases similar for AIRS, CrIS in 650-700 cm^{-1} region, but very different for water vapor due to sampling differences
- AIRS “ringing” due to me not doing AIRS frequency calibration before forming SNOs. TBD.

CrIS Radiometric Stability

Relative to SST, CO_2

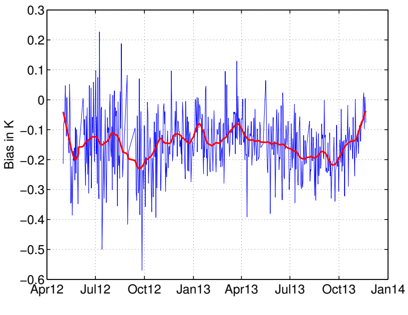

- Tropical ocean clear
- 1-Year differences far below 0.1K. Red curve is smoothed time series.

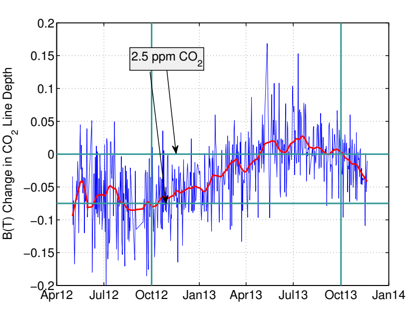

- CO_2 from ECMWF bias (791.5 cm^{-1}) - 0.27*bias(790 cm^{-1}).
- Second term removes any SST, H_2O variability.
- Oct 2012 through Oct 2013 shows 2.5 ppm growth rate (0.06K).

Conclusions

- CrIS spectral calibration continues to be stable and accurate
- UMBC will complete full analysis of Neon stability in the near future using CCAST
- CrIS high-resolution short-wave SDRs improved using period sinc basis function for apodization corrections.
- FOV-7 improvements needed for high-spectral resolution mode.
- AIRS/CrIS SNOs exhibit $\sim \pm 0.1$K agreement on a channel-by-channel basis with AIRS ($\sim$1080 channels).
- AIRS/CrIS comparisons will improve once AIRS SNOs are frequency calibration (by UMBC).
- AIRS $\longrightarrow$ CrIS conversion will make a combined AIRS, CrIS radiance climate data set possible, now at 11+ years length.

CrIS Calibration Equation

D. L. Mooney

Session 4b

STAR JPSS Annual Science Team Meeting

May 13 2014

The differences among processing approaches are small

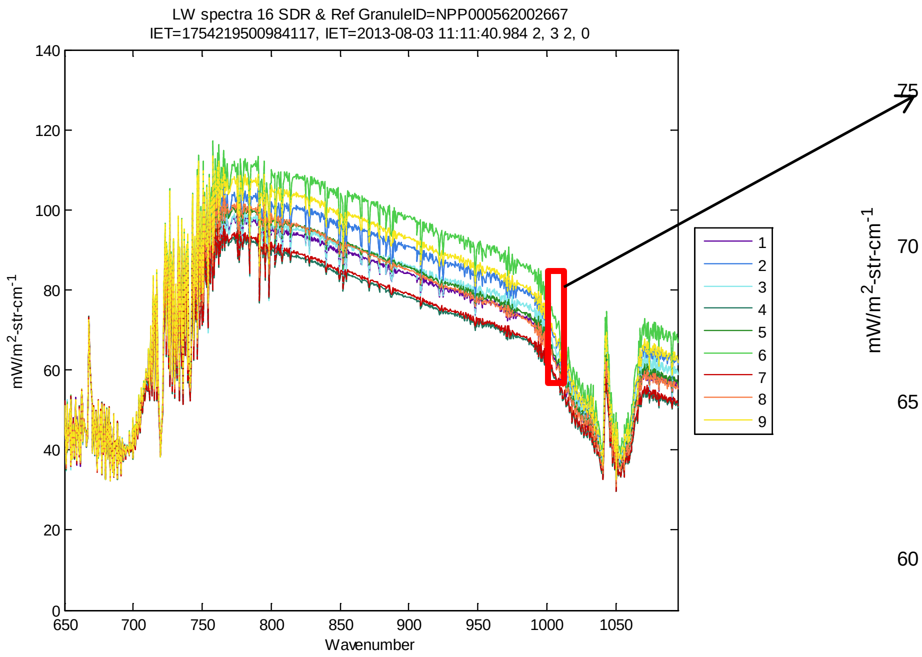

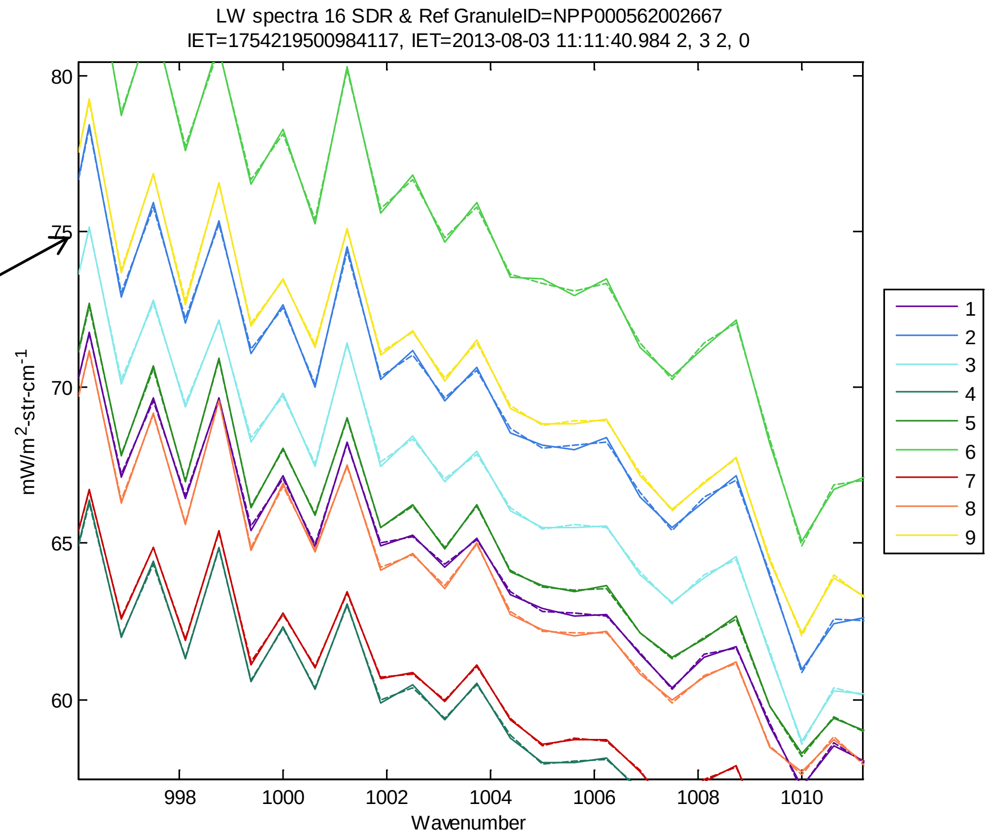

Solid - LL_old
Dashed - SDR

Difference IDPS-Ref and low Pass filtered difference

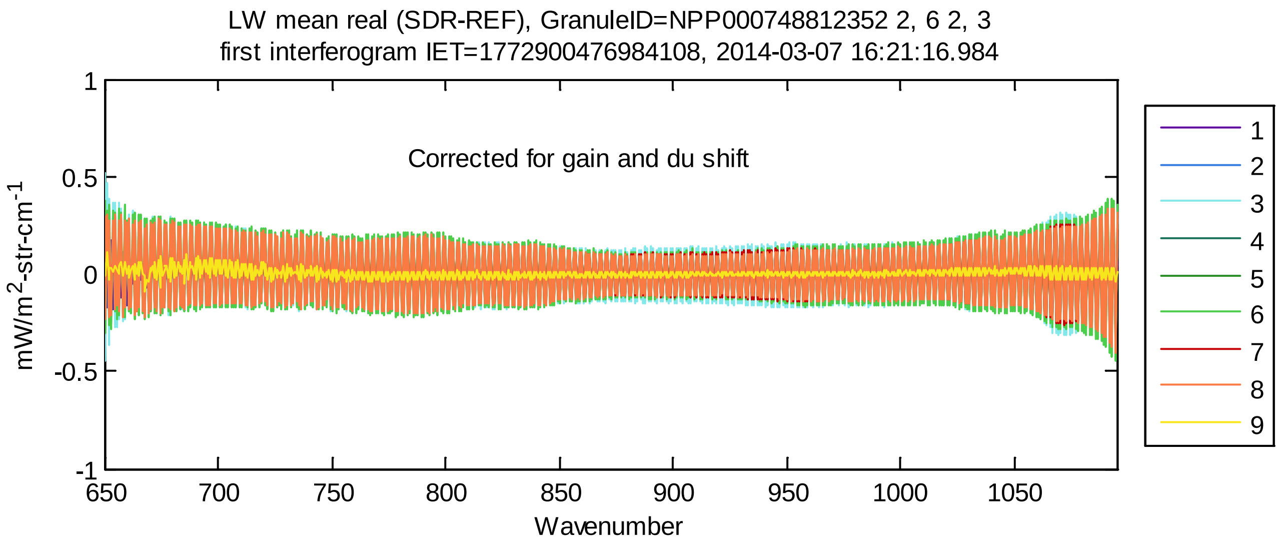

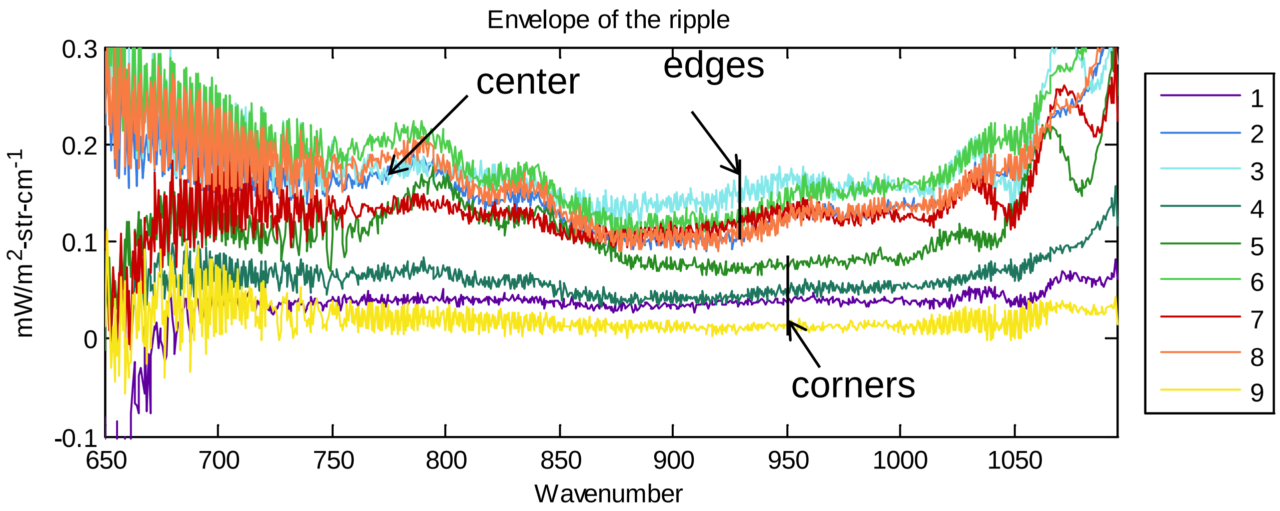

Determine gain and wavenumber shift

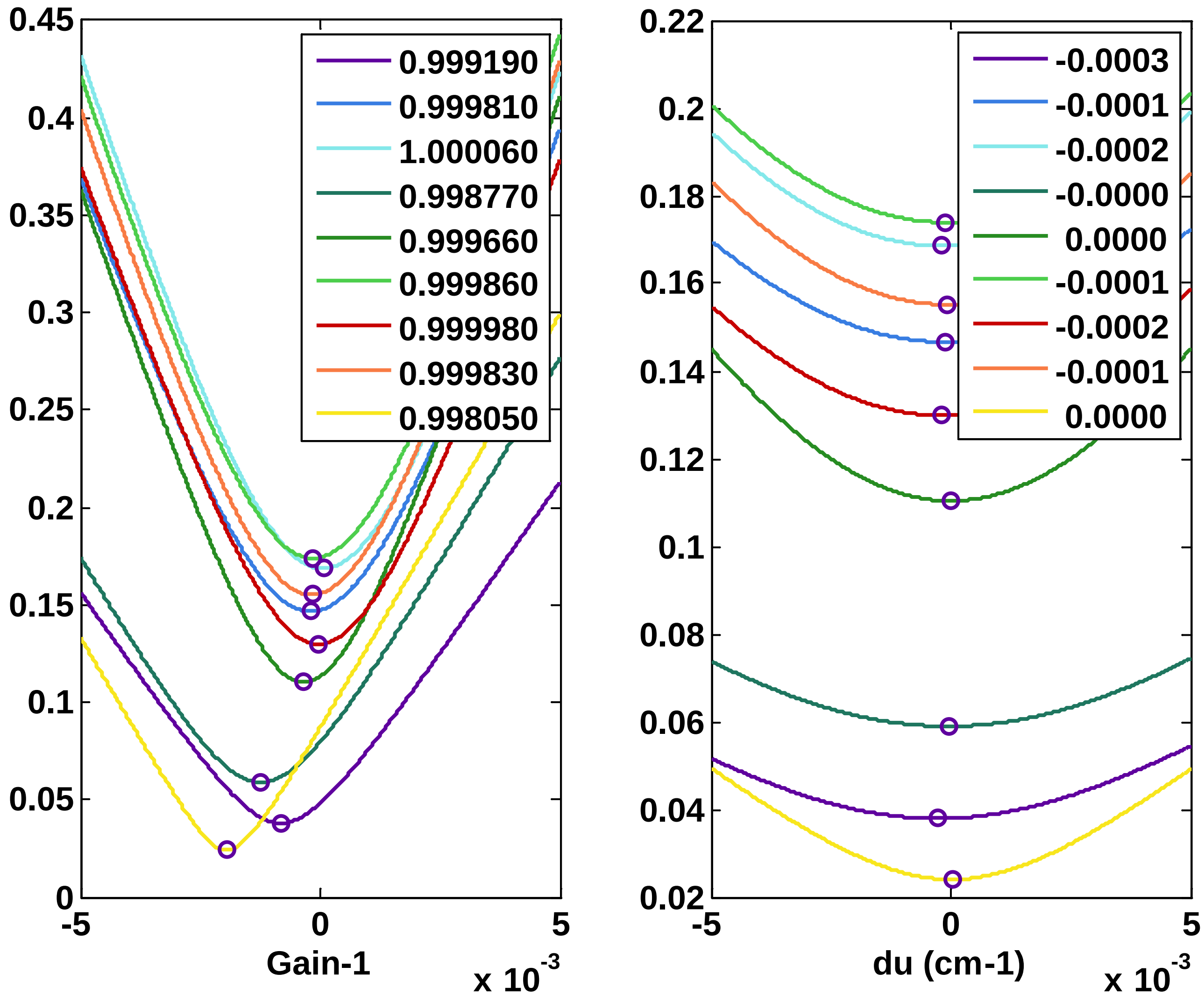

Corrected for gain and wavenumber shift

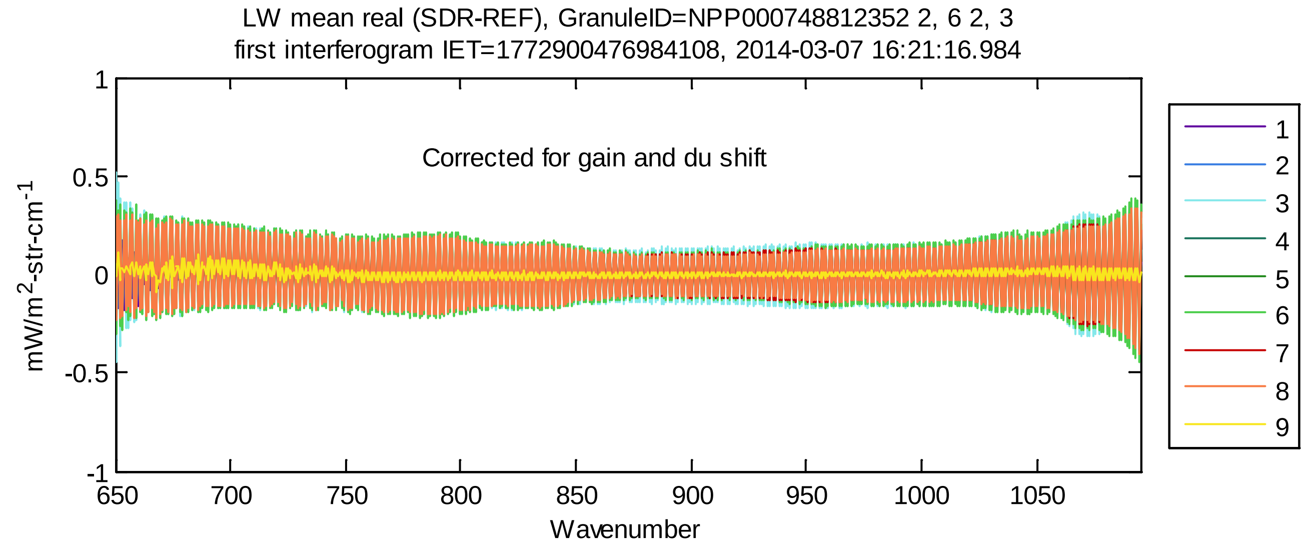

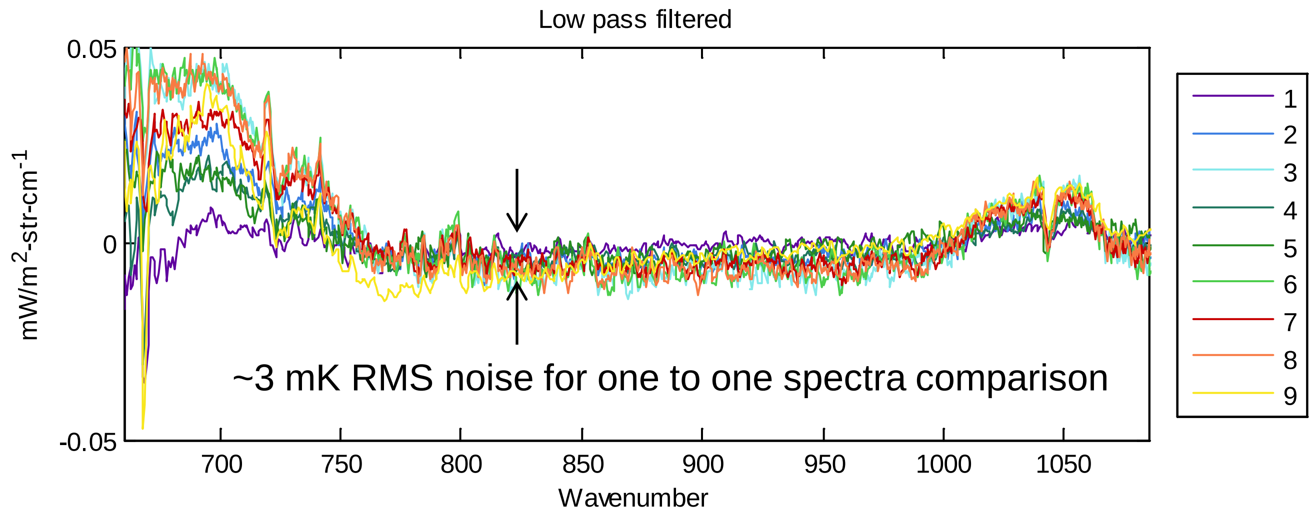

Envelope of ripple difference SDR-Ref for FOR=2 in Granule NPP 00055200266

- **We will use the envelope of ripple difference for comparing different calibration approaches**
- **Envelope by multiplying by [1,-1,1,-1,….]**

Ripple

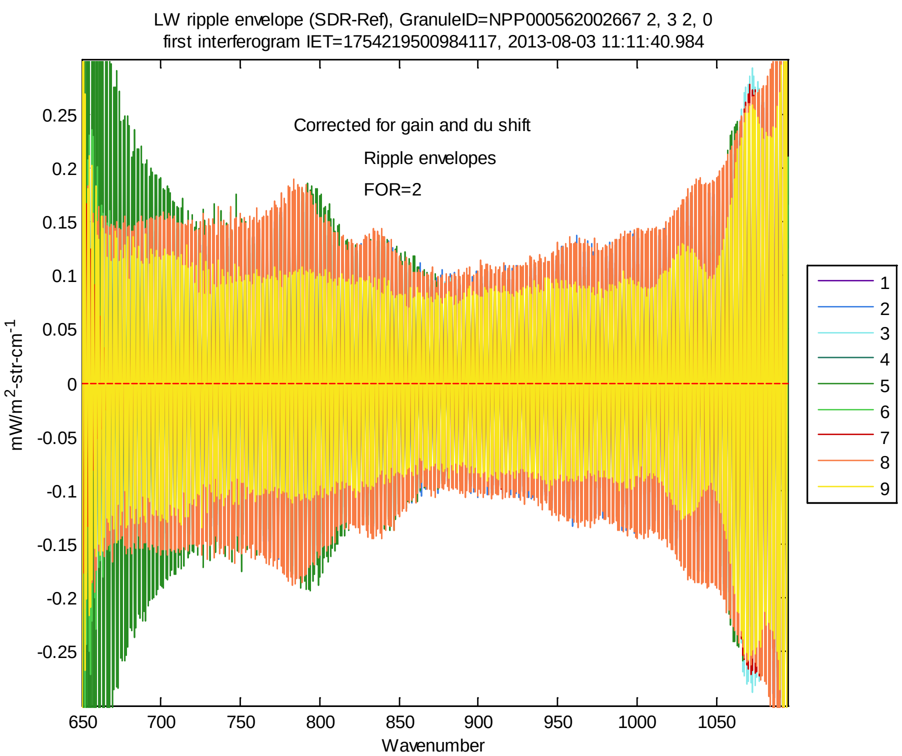

Envelope of ripple

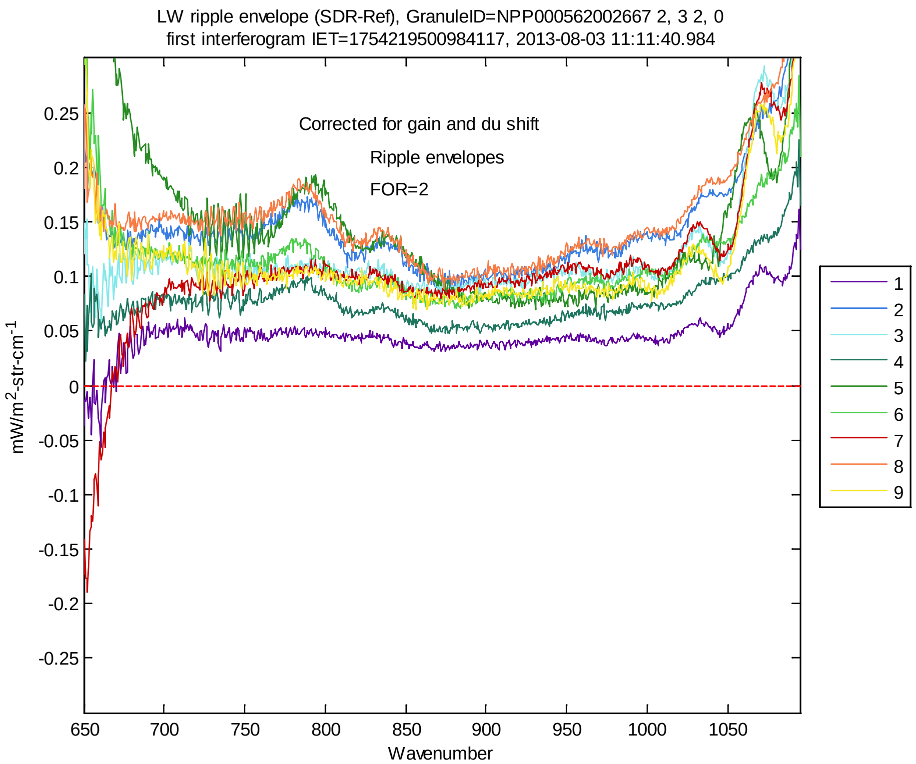

Examine a Range of spectra for different FOR

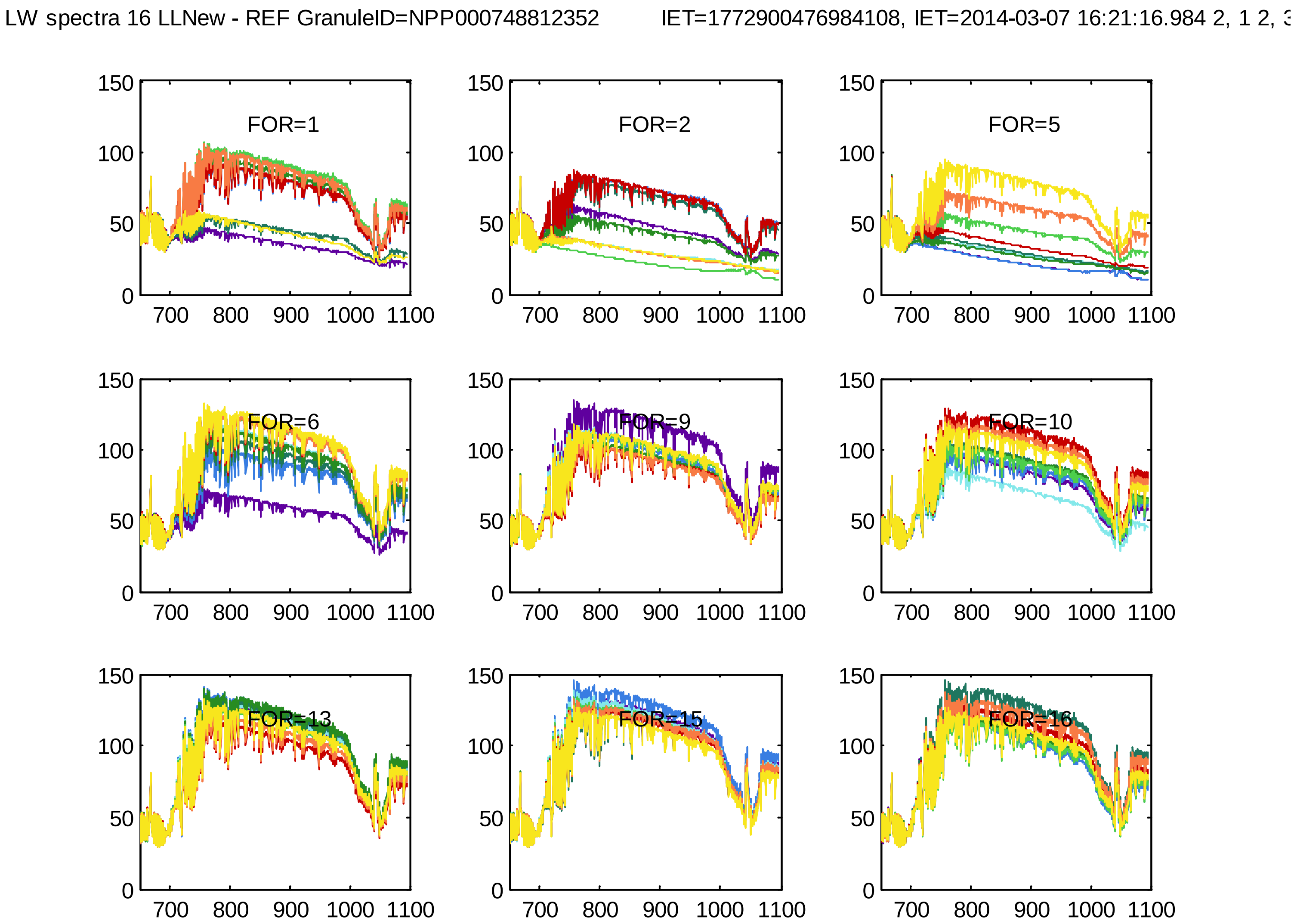

Ripple envelopes change with different FORs especially near the edges

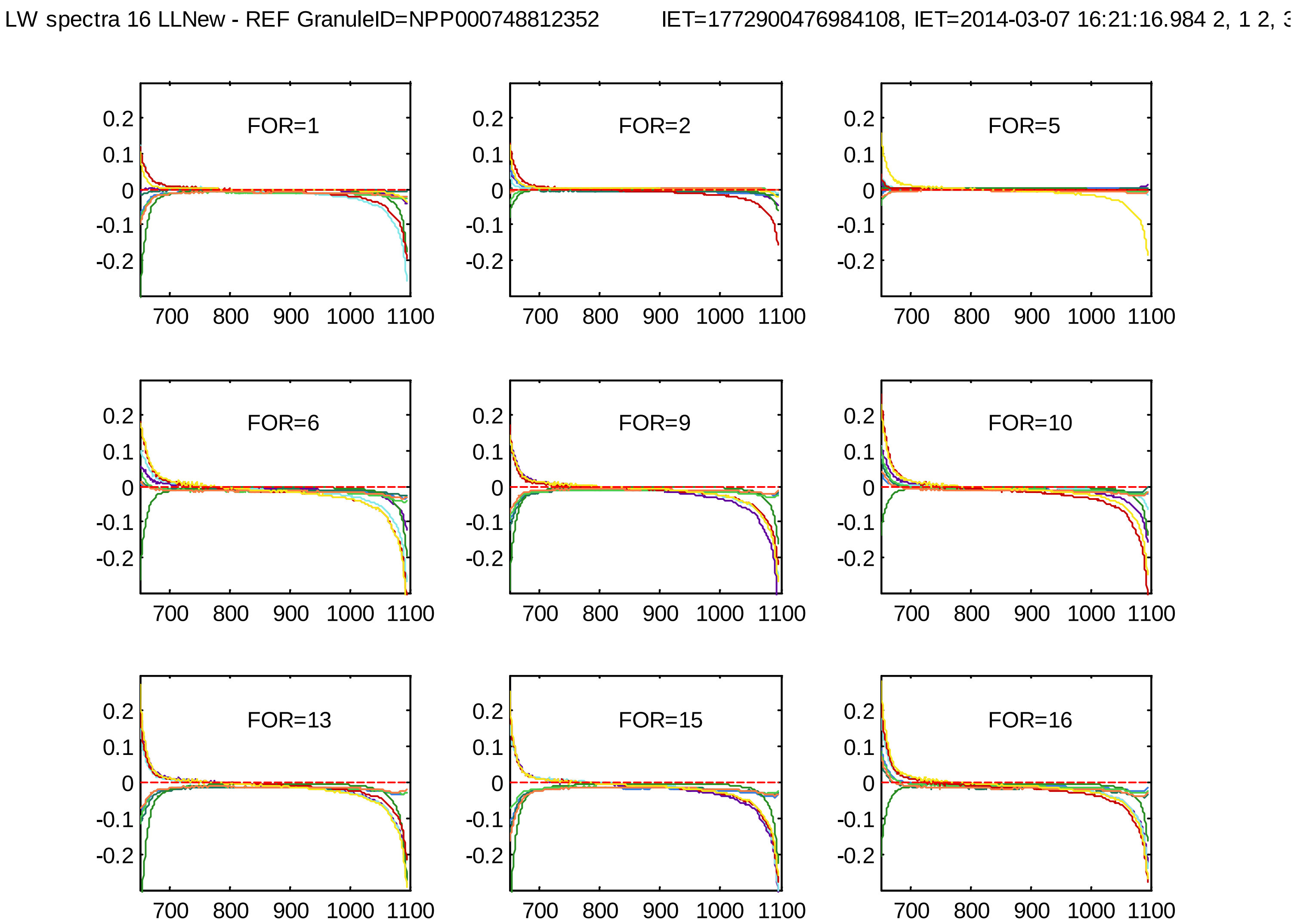

Calibration options

Item	Member	Calibration	CMO Principals	Calibration Order
1	IDPS	$N=(SA_u^{-1}\cdot F_{s\to u}\cdot f_{ATBD})\cdot\left\{\frac{S_E-S_{SP}}{S_{ICT}-S_{SP}}\cdot ICT(T,u_{sensor*(1+delta)})\right\}$	$SA_u^{-1}\cdot F_{s\to u}$	Calibration first, then CMO
2	ADL/CSPP	$N=(SA_u^{-1}\cdot F_{s\to u}\cdot f_{ATBD})\cdot\left\{\frac{S_E-S_{SP}}{S_{ICT}-S_{SP}}\cdot ICT(T,u_{sensor*(1+delta)})\right\}$		
3	Exelis (old)	$N=\left(SA_u^{-1}\cdot F_{s\to u}\cdot f_{ATBD}\right)\cdot\left\{\frac{S_E-S_{SP}}{S_{ICT}-S_{SP}}f_{BH}\cdot\left[SA_u^{-1}\cdot F_{s\to u}\right]^{-1}\cdot ICT(T,u_{sensor})\right\}$		
4	UMBC/UW** option A	$N=F_{s\to u}\cdot f\cdot SA_s^{-1}\cdot\left\{f\cdot\frac{FIR^{-1}\cdot(S_E-S_{SP})}{FIR^{-1}\cdot(S_{ICT}-S_{SP})}\cdot ICT(T,u_{sensor\_off\_axis})\right\}$	$F_{s\to u}\cdot SA_s^{-1}$	
5	CCAST Cal mode 1	$N=F_{s\to u}\cdot f\cdot SA_s^{-1}\cdot\left\{\frac{FIR^{-1}\cdot(S_E-S_{SP})}{FIR^{-1}\cdot(S_{ICT}-S_{SP})}\cdot ICT(T,u_{sensor\_off\_axis})\right\}$		
6	UMBC/UW** option B	$N=F_{s\to u}\cdot\left\{ICT(T,u_{sensor})\cdot f\cdot SA_s^{-1}\cdot\left\{f\cdot\frac{FIR^{-1}\cdot(S_E-S_{SP})}{FIR^{-1}\cdot(S_{ICT}-S_{SP})}\right\}\right\}$		
7	CCAST Cal mode 2	$N=F_{s\to u}\cdot f\cdot\left\{ICT(T,u_{sensor})\cdot SA_s^{-1}\cdot\left\{\mathrm{Re}\left[\frac{FIR^{-1}\cdot(S_E-S_{SP})}{FIR^{-1}\cdot(S_{ICT}-S_{SP})}\right]\right\}\right\}$		
8	LL(old)*	$N=\left\{\frac{M\cdot\left(FIR^{-1}\cdot(S_E-S_{SP})\right)}{M\cdot\left(FIR^{-1}\cdot(S_{ICT}-S_{SP})\right)}\right\}\cdot ICT(T,u_{user})$		CMO first, then Calibration
9	LL(new)	$N=\left\{\frac{F_{s\to u}\cdot SA_s^{-1}\cdot\left(FIR^{-1}\cdot(S_E-S_{SP})\right)}{F_{s\to u}\cdot SA_s^{-1}\cdot\left(FIR^{-1}\cdot(S_{ICT}-S_{SP})\right)}\right\}\cdot ICT(T,u_{user})$		
10	Proposed(1)	$N=F_{s\to u}\cdot f_{ATBD}\cdot\left\{\frac{SA_s^{-1}\cdot\left(FIR^{-1}\cdot(S_E-S_{SP})\right)}{SA_s^{-1}\cdot\left(FIR^{-1}\cdot(S_{ICT}-S_{SP})\right)}\cdot ICT(T,u_{sensor})\right\}$		
11	Proposed(2)	$N=ICT(T,u_{user})\cdot\left\{\frac{F_{s\to u}\cdot SA_s^{-1}\cdot f_{ATBD}\cdot\left(FIR^{-1}\cdot(S_E-S_{SP})\right)}{F_{s\to u}\cdot SA_s^{-1}\cdot f_{ATBD}\cdot\left(FIR^{-1}\cdot(S_{ICT}-S_{SP})\right)}\right\}$		
12	Exelis(new)	$N=\left\{\frac{\left(SA_u^{-1}\cdot F_{s\to u}\cdot(S_E-S_{SP})\right)}{\left(SA_u^{-1}\cdot F_{s\to u}\cdot(S_{ICT}-S_{SP})\right)}\right\}\cdot ICT(T,u_{user})$	$SA_u^{-1}\cdot F_{s\to u}$	

Ref

Calibration first then "CMO"

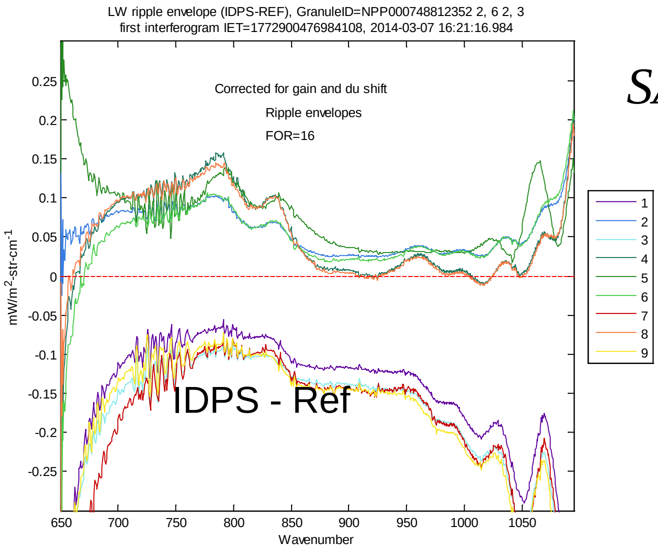

$$SA_s^{-1} \cdot F_{s \to u}$$

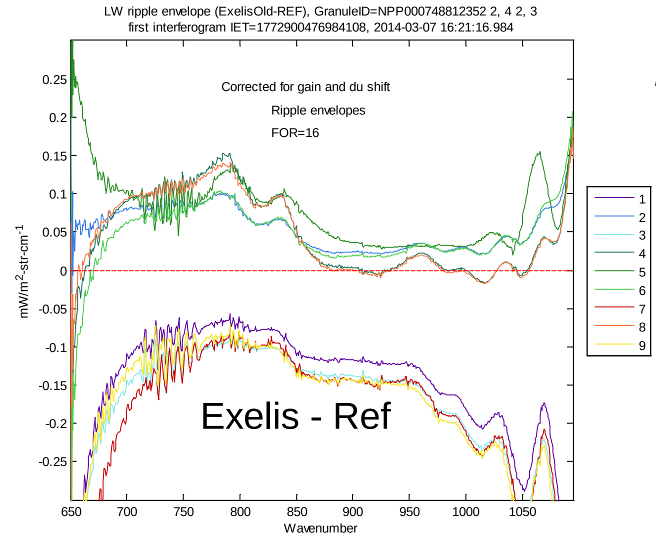

$$SA_s^{-1} \cdot F_{s \to u}$$

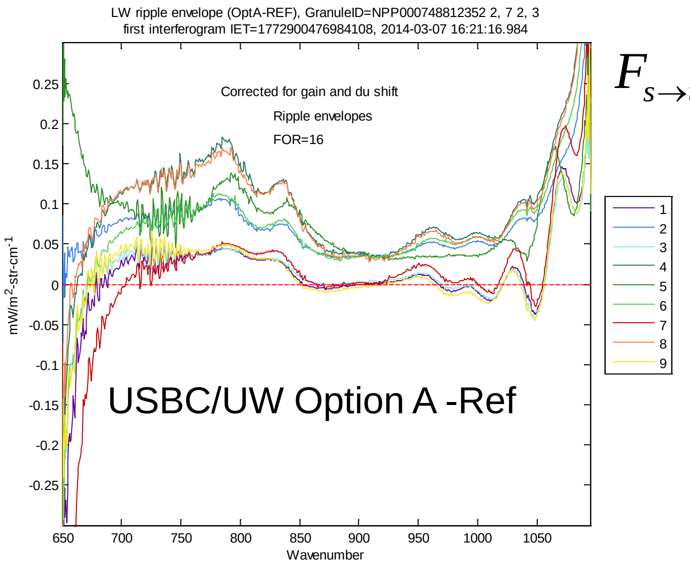

$$F_{s \to u} \cdot SA_s^{-1} \cdot$$

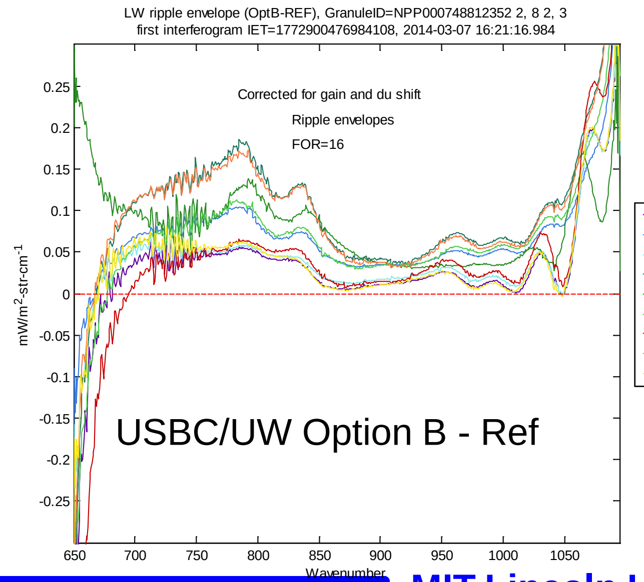

$$F_{s \to u} \cdot SA_s^{-1} \cdot$$

“CMO” first then calibration

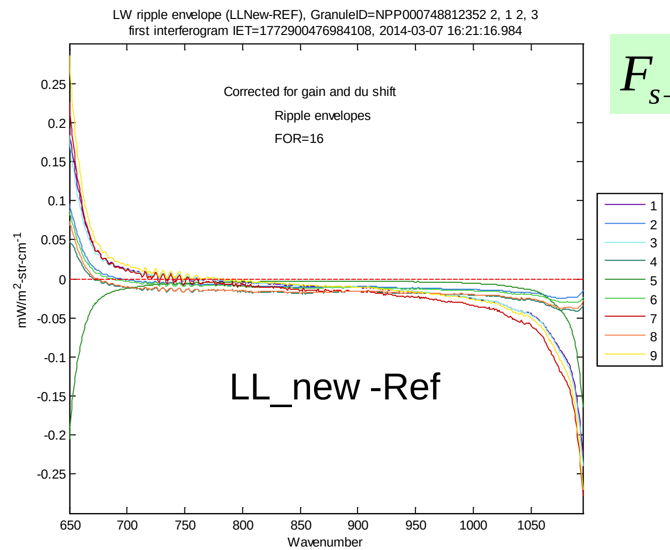

$$F_{s\rightarrow u}\cdot SA_s^{-1}\cdot$$

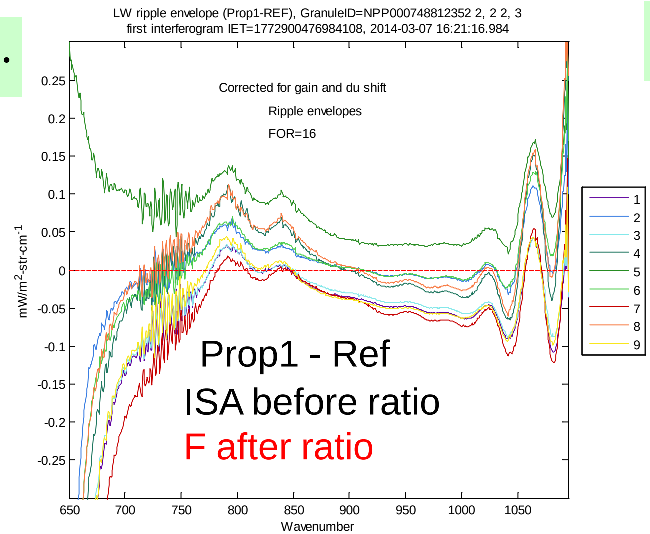

$$F_{s\rightarrow u}\cdot SA_s^{-1}\cdot$$

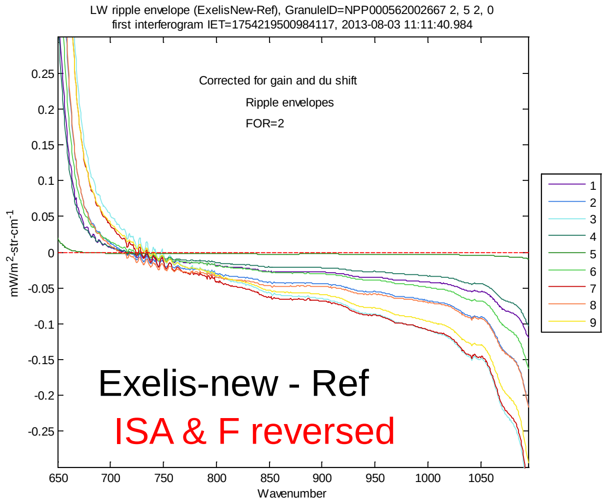

$$SA_s^{-1}\cdot F_{s\rightarrow u}$$

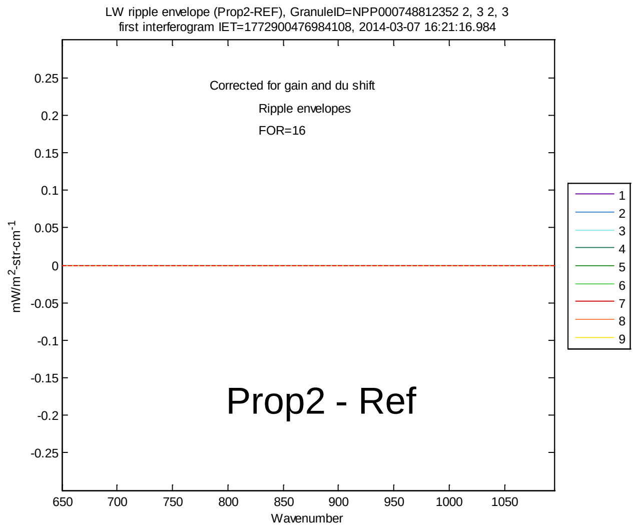

Doing the interpolation before/after the calibration ratio makes a difference (LW)

$$N = F_{s\to u}\cdot f\cdot SA_s^{-1}\cdot\left\{\frac{FIR^{-1}\cdot\left(S_E - S_{SP}\right)}{FIR^{-1}\cdot\left(S_{ICT} - S_{SP}\right)}\cdot ICT\left(T, u_{sensor\_off\_axis}\right)\right\}$$

$$N = ICT\left(T, u_{user}\right)\cdot\left\{\frac{F_{s\to u}\cdot SA_s^{-1}\cdot\left(FIR^{-1}\cdot\left(S_E - S_{SP}\right)\right)}{F_{s\to u}\cdot SA_s^{-1}\cdot\left(FIR^{-1}\cdot\left(S_{ICT} - S_{SP}\right)\right)}\right\}$$

$$N = F_{s\to u}\cdot f_{ATBD}\cdot\left\{\frac{SA_s^{-1}\cdot\left(FIR^{-1}\cdot\left(S_E - S_{SP}\right)\right)}{SA_s^{-1}\cdot\left(FIR^{-1}\cdot\left(S_{ICT} - S_{SP}\right)\right)}\cdot ICT\left(T, u_{sensor}\right)\right\}$$

Ratio after interpolation & ISA

Ratio before interpolation

Ratio before interpolation & ISA

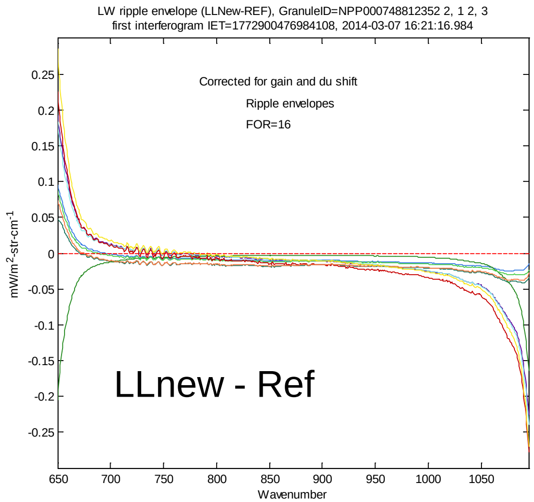

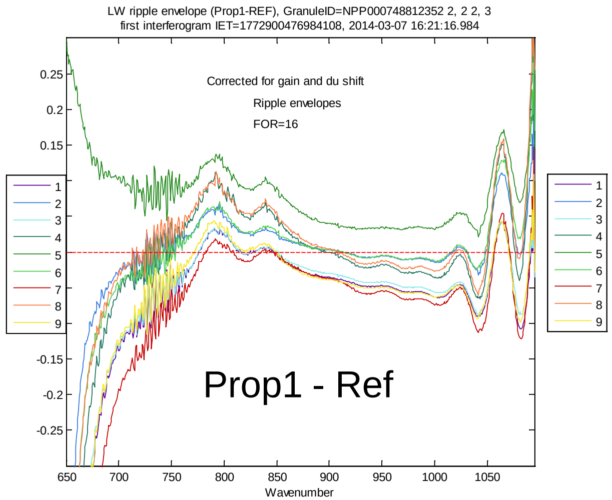

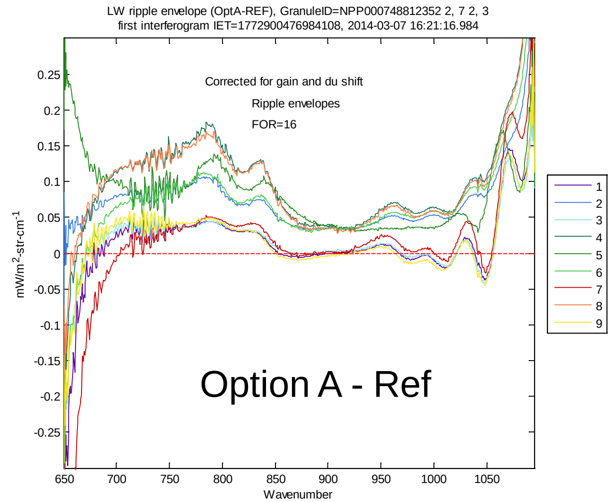

Ref= Prop2

$$N = ICT\left(T, u_{user}\right)\cdot\left\{\frac{F_{s\to u}\cdot SA_s^{-1}\cdot f_{ATBD}\cdot\left(FIR^{-1}\cdot\left(S_E - S_{SP}\right)\right)}{F_{s\to u}\cdot SA_s^{-1}\cdot f_{ATBD}\cdot\left(FIR^{-1}\cdot\left(S_{ICT} - S_{SP}\right)\right)}\right\}$$

Note: Ref does interpolation before ratio

Doing the interpolation before/after the calibration ratio makes a difference (SW)

$$N = \cdot ICT(T,u_{user}) \cdot \left\{ \frac{M \cdot \left(FIR^{-1} \cdot (S_E - S_{SP})\right)}{M \cdot \left(FIR^{-1} \cdot (S_{ICT} - S_{SP})\right)} \right\}$$

$$N = F_{s\to u} \cdot f \cdot SA_s^{-1} \cdot \left\{ \frac{FIR^{-1} \cdot (S_E - S_{SP})}{FIR^{-1} \cdot (S_{ICT} - S_{SP})} \cdot ICT(T,u_{sensor\_off\_axis}) \right\}$$

$$N = F_{s\to u} \cdot f_{ATBD} \cdot \left\{ \frac{SA_s^{-1} \cdot \left(FIR^{-1} \cdot (S_E - S_{SP})\right)}{SA_s^{-1} \cdot \left(FIR^{-1} \cdot (S_{ICT} - S_{SP})\right)} \cdot ICT(T,u_{sensor}) \right\}$$

Ratio after interpolation & ISA

Ratio before interpolation

Ratio before interpolation & ISA

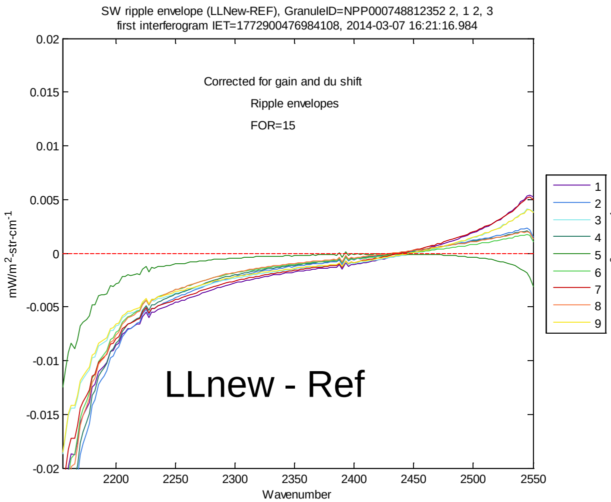

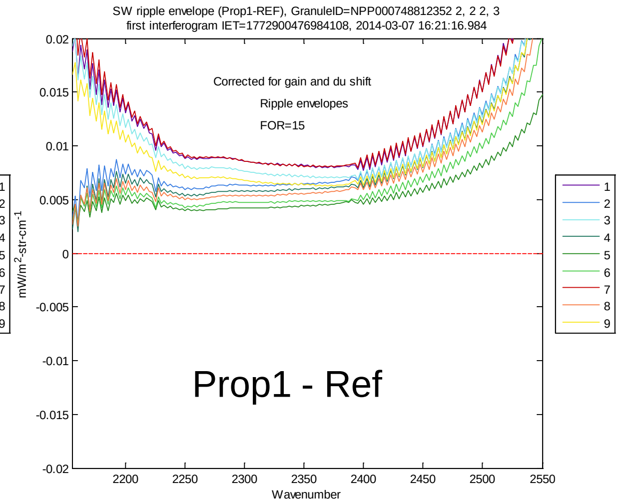

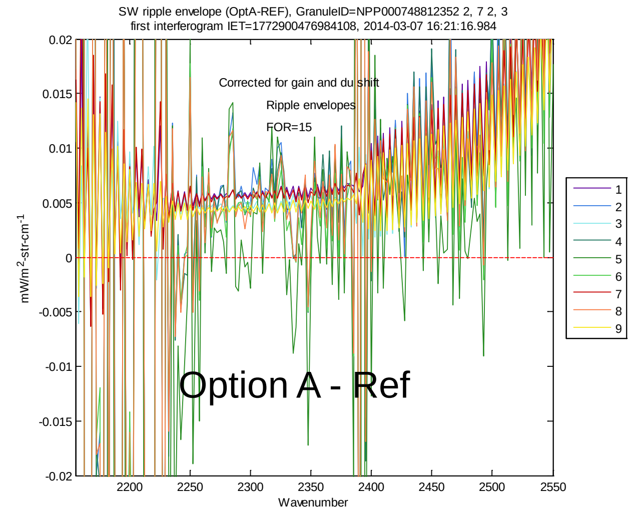

Ref= Prop2

$$N = ICT(T,u_{user}) \cdot \left\{ \frac{F_{s\to u} \cdot SA_s^{-1} \cdot f_{ATBD} \cdot \left(FIR^{-1} \cdot (S_E - S_{SP})\right)}{F_{s\to u} \cdot SA_s^{-1} \cdot f_{ATBD} \cdot \left(FIR^{-1} \cdot (S_{ICT} - S_{SP})\right)} \right\}$$

Note: Ref does interpolation before ratio

Conclusions

- Doing interpolation after calibration ratio gives a different result than interpolation & ISA before calibration ratio
- Difference is entirely a modulated ringing at the Nyquist
- Effective comparison of calibration results can be done by comparing ringing envelope
- There are two distinct classes of calibration algorithms
  - Interpolation (and ILS correction) before calibration ratio
  - Interpolation (and ILS correction) after calibration ratio
- Definition of ISA matrix is only consistent with Interpolation & ISA before calibration ratio\
- Further analysis is ongoing produce optimal extended resolution spectra with correct calibration equation